#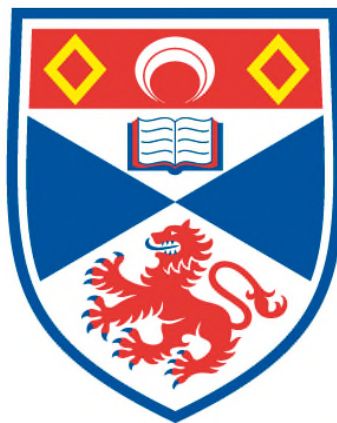 STRUCTURAL ANALYSIS OF THE POTENTIAL THERAPEUTIC TARGETS FROM SPECIFIC GENES IN METHICILLIN-RESISTANT STAPHYLOCOCCUS AUREUS (MRSA)

Xuan Yan

**A Thesis Submitted for the Degree of PhD
at the
University of St Andrews**

2011

**Full metadata for this item is available in
St Andrews Research Repository
at:
http://research-repository.st-andrews.ac.uk/**

**Please use this identifier to cite or link to this item:
http://hdl.handle.net/10023/2613**

Structural analysis of the potential therapeutic targets from specific genes in Methicillin-Resistant *Staphylococcus aureus* (MRSA)

Xuan Yan

050009756

A thesis submit for the degree of Doctor of Philosophy

School of Chemistry &

Biomedical Sciences Research Complex

University of St-Andrews

Supervisor – Prof. James H Naismith

TABLE OF CONTENTS

Declarations

1. Candidate's declarations:

I, Xuan YAN, hereby certify that this thesis, which is approximately 35,000 words in length, has been written by me, that it is the record of work carried out by me and that it has not been submitted in any previous application for a higher degree.

I was admitted as a research student in October, 2005 and as a candidate for the degree of Doctor of Philosophy in August 2006; the higher study for which this is a record was carried out in the University of St Andrews between 2005 and 2009.

Date: _____ Signature of candidate: _____

2. Supervisor's declaration:

I hereby certify that the candidate has fulfilled the conditions of the Resolution and Regulations appropriate for the degree of Doctor of Philosophy in the University of St Andrews and that the candidate is qualified to submit this thesis in application for that degree.

Date: _____ Signature of supervisor: _____

3. Permission for electronic publication:

In submitting this thesis to the University of St Andrews I understand that I am giving permission for it to be made available for use in accordance with the regulations of the University Library for the time being in force, subject to any copyright vested in the work not being affected thereby. I also understand that the title and the abstract will be published, and that a copy of the work may be made and supplied to any bona fide library or research worker, that my thesis will be electronically accessible for personal or research use unless exempt by award of an embargo as requested below, and that the library has the right to migrate my thesis into new electronic forms as required to ensure continued access to the thesis. I have obtained any third-party copyright permissions that may be required in order to allow such access and migration, or have requested the appropriate embargo below.

The following is an agreed request by candidate and supervisor regarding the electronic publication of this thesis:

Embargo on both [all or part] of printed copy and electronic copy for the same fixed period of two years (maximum five) on the following ground(s):

Publication would preclude future publication

Date: _____ Signature of candidate: _____

Signature of supervisor: _____

Acknowledgements

First and foremost, I would like to show my deepest gratitude to my supervisor, Professor James H Naismith a respectable, responsible and resourceful scholar, who has provided me with valuable guidance in every stage of the writing of this thesis. Without his enlightening instruction, impressive kindness and patience, I could not have completed my thesis. His keen and vigorous academic observation enlightens me not only in this thesis but also my future study.

I wish to express my warm and sincere thanks to Dr. huanting Liu who offered me great help and gave me important guidance during studies. Dr. Changjiang Dong deserves special thanks as another excellent teacher. They helped me to develop the fundamental and essential academic competence.

I shall extend my thanks to Dr. Lester Cater, Dr. Xiaofeng Zhu and Dr. Johnson who helped me to complete the data, great thanks for all their kindness, patience and help, and special gratitude give to Christina Wang.

My sincere appreciation also goes to all the colleagues in JHN lab, Stephen, Muse, Stefan, as well as anyone and everyone else.

Last but not least, I'd like to thank my parents, I could never finish this study without their support.

Abstract

The thesis describes over-expression, purification and crystallization of three proteins from *Staphylococcus aureus (S. aureus)*. *S. aureus* is an important human pathogen and methicillin-resistant *S. aureus* (MRSA) is a serious problem in hospitals nowadays. The crystal structure of 3-Methyladenine DNA glycosylase I (TAG) was determined by single-wavelength anomalous diffraction (SAD) method. TAG is responsible for DNA repair and is an essential gene for both MRSA and methicilin-susceptible *S. aureus* (MSSA). The structure was also determined in complex with 3-methyladenine (3-MeA) and was solved using molecular replacement (MR) method. An assay was carried out and the molecular basis of discrimination between 3-MeA and adenosine was determined.

The native crystal structure of fructose 1-phosphate kinase (PFK) from *S. aureus* was determined to 2.30 Å and solved using molecular replacement method. PFK is an essential enzyme involved in the central metabolism of MRSA. Despite extensive efforts no co-complex was determined, although crystals were obtained they diffracted poorly. An assay which can be used to test for inhibitors has been developed.

Mevalonate Kinase (MK) is another essential enzyme in MRSA and is a key drug target in the mevalonate pathway. Native data diffracting to 2.2 Å was collected. The structure was solved using multiple isomorphorus replacement (MIR) method. A citrate molecule was bound at the MK active site, arising from the crystallization condition. The citrate molecule indicates how substrate might bind. The protein was kinetically characterized. A thermodynamic analysis using fluorescence-based method

was carried out on each protein to investigate binding interactions of potential fragments and thus a drug design starting point.

List of Abbreviations

3-MeA	3-Methyladenine
a, b, c	Unit cell dimensions
α, β, γ	Angles of unit cell
Å	Angstrom
Ala (A)	alanine
Arg (R)	arginine
Asn (N)	asparagine
Asp (D)	aspartic acid
ASU	Asymmetric Unit
*Bam*HI	*Bacillus amyloliquefaciens* H restriction endonuclease I
Bar	barbamide
BLAST	Basic Local Alignment Search Tool
Bp	Base pairs
BER	Base excision repair
CCD	Charge-Coupled Device
CD	Circular Dichroism (Spectroscopy)
CV	Column Volume
Cys (C)	Cysteine
Da	Dalton
dH2O	deionised water
DNA	Deoxyribonucleic acid
DNAse I	deoxyribonuclease I
DMSO	Dimethyl sulfoxide
DTT	*Desulfotalea psychrophila*
EBI	European Bioinformatics Institute

EDM	electron density maps
EP	Eppendorf
E. COLI (E.coli)	*Escherichia coli*
EDTA	ethylenediaminetetraacetic acid
ESRF	European Synchrotron Radiation Facility
ExPASy	Expert Protein Analysis System
F.C.	Final Concentration
FAc	fluoroacetate
PFK	Phosphofrutose Kinase
F1P	Fructose 1-phosphate
FBP	Fructose-1,6-bisphosphate
FruA	D-fructose-1,6-diphosphate aldolase
Gln (Q)	Glutamine
Glu (E)	Glutamic acid
Gly (G)	Glycine
His (H)	Histidine
HPLC	High Performance Liquid Chromatography
I	Intensity
Ile	Isoleucine
IP	image plate
IPTG	isopropyl-β- D-thiogalactopyranoside
ITC	Isothermal Titration Calorimetry
K	Kelvin
Lac	lactose
LB	Luria Bertani
Leu (L)	Leucine
Lys (K)	Lysine
MAD	Multiple Anomalous Dispersion
MES	2-morpholinoethanesulfonic acid (buffer)
Met (M)	Methionine

MIR	Multiple Isomorphous Replacement
MIRAS	(the combination of)MIR with Anomalous Scattering
MME	mono-methyl ether
MR	Molecular replacement
MS	Mass Spectrometry
MW	Molecular Weight
NAD / NADH	nicotinamide adenine dinucleotide (oxidized / reduced)
NER	Nuleotide excision repair
NMR	Nuclear magnetic resonance spectroscopy
OD_{600}	Optical density at 600 nm
PBS	phosphate buffer saline
PCR	Polymerase Chain Reaction
PCT	Pre-crystallization Test
PDB	Protein Data Bank
PEG	poly ethylene glycol
PES	polypropylene serum (filter membrane)
Pfam	prorein family
Pfu	*Pyrococcus furiosus*
Phe (F)	phenylalanine
pI	isoelectric Point
PNP	purine nudeoside phosphate
Pro	promoter
Pro (P)	proline
r.m.s.d	Root-Mean-Square Deviation
RNA	ribonucleic acid
RONN	Regional Order Neuronal Network
RSC	Royal Society of Chemistry
rpm	Round per minute
SD	Standard deviation
SAD	Single Wavelength Anomalous diffraction

SAM	S-adenosyl-L-methionine
SDS-PAGE	sodium dodecyl sulfate – polyacrylamide gel electrophoresis
SeMet	selenomethionine
Ser (S)	serine
S.aureus	*Staphylococcus Aureus*
SIR	Single Isomorphous Replacement
SRS	Synchrotron Radiation Source, Daresbury Laboratory
Sso (SSO)	*Sulfolobus solfataricus*
SSPF	Scottish Structural Proteomic Facility
Ter	Terminator
TEV	Tobacco Etch Virus
Thr (T)	Threonine
TLS	Translation, libration and screw rotation
Tris	tris- (hydroxymethyl) aminomethane (buffer)
Trp (W)	Tryptophan
Tyr (Y)	Tyrosine
UV	Ultra Violet
Val (V)	valine
VDW	Van der Waals
Vm	volume of Uni cell

Chapter 1

"Introduction"

1.1 Bacterial infections and Methicillin-resistant *Staphylococcus aureus.*

1.1.1 Bacterial infections

Infectious diseases are one of the leading causes of death in both developed and underdeveloped countries. People with depressed immune system (e.g. breast feeding mothers and their babies) are predisposed to *staphylococcal* infections, such infections are commonly seen in hospitals and also a main causes of death (Bovill and Weir 1994; McGahee and Lowy 2000).

Staphylococci are a Gram-positive spherical bacterium that usually appears as "clusters resembling grapes" in electron microscope images (Song, Wachi et al. 1987; Peacock, de Silva et al. 2001). The bacterium is a common commensal infection of human beings and is usually carried in the nose or on the skin of otherwise healthy people (Keane and Cafferkey 1983; Berman, Schaefler et al. 1986). In 1884, two pigmented colony types of *Staphylococci* were described and both of them were named: *Staphylococcus epidermidis* and *Staphylococcus aureus* (Peromet, Schoutens et al. 1973; 1982). Over 20 species of *Staphylococcus* have been reported and described (Farr 1999), however only *S. epidermidis* and *S. aureus* normally infect humans (Karanas, Bogdan et al. 2000). *S. epidermidis* normally inhabits human skin while *S. aureus* usually found both on nasal mucosa and skin of healthy people. It also enters the body through wounds in the skin and cause systemic or blood infections (Daum 1998; Feder 2000; 2001).
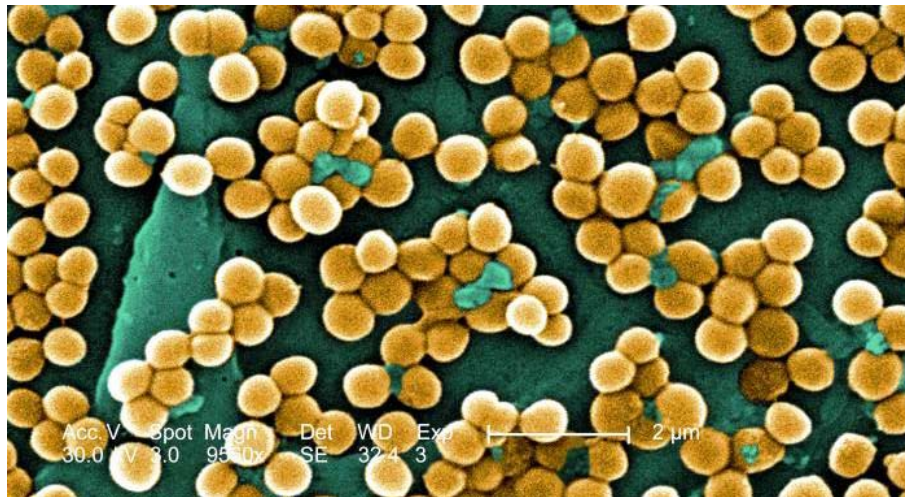
FIGURE 1.1: Scanning electron micrograph (SEM) of *S. aureus* bacteria. Magnified 9560x. (CDC/ Janice Haney Carr/ Jeff Hageman, M.H.S.)

S. aureus infection commonly results in skin diseases, styes, mastitis, neonatal infections and endocarditis (heart disease) (Lye, Leong et al. 1993; Frank, Marcinak et al. 2002). *S. aureus* is considered as a major cause of both "community-acquired" and "hospital-acquired" infections. Hospital-acquired refers to infections of wounds, surgical scars medical materials or devices such as catheters (Hone and Keane 1974; Okumura, Muraishi et al. 1993; Zaoutis, Toltzis et al. 2006).

FIGURE 1.2: Typical skin diseases caused by *S. aureus*. (Pictures taken from inernet).

About 20% to 25% of the population is always colonized with *S. aureus* on the skin or the nose (Karanas, Bogdan et al. 2000; Chen, Su et al. 2007). They are called "carriers" (when bacteria are present, but not causing any infection). A further 65% are intermittent carriers, and only 15% - 20% people never carry this organism (Peacock, de Silva et al. 2001). Some studies imply that the carriage of bacteria is one of the main risk factors for invasive infection (Martinez-Aguilar, Hammerman et al. 2003; Stankovic and Mahajan 2006). Healthy individuals (non-carriers) have a low risk of acquiring *S. aureus* invasive infection. Patients who have had surgery have the highest infection rate (Foster 2004; Lindsay and Holden 2004).

1.1.2 Methicillin-resistant *Staphylococcus aureus* (MRSA)

Before mid-1940's, death from bacteria infections were quite common, especially with *S. aureus,* which had a mortality rate up to 80% (Mitsuda 2002). Before the introduction of antibiotics in the 1940s, *S. aureus* was responsible for most hospital infections, primarily pneumonias (Bovill and Weir 1994; Graham 2002). At the beginning of the use of antibiotics (penicillin), all *S. aureus* infections were sensitive to penicillin (Panzaru, Gotia et al. 2002). However, antibiotic resistance developed in some *S. aureus* strains and other organisms within a very short time (Kanra, Caglar et al. 1985). As early as the 1950s, penicillin-resistant strains of *S. aureus* had reported for the first time (Rawal 1969; Song, Wachi et al. 1987). Then, methicillin (an analogue of synthetic penicillin) was introduced in 1959 and released onto the market

in 1960 used to treat penicillin-resistant *S. aureus* infections (Hone and Keane 1974; Giamarellou, Papapetropoulou et al. 1981). However, one year later, the United Kingdom first reported that some strains isolated from *S. aureus* had acquired resistance to this new antibiotic (Jovens, 1961). Soon methicillin-resistant *S. aureus* (MRSA) isolates were reported in other countries in Europe, then Australia, United States and some Asian countries (Japan and Vietnam) (Giamarellou, Papapetropoulou et al. 1981; Haley, Hightower et al. 1982; Boyce, White et al. 1983). By 1980, MRSA had spread throughout the world, and most of these MRSA strains were resistant to more than one antibiotic. MRSA, together with other antibiotic-resistant bacteria, cause over 60% of nosocomial infections in both developed and underdeveloped countries (Chang, Hsu et al. 1988; Farr 1999). As a result of the emergence of MRSA, *S. aureus* has re-emerged as a major health problem (Washer and Joffe 2006). MRSA infections now has become a significant issue and a priority task in hospitals worldwide (Branger, Gardye et al. 2003).
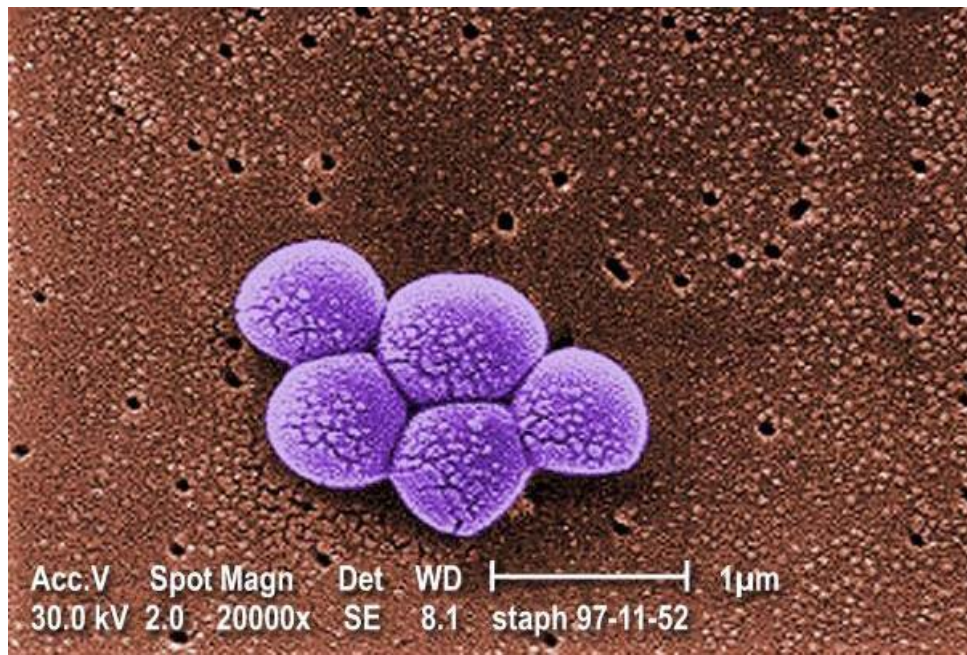
FIGURE 1.3: Scanning Electron Microscopy (SEM) micrograph of Methicillin-resistant *S. aureus* aureus NW15. Magnified 20, 000X. (CDC/Jim Biddle).

Until recently, MRSA infections had been limited mainly to patients in hospitals. However, the rise in "community-acquired" MRSA infections has raised new concerns. Infections are now occurring in healthy, non-hospitalized people who lack physical contact with healthcare personnel or other colonized patients (Herold, Immergluck et al. 1998). These incidents have raised serious concerns about the possibility of wide spread of MRSA outside the healthcare system. If MRSA were to become the major form of *S. aureus*, the treatment of bacterial infections will be much more difficult and expensive (Richet, Benbachir et al. 2003). Some strains are resistant to most regularly used antibiotics, with even vancomycin-resistance known (Milatovic 1986; Walsh, Fisher et al. 1996).

1.2 **Antibiotics resistance**

Antibiotics originally were defined as metabolites of small microbes that inhibit the growth or kill other microorganisms (Romano 1953; Mlynarczyk, Mlynarczyk et al. 1979). Now they refer more generally to drugs used for the treatment of bacterial infections. The first antibiotic, penicillin(Patelski and Hobby 1952; Fletcher 1984), was discovered in 1927 by Alexander Fleming (Hughes 1952; Lachowicz 1960) and first used for medical treatment in 1940s (Steinman 1962; Sabath, Wheeler et al. 1977). Penicillin changed medical care fundamentally, reduced disease and death, and in some cases eliminated the bacterial disease as a cause of death. Although the first antibiotics were natural compounds produced by other microorganisms, these were followed by some semi-synthetic antibiotics such as roxithromycin and clindamycin that derived produced by chemical modification of natural antibiotics (Kayser, Benner et al. 1970; Whipp 1987). Now over 10, 000 antibiotics have been characterized and synthesized and grouped into several different classes, and the most frequently used is the β-lactam class (Sieradzki, Leski et al. 2003; Kareiviene, Pavilonis et al. 2006)
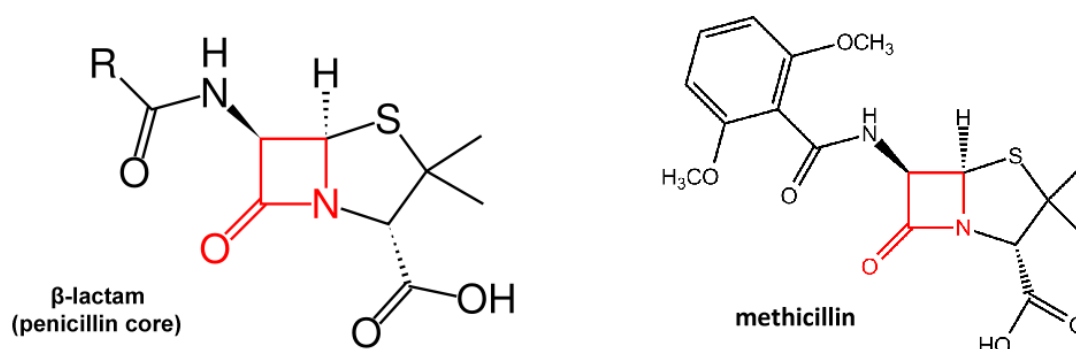
FIGURE 1.4: Molecular structures of penicillin-type antibiotics. β-lactam ring is shown in red.

1.2.1 Mechanism of antibiotic resistance

Antibiotics are natural products that evolved as a method of chemical defense to kill competing organisms. However, the evolution of production of these antibiotics in the bacterium requires co-evolution of resistance (Paulsen, Brown et al. 1996; Borges-Walmsley and Walmsley 2001). The term "antibiotic resistance" refers to the ability of bacteria to survive and grow in the presence of an antibiotic. Resistant bacteria thus continue to harm humans or animals during treatment.

Since antibiotics target the fundamental process in bacteria (Mlynarczyk, Mlynarczyk et al. 1979; Higashi, Wakabayashi et al. 1999) usually leading to cell death, evolutionary pressure thus rapidly selects drug resistant mutants. Antibiotic resistance is therefore essentially unavoidable and several common resistance mechanisms have evolved. The four main categories of antibiotic resistance mechanisms are: Modification to inactivate the drug; Efflux pumps to remove drugs; Cell wall changes to reduce drug entry and mutation of the target to reduce the drug inhibition (Whipp 1987; Ramage, Bachmann et al. 2002; Poole 2004).
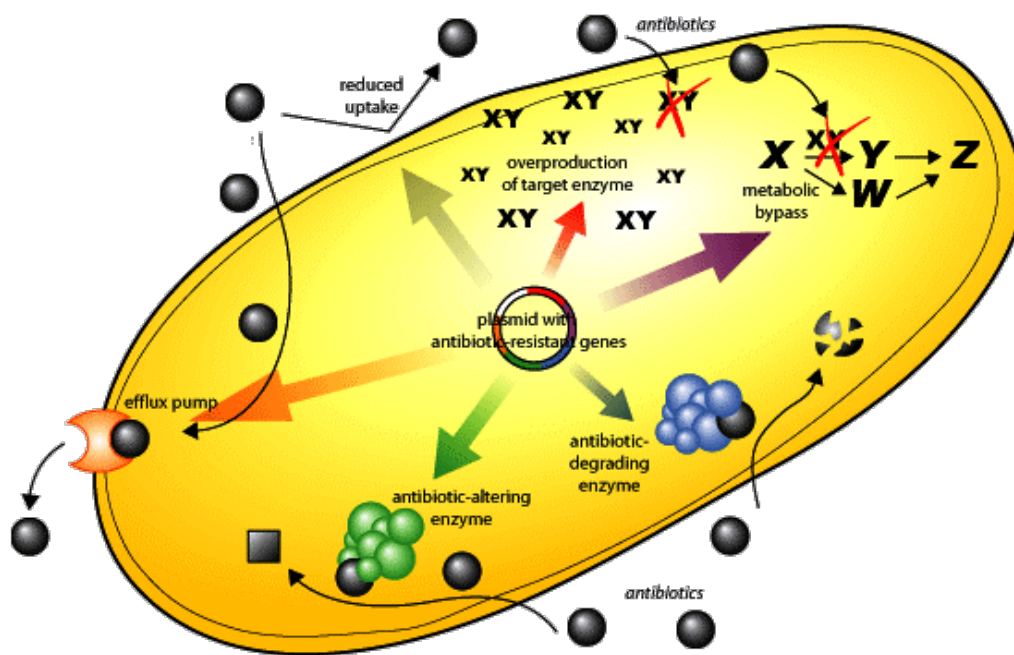
FIGURE 1.5: Main mechanisms of antibiotics resistance. Antibiotics are shown in grey spheres. Picture taken from The Science Creative Quarterly (Wilcox, Sara, 2004).

1.2.2 Chemical modification of the drug

All β-lactam antibiotics have a similar mechanism; they inhibit the formation of the cell wall by interrupting the peptidoglycan biosynthesis. (Powledge 2004; Xiao and Yao 2004). The β-lactam binds to penicillin-binding proteins (PBPs) in the cell wall of Gram-positive and Gram-negative bacteria, inhibiting them by forming covalent bonds with the active site residue (serine) (Katayama, Zhang et al. 2003; Poole 2004). Without PBPs, the transpeptidation reaction is prevented, and the peptidoglycan biosynthesis halts (Spratt and Cromie 1988). The β-lactam ring is the active group of these β-lactam class (penicillin-type) antibiotics. The β-lactamase enzyme hydrolyzes the β-lactam ring moiety breaking it open. Losing the ring conformation of β-lactam,

means the antibiotic is then unable to bind PBPs, and no longer inhibits cell wall biosynthesis (Massova and Mobashery 1998).

For some non β-lactam class antibiotics such as the aminoglycoside class (usually comprised of an amino group and a sugar group) (Crabtree, Pelletier et al. 1999), the antibiotic is covalently modified with moieties that change its function. Resistant bacteria express aminoglycoside-modifying enzymes that can add additional groups such as PO_3^{2-}, AMP or acyl group to the target, changing or reducing its affinity for RNA and thus its effectiveness (Shaw, Rather et al. 1993) (FIGURE 1.6).
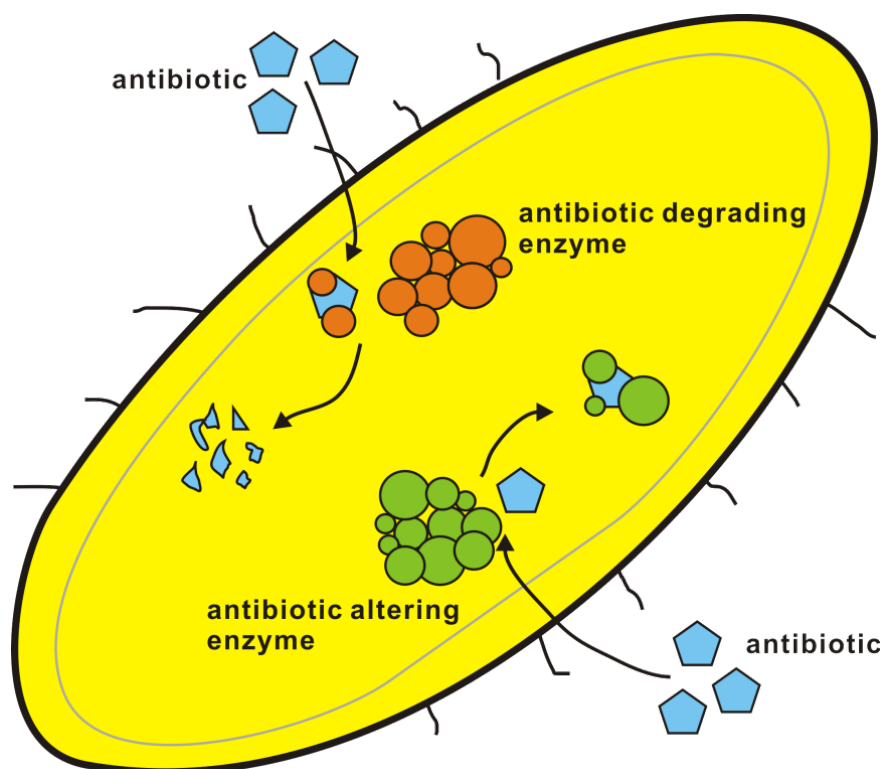
FIGURE 1.6: Chemical modification of the drug in cells. The conformation of antibiotics were changed by enzymes which expressed by antibiotic resistance gene in the cell. Then the antibiotics lose the activity to inhibit or kill the bacteria. Picture modified from The Science Creative Quarterly. (Yim, 2009)

1.2.3 Efflux pumps

The mechanism of efflux pumps is employed by both gram-positive and gram-negative bacteria. Efflux pumps can specifically recognize and pump out the antibiotic, lowering the concentration of the drug in the cell (Paulsen, Brown et al. 1996). By pumping the antibiotic out of the cell at a faster rate than it can diffuse in, the concentration of the antibiotic is remains below the effective level (Walsh 2000). Most of these pumps are trans-membrane proteins that mediate the expulsion of antibiotics and solvents from the cell (Levy 1992). Efflux pumps are a common self-protection mechanism by antibiotic producers (Kaatz 2002) (FIGURE 1.7).
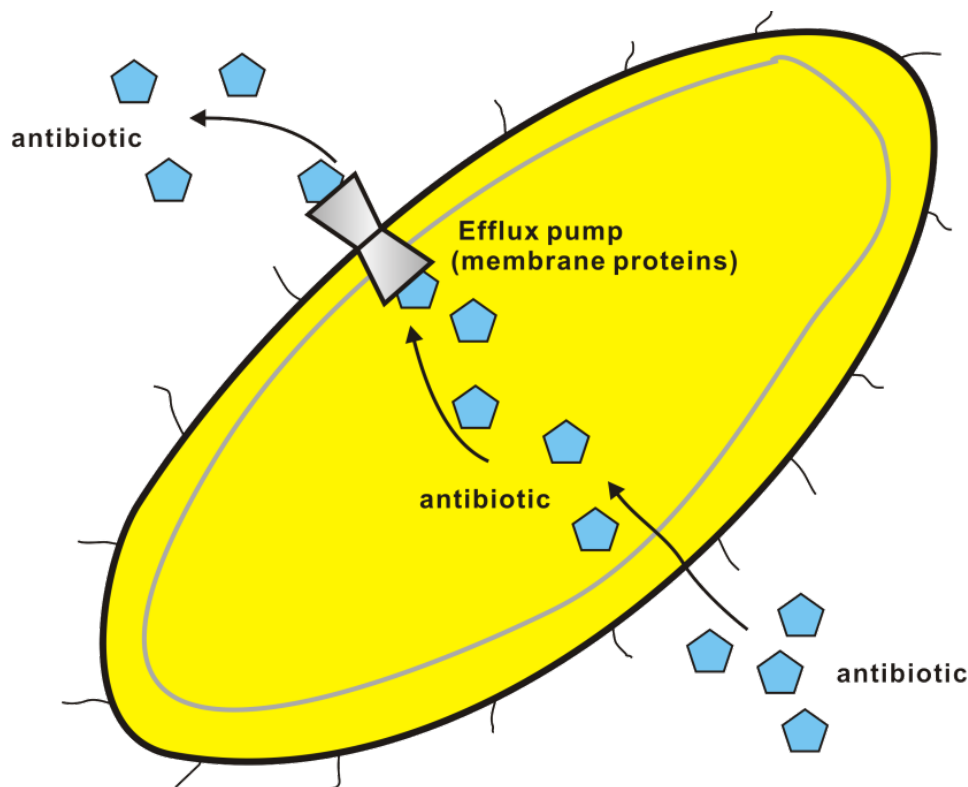
FIGURE 1.7: Efflux pumps mechanism in the cell. The efflux pumps are consisted by several membrane proteins. They keep pumping out the antibiotics out of the cell that the concentrations of antibiotics never get high enough to have its effective. Picture modified from The Science Creative Quarterly. (Yim, 2009)

1.2.4 The cell wall impermeability

The hydrophobic cell wall/outer membrane of bacterium cells is an important self-defense mechanism (Sieradzki and Tomasz 1997). The cell walls have selective permeability, meaning that they allow only certain molecules to pass through whilst stopping others. The lipid bilayer serves to slow the passage of antibiotics into the cell (Viriasov and Perelygin 1984; Urisu, Rahman et al. 2005). The permeability can be changed by expressing different proteins or altering the amount of the certain proteins (Asaoka, Yoshida et al. 1992; Dionne, Cain et al. 1996). In addition, recent studies have shown that cell wall/outer membrane impermeability often occurs in combination with other mechanisms such as efflux pumps, thus conferring the drug resistance (Gao, Laval et al. 2003).
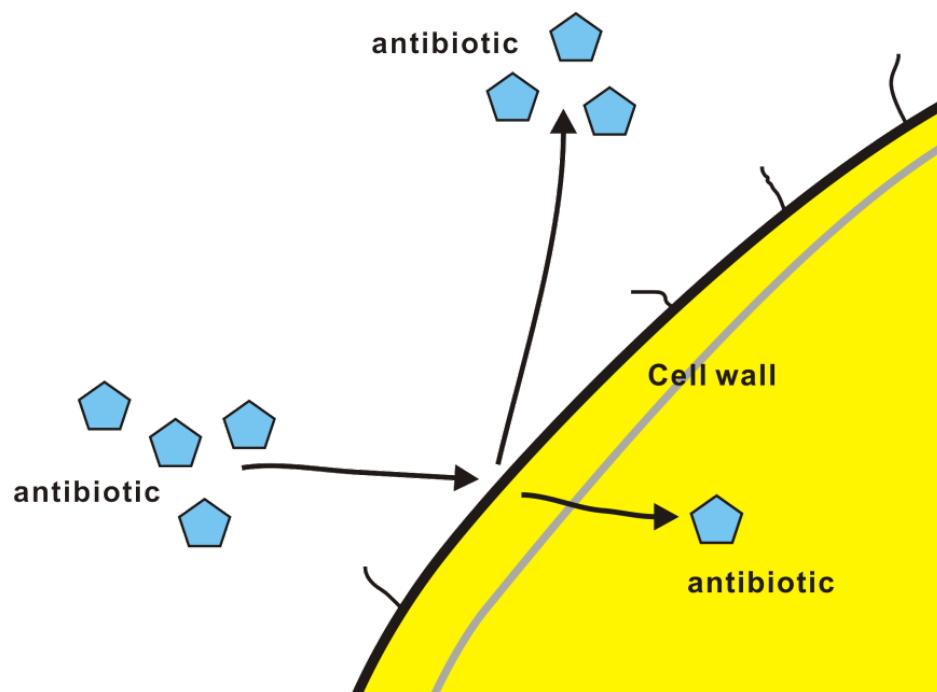
FIGURE 1.8: Cell wall/outer membrane impermeability mechanism in the cell. Picture modified from The Science Creative Quarterly (Yim, 2009).

1.2.5 Mutation of the drug target

Antibiotics target protein structure can be modified or mutated to relieve drug inhibition (Spratt 1994; Walsh 2000). The basis of the methicillin resistance in *S. aureus* is the acquisition of methicillin resistance gene (mecA), this gene can encode a protein which is called "methicillin-resistant penicillin-binding protein". This is an altered version of PBP, antibiotics such as methicillin can still bind to this PBP but with a much lower affinity (Song, Wachi et al. 1987; Chu, Plattner et al. 1996).

1.2.6 Multi-drug resistance

The spread of antibiotic resistance is driven by natural selective pressures placed on the bacterium by the continued use of antibiotics. It is also promoted by the promiscuity of gene transfer between bacteria (Levy 1998). Vancomycin was first introduced in 1958 and no clinical isolates of vancomycin-resistant bacteria observed until 29 years later (Rahman 1998). Vancomycin is still used in the clinic and is considered as the ultimate treatment of otherwise drug-resistant gram-positive bacterial infections (Lundstrom and Sobel 2000).

29 years are actually a long time as clinically significant resistance usually appears within only months to a few years after the introduction of a new antibiotic (Davies 1996), especially when it only targets one gene product. It is believed that the unusual time delay for vancomycin resistance is almost certainly due to the complexity of its resistance mechanisms, requiring the action of five gene products (Walsh, Fisher et al. 1996) and its relatively restricted usage.

The development of drug resistance in bacteria occurs by two main mechanisms, mutation of genes in chromosome followed by resistant strains selection and acquisition of resistance genes by harboring mobile elements (plasmids, transposons) (Arthur and Courvalin 1993; Davies 1994) (transposons are DNA sequences that can move from one location to another location with the genome). The methicillin resistance gene (*mecA*) in MRSA is usually carried by a plasmid known as "*S. aureus* cassette chromosome *mec* (SCC*mec*)". These plasmids replicate within the cell and subsequently spread to other cells, strains and even across species (Davies 1994). Transposons can excise themselves from one location to another, integrate into new location in a new bacterium, so antibiotic resistance genes encoded within transposons move between plasmids and genome (Tolmasky 2000; Scott 2002). Mobile genetic elements can accumulate more than one set of resistance genes from more than one organism; as a result, multi-drug resistant bacteria can emerge and transfer resistance to other species (Burrus, Pavlovic et al. 2002; Pembroke, MacMahon et al. 2002).
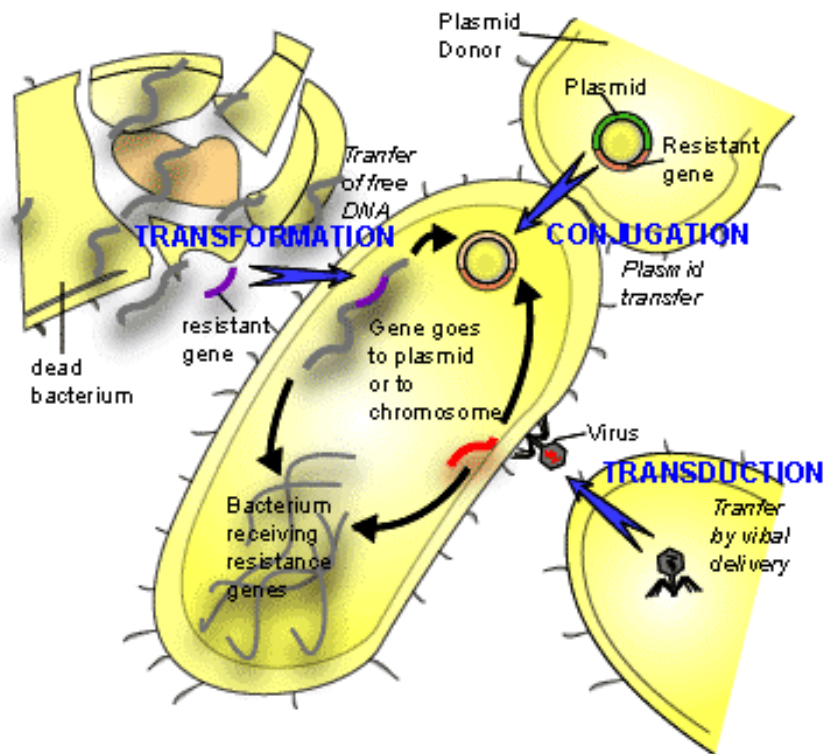
FIGURE 1.9: Horizontal transfer of the drug-resistant gene among bacteria. The resistant gene can be passed around bacteria strains by transformation, conjugation and transduction. Picture modified from The Science Creative Quarterly (Yim, 2009).

1.3 Genetics and Proteomics feature of resistance on *S. aureus*

1.3.1 MRSA252 and MSSA476 strains

To help to better understand the pathology of these disease-causing *S. aureus* bacteria, comparison of the proteomes of these MRSA and MSSA strains was carried out by the lab of Dr P. Coote (University of St Andrews) to identify proteins that could be important to pathogenesis, such proteins could lead to the identification of new drug targets in MRSA.

The genomes of the two disease-causing *S. aureus* strains have been sequenced and

annotated by The Sanger Institute Pathogen Sequencing Unit recently (Enright, Day et al. 2000). These two strains were clinically isolated, one strain represents the "hospital-acquired epidemic methicillin-resistant *S. aureus* (HA-EMRSA)" EMRSA-16 clone (MRSA252), which is found worldwide and is clinically prevalent lineage causing 50% MRSA infections in U.K (Johnson, Aucken et al. 2001).

MRSA252 was first isolated from a female patient in 1997 after a small-scale outbreak in a hospital (Johnson, Aucken et al. 2001; Moore and Lindsay 2002). MRSA252 is known to be resistant to methicillin, penicillin, erythromycin and ciprofloxacin (Johnson, Aucken et al. 2001).

The community-acquired MSSA476 was chosen for comparison, it can cause severe invasive disease in some immunocompetent children outside hospital settings. MSSA476 strain was isolated from a 9-year old boy in 1998 with systemic infection (Enright, Day et al. 2000). This strain is resistant to fusidic acid and penicillin, sensitive to most frequently used antibiotics, including ciprofloxacin, rifampicin, tetracycline, trimethoprim, erythromycin, gentamicin, amikacin, and methicillin. A comparative-genomics-method has been applied to *S. aureus* genomes to identify the key regions that might be responsible for virulence and antibiotic resistance (Holden, Feil et al. 2004).
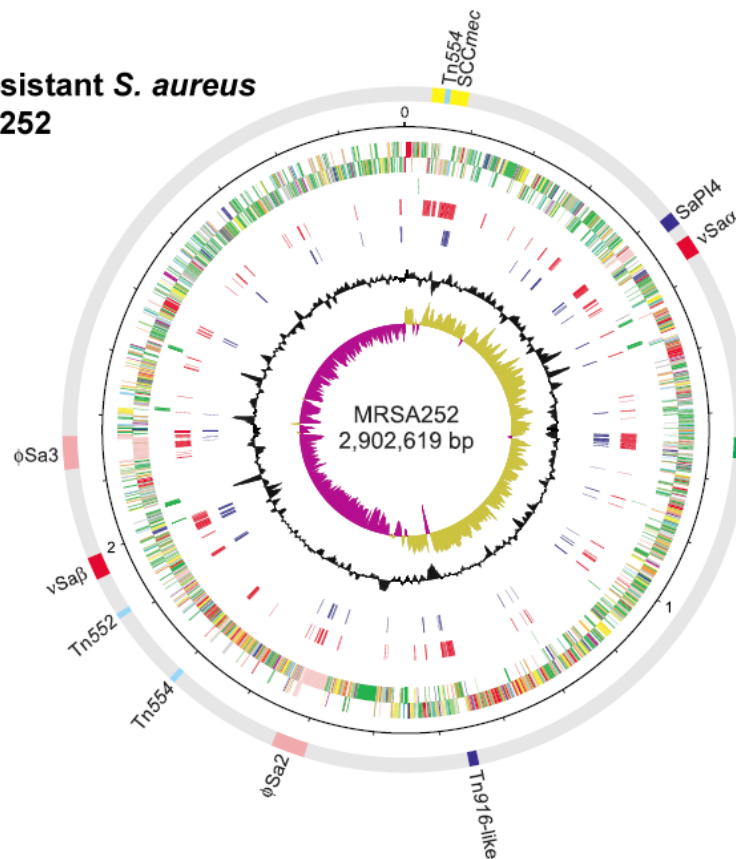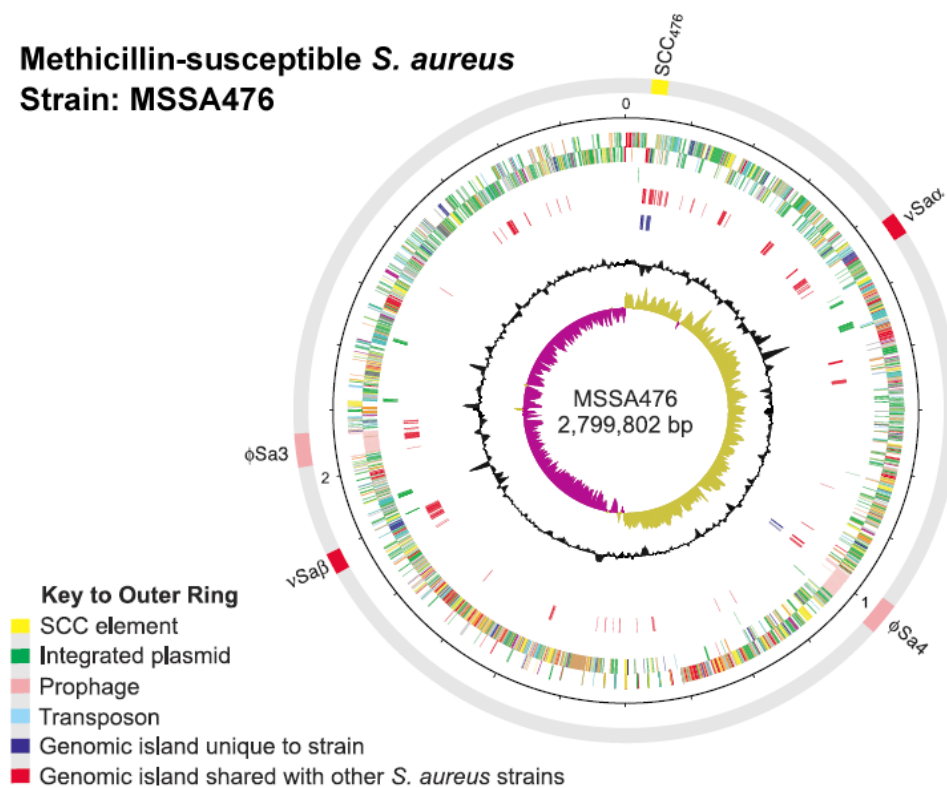
FIGURE 1.10: Circular diagrams of MSSA476 and MRSA252 chromosomes. Picture taken from (Holden, Feil et al. 2004)

1.3.2 Differences between MRSA252 and MSSA476

The MRSA252 chromosome has a size of 2,902,619 bp and contains 2,671 predicted protein-coding sequences (CDSs). While the MSSA476 is 2,799,802 bp in size and has 2,565 genes. Comparisons between these two chromosomes indicate that they are collinear with each other and also similar to those published *S. aureus* isolates such as MW2, Mu50, and N315 (Baba, Takeuchi et al. 2002; Feil, Cooper et al. 2003). The MRSA252 and MSSA476 genome sequences both have a common conserved core region. However their accessory genetic elements show some differences. About 6% of the genome is novel, including several unique genetic elements that are considered as critical for antibiotic resistance. Pseudogenes are known to be a regular feature of bacterial genomes and are found within the genomes of bacterial pathogens (Ross 1985) in particularly high numbers. Although MSSA476 is sensitive to methicillin, it contains a novel Staphylococcal chromosomal cassette (SCC) *mec*-like element. The integrated site of this element is same to SCC*mec* in MRSA252. However, this genetic element encodes a different protein compared with MRSA252.

	MRSA252	MSSA476
Length of sequence (bp)	2,902,619	2,799,802
G + C content	32.81	32.85
CDS count	2671	2565
Average length	896	882
GC percentage	33.52	33.59
tRNA	60	60
rRNA	16	19
5S	6	7
16S	5	6
23S	5	6
Stable RNAs	25	25
Pseudogenes	66	20
Transposons	3	0
SCC elemets	Type II SCCmec	SCC476

TABLE 1.1: Summary of the general features of MRSA252 and MSSA476 genomes.

Beyond the genetic diversity, the proteomics differences of these two strains may be important. We therefore reasoned that the MRSA252 up-regulated proteins may be particular important for pathogenicity with the potential for new drug targets embarked on the structural characterization. 2-Dimensional sodium dodecyl sulfate - polyacrylamide gel electrophoresis (SDS-PAGE) techniques were employed in identification of the differential expression level. Gels were silver-stained and proteins that were expressed differentially amount between the two strains were identified by eye (work of Dr. P. Coote (University of St Andrews)).

An initial 30 differentially expressed proteins were identified by Dr P. Coote (University of St-Andrews) as being significantly up regulated or down regulated. Then these potential targets were examined by peptide mass spectrometry (University of St-Andrews) by excised the target protein spots from the gels. An Investigator Progest Digestion Robot (Genomic Solutions) was using to perform these examinations. The web-based Mascot Search Engine (MSDB) (http://www.matrixscience.com/search_form_select.html) was used for peptide mass matching search.
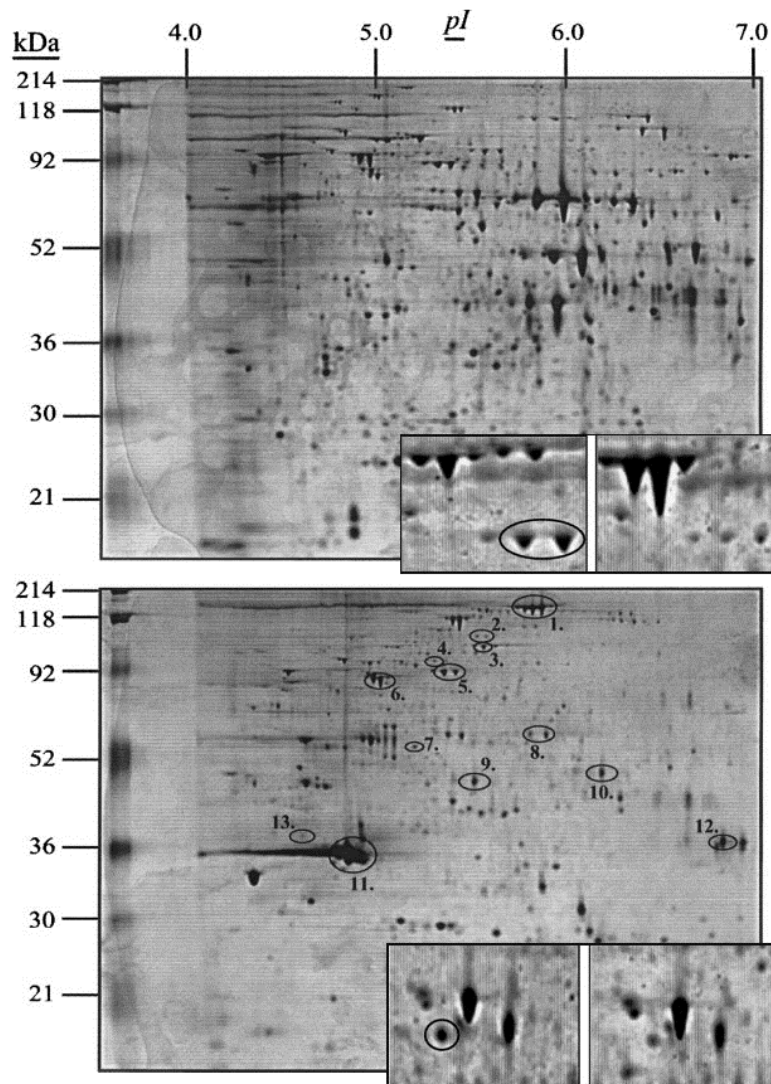
FIGURE 1.11: Result sample of silver stained 2D SDS-Page gel comparison of the proteomes of *S. aureus* MRSA252 and MSSA476.

After the identification of the potential targets, BLAST (Altschul, Madden et al. 1997) was used to determine that there was no protein structure deposited in the Protein Data Bank (PDB) with sequence homology (>70%). The sequences of the target proteins were assessed for suitability for structural study using some bioinformatics tools, such as the Regional Order Neural Network (RONN) application. RONN identifies disordered regions, which interfere with protein crystallization (Yang,

Thomson et al. 2005). After small-scale expression and solubility test, three proteins were selected for further structural study.
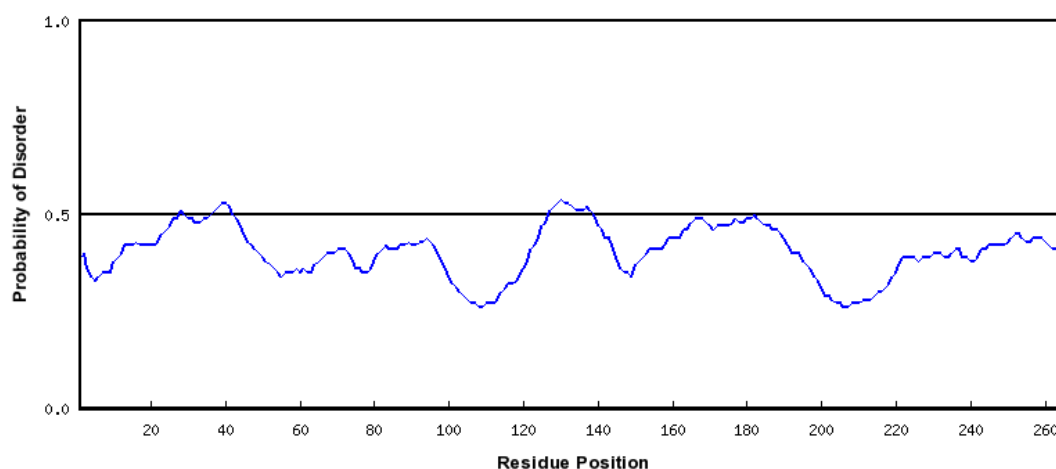
FIGURE 1.12: RONN plot of probability of disorder against residue number. The threshold value (0.5) for disorder is indicated. Residues with a probability above 0.5 predicted to be disordered, while those below 0.5 are predicted to order.

Name	Predicted function	Expression level description	Strain
TAG	3-methyladenine DNA glycosylase I	Up-regulated in MSSA476, down-regulated in MRSA252	MSSA476
PFK	1-Phosphofructokinase	Up-regulated in MRSA252 down-regulated in MSSA476	MRSA252
MK	Mevalonate Kinase	Up-regulated in MRSA252 down-regulated in MSSA476	MRSA252

TABLE 1.2: List of the potential drug targets selected from MRSA252 and MSSA476 by differential expression level between the two disease-causing strains.

1.4 Structural biology and Fragments-based drug discovery

1.4.1 Structural biology

Structural biology has been transformed biology over the last few decades, and more

progress is coming. This will be driven by advances in automation of protein expression, characterization, purification, crystallization, crystal mounting, x-ray diffraction, model building and Nuclear magnetic resonance (NMR) spectra interpretation.

X-ray crystallography is the most widely used method to investigate the three-dimensional (3D) structure of the protein. A protein that is essential for growth, survival or antibiotic resistance of a pathogen, is a potential drug target. The high-resolution crystal structure of such a protein can provide valuable information in drug discovery, especially if the structure of the protein contains potential lead inhibitor compounds bound at the active site. Protein complexes with drug can be obtained via either co-crystallization protein with compounds or the soaking method. Crystals can be soaked with individual hits separately or cocktails of up to 10 fragments from a library. The structure of the target protein in complex with the substrates or other compounds can help to identify the key residues that are involved in ligands recognition and catalysis.

The NMR method doesn't require any crystalline materials and works in solution or solid-state. NMR in solution depends on obtaining a sharp spectrum which in turn, depends on the rate of protein tumbling (Amano 2004). Large molecules which tumble slowly give broad weak band spectra which are difficult to interpret (Olofsson, Ippel et al. 2004).

1.4.2 Fragment-based drug discovery

Target proteins can be screened against compounds in high-throughput screening (HTS) (selection). The conceptual basis of fragment screening is that instead using large numbers of complex molecules, screening small amounts of less complex molecules increase the probability of potential drug hits. The term high-throughput screening (HTS) refers to that using modern techniques, such as automatic robotics, data processing and analysis, sensitive detectors and computer modeling. Fragments discovery is thought currently more likely to give better potential drug leads.
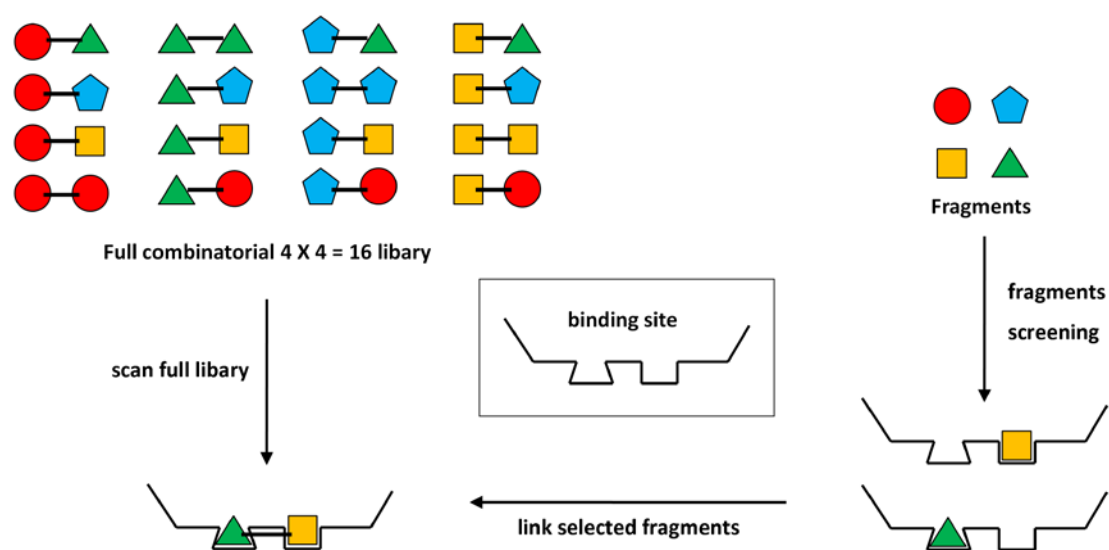
FIGURE 1.13: Fragments screening and normal compounds screening.

The thermal shift measures the change of the unfolding temperature of protein/fragments complex. Fragments that bind to the protein stabilize it. This technique is capable of high throughput selection (Nettleship, Brown et al. 2008).

The potential hits from the thermal shift assay can be further verified by either nuclear magnetic resonance (NMR) spectroscopy or isothermal titration calorimetry (ITC) or biochemical assay. Results of fragment identification provide a rational basis and starting point for further drug design and also contribute to the understanding the interaction between protein and ligands.

Targeted enzyme

Protein crystallization

X-Ray crystallography

Thermal shift assay   **Mutational study**

NMR, ITC   **Enzyme kinetics**

Virtual design & docking

Synthesis

Potential drug-like leads
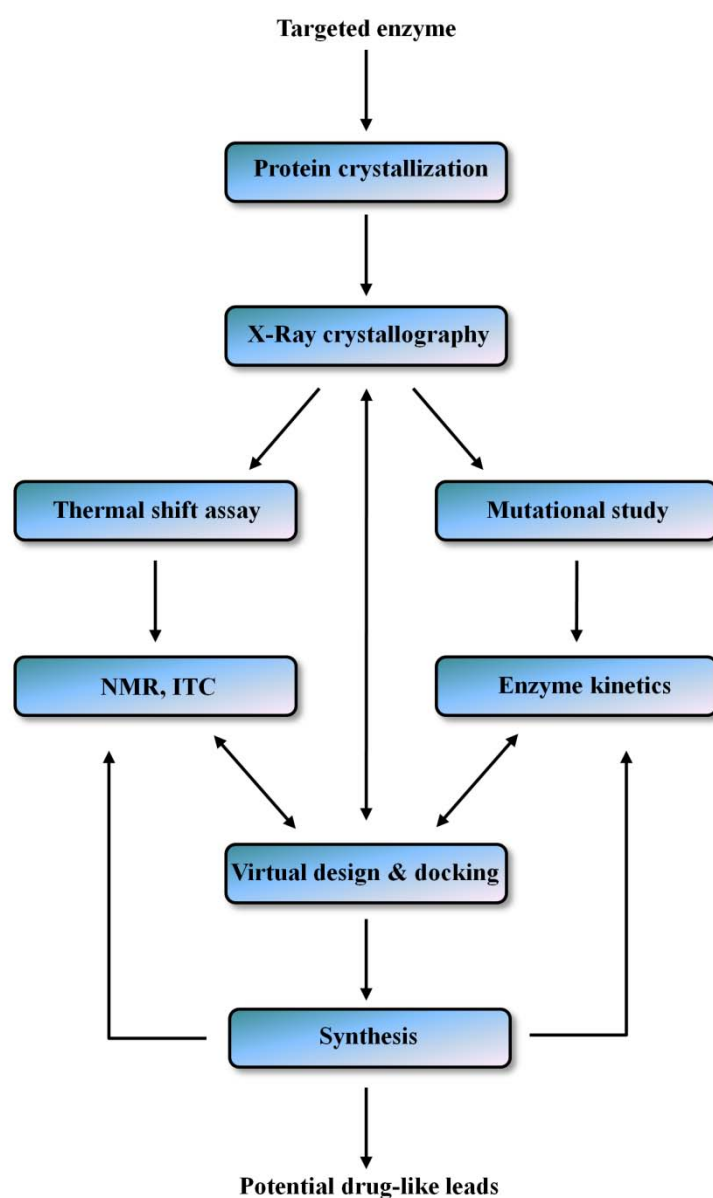
FIGURE 1.14: Schematic view of fragments-based drug discovery approach.

Chapter 2

"Structural studies of 3-Methyladenine DNA Glycosylase I from Methicillin-susceptible *Staphylococcus aureus* (MSSA), a member of the HhH DNA glycosylases family"

2.1 <u>Summary</u>

3-Methyladenine DNA glycosylase I (TAG) from *S. aureus* was successfully expressed in C43 (DE3) cells in Luria Broth (LB) culture medium and purified by a two-step purification approach using nickel-affinity column and size exclusion column. The identity and integrity of the protein was determined by mass spectrometry and SDS-PAGE. Native crystals of TAG were obtained from a Hampton Classics Screen [0.1M Tris-HCl pH 8.5, 2 M ammonium sulphate] using the sitting drop vapour diffusion method. The native structure was determined to 1.70 Å and solved using single-wavelength anomalous diffraction (SAD) method. The structure in complex with 3-methyladenine was obtained and solved using molecular replacement (MR) method. Fluorescence spectroscopy was used to determine the protein activity. A thermodynamic analysis using a fluorescence-based method (thermo-fluor) was carried out to investigate binding interactions of several ligands to TAG. The high resolution crystal structures of TAG and thermodynamic data contribute to the overall understanding of the interaction between TAG and its substrate. These findings show that TAG specificity binds 3-MeA rather than the normal base adenine.

2.2 Introduction

2.2.1 DNA damage and repair

The genetic information encoded within the DNA sequence and the structure of DNA is the basis of all life (except virus). However, the genetic information carrier, DNA, is constantly exposed to various kinds of challenge (Lindahl 1993). A variety of intracellular reactions and environmental compounds can induce unwanted chemical modification in the DNA bases.

Chemical reactions such as alkylation, oxidation or radioactive processes are all known (Friedberg, Aguilera et al. 2006). Moreover, DNA damage also occurs by the inherent chemical instability of nucleic acids during the replication process. If such changes are left uncorrected, the resulting lesion can cause genetic mutations or stalling of DNA normal replication which leading to cell apoptosis (Memisoglu and Samson 2000; Fromme and Verdine 2004). To defend against DNA damage, all organisms possess a series of self-defense mechanisms to repair the chemical change in their DNA and maintain the completeness, viability and stability of the genomic. (FIGURE 2.1)
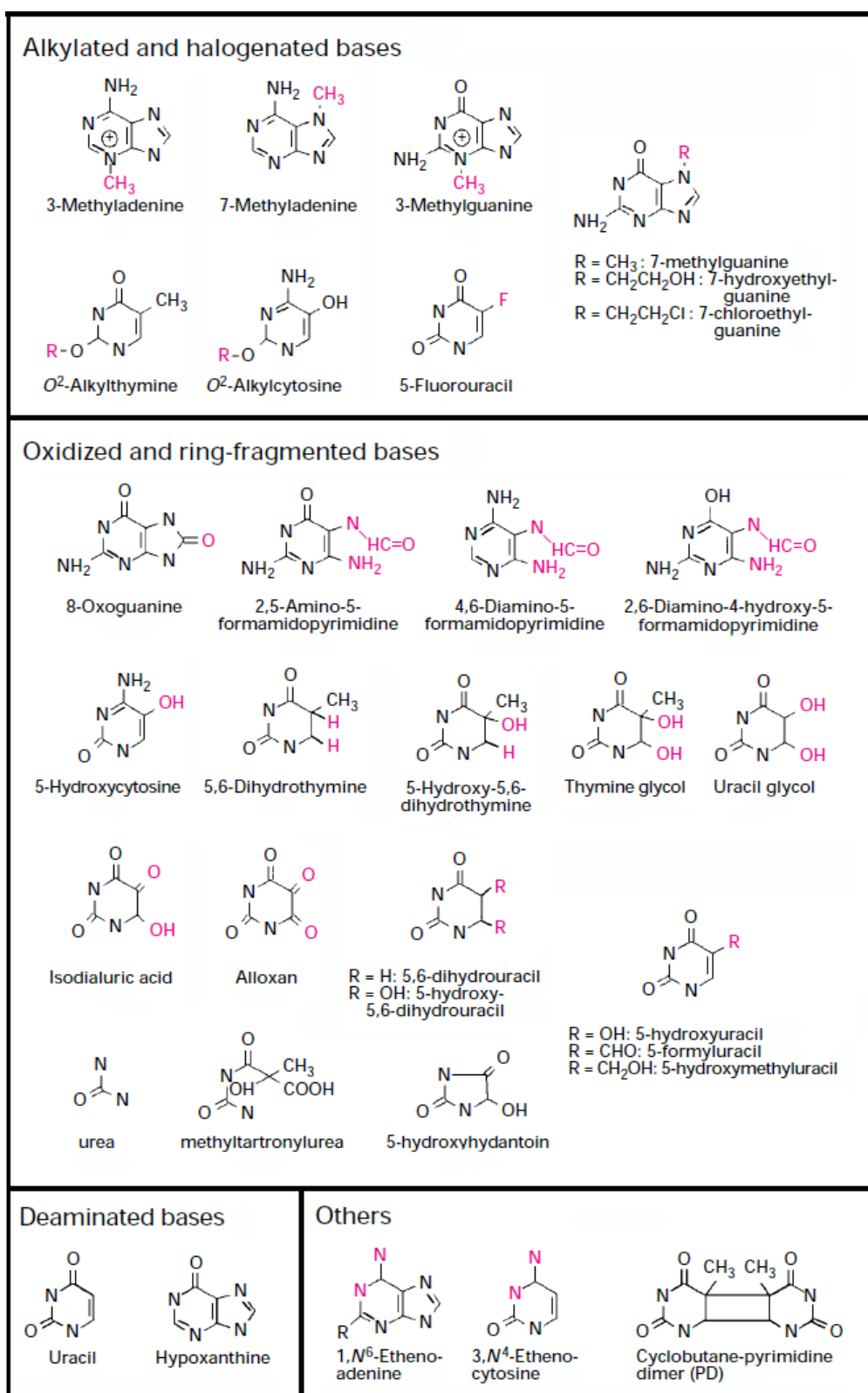
FIGURE 2.1: Chemical structure of typic al damaged DNA bases. Chemical groups not found in the normal DNA bases are shown in red label. Picture modified from (Krokan, Standal et al. 1997)

The organisms have evolved a variety of strategies for protecting their own genetic information since life began. The Nucleotide Excision Repair (NER) and Base Excision Repair (BER) are the two critical DNA repair pathways for recognizing and excising damaged DNA lesions (Fujii and Yamagata 2000; Krokan, Nilsen et al. 2000). The NER pathway is a complicated DNA repair system (Ackerman and Iakoucheva 2000; Dianov, Souza-Pinto et al. 2001), coordinating at least 20 different proteins to remove DNA adducts (Wood 1997), and about 30 other genes (Krokan, Standal et al. 1997) to complete repair. The NER pathway is an alternative DNA repair pathway for the excision of DNA damage induced by alkylation or oxidative as a backup system of the BER pathway (Samson, Thomale et al. 1988; Reardon, Bessho et al. 1997). (FIGURE 2.2)
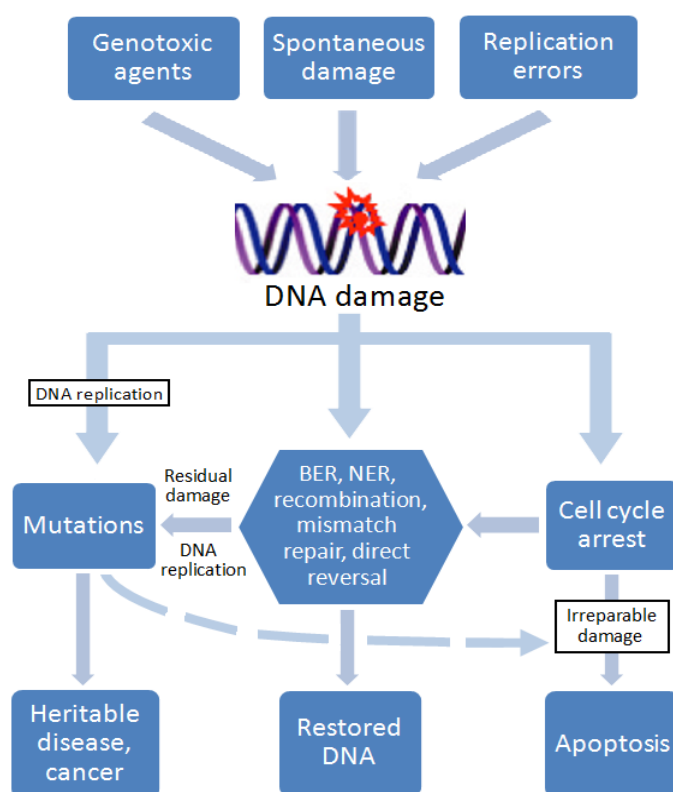
FIGURE 2.2: Schematic representation of cellular mechanisms evolved in the maintenance of the genome. Picture modified from (Krokan, Standal et al. 1997)

2.2.2 DNA glycosylases in Base Excision Repair pathway

The BER pathway is considered as the most significant self-defense mechanism and is triggered by the detection and then removal of damaged or abnormal bases such as radiated, alkylated, oxidized bases and even bases missing purine/pyrimidine (bases) (Meira, Burgis et al. 2005; Allen, Johnson et al. 2006). The initial step is carried out by different DNA glycosylases such as 3-MeA DNA glycosylase I or II (Bjelland and Seeberg 1996; O'Rourke, Chevalier et al. 2000). These DNA glycosylases remove different types of chemically modified or damaged bases by cleaving of the N-glycosidic bond between a base and the deoxyribose moieties of the nucleotide residue.

Once the abnormal base such as 3-MeA is recognized and removed by DNA glycosylases, the left remaining apyrimidinic/apurinc (AP) -site is then removed by AP-lyase or AP-endonuclease, which cleaves the DNA strand 3' or 5' to the AP-site, respectively (Korolev 2005). Deoxyribose phosphate residue is cleaved by 3'-phosphodiesterase and 5'- phosphodiesterase (Zharkov 2008). The resulting gap is filled by DNA polymerases. The DNA strand break is then repaired by either DNA ligase (I or III) at last to restore a normal and undamaged DNA strands (Seeberg, Eide et al. 1995; Baute and Depicker 2008) (FIGURE 2.3).
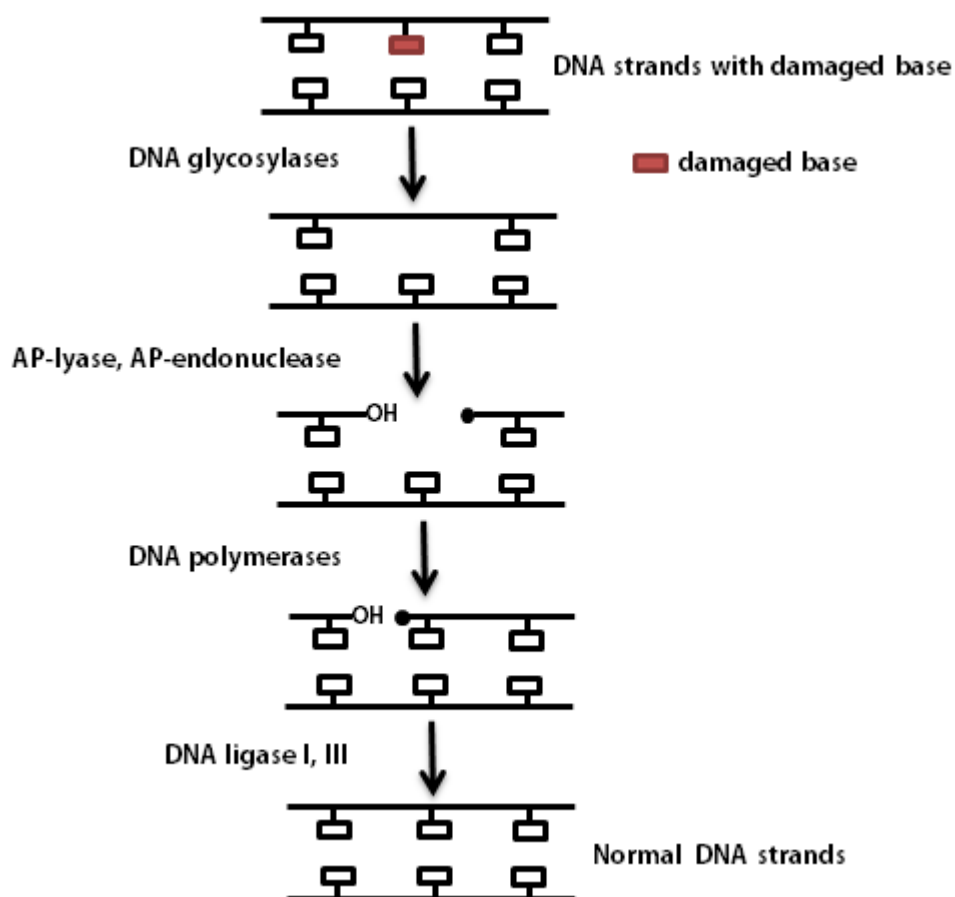
FIGURE 2.3: Diagram of the Base Excision Repair (BER) pathways. Shown above are the repairing steps and main components evolved in the BER pathway. Picture modified from (Memisoglu and Samson 2000)

At least eight different DNA glycosylases have been identified in the first step of the BER pathway (Krokan, Nilsen et al. 2000; Korolev 2005). All the DNA glycosylases could cleave glycosidic bonds of the damaged base, however they have differences in their range of ligand specificity (Seeberg, Eide et al. 1995; Korolev 2005). Most DNA glycosylases remove several structurally different damaged bases while a few of them have very narrow ligand specificities (Bjelland and Seeberg 1996; Korolev 2005). For instance, 3-Methyladenine DNA glycosylase II (AlkA) has the widest ligand specificity of all known DNA glycosylases and it can remove both damaged purines

39

and pyrimidines (Seeberg, Eide et al. 1995; Bjelland and Seeberg 1996). AlkA can remove 3-Methyladenine (3-MeA), 3-Methylguanine (3-MeG), 7-Methylguanine (7-MeG), 7-Methyladenine (7-MeA), O2-alkylcytosine, and O2-alkylthymine (Seeberg, Eide et al. 1995; Bjelland and Seeberg 1996; Hollis, Ichikawa et al. 2000). In contrast to AlkA, 3-Methyladenine DNA glycosylase I (TAG) in *E.Coli* is highly specific for 3-MeA base, although it also removes 3-MeG but with a much lower efficiency (Bjelland, Bjoras et al. 1993). Historically, DNA glycosylases that remove alkylated bases from DNA were called 3-Methyladenine DNA glycosylases, since 3-MeA was the first identified base (Lindahl 1976). Many of these DNA glycosylases have overlapping ligands specificities and they can serve back-up for each other for a more efficient purpose (Ikeda and Seki 2001; Korolev 2005).

2.2.3 The HhH DNA glycosylases family

The crystal structure of *E. Coli* thymine glycol DNA glycosylase (EndoIII) indicated a novel DNA binding motif, which is called the Helix-hairpin-Helix (HhH) motif (Thayer, Ahern et al. 1995). The HhH motif has a length of ~20 amino acids (Doherty, Serpell et al. 1996), consist two α-helices linked by a short hairpin loop which having the coincidental sequences (Phe/Leu)-Pro-Gly-(Ile/Val)-Gly. This motif presents in many DNA-binding proteins such as DNA polymerases and DNA glycosylases (Nash, Bruner et al. 1996). The motif binds DNA in a sequence independent manner (Doherty, Serpell et al. 1996) and it is considered as the key elements that involved in interactions with DNA (Sawaya, Prasad et al. 1997; Rafferty, Ingleston et al. 1998).

At least six different DNA glycosylases have been identified currently are the members of the HhH DNA glycosylase family, and each of them has multiple homologues (Doherty, Serpell et al. 1996; Dodson and Lloyd 2002; Dizdaroglu 2005). Although the sequence identity is low (~10 %) among the HhH DNA glycosylase family members (Drohat, Kwon et al. 2002), they all exhibit the signature HhH motif for DNA-binding. The hairpin loop of the HhH motif exhibits the signature sequence pattern (Phe/Leu)-Pro-Gly-(Ile/Val)-Gly, indicates that these DNA glycosylases may share a common mechanism for DNA-binding (FIGURE 2.4)
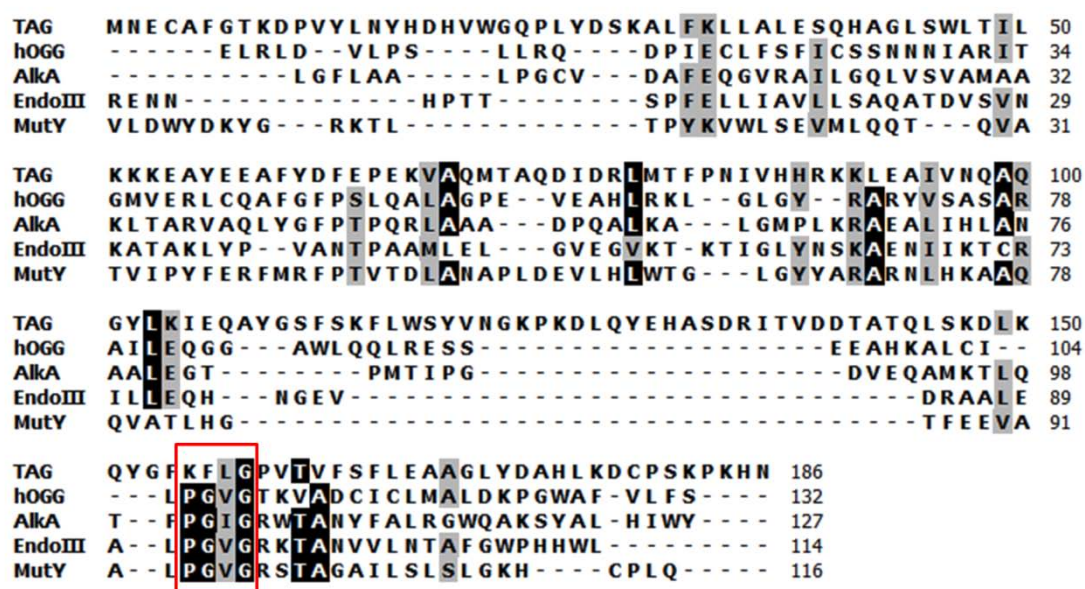
FIGURE 2.4: Sequence alignments of HhH family members. Alignment using BioEdit (Hall 1999) and DALI (Holm and Sander 1993) server. Identical residues in the sequences aligned are highlight in black, residues shaded grey indicate regions of sequence homology. The red box shows the conserved residues from the proposed DNA binding motif (HhH motif). The TAG, hOGG, AlkA, EndoIII and MutY each corresponds to 3-MeA DNA glycosylase I, 3-MeA DNA glycosylase II, thymine glycol DNA glycosylase and adenine-specific mismatch-DNA glycosylases.

Comparative studies on these HhH DNA glycosylases have provided valuable information about enzymatic mechanism and helped identify the critical amino acids

that are essential for DNA and ligand binding such as 3-MeA DNA glycosylase II (AlkA) (Labahn, Scharer et al. 1996; Hollis, Ichikawa et al. 2000). The crystal structure of *E. coli* AlkA in complex with DNA revealed that it used an activated water nucleophile to cleave to adenine mispaired with guanine (Guan, Manuel et al. 1998; Hollis, Ichikawa et al. 2000). This proposed mechanism is similar to adenine-specific mismatch-DNA glycosylases (MutY) (Fromme, Banerjee et al. 2004). Crystal structure of the human 8-oxoguanine DNA glycosylase (Bruner, Norman et al. 2000) also shows a similar DNA-binding mechanism to EndoIII, they both use a catalytic residues Lys for the nucleophile attack (Mol, Kuo et al. 1995; Thayer, Ahern et al. 1995).
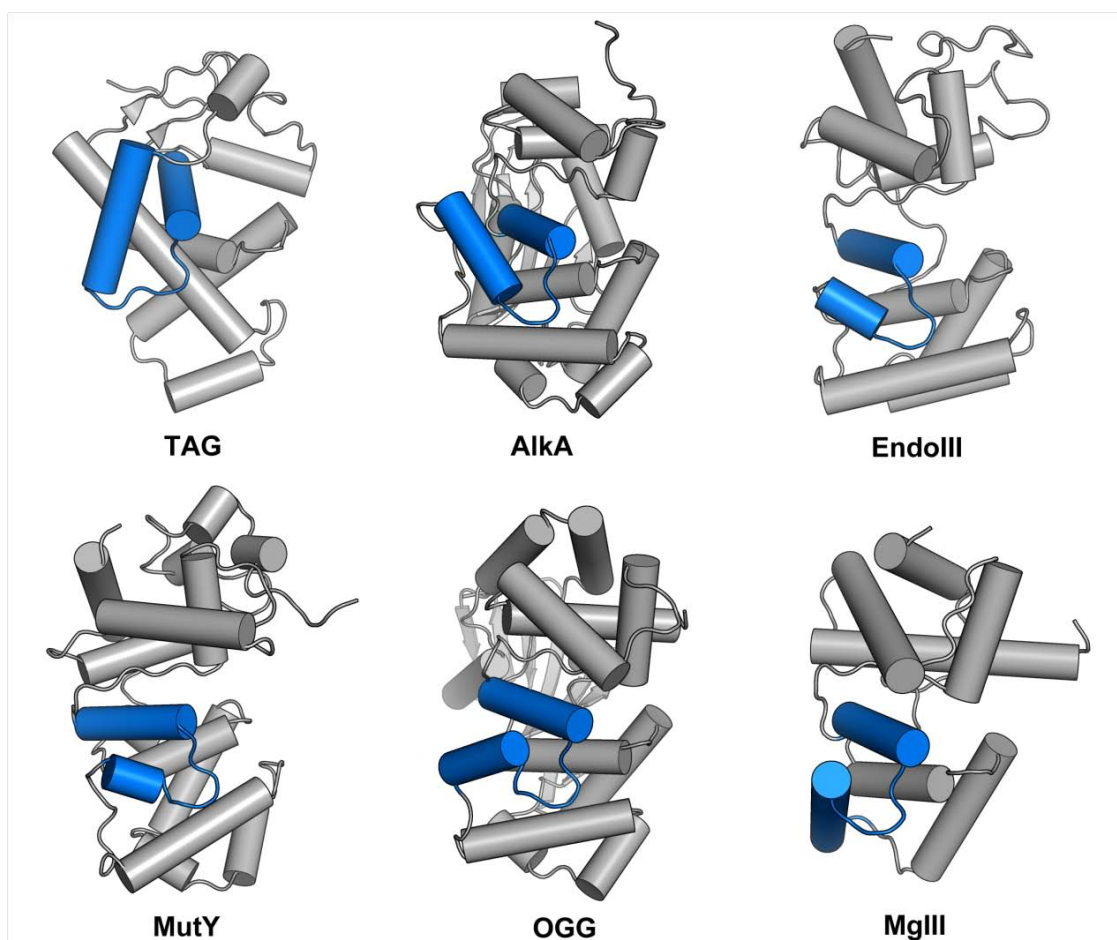
FIGURE 2.5: The HhH motif of DNA glycosylases. Schematic representation of the HhH subfamily DNA glycosylases structures. Helices are shown as grey cylinders and the HhH structure motif are shown in blue.

Enzyme	Source/Gene	References
Alkylbase-DNA glycosylases	*E. Coli* (TAG)	(Drohat, Kwon et al. 2002)
	E. Coli (AlkA)	(Labahn, Scharer et al. 1996)
	H. Pylori (MagIII)	(Eichman, O'Rourke et al. 2003)
Adenine-specific mismatch-DNA glycosylases	*E. Coli* (MutY)	(Guan, Manuel et al. 1998)
DNA glycosylases removing oxidized pyrimidines	*E. Coli* (EndoIII)	(Kuo, McRee et al. 1992)
DNA glycosylases removing oxidized pyrines	*S. Cerevisiae* (OGG)	(Bruner, Norman et al. 2000)

TABLE 2.1: List of some crystal and NMR structures of HhH subfamily of DNA glycosylases.

2.2.4 3-Methyladenine DNA glycosylase I (TAG) from *S. aureus*

Alkylated bases such as 3-MeA, 3-MeG and 7-MeG are cytoxic and mutagenic DNA lesions (Klungland, Fairbairn et al. 1992; Klungland, Bjoras et al. 1994), failure to repair leads to the stalling of regular duplication of DNA (Boiteux, Huisman et al. 1984), leading to more serious problems. Lesion repair begins by enzymatic hydrolysis of the glycosidic bond in DNA (the critical initial step of the BER pathway). The glycosidic bond of alkylated purine bases is usually hydrolyzed by two alkyl purine specific DNA glycosylases, 3-Methyladenine DNA glycosylase I (TAG) (Lindahl 1993) and II (AlkA) (Wyatt, Allan et al. 1999) (FIGURE 2.6).
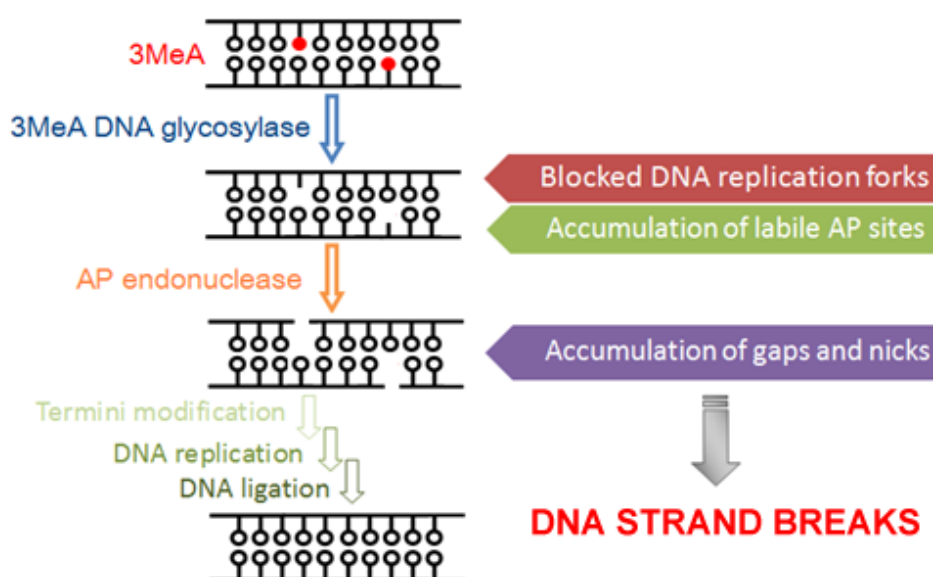
FIGURE 2.6: Schematic representation of BER intermediates results DNA strand breaks. Picture modified from (Memisoglu and Samson 2000)

3-methyladenine DNA glycosylase I (TAG) (E.C 3.2.2.20) is known as one of the

smallest member of the HhH family of DNA glycosylases (~186 residues, Mw: ~21 kDa) and has been shown that have a fairly narrow ligand specificity for the alkylated base, 3-MeA (Drohat, Kwon et al. 2002; Cao, Kwon et al. 2003). TAG shows very low overall protein sequences similarity compared with other HhH family DNA glycosylases (~8%). In *S. aureus* TAG, the highly conserved Pro-Gly-(Val/Ile)-Gly sequence pattern is not observed, replaced by Lys/Val-Phe-Val/Ile-Gly. Despite the low identity of overall sequences, *S. aureus* TAG still shows the conserved sequence motif at the HhH domain (FIGURE 2.7).
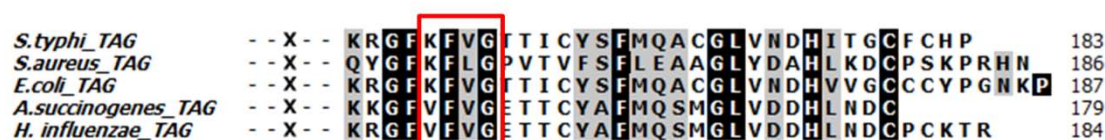
FIGURE 2.7: Sequence alignment of the the HhH motif in TAGs. The Highly conserved hairpin loop in HhH motif is highlighted by the red box.

The crystal structure of *S. aureus* TAG in complex with its product would provide valuable information to understand the DNA binding and base excision mechanism. There was no crystal structure of TAG bound to its product when we carried out this study, only a solution structure (NMR) of the *E. coli* TAG and an apo-form of TAG from *Salmonella typhi* (Cao, Kwon et al. 2003) (FIGURE 2.8). Maintaining of DNA is essential for the survival and evolution of *S. aureus,* making TAG a possible drug target. The protein is up-regulated in MRSA476, but down-regulated in MSSA252. Such proteomic differences implying that this protein may be important for the pathogenic strain. Structural study on this protein binding to its product and DNA will help us better understand the catalytic mechanism, and also contribute to inhibitor

design.
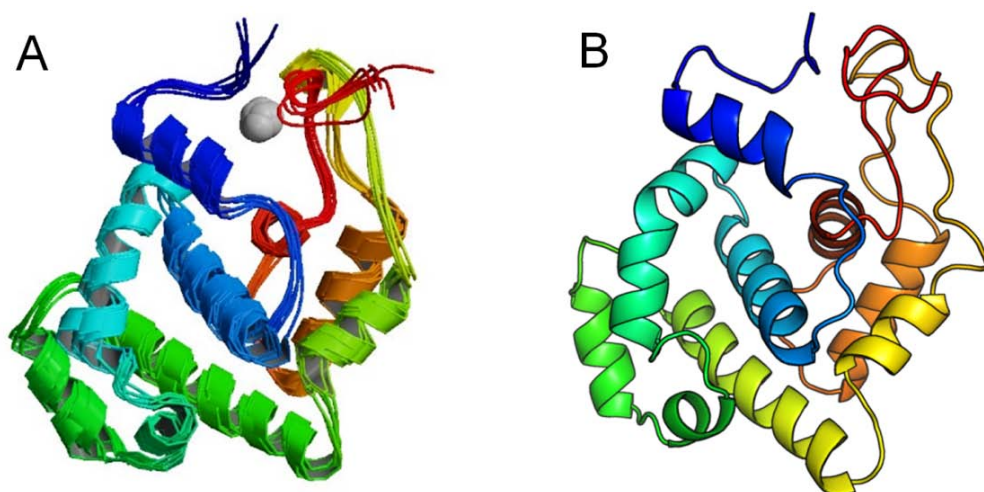
FIGURE 2.8: Cartoon representation of the NMR structure of [A] *E. coli* **TAG (PDB: 1P7M) and crystal structure of [B]** *Salmonella. Typhi* **TAG (PDB: 2OFK). Zn2+ ion is shown in grey sphere.**

2.3 Materials & Methods

2.3.1 Overexpression and purification of TAG

Protein Expression

The TAG plasmid DNA (pDEST14-TAG) was transformed into *E. coli* C43 (DE3) cells (Novagen) and plated onto Ampicillin agarose plates. Single colonies were picked up and grown in 10 ml Luria Broth (LB) medium supplemented with 100 µg/ml ampicillin at 37 ℃ overnight. The overnight cultures were used to inoculate 500 ml of LB medium in 2 L flasks and grown to an OD_{600} of 0.6–0.8 at 37 ℃. The temperature was then reduced to 30 ℃ and protein over-expression was achieved by induction with 1.0 mM isopropyl β-D-1-thiogalactopyranoside (IPTG) for 6 hours. Induced cells were harvested by centrifugation at 10500 X g for 15 minutes (Beckman

Avanti J20-XP, JL8.100 rotor). The cells were then re-suspended in PBS and stored at -80 ℃ until required.

Protein Purification

After harvest, the induced cells were re-suspended in lysis buffer (150 mM NaCl, 2 mM DTT, 20 mM imidazole and 50 mM Tris-HCl, pH 7.75) at room temperature for 30 minutes. The cells were disrupted by sonication for 8 cycles of 45 seconds, interrupted by 1 minute periods on ice after addition of 20μg/ml DNAse I, one tablet of protease inhibitor was added. To ensure that the DNA was digested by DNAse I, the mixture was kept at 4℃ for another 20 minutes. After addition of 2 mM EDTA, the mixture was centrifuged for 45 minutes at 20,000 rpm at 4 C. Then the supernatant fraction was passed through a 0.22 µm syringe filter (Millipore) and collected for further purification.

The supernatant containing TAG protein was applied to a charged Histrap Nickel Sepharose, high performance column (Amersham Biosciences), which had been equilibrated already with the lysis buffer. The unbound and weakly bound protein were removed by extensive washing with the wash buffer (300 mM NaCl, 2 mM DTT, 30 mM imidazole and 50mM Tris-HCl, pH 7.75). Essentially pure TAG protein was eluted with the elution buffer (500 mM NaCl, 2mM DTT, 500 mM imidazole and 50 mM Tris-HCl, pH 7.75). The eluted protein was then incubated with 1 ml of 2 mg/ml His-tagged tobacco etch virus protease (TEV) (approximate ratio 20:1 protein: protease) to remove the N-terminal polyhistidine tag (his-tag) at room temperature, the TAG protein and TEV mixture was dialyzed against 500 mM NaCl, 2 mM DTT

and 50 mM Tris-HCl, pH7.75 for 4 hours to remove the high concentration imidazole. The progress of cleavage was checked by SDS-PAGE, on completion the product mixture was passed through a 0.22 μM syringe filter membrane (Millipore) and a second Ni-NTA column to remove any uncleaved protein. The flow through was then concentrated to approximately 5 ml for size exclusion chromatography/gel filtration. Any precipitant was removed by centrifugation at 15000 X g for 15 min (4℃, Beckman Avanti J20-XP JA25.50 rotor). Size exclusion/gel filtration was applied on a Superdex™ 200 size exclusion chromatography column (Amersham Biosciences). The buffer used for column equilibration and gel filtration was consisting of 150 mM NaCl, 20 mM Tris-HCl pH 7.75 and 2 mM DTT. After the gel-filtration step proteins were judged to be pure by Coomassie™ Blue-stained gels and their integrity was confirmed by mass spectrometry (University of St Andrews). In total it was estimated 30 mg pure TAG native protein was obtained from 4 L of cell culture. According to the results of pre-crystallization Test (PCT), the protein was then concentrated to 20 mg/ml and 10 mg/ml respectively and dialyzed into 150 mM NaCl, 50 mM Tris-HCl, pH 7.75 prior to crystallization. Some of protein was flash-frozen in liquid nitrogen for long term storage.
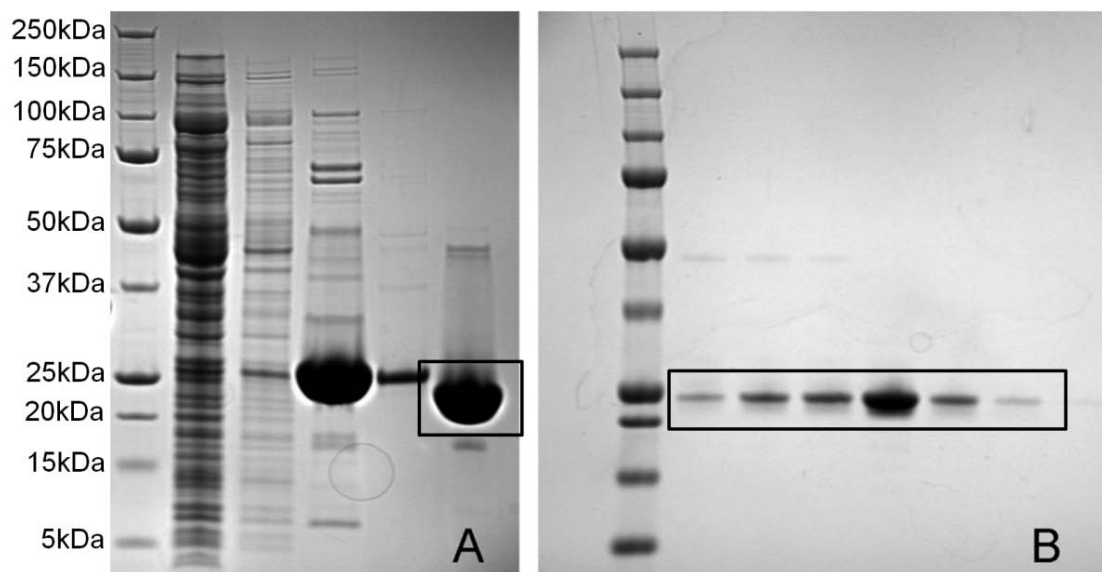
FIGURE 2.9: Coomassie Blue stained SDS-PAGE gels of TAG. [A]TAG purification and TEV cleavage. [B] TAG gel filtration fractions. The protein standards marker is labeled in [A] and pure cleaved protein is highlighted by a black square.

Binding buffer	500 mM NaCl, 2 mM DTT, 50 mM phosphate buffer, pH 7.75 (11.25 mM NaH_2PO_4, 38.75 mM Na_2HPO_4), 10 mM imidazole
Wash buffer	500 mM NaCl, 2 mM DTT, 50 mM phosphate buffer, pH 7.75 (11.25 mM NaH_2PO_4, 38.75 mM Na_2HPO_4), 35 mM imidazole
Elution buffer	500 mM NaCl, 2 mM DTT, 50 mM phosphate buffer, pH 7.75 (11.25 mM NaH_2PO_4, 38.75 mM Na_2HPO_4), 500 mM imidazole
Dialysis buffer	500 mM NaCl, 2 mM DTT, 50 mM phosphate buffer, pH 7.75 (11.25 mM NaH_2PO_4, 38.75 mM Na_2HPO_4), 10% glycerol, 1 mM EDTA
Gel-filtration buffer (Crystallization buffer)	150 mM NaCl, 50 mM Tris-HCl buffer, pH 7.75

TABLE 2.2: Buffer used in each step of *S. aureus* TAG purification.

## 2.3.2 Crystallization, optimization and diffraction test.

Crystallization

Attempts were made to crystallize both apo-form TAG and a complex crystal.

Concentrated protein in gel filtration buffer was screened using sitting drop vapour

diffusion technique. Two protein concentrations of 20 and 10 mg/ml were screened at 20 ℃ with a drop size of 0.2 μl (containing 0.1 μl of protein and 0.1 μl precipitant), set up against 100 μl reservoir solution. The protein mixture drops were prepared using a nano-drop crystallization robot (Cartesian Honeybee), which is a part of the Hamilton-Thermo Rhombix system. Crystal screens employed in the study include JMac, Nextal-The Classics, Nextal-pH Clear, KBS Wizard, Nextal-JCSG, Nextal-PE. All the sitting drop trials were kept in a quiet room to avoid any disturbance and held at 20 ℃.

TAG crystals was obtained in 24 hours from several conditions. Optimization of the initial 3 - 4 most visually promising hits, including at least one at each concentration, were performed to confirm crystals were protein crystals rather than salt. Improved crystals could be obtained from a number of optimized screens around the original conditions. The crystals grew to typically 0.1 to 0.2 mm^3. The best crystals, judged by size and regular shape, were obtained from variation of Hampton Classics Screen 82 [0.1M Tris-HCl pH 8.5, 2 M ammonium sulphate].
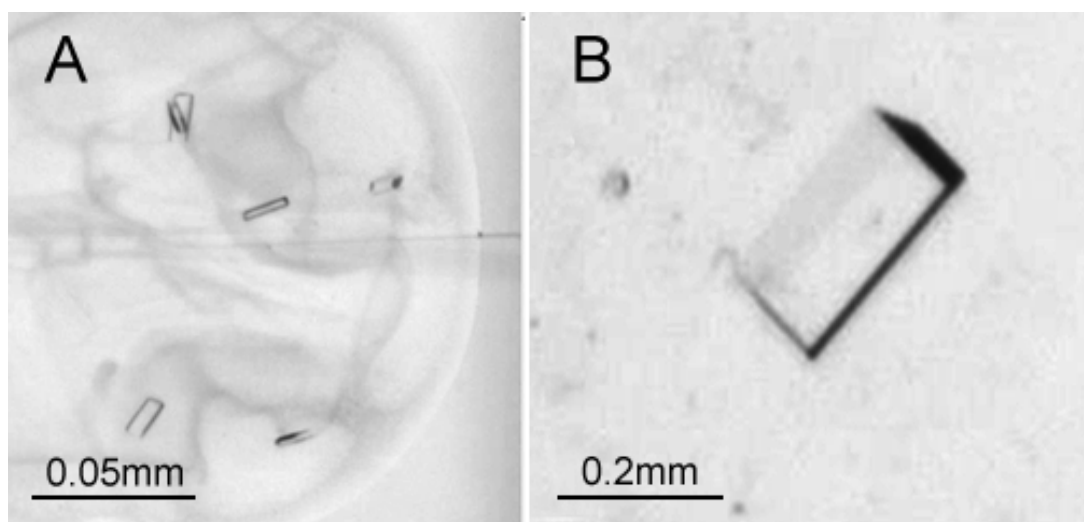
FIGURE 2.10 Native TAG crystals. [A] Native TAG crystal grown in nano drop. [B] Native TAG crystal after optimization at similar condition.

TAG protein in complex with 3-methyladenine (3-MeA)

3-MeA (Sigma-Aldrich) was dissolved in the gel filtration buffer as a stock solution to a concentration of 100 mM/mL. Two concentrations of 20 mg/ml and 10 mg/ml of native TAG protein were pre-incubated with 10 mM and 5 mM 3-MeA solution for at least 6 hours at 4 °C. The mixture was centrifuged at 15000 X g for 2 minutes (Eppendorf Centrifuge 5415D) to remove any insoluble ligand and protein precipitant. Crystallization trials were set up using the same method and system as the native TAG but at 4 °C. 3-MeA and TAG complex crystals were grown in cold room (temperature = 4 °C). All the drops were imaged and checked periodically.

Initial crystals (FIGURE 2.11A) were found from a Hampton screen after about 7 days. An optimization attempt around this condition was made to produce better quality complex crystals that were suitable for synchrotron. However, we could only

grow crystal clusters (FIGURE 2. 11B) from optimization trails, no single crystal observed in all optimized drops. In order to get a single piece of crystal, we had to break the crystal cluster by needle under microscope. The flash-freezing method was used to store the single piece crystals for further data collection.
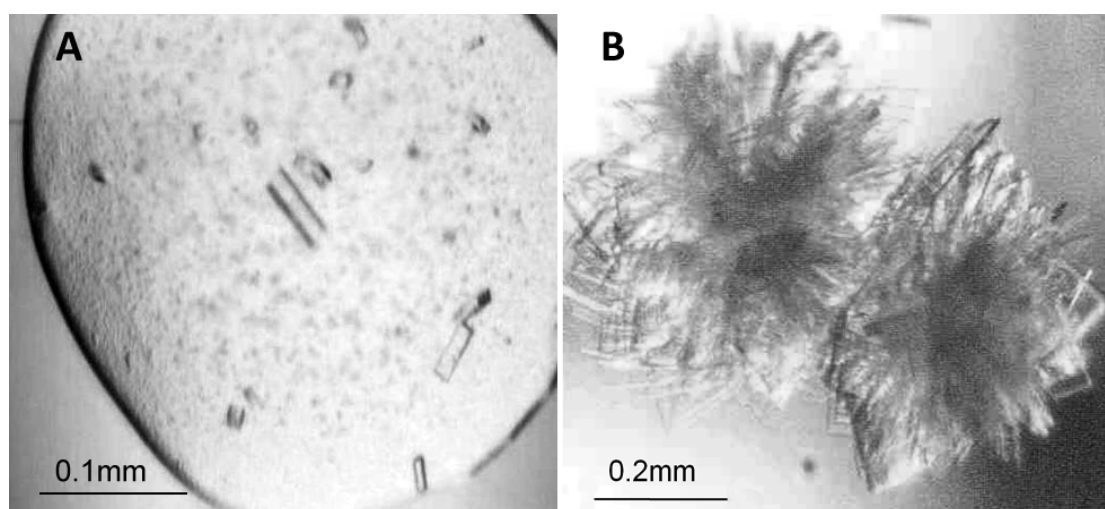
FIGURE 2.11: TAG/3-MeA complex crystal and clusters. [A] TAG/3-MeA complex crystals grown in nano drop. [B] Crystals cluster of TAG/3-MeA complex after optimization at similar condition.

To test the crystals diffraction quality, the in house X-ray generator (Rigaku-MSC Micromax-007 HF) system was used to screen the potential candidate crystals, which produced Cu Kα radiation (λ=1.5418Å) with Osmic mirrors. The crystals were firstly cryo-protected with 20% – 25% glycerol added to mother liquid before X-ray exposure. For the quick screen test, we use 30 second exposure time and 0.5 oscillations range. The crystal diffract to 2.1 Angstrom at the edge (image not shown) which indicated that the crystals we had were protein crystals, and crystals from same condition might diffract to an even higher resolution at European Synchrotron

Radiation Facility (ESRF). Larger crystals from same condition were flash-frozen in liquid nitrogen for synchrotron data collection.

### 2.3.3 Data collection strategy and initial processing

Native TAG data collection

TAG crystals diffraction data were collected on BM14 beamline at ESRF. Crystals were cryo-protected by adding 2 µl of 25% glycerol or PEG 200 (20%) to the protein drop. It seems PEG 200 gave more reliable cryo-protection than glycerol. Once a single crystal had been selected and soaked in cryo-protectant it was mounted on a cryo-loop and flash cooled to -173 ℃ in liquid nitrogen (Garman 1999). A high resolution data set that diffracted to 1.7Å was collected, using an exposure time of 10 second and 1° oscillations angle per frame, and the crystal to detector distance was 114.2 mm. 230 images were collected in this step. All the images were firstly indexed and integrated in DENZO and SCALEPACK (Otwinowsky, 1997). The program suggested that, the native crystal lattice belonged to the C 2 Laue group with cell dimension of a= 107.4 Å, b= 63.1 Å, c=38.4 Å, α=90.00, β=109.24, γ=90.00. The program POINTLESS, implemented within CCP4 program suite (Collaborative Computational Projects, Number 4 (Thornsberry 1994)), was used to confirm the Laue group and to suggest a space group C21.
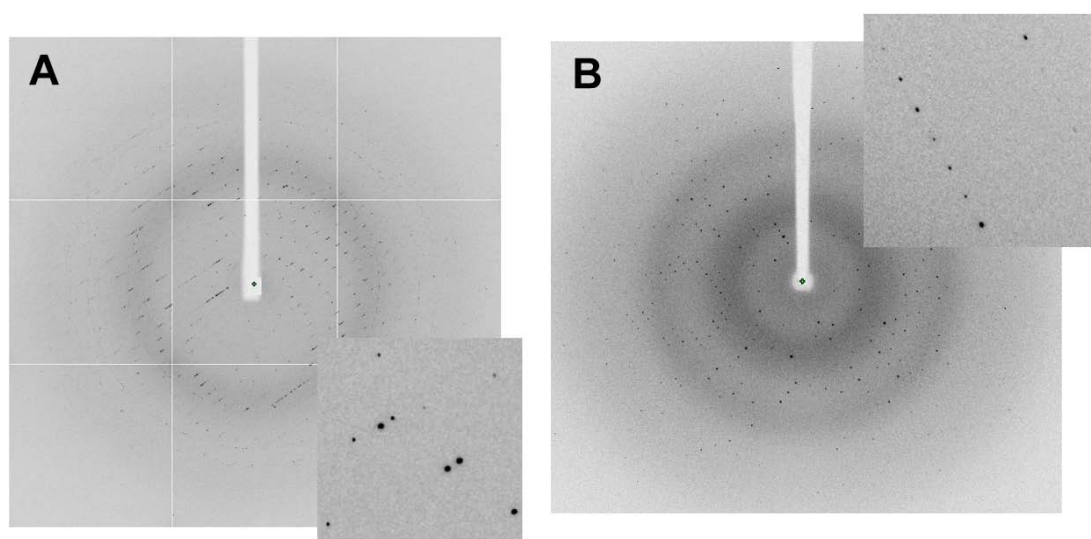
The TAG/3-MeA complex crystal diffraction data was collected on a single fragment of a big crystal cluster. The crystal was cryo-protected by adding 25% glycerol to the

mother liquid and frozen at -173℃ in liquid nitrogen. A 1.8 Å data set was collected

from this single piece of crystal on ESRF ID14-2. The incident X-ray beamline had a

wavelength of 0.934 Å. Data were recorded on a MARCCD detector with a crystal to

detector distance of 112.63 mm. Indexing with MOSFLM revealed that the crystal

had a same space group as native TAG.

An attempt to solve the structure by Molecular Replacement (MR) was made with

AMoRe (Navaza 1994), MOLREP (Vagin and Teplyakov 2000) and PHASER of the

CCP4 program suite, but ultimately proved unsuccessful. The available crystal MR

structure model was of low sequence homology (<20%), they failed to provide any

significant solution, and the NMR model also failed to solve the structure (Protein

Data Bank, Code: 1NKU, sequence identity 43%). However, as indicated by previous

studies from the other group (Cao, Kwon et al. 2003; Kwon, Cao et al. 2003), TAG

binds tightly with Zn^{2+}, and were able to use the anomalous signal from this bound

metal to solve the structure by Single-wavelength Anomalous Dispersion (SAD)

technique. In order to obtain the strongest Zn anomalous signal, the wavelength was

changed to 1.282 Å (the Zn^{2+} edge), the data were collected. Diffraction image and

data collection statistics are shown in FIGURE 2.13 and TABLE 2.3, respectively.
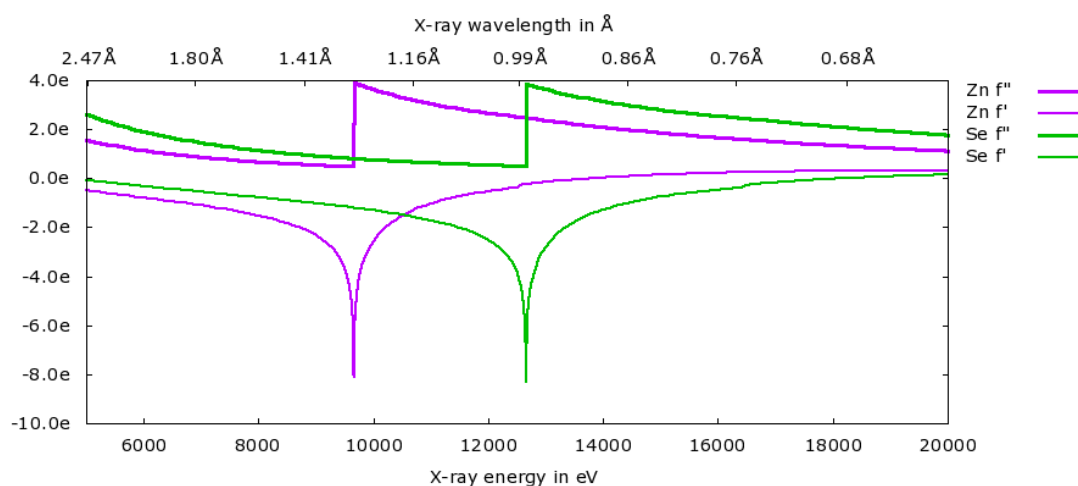
FIGURE 2.12: Plot of theoretical f' and f" for Zn and Se under different X-ray wavelength. Image was made by a web-based X-ray Anomalous Scattering Coefficients check tool http://skuld.bmsc.washington.edu/scatter/

FIGURE 2.13: X-ray diffraction pattern of TAG and TAG/3-MeA complex crystals. [A] native TAG determined to 1.7 Å at the ESRF, The resolution at the edge of the detector is 1.5 Å. [B] X-ray diffraction pattern of TAG/3-MeA complex crystals to 1.8 Å at the ESRF beamline ID14-EH2. The resolution at the edge of the detector is 1.6 Å.

Data collection	apo TAG SAD	TAG/3-MeA complex
Wavelength (Å)	1.282 Å	0.933Å

Resolution (Highset Shell) (Å)	50 - 1.70 (1.76 – 1.70)	30 - 1.80 (1.83-1.80)
Unit cell	a=107.46, b=63.10, c=38.47 $\alpha = \gamma =90.00$, $\beta = 109.24$	a=107.46, b=63.10, c=38.47 $\alpha = \gamma =90.00$, $\beta = 109.24$
Space Group	$C2_1$	$C2_1$
Unique reflections	24735 (5369)	93166 (17865)
Average redundancy	9.2 (7.8)	4.1 (1.5)
Data Completeness (%)	98 (86)	100 (92)
$I/\sigma\ (I)$	24.8 (4.3)	18.6 (3.9)
R_{merge}*	0.05(0.304)	0.09 (0.49)

TABLE 2.3: Summary of data collection statistics for Native TAG crystal and TAG/3-MeA complex crystals.

2.3.4 Structure solution and model refinement

Native TAG structure

The program SHELXC/D/E in CCP4 suite (Collaborative Computational Projects, Number 4 (Thornsberry 1994)) was used to identify the location of Zn and calculate the phases. SHELX C was used to prepare and analyze the SAD data. SHELX D was used to find the anomalous scatters and SHELX E to carry out density medication and calculated the phases. The TAG protein contains 2 cysteines, 1 Zn^{2+} atom is expected in the structure. The estimated solvent content is 56% with one monomer in the asymmetric unit. The CC All/Weak value from SHELX D is 31.47/23.70 which means a meaningful solution for this dataset. The heavy atom positions were used to calculate the phases, with density modification being used to break the phase

ambiguity. The initial phases were then improved by SOLVE/RESOLVE (Terwilliger 2003). The program ARP/wARP (Perrakis, Morris et al. 1999) was then used to auto-build the TAG model. At this stage, 7 chains of 159 residues in total were built in the new model after 50 building cycles with an R_{factor}/R_{free} of 0.29/0.35. The rest of model building was straightforward. Manually model building and refinement was applied using the WinCoot (Emsley and Cowtan 2004) and REFMAC5 (Murshudov, Vagin et al. 1997)

```
-------------------------------------------------------------------
PSUM 88.69  PSMF Peaks: 44 20 18 16 14 14 13 12 12 12 11 11
Try 100:12  Peaks 99 62 50 23 13 8
R = 0.544, Min fun  = 0.559, <cos> = 0.506, Ra = 0.448
Try   100, CC All/Weak 25.86 / 18.87, best 31.47 / 23.70, best PATFOM 23.82
PATFOM  9.52
===================================================================
```

FIGURE 2.14: SHELX D output of the TAG dataset.

3-MeA and TAG complex structure

The 1.8 Å data sets of TAG/3-MeA complex crystal were indexed and merged in the space group C121, same as native TAG structure. The TAG/3-MeA complex structure was solved using the native TAG structure as the search model (PDB ENTRY CODE: 2JG6). Automated molecular replacement with the PHASER program (McCoy 2007) in CCP4 program suite produced one solution with high rotation function Z (18.9) and translation function Z (TF-Z) score of 30.2, which suggested that the molecular replacement phasing with search model was successful. In this step, all residues were already given in the solution with an initial R factor and R_{free} of 0.31 and 0.37 respectively. WinCoot (Emsley and Cowtan 2004) and REFMAC5 (Murshudov, Vagin

et al. 1997) were subsequently used to build and refine the final TAG complex model. Both the native and the complex TAG structure were refined using the REFMAC5 in CCP4 Suite with translation, libration and screw rotation parameters (TLS) (Potterton, Briggs et al. 2003; Winn, Murshudov et al. 2003). Water molecules were added to the model automatically using ARP/wARP (Perrakis, Morris et al. 1999) in CCP4 program suite. Ligand libraries were prepared using PRODRG (Schuttelkopf and van Aalten 2004). The 3-MeA molecule was modeled into the unbiased Fo-Fc map when the electron density was unambiguous. The final model was validated by a web-based protein structure validation service (http://molprobity.biochem.duke.edu/). Crystallographic figures were made using PyMOL™ (Version 1.1r1 – Delano Scientific) unless otherwise stated. The protein surface electrostatic potential was calculated using APBS (Adaptive Poisson-Boltzmann Solver), a PyMol™ plugin tool (Baker, Sept et al. 2001). The native TAG and complex model refinement statistics are summarized in TABLE 2.4

Refinement	Native TAG	TAG/3-MeA complex
Clashscore	3.01	2.9
Rotamer outliers (%)	0.00%	1.00%
Cβ deviations >0.25 Å	0	0
Residues with bad bonds/angles (%)	0.00%	0.00%
MolProbity Score (percentage (%))	1.13 (99)	1.08 (100)
Ramachandran favoured/outliers (%)	97.83%	98.49%
R_{work}	0.163	0.169
R_{free}	0.193	0.201
r.m.s.d bond lengths(Å)/angles	0.009/1.093	0.008/1.147

**TABLE 2.4: Model refinement and validation statistics of native TAG and TAG/3-MeA complex.**

2.3.5 Fluorescence spectroscopy assay for TAG

The assay for TAG used a previously reported fluorescence method (Drohat, Kwon et al. 2002), which is based on fluorescence quenching of a protein tryptophan by adenine. The decrease in tryptophan fluorescence intensity of TAG (2µM) is monitored during addition of increasing amounts of 3-MeA (10 – 500µM) at 20 ℃. Excitation wavelength was 280 nm and emission 335 nm with buffer of 50 mM Tris-HCl pH7.5 and 150 mM NaCl.

We also investigated the binding of the normal base adenine under same condition as 3-MeA as the control experiments. All the reagents and assays auxiliary enzymes were purchased from Sigma-Aldrich. Three repeat measurements were carried out to make sure the data are consistent. Data were re-plotted in Grafit graphic analysis program. No significant binding of the normal base adenine was detected even at a high concentration of 350 μM. *S. aureus* TAG has a highly degree of ligand specificity for 3-MeA over adenine.
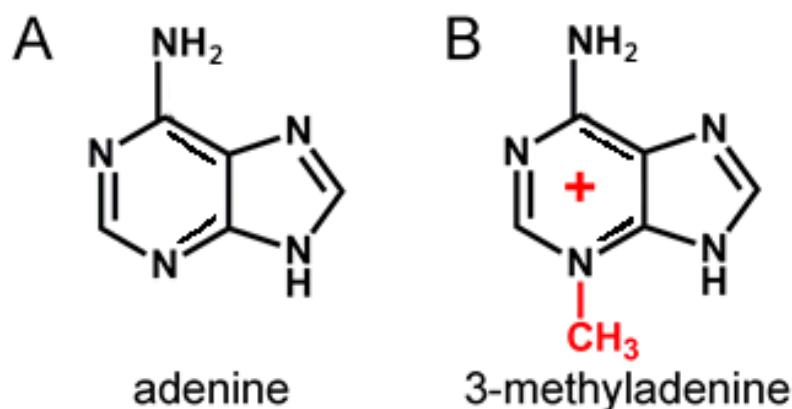
FIGURE 2.15: chemical structure of normal base adenine and the alkylated base adenine, 3-methyladenine.
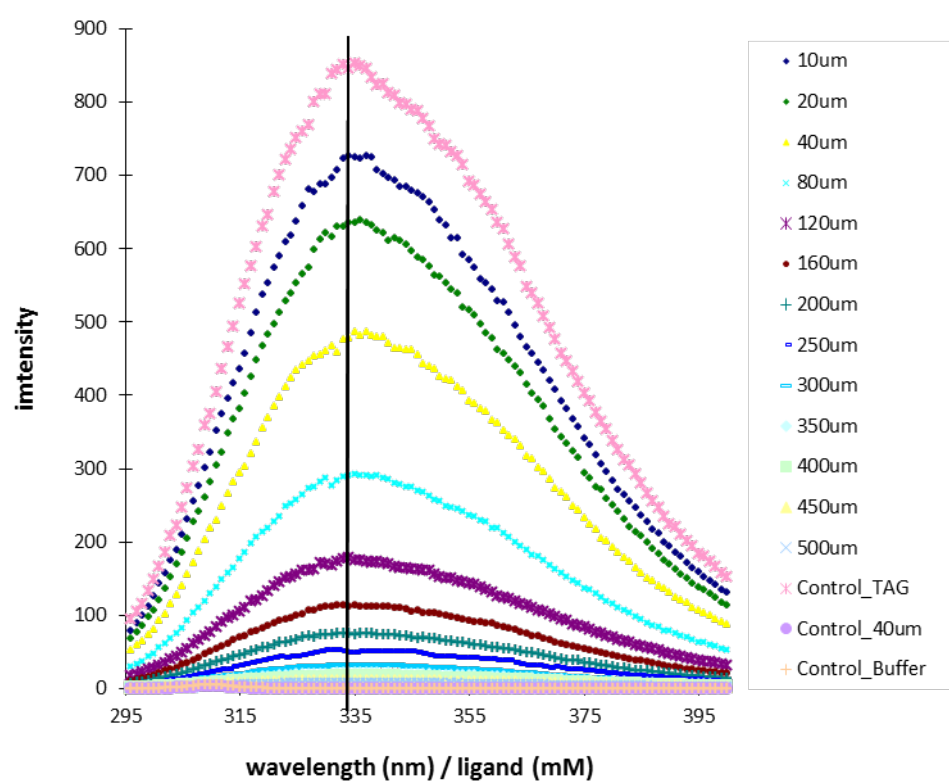
FIGURE 2.16: Fluorescence spectroscopy assay for TAG/3-MeA binding at 335 nm.
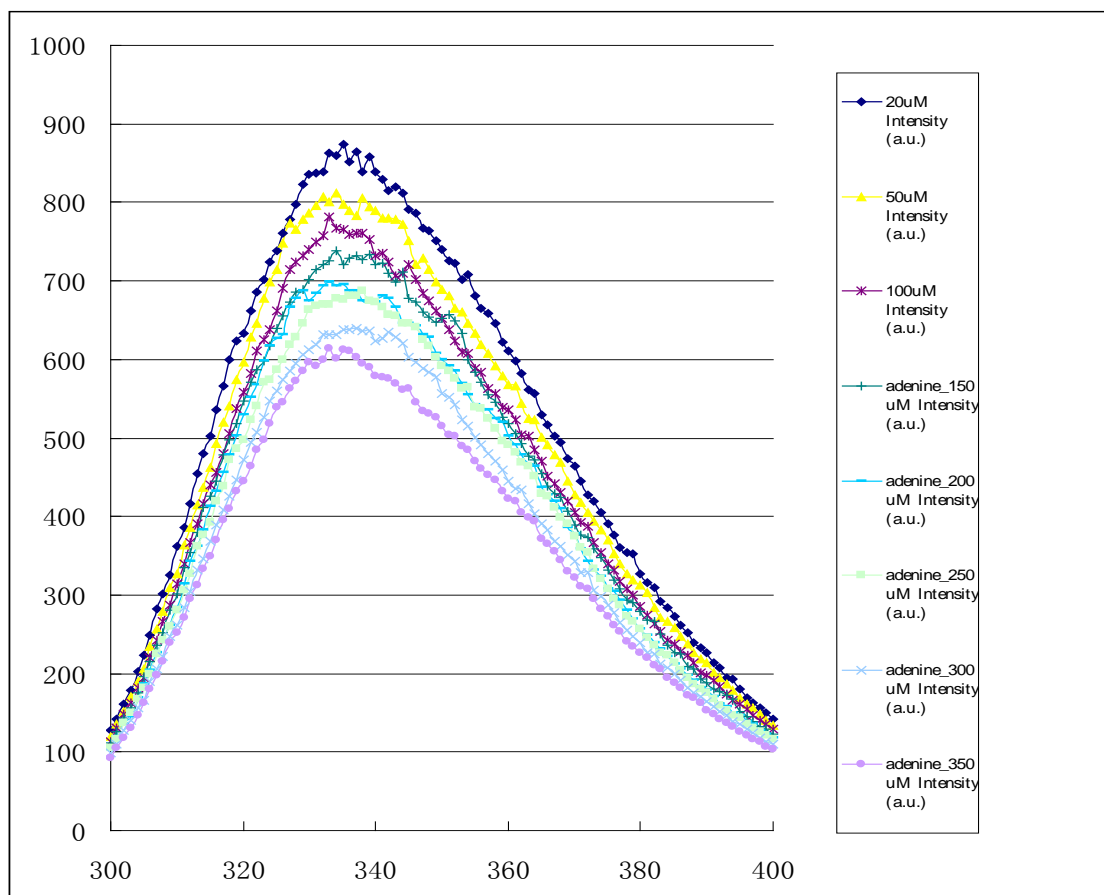
FIGURE 2.17: Fluorescence spectroscopy assay for TAG/adenine binding at 335 nm.

2.3.6 Thermofluor study on *S. aureus* TAG

The fluorescence-based thermal shift assay (Thermofluor) is applied for the fragments screening method for finding the potential hits for the target protein. The changes of protein thermodynamic stability upon fragments binding are evaluated by a thermal unfolding curve. The midpoint temperature (T_m) of the protein unfolding transition is considered as the key guideline for the fragments evaluation.

The Thermofluor assay for TAG fragments screening was performed in a commercially available real-time PCR instrument (Lo, Aulabaugh et al. 2004), where

thermal melting curves of buffer/fragments condition can be screened rapidly in high-throughput mode (96 samples in 2 hours).

Sample preparation

The TAG protein used in this thermo shift assay was also expressed in *E. coli* C43 (DE3). Purification of the protein was performed as same as described previously, the TAG Gel-filtration buffer was consisting of 150 mM NaCl, 20 mM Tris-HCl pH 7.75, 10 mM b-mercaptoethanol and 2 mM ethylenediaminetetraacetic acid (EDTA). The protein was concentrated to 50 mM/ML and kept at -80℃ for further use. The original stock 5000X concentrate SYPRO Orange (molecular probe, Dye) (Invitrogen) in DMSO was firstly diluted to 25X by TAG gel-filtration buffer. All the compounds were dissolved in DMSO to a final concentration of 200 mM and kept at 4 ℃ for further use.

Thermofluor assay

To apply the Thermo shift assay, solutions of 5 µL SYPRO Orange, 5 µL TAG protein, 4.5 µL compound solution, and 35 µL TAG gel-filtration buffer were added to the well of a 96-well iCycle iQ PCR plate (Bio-Rad, Hercules, CA). For the control samples, 5 µL DMSO and buffer was added instead of compounds solution. All the plates were sealed and heated in an iCycle iQ5 Real-Time PCR detection system (Bio-Rad) from 25 ℃ to 98 ℃ in increment of 0.5 ℃ per minute. The fluorescence intensity of each well of the plates was monitored and recorded automatically by a

charge-coupled device (CCD) camera. The wavelengths of excitation and emission were 490 and 530 nm. Measurements were repeated twice. The melting curves were generated by the program iCycler iQ Optical System. The data could be further processed using the same program and Origin. Those fragments that induced a shift of *Tm* over 2 ℃ were considered as positive hits.
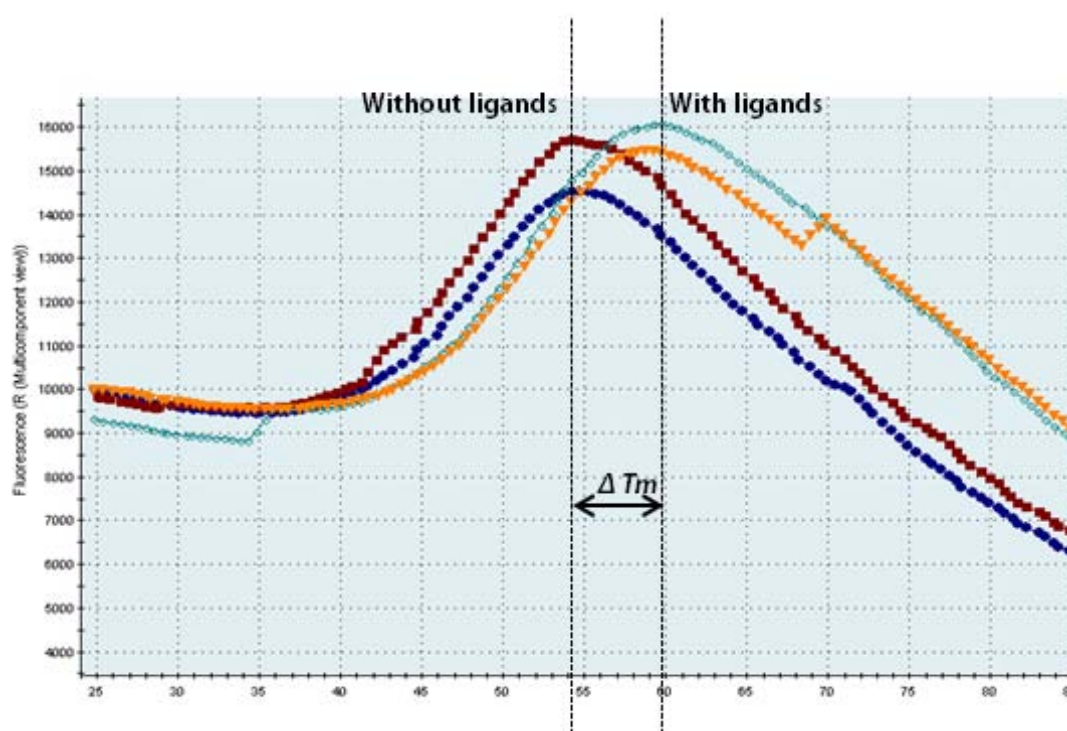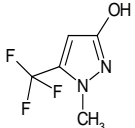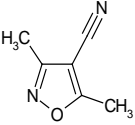

FIGURE 2.18: The fluorescence-based thermal shift assay.
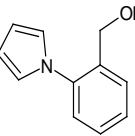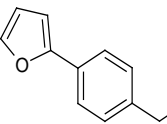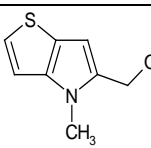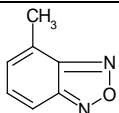
Results / Potential hits

16 potential hits out of 476 fragments were obtained by thermal shift assay against TAG. 6 of them were considered as obvious improvement.

Fragments	Structure	Formula	ΔT_m (℃)

63

Compound name	Structure	Formula	Hits
1-methyl-5-(trifluoromethyl)-1H-pyrazol-3-ol		C5H5F3N2O	2
3,5-dimethyl-4-isoxazolecarbonitrile		C6H6N2O	3
[2-(1H-pyrrol-1-yl)phenyl]methanol		C11H11NO	3
[4-(2-furyl)phenyl]methanol		C11H10O2	4
(4-methyl-4H-thieno[3,2-b]pyrrol-5-yl)methanol		C8H9NOS	4
4-methyl-2,1,3-benzoxadiazole		C7 H6 N2 O	6

TABLE 2.5: The positive hits of the thermal shift assay for TAG

The top hits for TAG are quite similar to the real TAG product, 3-methyladenine (3-MeA). They all have a benzene ring group linked to a NH_2 group. It seems that this part in protein – compound interactions is vital.

However, there are so many other factors influencing the results of the thermal shift assay, the protein stability is highly susceptible to buffer condition such as temperature, salt type and concentration, pH and ionic strength of the buffer. The next step is producing some complex crystals with these potential fragments by either co-crystallization or cocktail soaking techniques.

2.4 Results & Discussion

2.4.1 Overall structure of TAG and TAG/3-MeA complex

TAG overall crystal structure

The final refined native TAG structure model consists of 186 residues with an R_{factor} and R_{free} of 0.16/0.20. The monomer structure appears as an "ellipse shape" and contains 10 α-helices and 2 β-sheets. The final model of TAG/3-MeA complex monomer has 188 residues. The two additional residues (Gly-Ala) were attached to the N-terminus and result from the cleavage of His-tag. An examination of the Protein Data Bank (PDB) for similar structures using the web-based protein structure comparison service SSM at European Bioinformatics Institute (EBI) http://www.ebi.ac.uk/msd-srv/ssm/ (Krissinel and Henrick 2004) shows that the *S. aureus* TAG shared a common overall fold with other TAG. The r.m.s.d with these monomers is in the range 1.2 – 1.8 Å. (TABLE 2.6)

Source	N_{align}	r.m.s.d(Å)	Seq identity	Citation
E. coli TAG (1P7M)	174	1.79	43%	(Cao, Kwon et al. 2003)
S. typhi TAG (2OFK)	177	1.26	40%	(Metz, Hollis et al. 2007)

TABLE 2.6: strucuture alignment of *S. aureus* TAG using SSM at European Bioinformatics Institude (EBI) http://www.ebi.ac.uk/msd-srv/ssm/ (Krissinel and Henrick 2004). N_{align} indicates the residues aligned.

The TAG structure consists of two main domains. Helices α1- α8 consist the bottom domain (large domain), this domain is highly conserved in HhH DNA glycosylase family (Mol, Kuo et al. 1995; Eichman, O'Rourke et al. 2003) and contains the HhH

DNA binding motif. The HhH motif in TAG is composed by helices α9, α10 and the loop between them (FIGURE 2.21). This signature HhH motif is mainly responsible for DNA binding (Fromme and Verdine 2002; Metz, Hollis et al. 2007). β-strands β1, β2 and the N-, C-terminal loop consist the upper domain (small domain). Structural comparison indicates the small domain is less conserved among the HhH DNA glycosylase members.
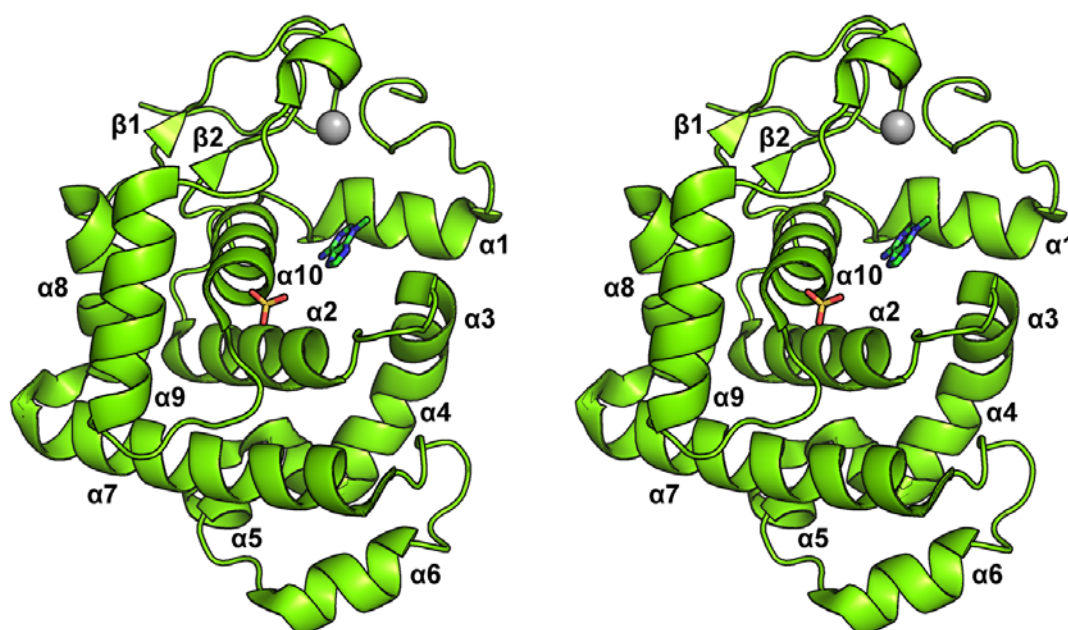
FIGURE 2.19: Stereo view of overall structure of TAG in complex with 3-MeA monomer A. Zn^{2+} iron is showing as a green sphere, the product 3-MeA is showing as stick in green and blue color and sulfate is showing as stick in red and yellow. N-Terminal is shown in blue, C-Terminal starts from the orange loop. All the helices and sheets are labeled.
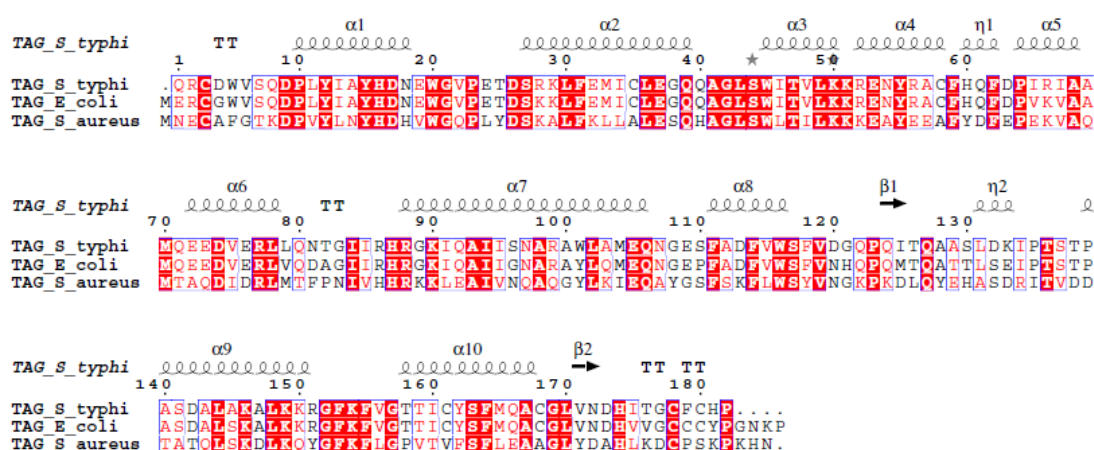
FIGURE 2.20: Structure-based sequence alignment of *S. aureus, S.typhi, E.coli* TAG. The secondary structural elements of TAG are shown. Sequence alignment using ClusterW (Larkin, Blackshields et al. 2007) and ESpript (Gouet, Robert et al. 2003).
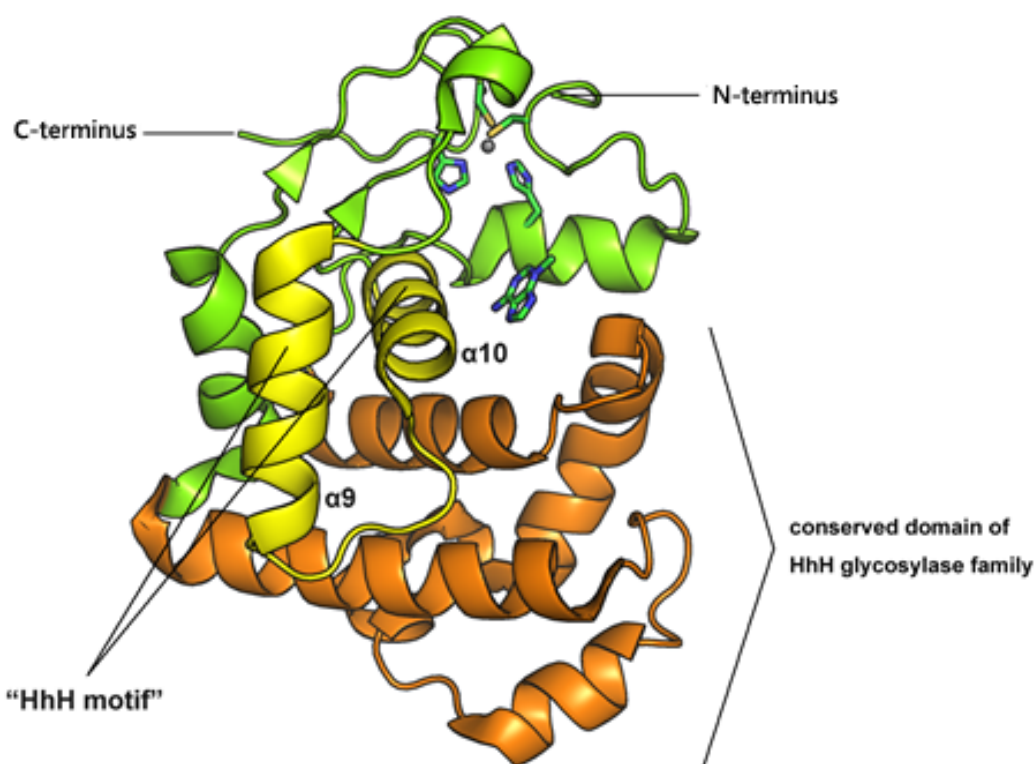
FIGURE 2.21: Stereo view of crystal structure of TAG/3-MeA complex. The HhH motif is labeled and highlighted in yellow. The remaining conserved helical domain of the HhH glycosylase subfamily is shown in orange. The structures elements are unique to TAG are colored in green. 3-MeA is shown in green and blue sticks to indicate the binding pocket of TAG. Zn^{2+} ion is shown in grey sphere.

A web-based "protein interfaces, surfaces and assemblies" (PISA) analysis software http://www.ebi.ac.uk/msd-srv/prot_int/pistart.html (Krissinel and Henrick 2005) indicates that both the apo-form *S. aureus* TAG and complex structure are monomers and this is consistent with gel filtration result. There is no major structural difference observed between the apo-form and complex TAG structure. Other members of HhH DNA glycosylases are also reported to be monomeric such as *S. typhi* TAG (Eichman, O'Rourke et al. 2003; Metz, Hollis et al. 2007) and MagIII (Eichman, O'Rourke et al. 2003). A Zn^{2+} ion is bound at the same location as the apo-form TAG structure. A sulfate molecule is observed in TAG/3-MeA structure, presumably from the crystallization condition. A 3-MeA molecule is bound at the active site, and the surface electrostatic charge is strongly negative. The loop in the signature HhH motif has a positive electrostatic surface.

The Zn binding site is located at the centre of N-terminal loop and C-terminal loop (FIGURE 2.22). This binding site has as might be expected, a strong negatively charged electrostatics surface. Four conserved residues (Cys4, His17, His175 and Cys 179) ligate the Zn ion within the normal Zn atoms distance. The distance of each residue to the Zn is 2.3 Å, 2.1 Å, 2.1 Å and 2.3 Å, respectively. Cys4 and His17 both from N-terminal loop while His175 and Cys179 are from C-terminal loop. The Zn ion seems likely act as a pin that tethers the N-terminal and C-terminal loops, stabilizing these flexible structure elements and holding the active site, also increasing the overall stability of the whole structure (Drohat, Kwon et al. 2002; Kwon, Cao et al. 2003).
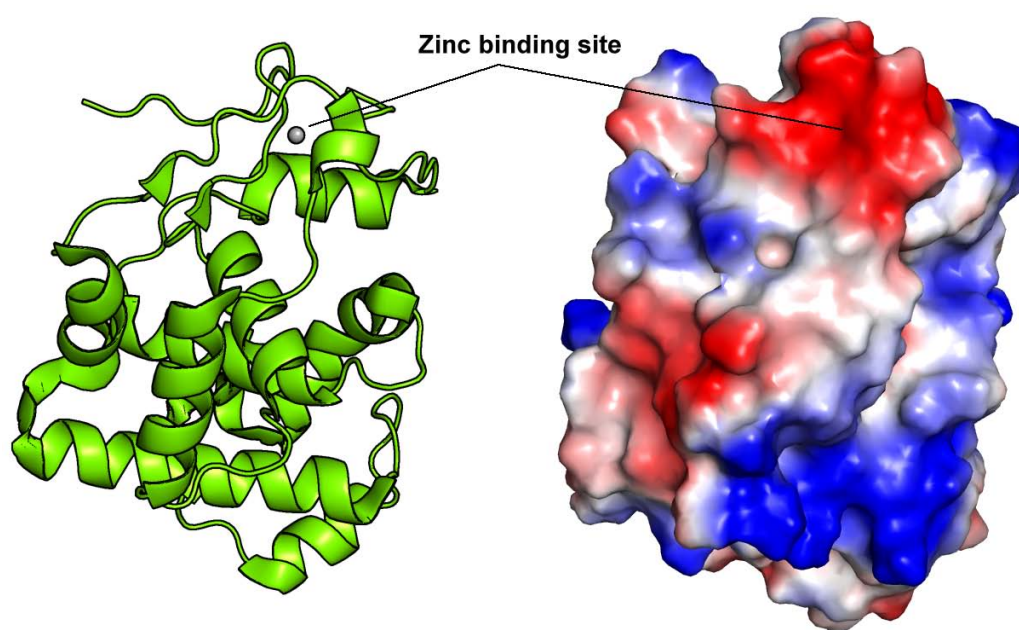
FIGURE 2.22: Cartoon representation of the Zn^{2+} binding site of *S. aureus* TAG. The solvent-accessible surface of TAG colored based on the electrostatics potential from -7 to +7 kT/e, calculated using ABPS tools in PyMol™. Positive charge is shown in blue and negative charge is shown in red.
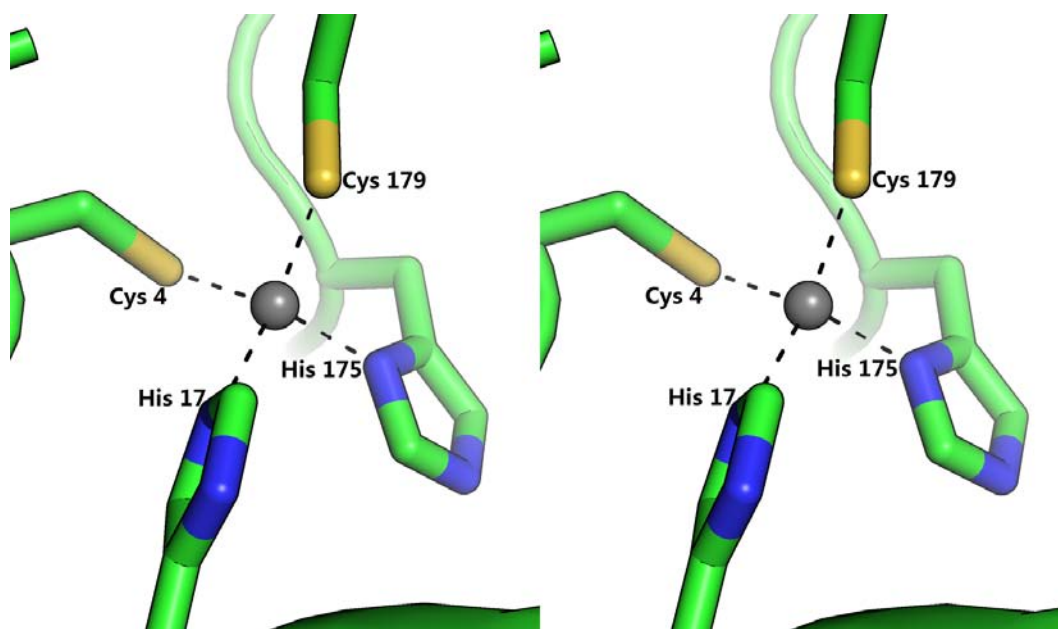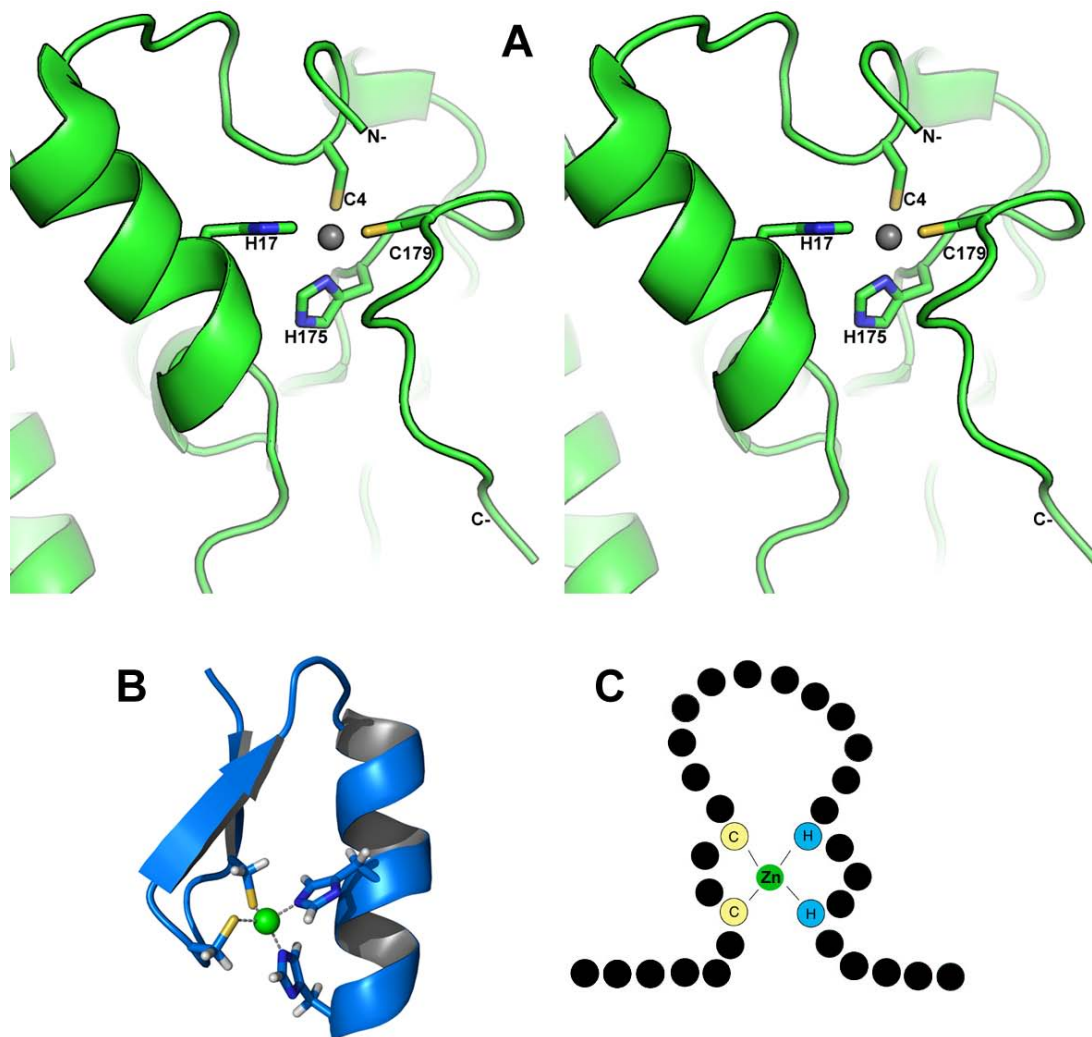

FIGURE 2.23: Stereo view of the Zn^{2+} binding pocket. Zn^{2+} ion is shown in grey sphere. Hydrogen bonds are depicted as black dashed lines. Residues that might interact with the Zn^{2+} ion are labeled in black letters.

The same Zn binding motif is also found in other structures of the TAG family such as *E.coli* TAG (Kwon, Cao et al. 2003) and *S. typhi* TAG (Metz, Hollis et al. 2007). Sequence alignment of TAG family protein shows this "Cys-His-X-His-Cys" motif is highly conserved (FIGURE 2.24). This Zn binding structure motif is distinct from the other normal "Zn^{2+} finger motif" found in eukaryotes (Berg 1990; Berg 1990) and other DNA glycosylases like human OGG (Fromme and Verdine 2002) and MutM (Gilboa, Zharkov et al. 2002). The normal Zn^{2+} finger motif in these structures are similar, they usually consists of 2 – 4 cysteines, and the order of these residues is usually Cys-X-Cys-X-Cys-X-Cys (Berg 1990; Kwon and Smerdon 2003), X represents up to about 20 amino acids. The normal Zn^{2+} finger motif stabilizes the two adjacent β-sheets and α-helix, which cluster in the region of a turn (Jasanoff, Kochoyan et al. 1992; Kirthi and Savithri 2003). However the Zn binding motif in *S. aureus* TAG is composed of two Cys-X-His sub-motifs, separated by 158 amino acid residues. This arrangement in TAG is significantly different from other Zn^{2+} finger motifs (FIGURE 2.25).


```
S.aureus   - - - - - - - M N E C A F G T K D P V Y L N Y H D H - X - D A H L K D C P S K P K H N   186
P.lumine   M E L T R M E L T R C H W V T S D P Q Y L A Y H D N - X - N D H I T D C L C R K - - -   190
H.influe   - - - - M Q Q I T R C P W V G E Q P I Y I D Y H D K - X - D D H L N N C P C K T R - - -   187
P.multoc   - - - - - - M K T R C S W V G N S T I Y R D Y H D H - X - N D H L N D C C C K - - - - -   183
A.aphrop   - - - - - - M A R R C A W A E S S Q L Y R D Y H D N - X - N D H W N Q C H S K T A N K A   188
B.brevis   - - - - - - - M N R C G W V N Q D P I Y M D Y H D H - X - N D H V A T C D L Y Q K N - -   185
S.protea   - - - - - M I N E R C G W V T A D P L Y L E Y H D K - X - N D H L T G C L C Y P K P - -   187
Y.rohdei   - - - M N M D L Q R C G W V T S D P L Y L A Y H D E - X - N D H L A S C F C H P D N A V   192
E.coli     - - - - - - - M E R C G W V S Q D P L Y I A Y H D N - X - N D H V V G C C C Y P G N K P   187
```

FIGURE 2.24: Sequence alignment of the conserved Cys-His-His-Cys structure motif of the TAG family. The sequences of the TAG family were obtained from BLAST search using *S. aureus* TAG sequence. The Zn^{2+}-binding Cys-His-His-Cys cluster is highlighted in red box.

FIGURE 2.25: Cartoon representation of the Zn^{2+} snap motif in TAG and normal Zn^{2+} finger motif. [A] A stereo view of the Zn^{2+} binding site in TAG. [B] Cartoon representation of the normal Zn^{2+} finger motif. [C] Schematic view of the normal Zn^{2+} finger motif.
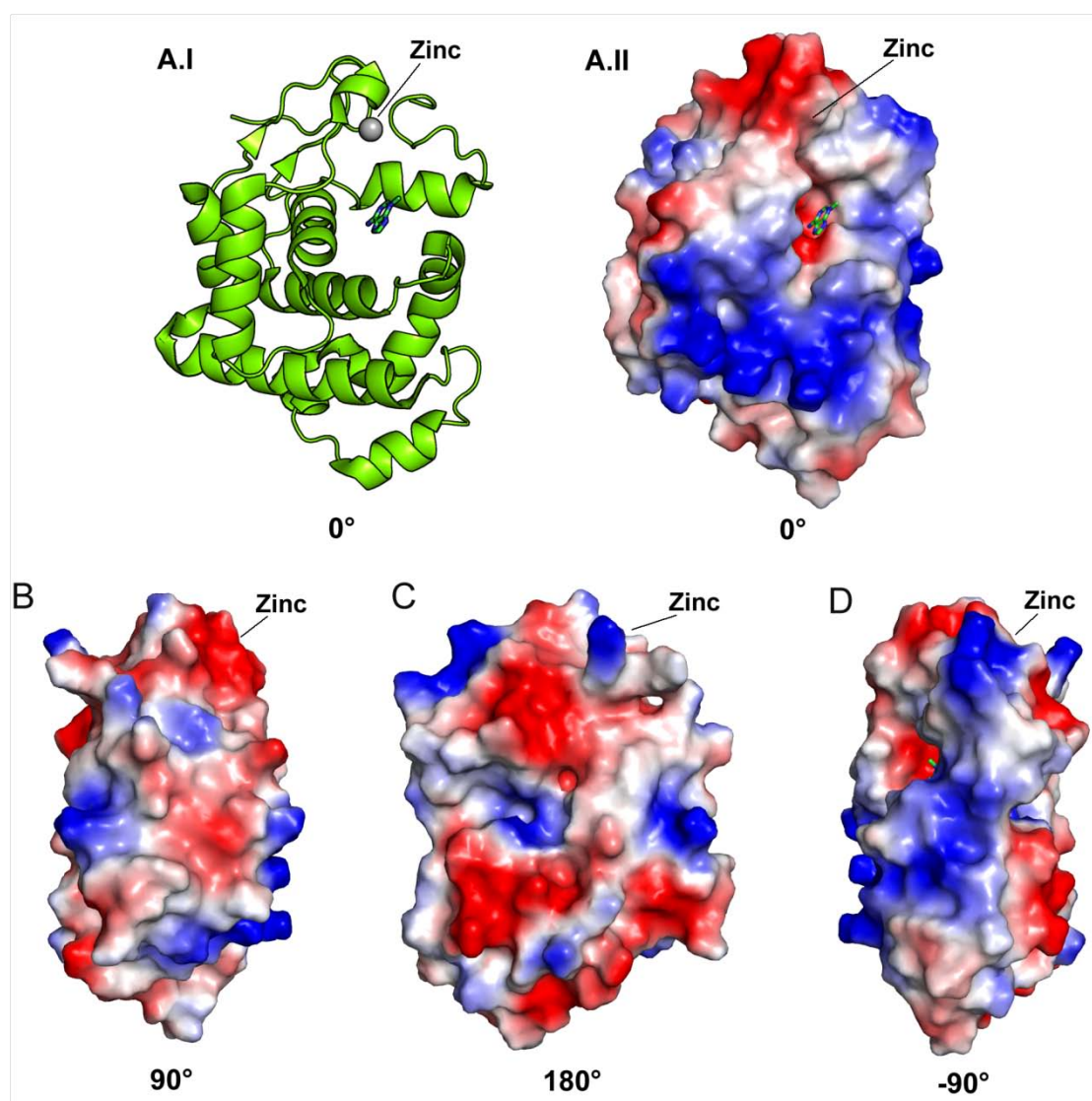
FIGURE 2.26: Solvent accessible surface of TAG colored according to electrostatics potential. **[A.I].[A.II] Cartoon representation and surface electrostatics potential of TAG structure. [B].[C].[D] The solvent-accessible surface of TAG colored based on the electrostatics potential from -7 to +7 kT/e, calculated using ABPS tools in PyMol™. Positive charge is shown in blue and negative charge is shown in red. 3-MeA is shown as green and blue stick to indicate the ligand binding pocket of TAG.**

2.4.2 The recognition site of *S. aureus* TAG

The helix α10 is close to the product 3-MeA (< 4.8 Å) and involved in active site, residues from this helix interact with 3-MeA directly. Although 3-MeA and adenine have similar structures, the electron density map shows clearly that the 3-MeA is

bound (FIGURE 2.27).
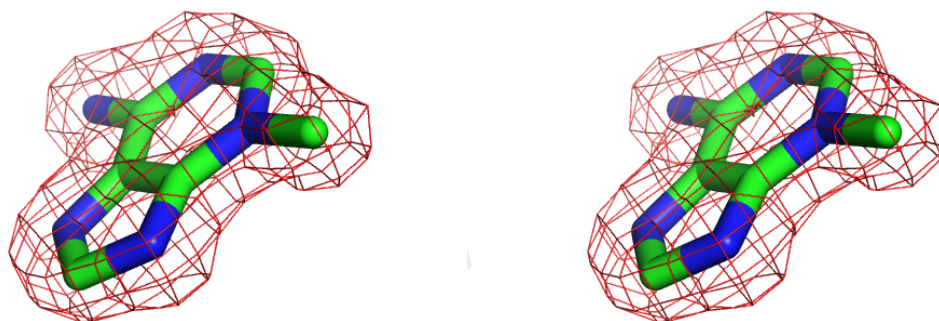
FIGURE 2.27: Stereo view of unbiased Fo-Fc electron-density map (red mesh) contoured at 3 σ with the final refined 3-MeA superimposed.

The 3-MeA binding pocket is constituted by the four helices α1, α2, α3, α10 and the loop between helices α2 and α3 (FIGURE 2.29). Helix α1 also involved in the Zn^{2+} binding motif, while α10 is a part of the HhH motif. The four helices are highly conserved in the HhH family of DNA glycosylases. The overlap between HhH motif and product recognition pocket is consistent with recognition of both DNA strand and an alkylated base. The recognition pocket shows a very strong negative electrostatic surface charge (FIGURE 2.28). The orientation of the ring is assigned by hydrogen bonds since the nitrogen and carbon atoms are indistinguishable at this resolution.
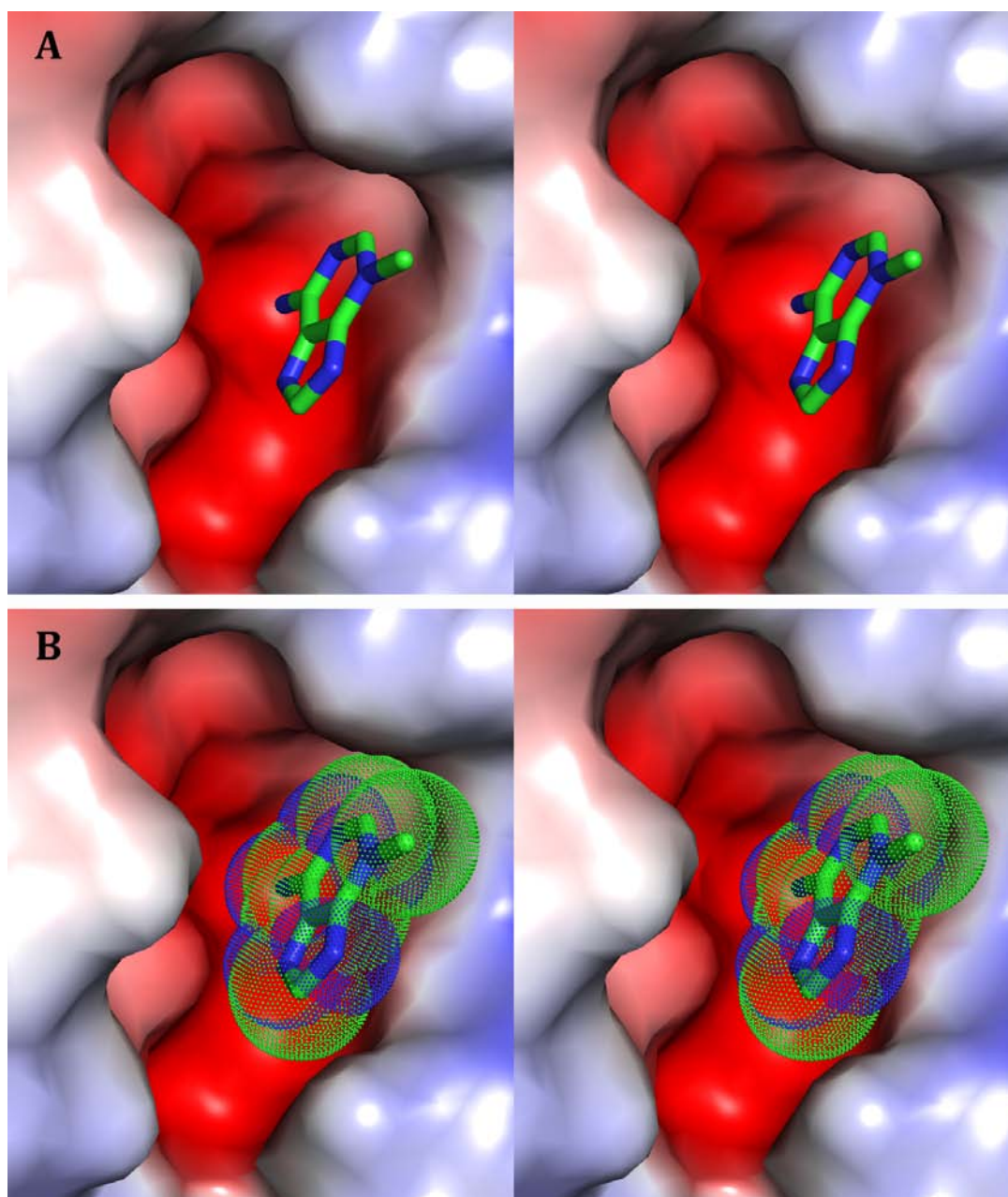
FIGURE 2.28: The electrostatics surface potential of the active site of TAG. The solvent-accessible surface of TAG colored based on the electrostatics potential from -7 to +7 kT/e, calculated using APBS tools in PyMol™. Positive charge is shown in blue and negative charge is shown in red. 3-MeA is shown in green and blue stick.
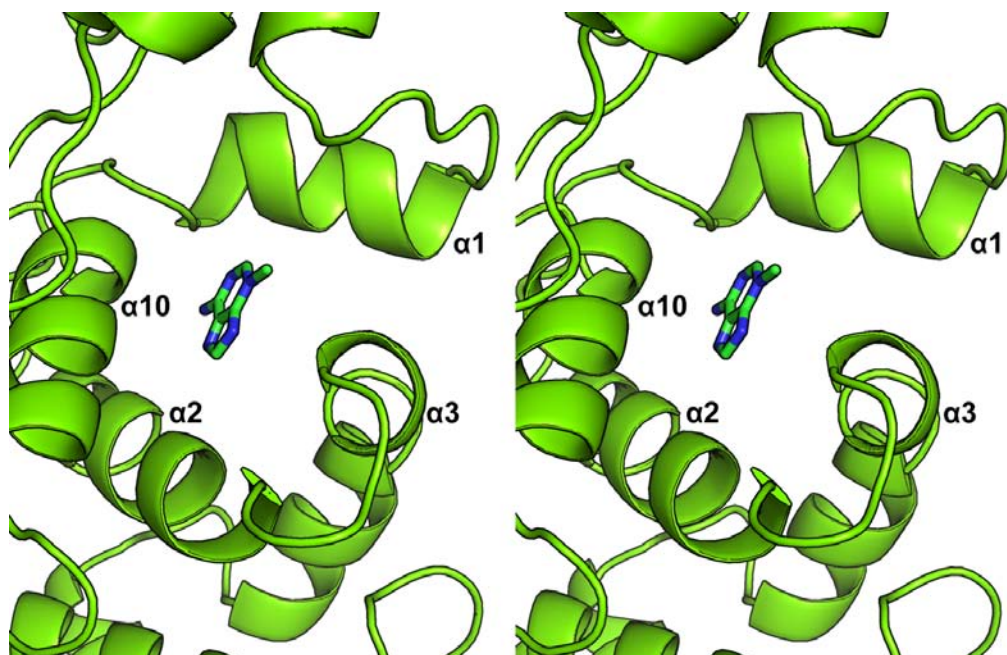
FIGURE 2.29: Stereo view of the active site of TAG. 3-MeA is shown in green and blue sticks. All the helices were labeled in black.

A closer look of the product binding site of TAG revealed that in total 8 residues from helices α1, α2, α3 and α10 involved in 3-MeA binding. These residues form a deep hydrophilic cavity for the product and solvent to access. The 3-MeA is fixed by hydrogen binding and a series of interactions with residues in the active site. Tyr16 from helix α1 and Glu38 from helix α2 hydrogen bond 3-MeA. Water molecules bridge from 3-MeA to the main and side chain of Trp46, Trp21, Phe6 and Ser164 from helix α10. Trp46 stacks against the hydrophobic face of 3-MeA. Compared to the apo-form protein, the water molecules W1 and W2 remain unchanged after the 3-MeA binding, however, three water molecules W3, W4 and W5 are replaced by 3-MeA molecule. The 3-MeA molecule also recruits 3 water molecules, created a new water-mediated interaction network and may enhance the binding of 3-MeA (FIGURE 2.30).
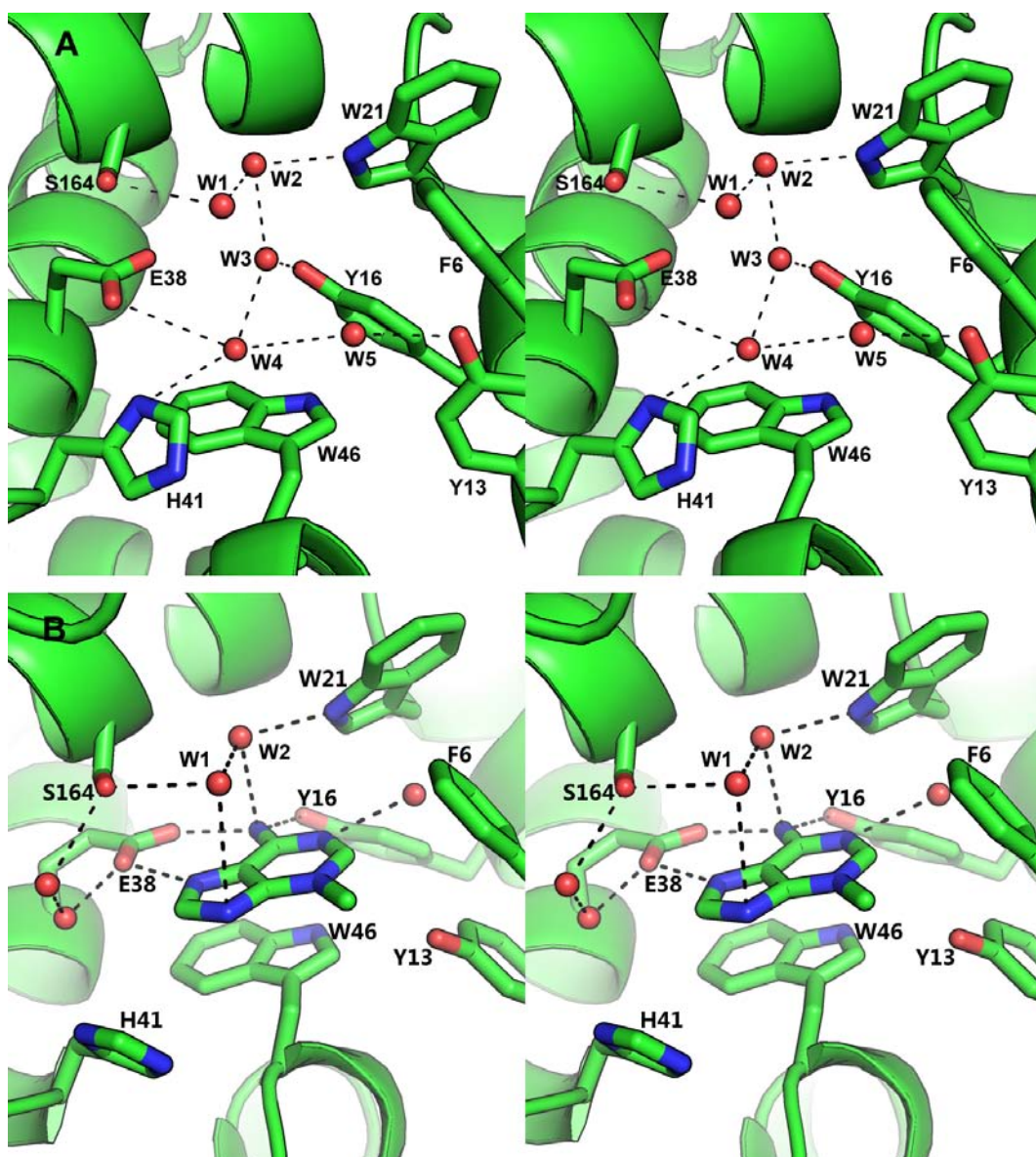
FIGURE 2.30: Stereo view of key interactions in the active site. [A]apo-form TAG protein. [B] TAG in complex with 3-MeA. Protein residues are shown in green, 3-MeA in green and blue, and water molecules as red sphere. Hydrogen bonds are depicted as black dashed lines. Residues that might interact with the ligand are labeled in black letters.

Superposition of the 3-MeA binding site of apo-form TAG and TAG/3-MeA complex monomer A shows no major difference (FIGURE 2.31). Glu38 and Tyr16 directly interactions with the 3-MeA molecule and have moved towards to the ligand by 0.8Å. Trp46, Phe6 and Ser164 are slightly closer to the 3-MeA molecule (0.3 Å). The side

chain orientation change of His41 and Tyr13 reflects change in the water-mediated

network upon 3-MeA binding (FIGURE 2.32).
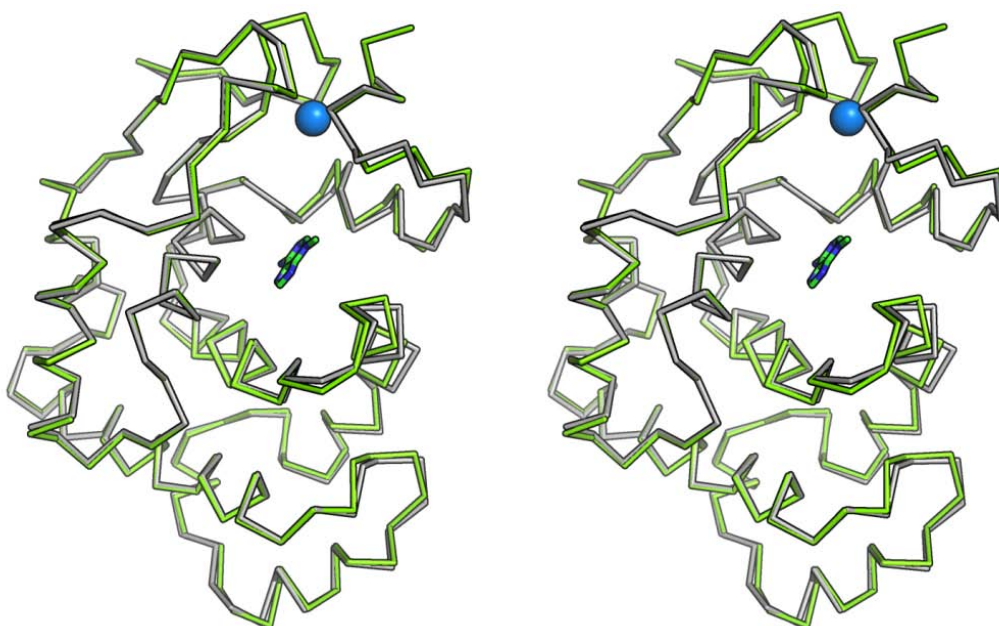
FIGURE 2.31: **Stereo view of superimposed structure of TAG/3-MeA and native TAG (stick view). The 3-MeA is superimposed to indicate TAG active site. Native TAG is shown in grey Cα trace. TAG/3-MeA complex is shown in green Cα trace. The Zn^{2+} ion is shown in blue sphere to indicate the Zn^{2+} binding site of TAG.**
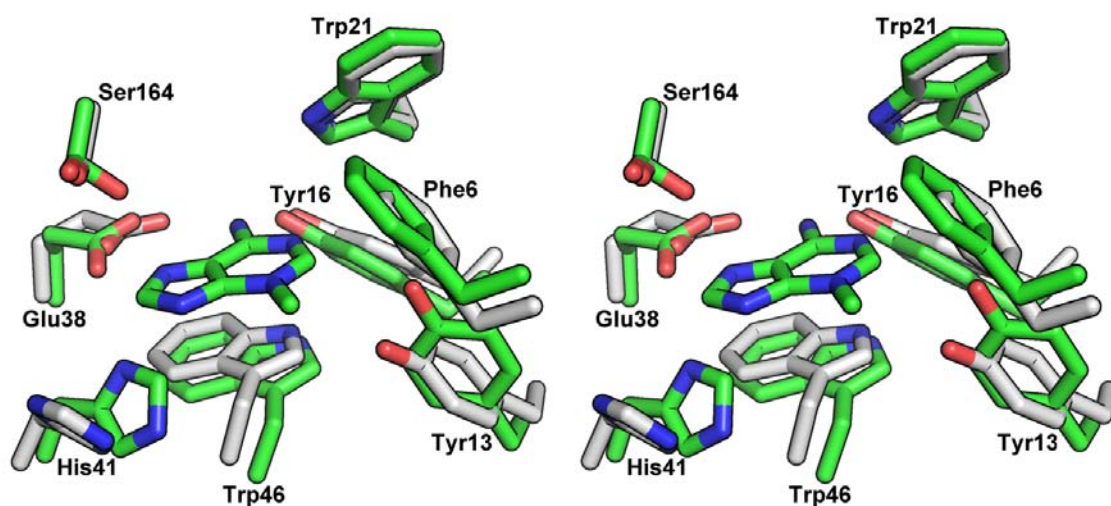
FIGURE 2.32: Stereo view of superimposed binding site of TAG and TAG/3-MeA complex structures. The native TAG residues is shown in white, the TAG/3-MeA complex residues is shown in green, Native TAG and TAG/3-MeA complex share same black labels.

2.4.3 3-methyladenine recognition of TAG

The results of fluorescence spectroscopy assay shows that *S. aureus* TAG has much

stronger binding affinity for 3-MeA than adenine. This result matches that seen with

the *E. coli* TAG (Bjelland, Bjoras et al. 1993; Drohat, Kwon et al. 2002).
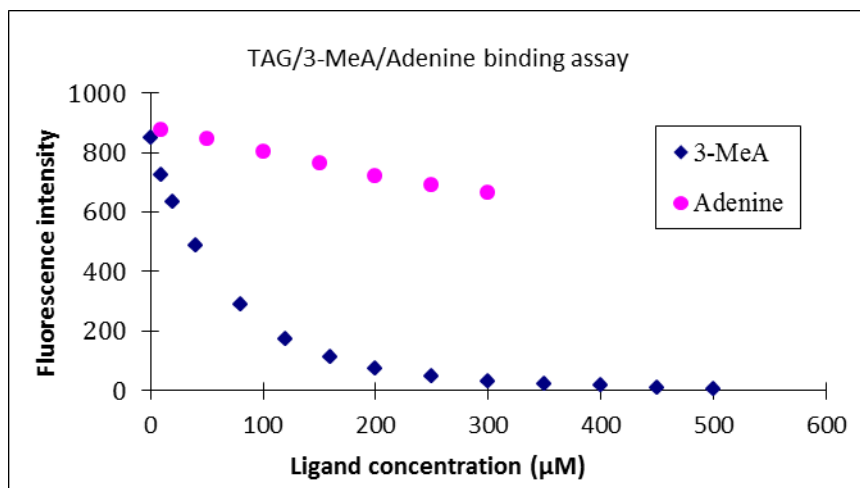
FIGURE 2.33: Tryptophan fluorescence studies of 3-MeA and noemal base adenine binding to TAG. TAG shows a 90% decreace in its Tryptophan fluorescence intensity upon binding 3-MeA (dark blue diamond) but not adenine (red dots).
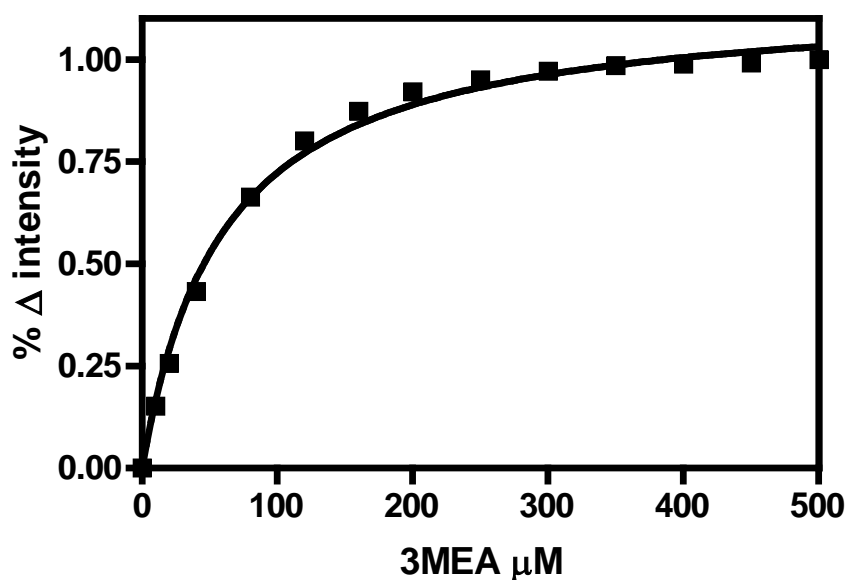
FIGURE 2.34: Reploted data for TAG upon 3-MeA binding. The K_d for 3-MeA determined from these data is 59.7 µM. 95% confidence intervals, 50.72 – 68.75 (µM).

The main difference between 3-MeA and adenine on structure is that 3-MeA has a methyl group on the ring (FIGURE 2.35). This additional methyl group on 3-MeA create a rearrangement of electron, thus make the 3-MeA base positive charged in DNA context. Although residues Glu38 and Tyr16 in 3-MeA binding site should possess similar hydrogen bonds with adenine, the interaction with Glu38 is probably different. In neutral adenine the carboxylate which is electron rich that will clash with the electrons on adenosine. This clash will be significantly reduced by the presence of the positive charge on 3-MeA, which will tend to reduce electron density on the ring nitrogen atom. The electrostatics surface potential shows the recognition site is strongly negatively (FIGURE 2.36). The negatively charged cavity binds the positively charged 3-MeA is preference over the normal base adenine. TAG uses this "surface electrostatics selection" mechanism to ensure its specificity for ligand. Such "surface electrostatics selection" effect also observed in other members of HhH DNA glycosylases, such as *H. pylori* MagIII (Eichman, O'Rourke et al. 2003). MagIII can specific binding with the methylated adenine like 3-MeA, but binding affinity for the normal base adenine is low.
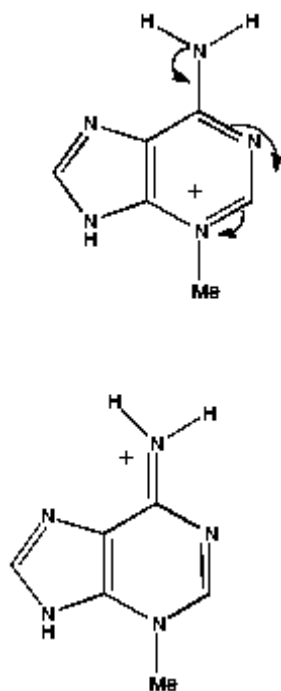
FIGURE 2.35: Chemical structure of the 3-methyladenine and normal base adenine.
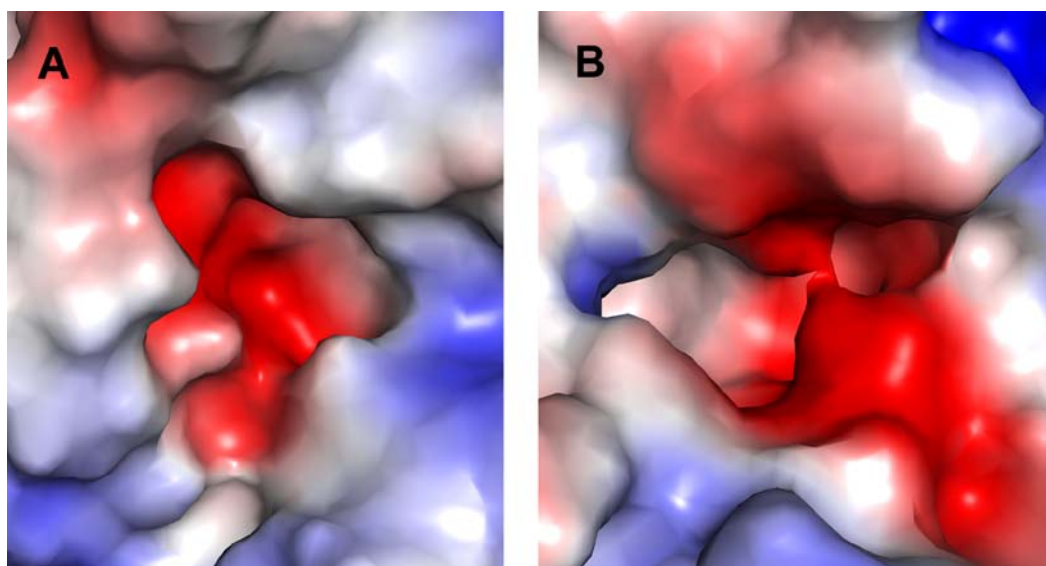
FIGURE 2.36: surface electrostatics potential of the active site of TAG [A] and MagIII [B]. The solvent-accessible surface of protein colored based on the electrostatics potential from -7 to +7 kT/e, calculated using APBS tools in PyMol™. Positive charge is shown in blue and negative charge is shown in red.

A feature of the TAG binding site is the "aromatic-rich" with stacking interactions

(Trp46). There are five aromatic residues surrounding the 3-MeA (FIGURE 2.37), Trp 21, Trp46, Tyr13, Tyr16 and Phe6. This phenomenon, aromatic residues clustering around the electron-deficient purines, is a common feature and widely observed in the bacteria and animal 3-MeA DNA glycosylases (Hollis, Ichikawa et al. 2000; Lau, Wyatt et al. 2000) (Thayer, Ahern et al. 1995). These aromatic residues are rich in electrons, and such an electron-rich setting is well suited for positively charged alkylated purines. This aromatic effect has been demonstrated to be vital for the 3-MeA recognition and binding (Hollis, Ichikawa et al. 2000; Eichman, O'Rourke et al. 2003) (Labahn, Scharer et al. 1996). Mutational studies on the aromatic residues in *S. typhi* TAG revealed that substitution of the active site aromatic residues such as Trp46Ala and Trp6Ala both resulted an approximately 10-fold drop of the base excision activity (Metz, Hollis et al. 2007). We predict that the distribution of active site surface electrostatic potential and the aromatic-rich effect are likely to enhance the 3-MeA recognition and binding for *S. aureus* TAG.
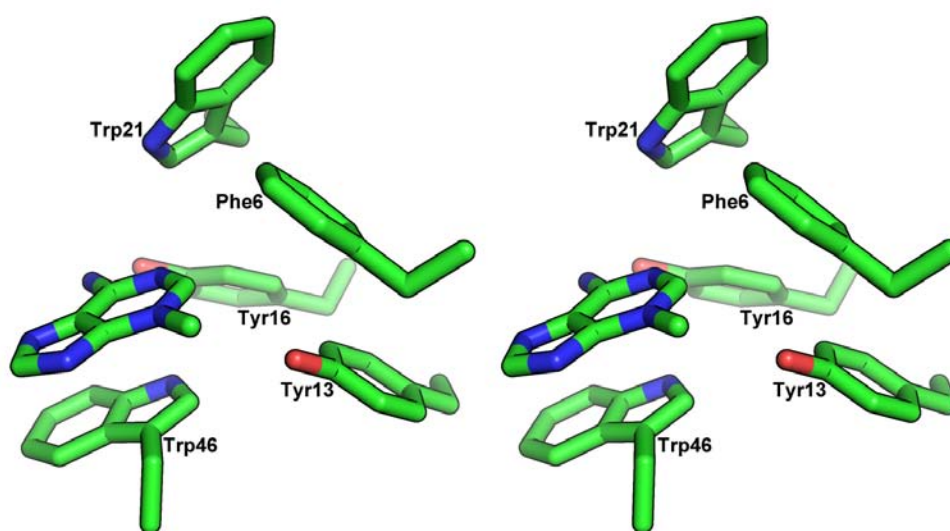
FIGURE 2.37 Stereo view of the aromatic residues around 3-MeA at the active site of TAG. All the aromatic residues around 3-MeA are labeled.

2.4.4 3-MeA recognition of TAG

3-MeA recognition in *S. aureus* TAG is mainly achieved by hydrogen bonds between the product and conserved active site residues Glu38 and Tyr16. A multiple sequence alignment shows that these two residues are highly conserved in TAG family (FIGURE 2.38). Mutational studies on these two residues of *S. typhi* TAG demonstrated the binding affinity of 3-MeA of the mutant Glu38Ala reduced affinity approximately 300-fold, whereas Tyr16Phe mutant reduced affinity only 12-fold (Metz, Hollis et al. 2007). These results are consistent with the mutational studies of *E. coli* TAG (Cao, Kwon et al. 2003) and indicate that these two residues are the key determinant for 3-MeA binding. The crystal structure of *S. aureus* TAG/3-MeA complex is consistent with the observation that Glu38 is the most important residue.
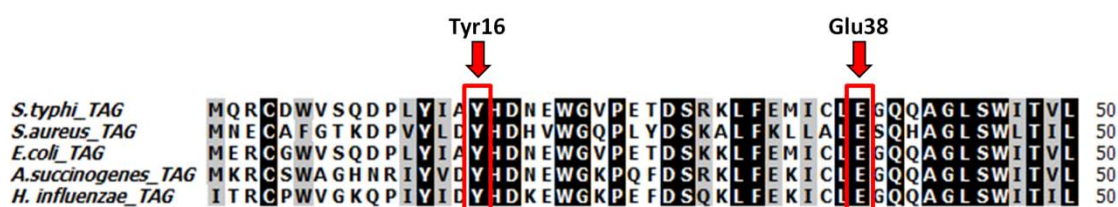
FIGURE 2.38: Sequence alignments of TAG family members. Alignment using BioEdit (Hall 1999) residues in the sequences aligned are highlight in black, residues shaded grey indicate regions of sequence homology. The red box shows the highly conserved residues Tyr16 and Glu38.
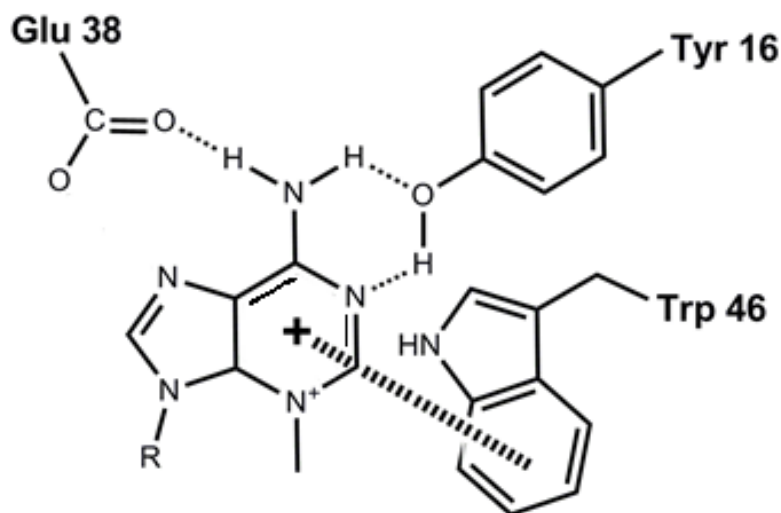
FIGURE 2.39: Interactions of 3-MeA and residues in TAG active site. R = Rest of potential interaction with DNA. This figure was generated by CHEMDRAW.

The HhH structure motif is highly conserved in HhH DNA glycosylases and considered to be the key elements for DNA binding (Doherty, Serpell et al. 1996; Hollis, Ichikawa et al. 2000; Drohat, Kwon et al. 2002). Crystal structure of these DNA glycosylases in complex with DNA such as OGG (Bruner, Norman et al. 2000) and AlkA (Hollis, Ichikawa et al. 2000) show HhH motif is the main element binds with DNA. Based on the structures of AlkA/DNA complex, a model of *S. aureus* TAG in complex with DNA was constructed for structure comparison by superposition of the DNA from the *S. typhi* TAG/DNA complex model (PDB entry: 3D4V) onto the *S. aureus* TAG/3-MeA complex structure.

The *S. aureus* TAG/3-MeA/DNA complex model shows that the modeled DNA is binds the HhH motif, and the electrostatic potential around the HhH motif is positively charged, consistent with recognition of negative charged phosphate. The electrostatics distribution is predicted to be essential for DNA binding (Eichman,

O'Rourke et al. 2003). The alkylated base binding site is close to the DNA (~ 6 Å).

Such structural architecture should contribute to the binding of the 3-MeA. TAG uses

the loop between α2 and α3 to insert the minor groove of the DNA strands for a closer

binding purpose. The loop in the HhH motif is predicted to have significant

interactions with the DNA strands. This model is also consistent with the *S. typhi*

TAG/DNA model matches that determined by Eichman group (Metz, Hollis et al.

2007) (PDB CODE: 2OFI).
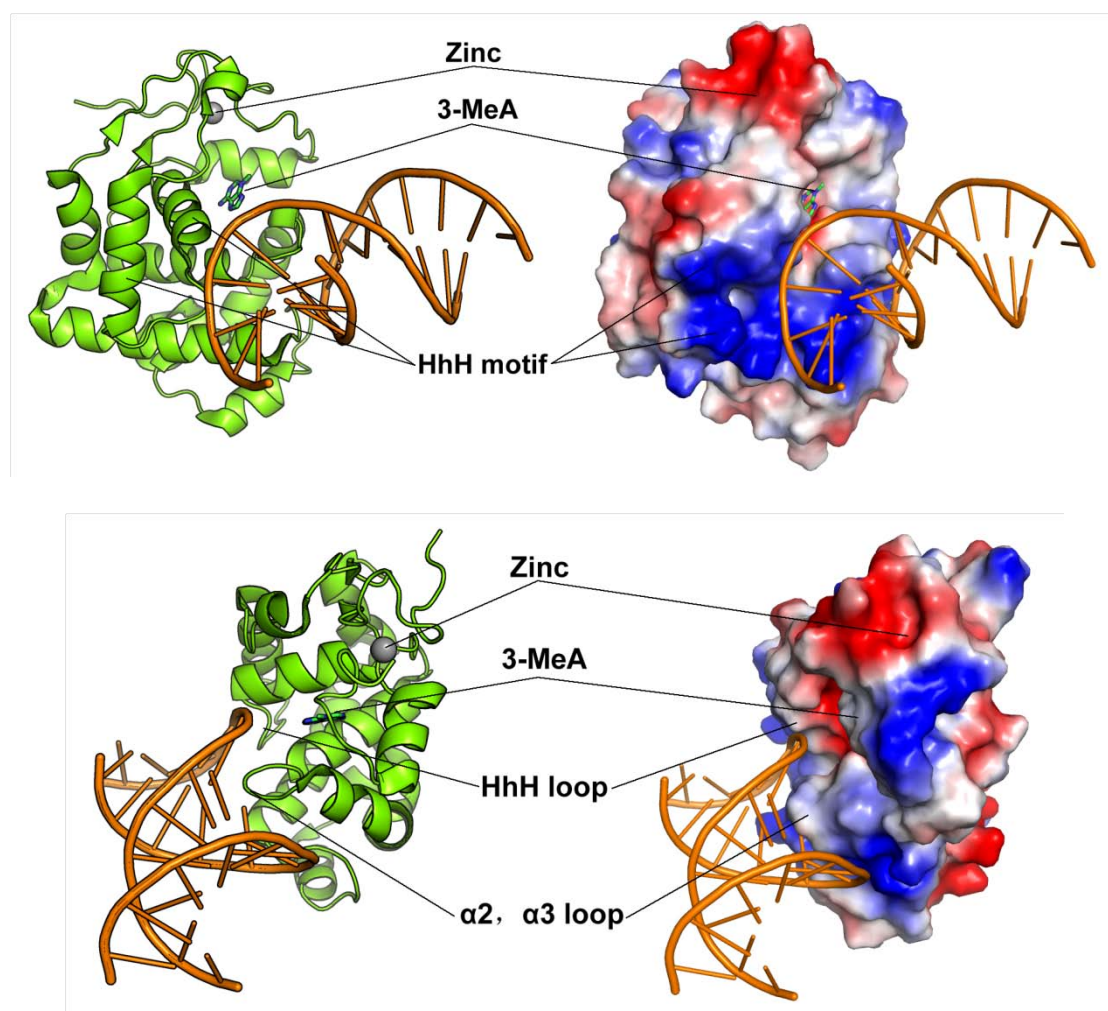
FIGURE 2.40: The structure of TAG-DNA complex model. The HhH structural motif is highlighted in blue. The remaining conserved helical domain of the HhH DNA glycosylase subfamily is shown in grey. The structures elements are unique to TAG are colored in green. DNA is shown in orange sticks. 3-MeA is shown in green and blue sticks to indicate the binding pocket of TAG.

Superimposition of the active site residues shows that the main residues that involved in ligand binding are highly conserved. His41 in *S. aureus* TAG corresponding to Gln41 in *S. typhi* TAG, while Phe6 in *S. aureus* TAG corresponding to Trp6 in *S. typhi* TAG, both are aromatic residues. This highly conserved active site setting indicates that they are using a common mechanism in 3-MeA recognition and binding.
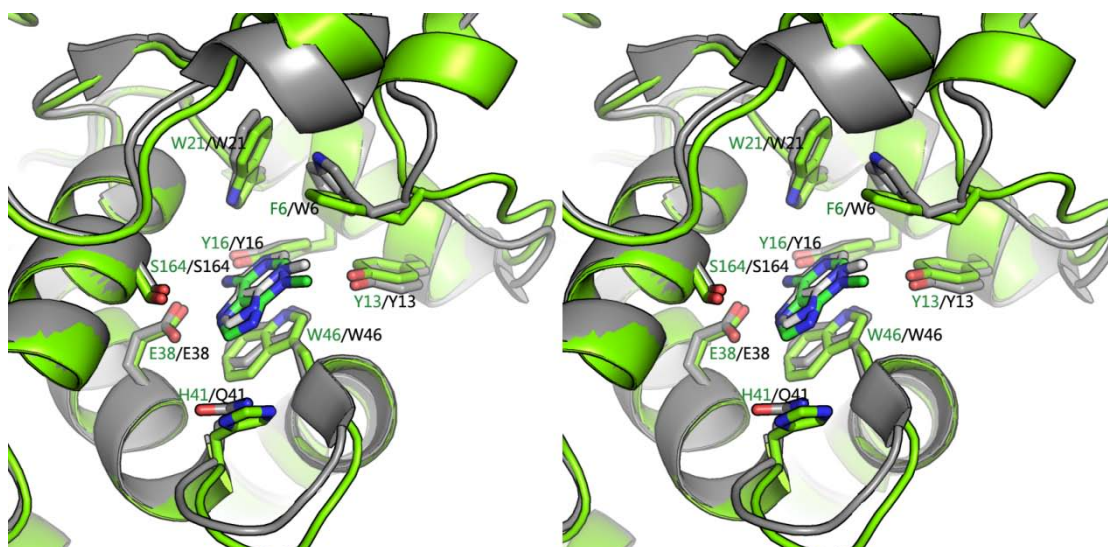
FIGURE 2.41: Stereo view of superimposed of the active site residues of *S. aureus* TAG and *S. tphi* TAG. The *S. aureus* TAG is shown in green, the *S. typhi* TAG is shown in grey. The key active site residues are labeled in green (*S. aureus* TAG) and black (*S. typhi* TAG), respectively. The 3-MeA from *S. aureus* TAG are colored in green, the 3-MeA from *S. typhi* TAG are colored in grey.

2.4.5 Future work

This study has provided a general insight into the 3-MeA binding of TAG. However, questions were left for answers. We still need to further investigate the mechanism of TAG/DNA binding. Full DNA complex and further inhibition studies and genetic knockout studies are significant for inhibitor designing.

Chapter 3

"Structural studies of Fructose 1-phosphate kinase from Methicillin-resistant *Staphylococcus aureus, a member of the ribokinase-pfkB family*"

3.1 <u>Summary</u>

Fructose 1-phosphate kinase (PFK) is a ribokinase-pfkB family enzyme that catalyzes the second step of the fructose metabolite pathway. The enzyme has been postulated to be active in *S. aureus* and related bacteria. In this chapter, the putative PFK over-expression, purification, crystallization and structure solution are described. The protein could not be expressed in soluble form using *E. coli* with IPTG induction. The soluble protein was however obtained using auto-induction at a lower temperature. Crystallization conditions for the native PFK were identified and the structure of PFK was obtained to 2.3 Å. The protein was characterized by a biochemical assay as a fructose 1-phosphate kinase. However all attempt to solve the structure of PFK in complex with fructose 1-phophate were unsuccessful due to low quality of complex crystals. A thermodynamic analysis using thermofluor method was also carried out to investigate binding interactions of different fragments to PFK.

3.2 Introduction

3.2.1 Fructose, glucose and glycolysis

Sugars are vital for cells because they are a source of energy and carbon. Sucrose, lactose, glucose, galactose and fructose are commonly used in the energy flux system (Balakrishnan and Van den Broeck 2005) Among these sugars, glucose is the most important one because it is the main energy source for most organisms (Fairclough and Houston 2004). Fructose is a structural isomer of glucose and is used in the metabolism. Ribulose, fucose and xylulose are relatively rare and are only processed by some specialized microorganisms (Staudacher, Altmann et al. 1999; Carretero-Paulet, Ahumada et al. 2002). In nature, fructose is commonly found at high levels in various varieties of fruit, in honey and in some root vegetable (e.g. yams or sweet potatoes) (Park and Yetley 1993). Fructose is the sweetest of all simple sugars (Binet, Rager et al. 1998; Ehringer, Chiang et al. 2001). Nowadays the overall consumption of fructose is increasing because of its used as high-fructose corn syrup (HFCS) in the food industry as a sweetener for candies, cakes and drinks (Luz, Rodrigues et al. 2008)

After sugars are transported into the cell, they are phosphorylated by specific sugar kinases (Gschaedler, Thi Le et al. 1994). The addition of negatively charged phosphoryl groups prevents the leakage of neutral sugars through the cell membrane,

trapping them inside the cell, in preparation for further digestion by catabolic or anabolic pathways (Crouzoulon 1973; Fujisawa, Riby et al. 1991). The main catabolic pathway is called glycolysis, with glucose as the key sugar source (Van Rooyen, McCarthy et al. 2002). In the glucose pathway, glucose 6-phosphate (G6P) is the product of the first phohsphorylation step by hexokinase (Bork, Sander et al. 1993). G6P is converted to fructose 1, 6-phosphate (F16P) via phosphoglucose isomerase and fructose 6-phosphate kinase (Selig, Xavier et al. 1997). This is the committed step in the glycolysis process, because the metabolite fructose 1, 6-phosphate is the key product for further glycolysis and fructose 6-phosphate kinase is the limiting enzyme (Draborg, Villadsen et al. 1999; Hansen, Arnfors et al. 2007). Following a series of chemical reactions, F16P is eventually converted to Acetyl-CoA by a series of enzymes and finally enters the tricarboxylic acid cycle (TCA-cycle). This process is shown in FIGURE 3.1 below.
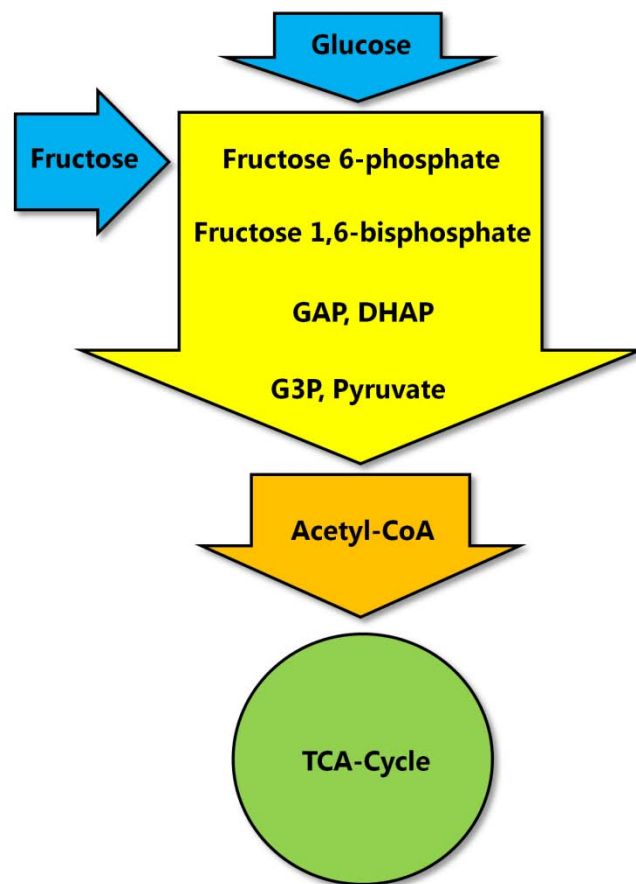
FIGURE 3.1: Schematic view of the glucose glycolysis pathway.

3.2.2 Fructolysis and fructose 1-phosphate pathway

Some bacteria utilize fructose instead of glucose as their main sources of energy and carbon. In these cases, fructose is utilized by an alternative metabolic pathway that avoids the rate limiting enzyme (fructose 6-phosphate kinase) but still produces acetyl-CoA (Papadopoulos and Roe 1957) (FIGURE 3.1). The fructose metabolism usually occurs in the liver using a unique active enzyme system (Van Schaftingen, Detheux et al. 1994). In this fructose metabolic pathway, the first step is carried out by fructokinase (FK), which converts fructose into fructose 1-phosphate (F1P) (Gunther, Sillero et al. 1967). F1P is not only an intermediate in this pathway but also a

stimulator of glucokinase. F1P specifically binds to the regulatory protein of glucokinase, thus preventing it from inhibiting the enzyme, The activity of glucokinase is affected by an inhibitory binding protein, the protein binding affinity for glucokinase is enhanced by binding F6P, and decreased by binding with F1P (Van Schaftingen, Detheux et al. 1994). The second enzyme in fructose metabolite pathway is fructose 1-phosphate aldolase, which break F1P down to D-glyceraldehyde and Dihydroxyacetone-phosphate for further chemical reaction (Hers and Kusaka 1953). In this case, fructose is catabolized directly through the fructose 1-phosphate pathway. This direct metabolic pathway has only been discovered in the liver and muscles (Hagopian, Ramsey et al. 2005).

Fructose can also enter the glucose pathway (Niculescu, Veiga-da-Cunha et al. 1996). In this alternative route shown in FIGURE 3.2, the second step is replaced by an ATP-dependent phosphorylation reaction of fructose 1-phosphate by fructose 1-phosphate kinase (1-PFK) that yields the critical metabolite in the glucose pathway, fructose 1, 6-bisphosphate (Davies, Detheux et al. 1990). In this process, fructose acts as a supplement for glucose to some extent because fructose can also be phosphorylated to F16P by the sugar kinases such as fructokinase and fructose 1-phosphate kinase (Selig, Xavier et al. 1997). Both fructose metabolite pathways are essential for the survival of *S. aureus* (Kizaki and Sawada 1997).
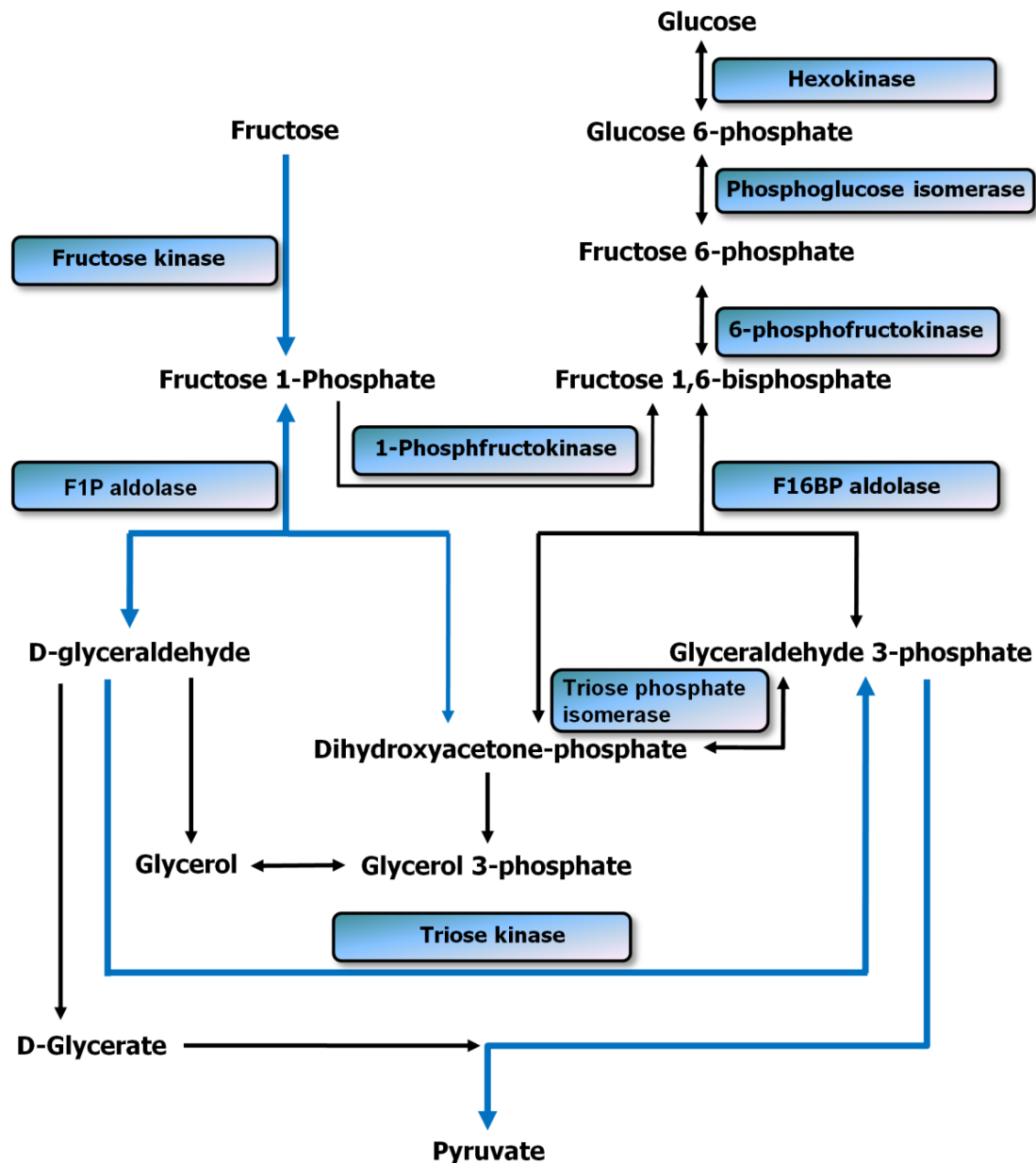
FIGURE 3.2: Schematic views of the Fructose and the associated glucose pathway. The fructose metabolism pathway is highlighted in blue arrows. Key enzymes involved in fructose metabolism are indicated by blue box. Picture adopted from (Hagopian, Ramsey et al. 2005).

3.2.3 Ribokinase-pfkB family

Kinases that catalyze sugar phosphorylation are called sugar kinases. All of the sugar kinases can be classified into three major distinct nonhomologous superfamilies.

The hexokinase family contains many eukaryotic and prokaryotic sugar kinases with different specificities. The second is the galactokinase family (GHMP kinase family), which contains several bacterial and yeast galactokinases, mevalonate kinase, phosphomevalonate kinase and homoserine kinases. The third family, ribokinase family, comprises bacterium fructokinases, prokaryotic and eukaryotic ribokinases, the minor isoform fructose 6-phosphate kinase, fructose 1-phosphate kinase, tagatose 6-phosphate kinase and a new member inosine-guanosine kinase (Bork, Sander et al. 1993). Members from these three distinct families of sugar kinases appear to have a different 3D fold (FIGURE 3.3).
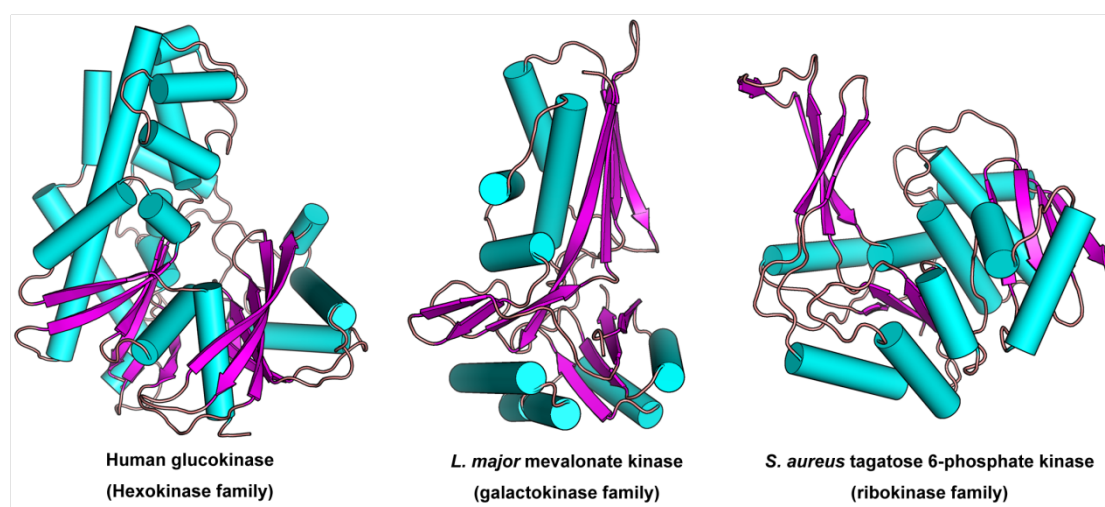
FIGURE 3.3: Typical folds of three distinct kinase families. Including human glucokinase from hexokinase family, L. major mevalonate kinase from galactokinase family and *S. aureus* tagatose 6-phosphate kinase from ribokinase family.

The amino acid sequence search suggests that the putative fructose 1-phosphate kinase from *S. aureus* is a member of the ribokinase-pfkB family of carbohydrate kinase. The most closely related proteins suggested by a BLAST search are

fructokinase, phosphotagatokinase, ketohexokinase, adenosinekinase and the minor fructose 6-phosphate kinase. Multiple sequence alignment shows that the putative *S. aureus* PFK has the conserved sequence motifs I and II (FIGURE 3.4) of the ribokinase family (Sigrell, Cameron et al. 1998; Li, Kwok et al. 2002; Zhang, Dougherty et al. 2004). The putative *S. aureus* PFK exhibits these characteristics to share a similar overall fold with the other members of the ribokinase-pfkB family.

FIGURE 3.4: Multiple sequences alignment of 4 ribokinase family enzymes. Sequences are the putative *S. aureus* PFK (1PFK_STAAU), D-tagatose-6-phosphate kinase from *S. aureus* (LACC_STAAU), 6-phosphofructokinase from *Escherichia coli* (6-PFK_ECOLI) and human ribokinase (RBKS_HUMAN). Identical residues in the sequences aligned are highlighted in black, and residues shaded grey indicate regions of sequence homology. The two red boxes indicate the conserved motifs 1 and 2, which have been identified previously as the potential ATP/PPi binding motif for the ribokianse family. Sequence alignment was carried out using BioEdit (Hall 1999) and DALI (Holm and Sander 1993) server.
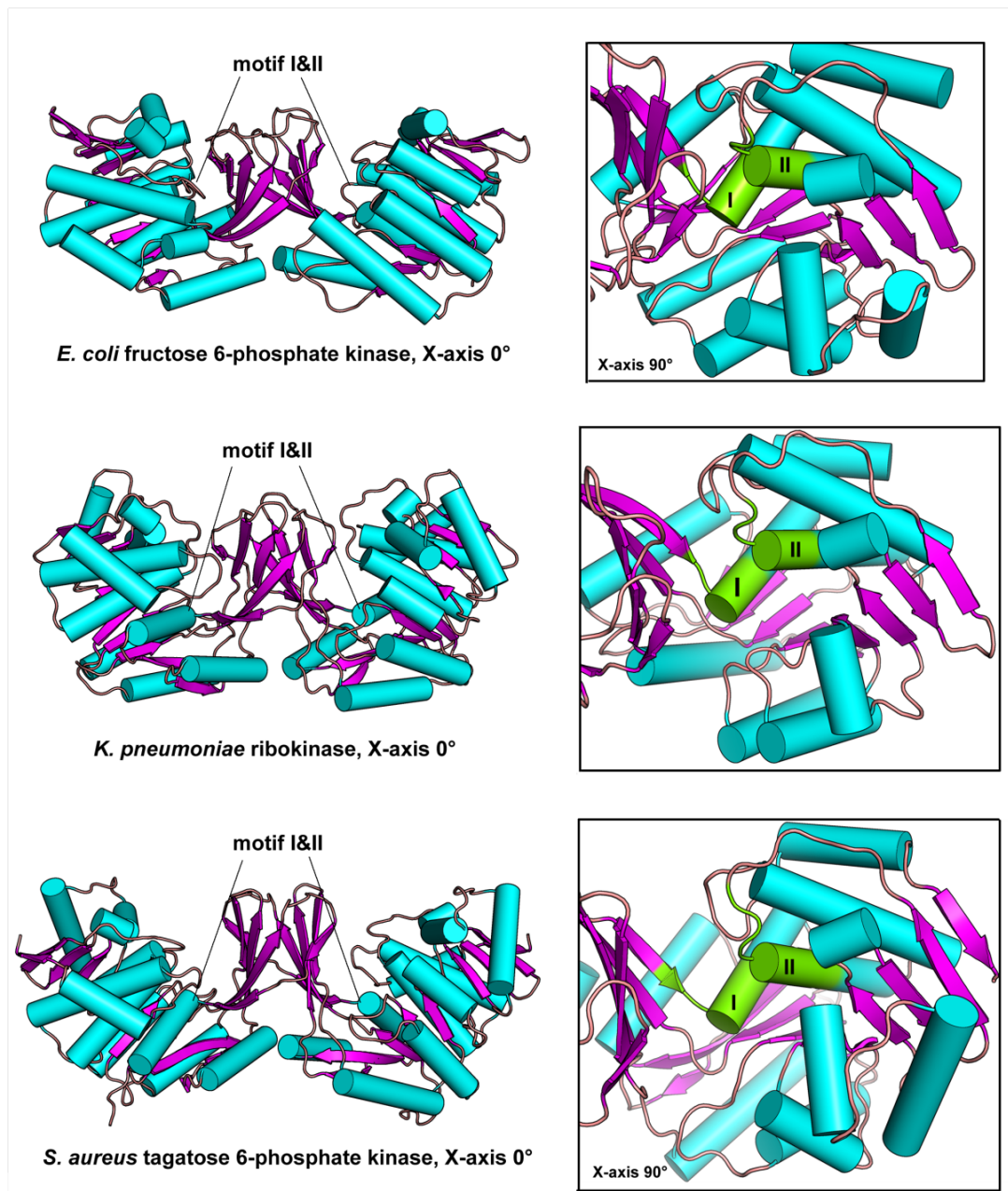
FIGURE 3.5: Localization of conserved structure motifs I and II in ribokinase family enzymes.

3.2.4 Fructose 1-phosphate kinase (1-PFK) from *S. aureus*

Fructose 1-phosphate kinase (systematic name ATP: D-fructose 1-phosphate 6-phosphotransferase (E.C. 2.7.1.56)) is also referred to as 1-phosphofructokinase (1-PFK). This ATP-dependent enzyme is crucial for the alternative route of fructose

metabolites and for fructose entry into the glucose pathway. This enzyme was first identified in *Bacteroides symbiosus* (Reeves, Warren et al. 1966) and later in other organisms such as *Pseudomonas putida* and *E. coli* (Bang, Baumann et al. 1977; Orchard and Kornberg 1990). Substrates of 1-PFK and other members of ribokinase-pfkB family are quite similar (FIGURE 3.4), with only minor differences on the location of the hydroxyl group of the sugar moieties for enzymes such as tagatose 6-phoshate kinase (LacC) (E.C 2.7.1.144) and fructose 6-phosphate kinase (E.C 2.7.1.11). The reactions of these substrates are similar, the phosphate group is added to a primary hydroxyl group attached to a five membered ring, generating biphosphate products such as fructose 1, 6-bisphosphate.
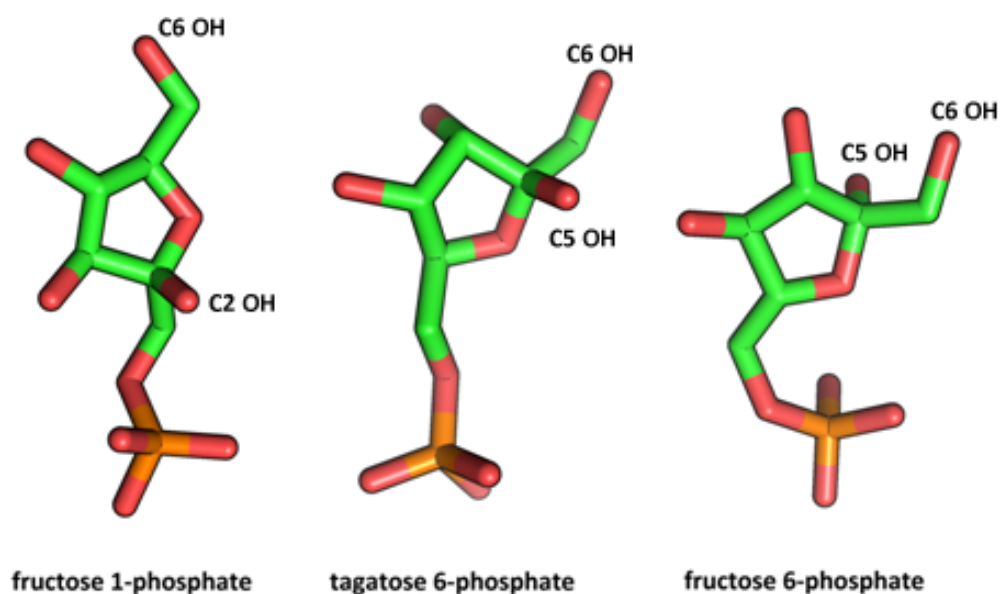
FIGURE 3.6: cartoon representation of the substrates for ribokinase family members.
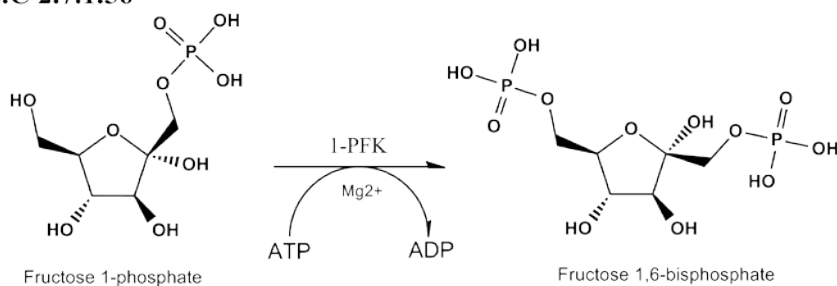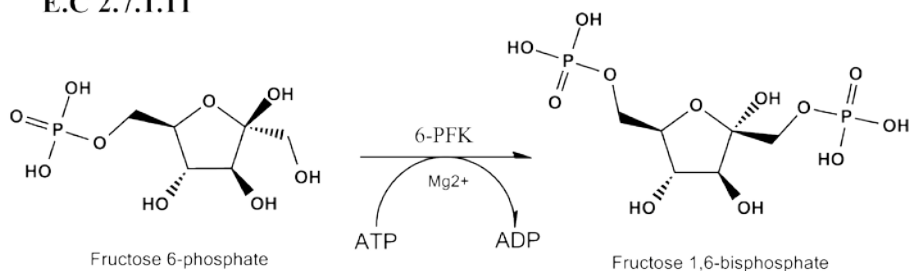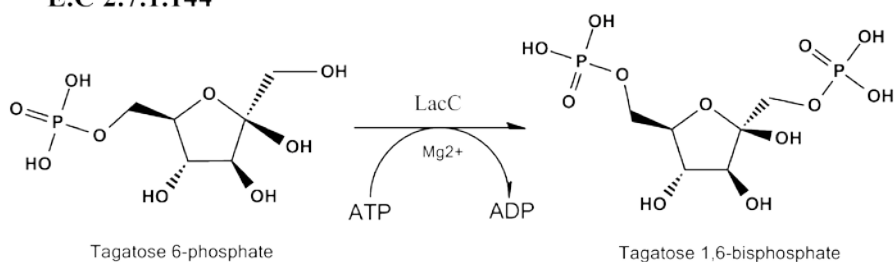
FIGURE 3.7: The reactions catalyzed by enzymes from ribokinase-pfkB family. fructose 1-phosphate kinase (E. C 2.7.1.56), fructose 6-phosphate kinase (E.C 2.7.1.11) and tagatose -6 phosphate kinase (LacC) (E.C 2.7.1.144).

There was no structural information available on the structure of fructose 1-phosphate kinase when the project started. 2D gel electrophoresis in Peter Coote's laboratory (University of St Andrews) revealed that the putative *S. aureus* PFK is up-regulated in MRSA252 and down-regulated in MSSA476. Structural studies on this enzyme will help us better understand the catalytic mechanism of this enzyme, and may contribute

97

to drug design.

3.3 <u>Materials & Methods</u>

3.3.1 Over-expression and purification of PFK

IPTG induction and Auto-induction

Attempts to express PFK using IPTG induction were unsuccessful since all the protein was recovered in the insoluble fraction, even when the expression was carried out at lower temperatures (16°C and 25°C). Next, protein over-expression was attempted using the auto-induction media as described by Studier. (Studier. 2005).The PFK plasmid was firstly transformed into *Escherichia coli* BL21 (DE3) cells (Novagen) and plated onto ampicillin agar plates. Single colonies were grown in 10 ml LB medium overnight, supplemented with 100 µg/ml ampicillin. Then 1ml of a 10 ml overnight culture was used to inoculate 50 ml of LB and cells were harvested, after overnight incubation at 37 ℃, at 2000 X g and re-suspended in 20 ml PBS. 500 ml of auto-induction growth medium in a 2L baffled flasks, supplemented with 100 µg/ml ampicillin, was inoculated with 5 ml re-suspended cells and grown at 37 ℃, with shaking at 300 r.p.m for 4 hours to start bacterial growth. The temperature was then lowered to 25 ℃ and left for 48 hours, allowing bacterial subsequent self-induction of protein expression and growth to reach saturation (OD_{600}~5.0). Cells were then harvested at 10500 x g and then re-suspended in 50 mM Tris-HCl pH 7.75, 150 mM NaCl and 15 mM imidazole.
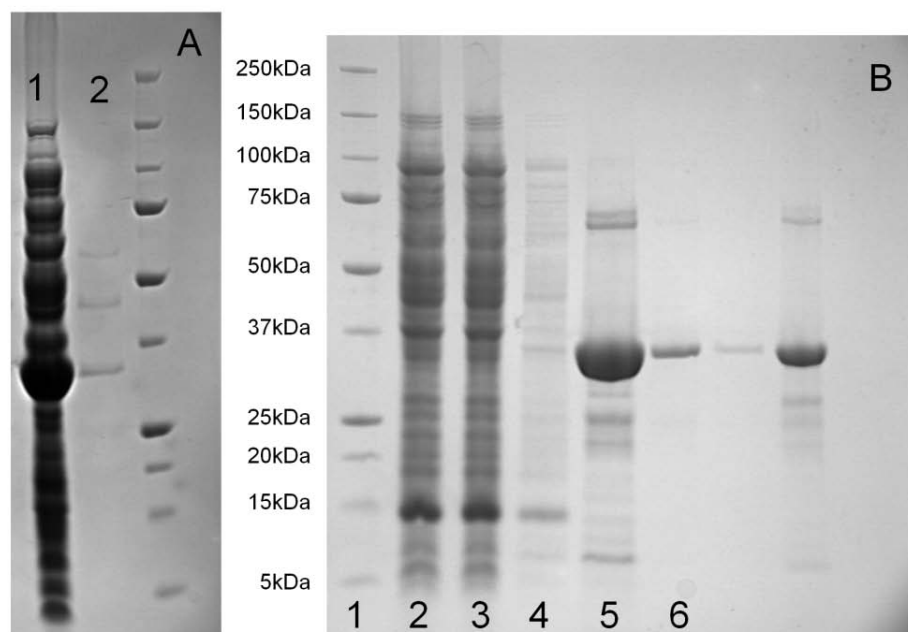
FIGURE 3.8: Comparison of IPTG-induced and auto-induced over-expression of PFK.
Coomassie Blue stained SDS-PAGE gels of *S. aureus* PFK. [A.1] crudes flow through of TPTG
induction [A.2] first elution of IPTG induction. [B.1]protein marker. [B.2] crudes flow through
first part. [B.3] crudes flow through second part. [B.4]wash flow throgh. [B.5] first elution from
nickel column. [B.6] second elution.

Purification

Soluble protein was firstly extracted by incubation with 100 µg/ml Lysozyme and 20

µg/ml DNase I (Sigma) before lysis, followed by two passes through a Constant cell

disruptor (Constant systems). The soluble and insoluble fractions were separated by

centrifugation for 45 minutes at 75500 x g. The same purification procedure was used

for PFK purification as described earlier for TAG (Section 2.3.1) except that sodium

phosphate buffer (11.25 mM NaH_2PO_4, 38.75 mM Na_2HPO_4) was used in place of

Tris-HCl. Eluted protein was incubated with 1 ml of 2 mg/ml tobacco etch virus

protease (TEV) (approximate ratio 20:1 protein: protease) to remove the polyhistidine

tag at room temperature in buffer containing 500 mM NaCl, 2 mM DTT and 50 mM

99

phosphate buffer, pH7.75 for 4 hours to remove the high concentration imidazole. The progress of cleavage was checked by sodium dodecyl sulphate polyacrylamide gel electrophoresis (SDS-PAGE). Although TEV protease was able to cleave the His-tag on PFK, it took much longer time than expected (typically <5 hrs). The protein had to be incubated at room temperature for over 5 days changing the TEV protease and dialysis buffer once a day. Although an optimization attempt on cleavage condition was performed by varying buffer, salt concentration, pH, temperature and glycerol, the best result was only 50 % cleavage after three days of incubation. (FIGURE 3.9)
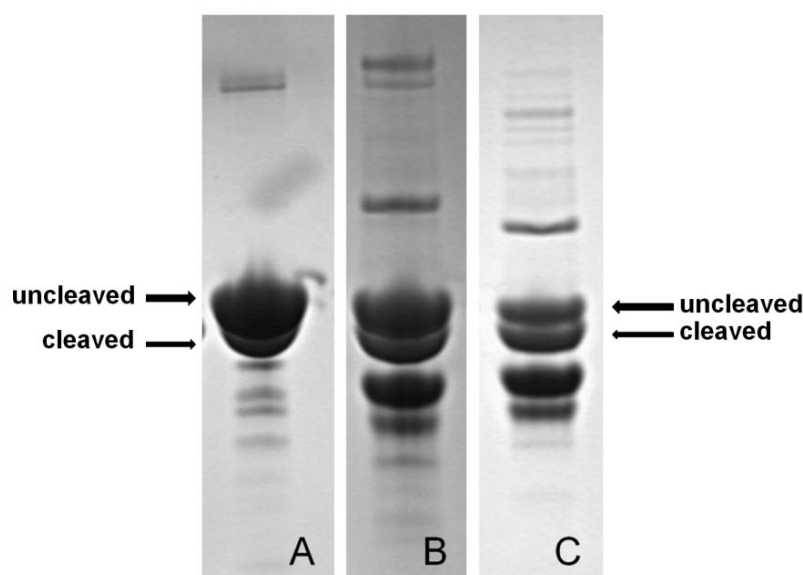
FIGURE 3.9: Coomasie Blue stained SDS-PAGE of PFK TEV protease cleavage in three days. [A] after 12 hours at 4 ℃; [B] after 36 hours at 4 ℃; [C] after 60 hours at 4 ℃

Although the His-tag was never fully cleaved, the second nickel column was able to separate the tagged and untagged protein. The protein-TEV mixture was passed through a 0.22 μM syringe filter membrane (Millipore) and a second Ni-NTA column to remove any non-cleaved protein, His-tag and TEV protease. Then the flow through

was concentrated to approximately 5 mL before further purification by size exclusion gel filtration. Any precipitant was removed by centrifugation at 35000 x g for 10 min (4℃, Beckman Avanti J20-XP JA25.50 rotor). Sample was applied on a Superdex™ 200 size exclusion chromatography column (Amersham Biosciences). Each step of purification was monitored by SDS-PAGE. After the gel-filtration step, the protein was judged to be pure by Coomassie™ Blue-stained gels and their integrity was confirmed by mass spectrometry using University of St Andrews mass spectrometry service. In total it was estimated 16 mg pure PFK native protein was obtained from 4 L of cell culture. According to the results of Pre-Crystallization Test (PCT), the protein was then concentrated to 12 mg/ml and 6 mg/ml and dialyzed into 150 mM NaCl, 20 mM Tris-HCl, pH 7.75 prior to crystallization. Some of protein was flash-frozen in liquid nitrogen for long term storage. Buffer used in each step were detailed in TABLE 3.1.

Protein View

Match to: **Q6GIU3** Score: **1160** Expect: **6.4e-110**
Putative phosphofructokinase - Staphylococcus aureus (strain MRSA252)

Nominal mass (M_r): **32639**; Calculated pI value: **4.66**
NCBI BLAST search of Q6GIU3 against nr
Unformatted sequence string for pasting into other applications

Taxonomy: Staphylococcus aureus subsp. aureus MRSA252

Sequence Coverage: **65%**

Matched peptides shown in **Bold Red**

```
  1 MIYTVTFNPS IDYVIFTNDF KIDGLNRATA TYKFAGGKGI NVSRVLKTLD
 51 VESTALGFAG GFPGKFIIDT LNNSAIQSNF IEVDEDTRIN VKLKTGQETE
101 INAPGPHITS TQFEQLLQQI KNTTSEDIVI VAGSVPSSIP SDAYAQIAQI
151 TAQTGAKLVV DAEKELAESV LPYHPLFIKP NKDELEVMFN TTVNSDADVI
201 KYGRLLVDKG AQSVIVSLGG DGAIYIDKEI SIKAVNPQGK VVNTVGSGDS
251 TVAGMVAGIA SGLSIEKAFQ QAVACGTATA FDEDLATRDA IEKIKSQVTI
301 CVLDGE
```

FIGURE 3.10: gel-filtration elutions profiles and SDS-PAGE of the putative *S. aureus* PFK.

Binding buffer	**500 mM NaCl, 2 mM DTT, 50 mM phosphate buffer, pH 7.75 (11.25 mM NaH$_2$PO$_4$, 38.75 mM Na$_2$HPO$_4$), 10 mM imidazole**
Wash buffer	**500 mM NaCl, 2 mM DTT, 50 mM phosphate buffer, pH 7.75 (11.25 mM NaH$_2$PO$_4$, 38.75 mM Na$_2$HPO$_4$), 35 mM imidazole**
Elution buffer	**500 mM NaCl, 2 mM DTT, 50 mM phosphate buffer, pH 7.75 (11.25 mM NaH$_2$PO$_4$, 38.75 mM Na$_2$HPO$_4$), 500 mM imidazole**
Dialysis buffer	**500 mM NaCl, 2 mM DTT, 50 mM phosphate buffer, pH 7.75 (11.25 mM NaH$_2$PO$_4$, 38.75 mM Na$_2$HPO$_4$), 10% glycerol, 1 mM EDTA**
Gel-filtration buffer	**150 mM NaCl, 50 mM Tris-HCl buffer, pH 7.75**

TABLE 3.1: Buffers used in each step of *S. aureus* PFK purification.

3.3.2 Crystallization and optimization of *S. aureus* PFK

Purified PFK protein was concentrated to 12 mg/ml and 2mM DTT was added prior to screening for crystallization conditions. The sitting drop method was employed for crystal screening, using a drop size of 0.3 μl, containing 0.15 μl protein and 0.15 μl precipitant, against 80μl screen buffer. The nano-drop crystallization robot (Cartesian Honeybee) from Hamilton-Thermo Rhombix system was also used to perform this screening. The crystal screens employed for this initial crystal screening included JMac, Nextal-The Classics, Nextal-JCSG, Nextal-PEGs (Hampton Research). All the sitting drop trials were incubated at 20 °C. Initial crystals were obtained from Hampton Classics screen condition 87 [0.2 M Ammonium acetate, 0.1M Sodium citrate tribasic dihydrate pH 5.6, 30% w/v PEG 400] and JMAC screen condition 74 [0.1 M HEPES pH 7.5, 2.0M Ammonium Sulphate, 0.2M Lithium Sulphate] after 2 days incubation. An optimization screen around these conditions was carried out to produce better quality crystals suitable for X-ray diffraction. Some large crystals were

observed in an optimized condition containing 0.2 M Ammonium acetate, 0.1M

Sodium citrate tribasic dihydrate pH 5.6, 28% w/v PEG 400, using a drop with 3 µL

protein and 3µL precipitant equilibrated against a reservoir of 100 µL buffer. The

diffraction quality was tested in house using the Rigaku 007 rotating anode X-ray

generator. Crystals were cryo-protected by adding 20% – 25% glycerol to the buffer

above before being flash-frozen for synchrotron source data collection. The crystals

are shown in FIGURE 3.11
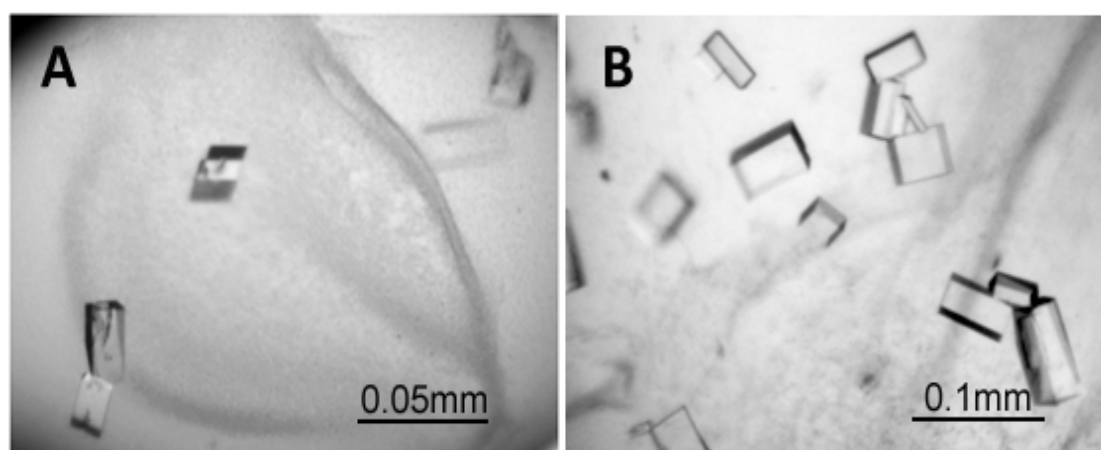
FIGURE 3.11: *S. aureus* **PFK crystals. [A] Native PFK crystals grown in a nano drop from Hampton Classics Screen 87, 0.2 M Ammonium acetate, 0.1M Sodium citrate tribasic dihydrate pH 5.6, 30% w/v PEG 400. [B] PFK crystals after optimization at similar condition.**

In order to produce complex crystals of PFK with its substrate and co-factor,

co-crystallization method was attempted using 5 mM substrate F1P and 5 mM

AMP-PNP. AMP-PNP, an analogue of ATP, is resistant to hydrolysis because the O

atom between γ- and β-phosphate is replaced by N atom. F1P and AMP-PNP were

both dissolved in PFK gel-filtration buffer. The protein and ligands solution were

mixed gently and pre-incubated for 6 hours at 4°. The protein and ligands mixture was

then centrifuged at 35000 x g for 2 min (Eppendorf Centrifuge 5415D) to remove any

insoluble compounds and precipitated protein. Crystallization of PFK in complex with F1P and AMP-PNP was attempted using sitting drop method and screening buffers as described in Chapter 2. Crystals were appeared after approximately one week. The best crystals appeared in a Hampton PEGs Screen 27 [0.2M Sodium acetate trihydrate, 20 %w/v polyethylene glycol 3350]. These crystals were then optimized to produce larger crystals (FIGURE 3.12)
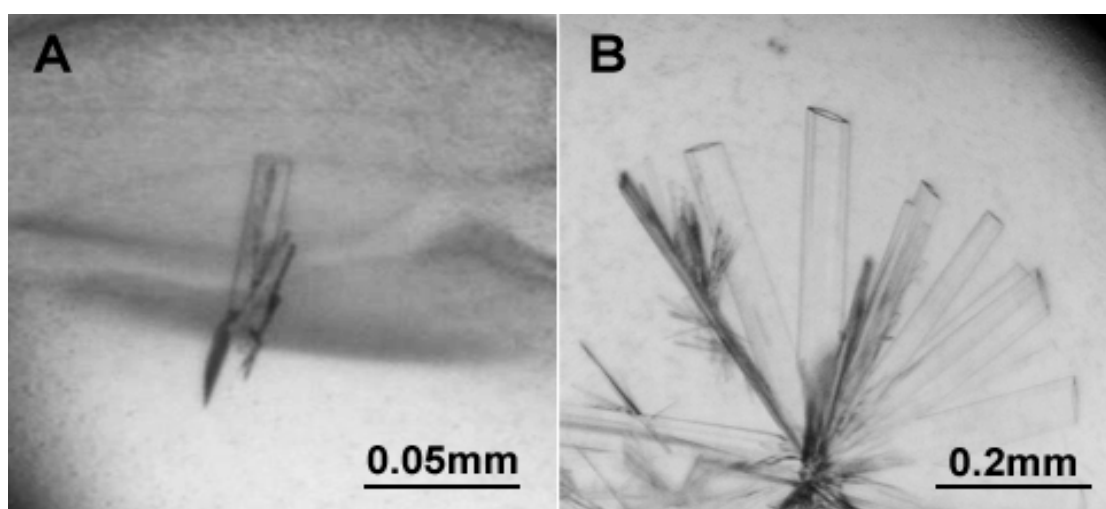
FIGURE 3.12: *S. aureus* **PFK complex crystals. [A] PFK complex crystals grown in a nano drop from Hampton PEGs Screen 27, 0.2M Sodium acetate trihydrate, 20 %w/v polyethylene glycol 3350. [B] PFK complex crystals after optimization under identical conditions.**

3.3.3 Data collection and initial processing

Native PFK

Crystals were cryo-cooled in liquid nitrogen 25% PEG 400 as cryo-protectant. A 2.2 Å dataset was collected on native PFK crystals at ESRF Beam-line BM14. 180 images were collected using an exposure time of 10 seconds and a crystal to detector distance of 280 mM. The wavelength used for data collection was 0.976 Å. An

example of the diffraction pattern obtained is shown in FIGURE 3.13. The spots

appeared to be split, but initial processing using MOSFLM seemed to work well,

suggesting that the crystal lattice belonged to the P222 Laue group with cell

dimensions of a=85.01 Å, b=160.26 Å, c=40.74 Å; $\alpha=\beta=\gamma=90.00°$. Data were

processed and integrated using these parameters and then merged in SCALA.

Program POINTLESS suggested that the space group $P2_12_12_1$. Data were indexed in

this space group and merged using SCALA. X-ray data collection statistics are

presented in FIGURE 3.13 and TABLE 3.2, respectively.
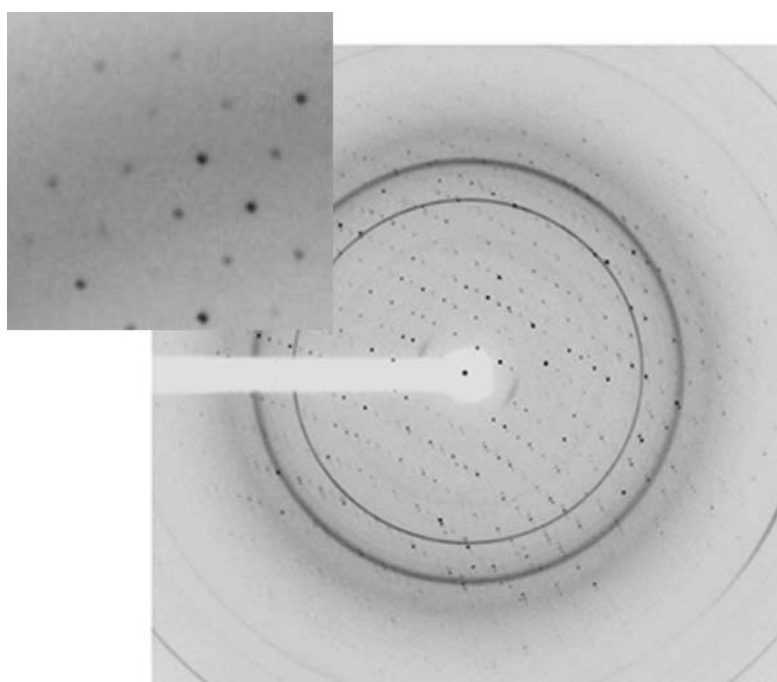
**FIGURE 3.13 X-ray diffraction pattern of *S. aureus* PFK crystals at the ESRF beamline BM14.
The resolution at the edge of the detector is 2.26 Å.**

Data collection	Native PFK
Wavelength (Å)	0.976
Resolution (Highset Shell) (Å)	19.7 - 2.30 (2.36-2.30)
Unit cell	a=85.01, b=160.26, c=40.74; α=β=γ=90.00
Space Group	$P2_12_12_1$
Unique reflections	24100
Average redundancy	4.8 (4.8)
Completeness (%)	99.5(94.5)
R_{merge}	0.09(0.42)
$I/\sigma (I)$	12.8(3.7)

TABLE 3.2 Summary of data collection statistics for native PFK crystal collected at the ESRF

PFK complex crystal data collection

The in house X-ray generator (Rigaku-MSC Micromax-007 HF) system was used to screen the optimized PFK crystals in complex with F1P and AMP-PNP. The crystal was cryo-protected by adding 25% glycerol to the mother liquor before diffraction screening, 360 images were collected using 45 seconds exposure time with 0.5° oscillation angle. The wavelength and crystal to detector distance used in data collection were 1.5418Å and 70 mM, respectively. Unfortunately, as can be seen from the diffraction pattern, the spots are smeared in some area. As a result, the dataset could not be processed using either HKL2000 or MOSFLM. Despite several attempts, no higher or better diffraction could be obtained with PFK complex crystals.
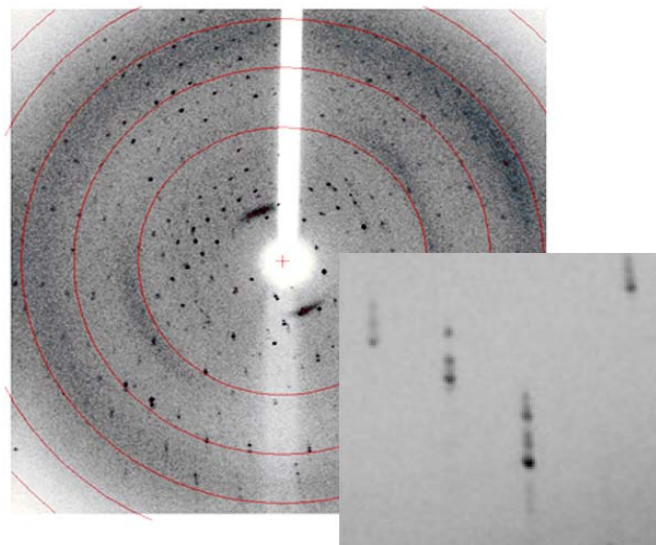
FIGURE 3.14: X-ray diffraction pattern of *S. aureus* PFK crystals using an in-house X-ray generator system (Rigaku-MSC Micromax-007 HF). The resolution at the edge of the detector is 3.2 Å.

3.3.4 Data processing, structure solution and model refinement

Native PFK data set

The native PFK dataset was indexed and merged in space group $P2_12_12_1$. The Mathews coefficient calculation suggested that each asymmetric unit contained two molecules, with a solvent content of 48%. Molecular replacement was attempted because a similar structure from another organism was found with 41% sequence identity in the PDB (fructose 1-phosphate kinase from *Bacillus halodurans*. PDB entry: 2ABQ). Using this structure as the search model, the program PHASER from CCP4 program suite was able to give a partial solution with rotation function Z of 12.1 and translation function Z of 17.4 as the starting model.

The initial solution from PHASER was improved using an in-house procedure developed by Dr Kenneth Johnson, which took the search models, and then generated

multiple new models. These models were subjected to the simulated annealing process in CNS, and the regions where the atomic coordinates of the models converged were used as a starting point for new model, the process was iterative. This method was used to build as much of the model as possible, resulting in 374 residues. Examination of the maps produced by this model in program Xfit showed a domain shift between the putative *S. aureus* PFK and 2ABQ structure. The domain was fitted using the real space rigid body refinement procedure in Xfit and SCRWL was used to correct the side chains of the model. Cycles of refinement in REFMAC5 and Xfit from CCP4 program suite were subsequently used to produce a starting model (R_{factor} = 0.37). From this initial starting model, I refined the structure using WinCoot and REFMAC5 to refine and build the final model. Water molecules were added to the model automatically using ARP/wARPs. The final model was validated by a web-based protein structure validation service "MolProbity" (Lovell, Davis et al. 2003) (http://molprobity.biochem.duke.edu/). The refinement and validation statistics of native PFK structure is summarized in TABLE 3.3

Refinement	Native PFK
Clashscore	12.09
Rotamer outliers (%)	2.19%
Cβ deviations >0.25 Å	0
Residues with bad bonds/angles (%)	0.00/0.00
MolProbity Score (percentage)	1.98 (91%)
Ramachandran favoured/outliers (%)	97.53/0
R $_{factor}$	0.215
R $_{free}$	0.276
r.m.s.d bond lengths(Å)/angles	0.011/1.197

TABLE 3.3: Model refinement and validation statistics of native PFK structure.

3.3.5 *S. aureus* PFK enzyme activity assay

S. aureus PFK enzyme activity assays was carried out using Mass spectrometry (University of St Andrews), The experiment was carried out to differentiate the reaction product fructose 1,6-bisphosphate, which has a molecular weight of ~339 Da from the substrate fructose 1-phosphate (~259 Da). This difference can be distinguished by mass spectrometry analysis. The assay solution consisted of 100 mM ammonium pH 7.5, 3 mM F1P, 0.5 mM MgCl2 and 2.5 mM ATP. After pre-incubation at 25 ℃ the reaction was started by the addition of PFK at an appropriate dilution (2 µg). All reagents were purchased from Sigma-Aldrich. Reactions in absence of ATP, F1P and *S. aureus* PFK under same condition were used for controls (data not shown). All the experiments were repeated twice to make sure the data was consistent. The mass spectrometry data are shown in FIGURE 3.16.
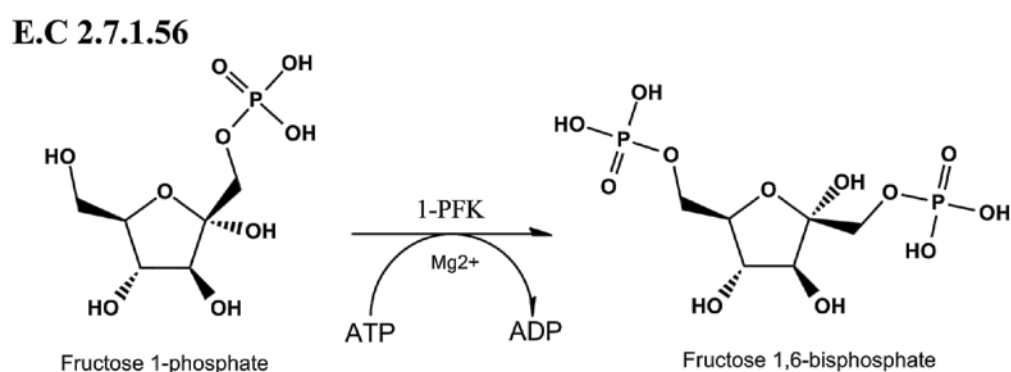
FIGURE 3.15: Reaction of E.C 2.7.1.56, Phosphorylation of Fructose 1-phosphate by 1-PFK
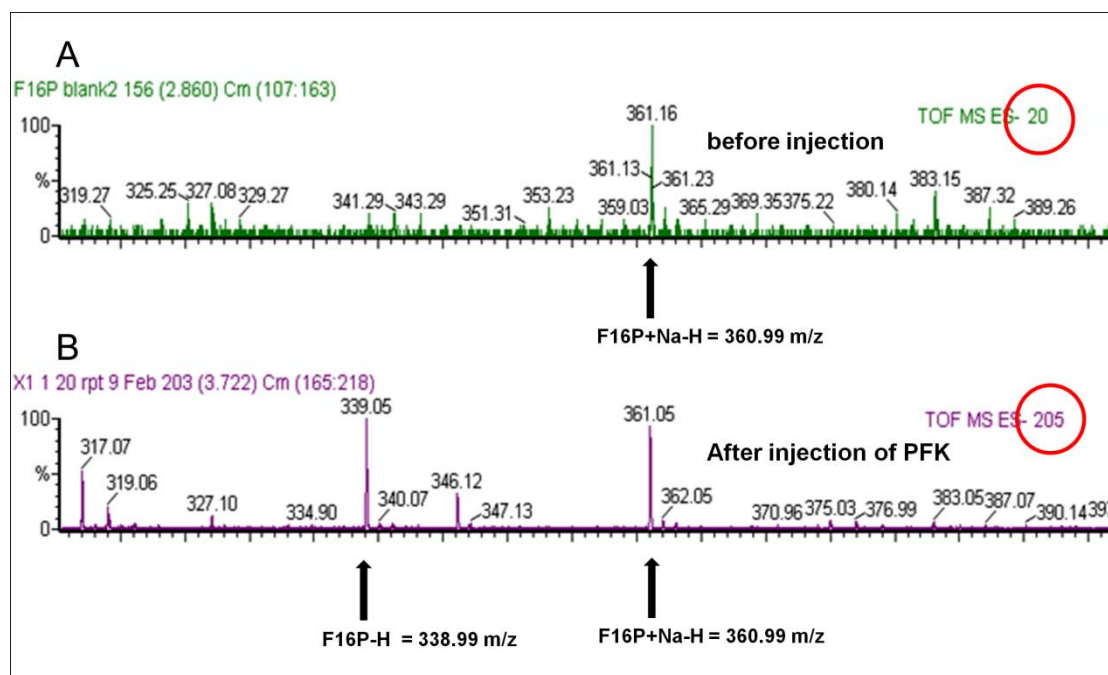
FIGURE 3.16: Mass spectrometry analysis of the assay mixture before and after addition of PFK. [A] Mass spectrometry analysis of the assay mixture before PFK was injected. [B] Mass spectrometry analysis of the assay mixture after injection of PFK. The ion count is circled in red, indicating the very latge increace in the intensity of the peak at 399.05.

The reaction product fructose 1, 6-bisphohsphate has a estimated mass of 339 m/z with hydrogen, 361 m/z with sodium ion. The count in red circle indicates the concentration of reaction product fructose 1,6-bisphosphate salt. Before the addition of putative *S. aureus* PFK, the 361.16 peak (possible Na adduct is very low. The small peak may be contaminating F16BP (although the peak at 399 is missing) (FIGURE 3.16A). FIGURE 3.15B shows the mass spectrometry analysis of the assay mixture after injection of PFK with strong peaks at 399.05 (F16BP) and 361.05 (F16BP + Na). This result strongly suggested that the putative *S. aureus* PFK can catalyze the phosphorylation reaction of F1P to F16BP.

The kinetics study on PFK was based on a coupled enzyme reaction (FIGURE 3.17)

using initial rates method. The PFK activity was measured by coupling the formation of F 1,6-BP to the oxidation of NADH via three enzymes, fructose 1,6-bisphosphate aldolase (F16P aldolase), triosephosphate isomerase (TIM) and glycerol 3-phosphate dehydrogenase (Davies, Detheux et al. 1990; Niculescu, Veiga-da-Cunha et al. 1996). The enzyme activity was determined by measuring the decrease of optical density at 340 nm using a spectrometer at room temperature (25 °C). The standard assay system was 1 mL solution mixture contained 100 mM Tris-HCl, pH 7.5, 0.2 mM NADH, 5 mM MgCl2, 1 mM EDTA, 2 mM ATP and 5-8 units each of F16P aldolase, TIM and glycerol 3-phosphate dehydrogenase. The final volume of the reaction mixture was 1 ml. The mixture was mixed gently and the back group rate for the oxidation of NADH was measured for 2 minutes before addition of PFK. The reaction was monitored for an additional 30 seconds. A unit enzyme activity is defined as the amount of enzyme producing 1 µmol fructose 1,6-bisphosphate per minute. The K_m for F1P was determined using an enzymes assay mixture containing 2 mM ATP, 0.5 – 12 mM F1P, and 1µg of pure *S. aureus* PFK. All coupling enzymes and chemicals were tested in absence to make sure that the rate of the standard assay is not limited by them. All the reagents and assays auxiliary enzymes were purchased from Sigma-Aldrich. Three repeat measurements were carried out to make sure the data are consistent.
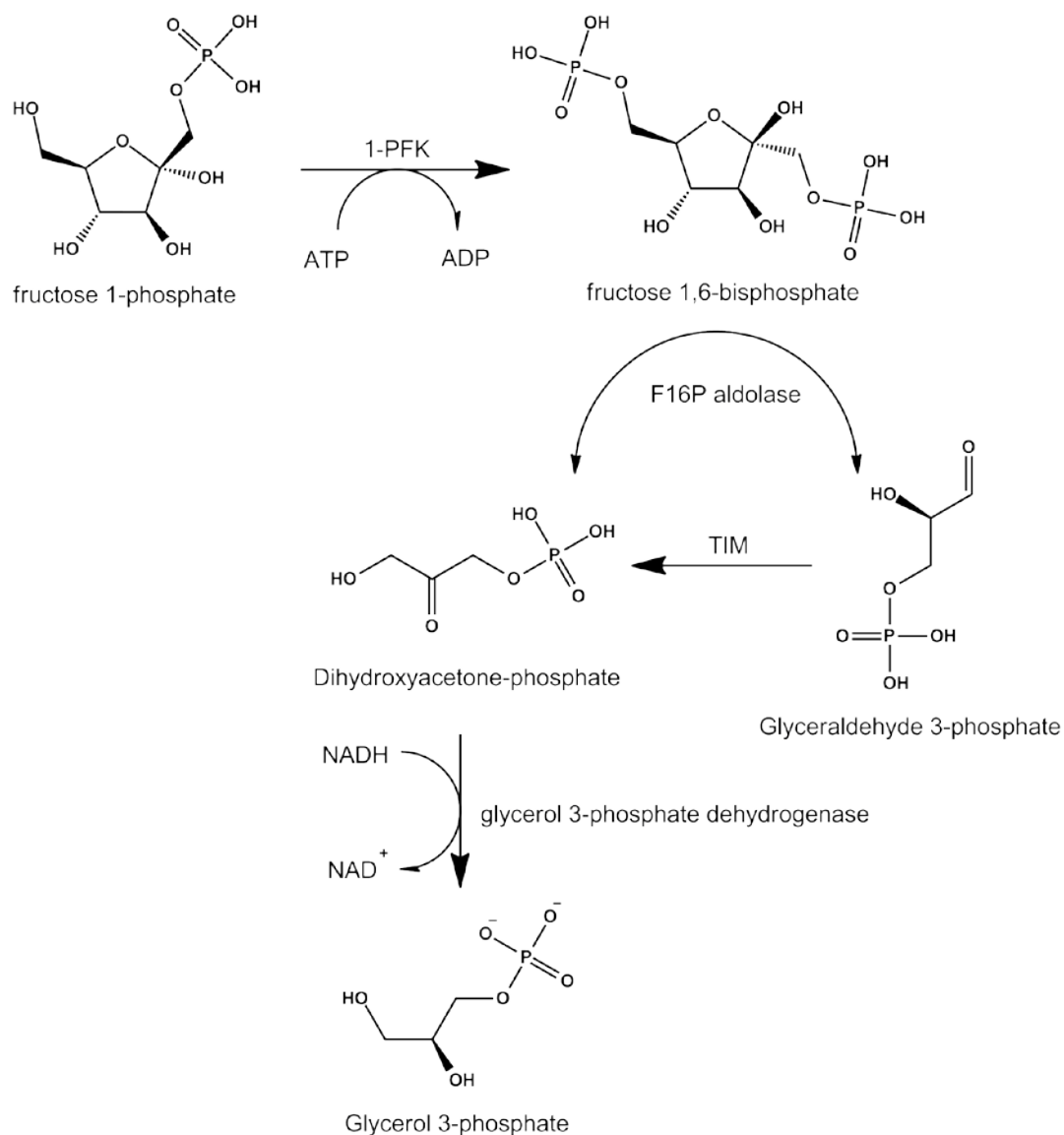
FIGURE 3.17: Chemical Diagram of the coupled reaction of formation of F 1,6-BP to the oxidation of NADH via three related enzymes, fructose 1,6-bisphosphate aldolase (F16P aldolase), triosephosphate isomerase (TIM) and glycerol 3-phosphate dehydrogenase.

Data repotted in Grafit graphic analysis program. K_m of *S. aureus* PFK for fructose 1-phosphate obtained using the Michaelis – Menten equation. The apparent K_m of *S. aureus* PFK for F1P was determined to approximately 410 µM when enzyme was measured in the presence of 1 mM ATP and 5 mM $MgCl_2$.
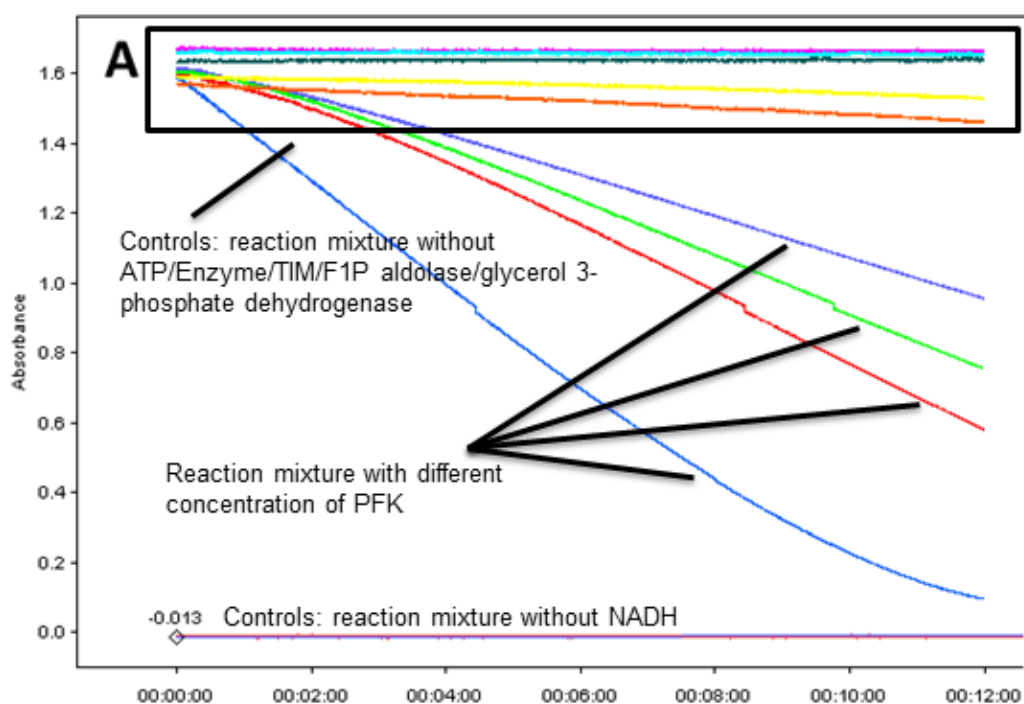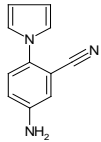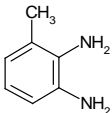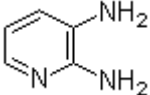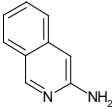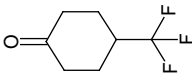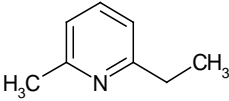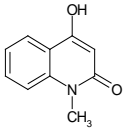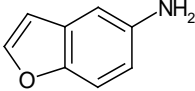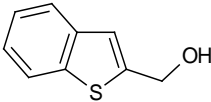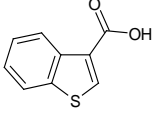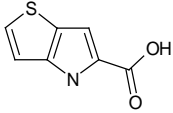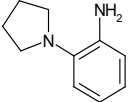
FIGURE 3.18: Enzyme kinetics study on *S. aureus* PFK.The apparent K_m of *S. aureus* PFK for F1P was approximately 410 μM when enzyme was measured in the presence of 1 mM ATP and 5 mM MgCl₂

3.3.6 Thermofluor study on *S. aureus* PFK

The Thermofluor assay is also applied for finding the potential hits for *S. aureus* PFK. The same sample preparation and assay protocol are employed as described before (Chapter 2.3.6). All the samples were repeated twice at the same condition. The melting curves were generated and analyzed by the program iCycler iQ Optical System. Positive hits are those fragments that induce a shift of Tm over 2℃.

Results / Potential hits

24 potential hits out of 476 fragments were obtained by thermal shift assay against TAG. 16 of them were considered as clearly shifting the thermal stability.

Fragments	Structure	Formula	ΔT_m (°C)
5-amino-2-(1H-pyrrol-1-yl)benzonitrile		C11 H9 N3	2
3-methylbenzene-1,2-diamine		C7 H10 N2	2
pyridine-2,3-diamine		C5 H7 N3	2
isoquinolin-3-amine		C9 H8 N2	2
4-(trifluoromethyl)cyclohexan-1-one		C7 H9 F3 O	2
2-ethyl-6-methylpyridine		C8 H11 N	3
4-hydroxy-1-methyl-1,2-dihydroquinolin-2-one		C10 H9 N O2	2
1-benzofuran-5-amine		C8 H7 N O	2
1-benzothiophen-2-ylmethanol		C9 H8 O S	3
1-benzothiophene-3-carboxylic acid		C9 H6 O2 S	3
4H-thieno[3,2-b]pyrrole-5-carboxylic acid		C7 H5 N O2 S	3
4-methyl-4H-thieno[3,2-b]pyrrole-5-carboxylic acid		C8 H7 N O2 S	3
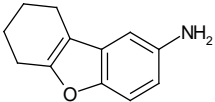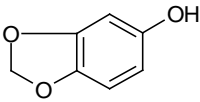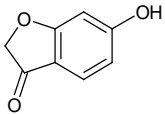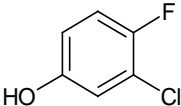
6,7,8,9-tetrahydrodibenzo[b,d]furan-2-amine		C12 H13 N O	4
1,3-benzodioxol-5-ol		C7 H6 O3	3
6-hydroxy-2,3-dihydrobenzo[b]furan-3-one		C8 H6 O3	3
3-chloro-4-fluorophenol		C6 H4 Cl F O	4

TABLE 3.4: The positive hits of the thermal shift assay for PFK

3.4 Results & Discussion

3.4.1 Overall structure of *S. aureus* PFK

The final model of *S. aureus* PFK monomer consists of 306 amino acids residues with an R_{factor} of 0.21 and R_{free} of 0.26. The *S. aureus* PFK monomer appears as a "bowl-with- lid shape" with two distinct structural domains. There are 14 β-sheets and 10 α-helices in a monomeric structure. An examination of the Protein Data Bank (PDB) for similar structures using the web-based protein structure comparison service SSM at European Bioinformatics Institute (EBI) http://www.ebi.ac.uk/msd-srv/ssm/ (Krissinel and Henrick 2004) shows that the *S. aureus* PFK shared a common overall fold with other members of ribokinase-pfkB family and the r. m. s. deviation of Cα atoms with these monomers is in the range 1.5 – 2.3 Å.

Source	N_{align}	r.m.s.d ($\overset{\circ}{A}$)
S. aureus tagatose 6-phosphate kinase (LacC)	296	1.86
B. halodurans fructose 1-phosphate kinase	302	1.75
E. faecalis tagatose 6-phosphate kinase	294	1.61
E. coli fructose 6-phosphate kinase	289	1.86
T. maritama fructose 1-phosphate kinase	282	2.28

TABLE 3.5: Structure alignment of *S. aureus* fructose 1-phosphate kinase using SSM at European Bioinformatics Institude (EBI) http://www.ebi.ac.uk/msd-srv/ssm/ (Krissinel and Henrick 2004). N_{align} indicates the residues aligned.

The tertiary structure of a PFK monomer is composed of two domains (FIGURE 3.24). The large domain appears as 3 layers (α/β/α) like a sandwich, consists of 10 β-sheets and 10 α-helices and comprises the residues 1-5, 38-82, and 109-306. Residues 109-217 present a typical Rossmann-fold (Sigrell, Cameron et al. 1998) in the centre of the large domain comprising of α3-α7 and β8-β10. β-strands β4, β5, β12-14 extend the entire length of these parallel β-strands. The central β-strands are surrounding by 5 α-helices on each side. A smaller domain comprising of residues 9-36 and 88-102, forms 5 β-strands which attaches to the main domain like a lid. The four large strands β2, β3b, β6 and β7 of this domain form an anti-parallel sheet, the small strand sits apart β3b. The two domains are connected by four loops (residues 5-9, 36-38. 82-88.102-109).

The structure of the monomer appears like an open clam shell with a large gap between both domains. These features suggest a potential flexibility at the connecting loops, which may result in conformational changes with the loops acting as hinges. The Rossmann fold structure architecture and the "4+1 β-sheets" lid domain are highly conserved among the pfkB family proteins (FIGURE 3.28). Structure comparison shows the predicted locations of active site for substrate and co-factor binding are likely to be similar to other members of ribokinase-pfkB family. These structures include Fructose-1-phosphate kinase from *Bacillus halodurans* (PDB code: 2ABQ), D-tagatose-6-phosphate kinase from *S. aureus* (PDB code: 2JGV), fructose 6-phosphate kinase from *Escherichia coli* (PDB code: 3CQD) and 1-phosphofructokinase from *Thermotoga. maritama* (PDB code: 2AJR). All main structure elements are labeled in FIGURE 3.19 and FIGURE 3.20.
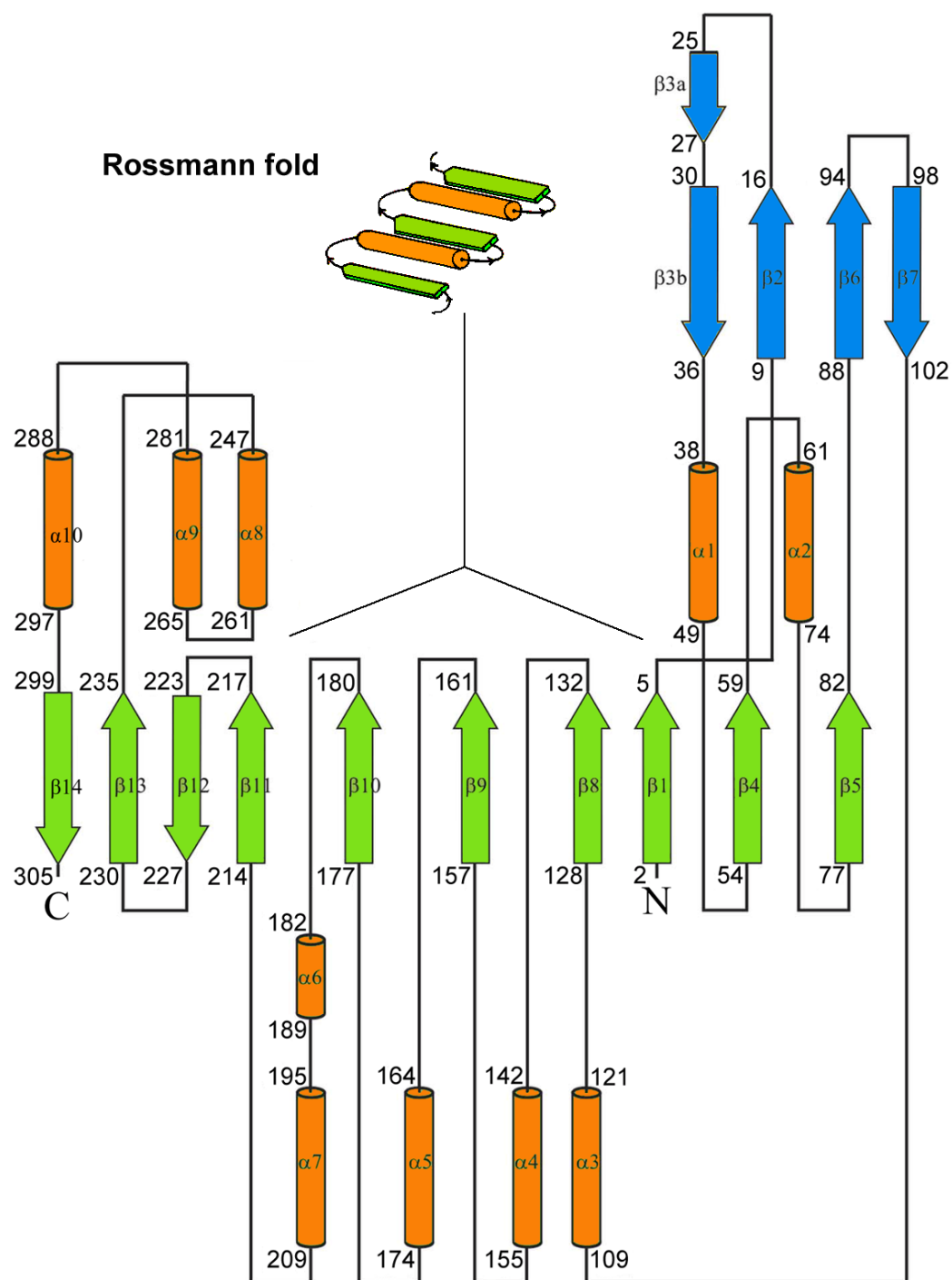
FIGURE 3.19: Schematic view of native PFK monomer A. N-Terminal is shown in blue, C-Terminal starts from the orange loop. Helices are shown in orange cylinder. β-sheets in large domain are colored in green arrows, β-sheets from the lid domain are colored in blue arrows.
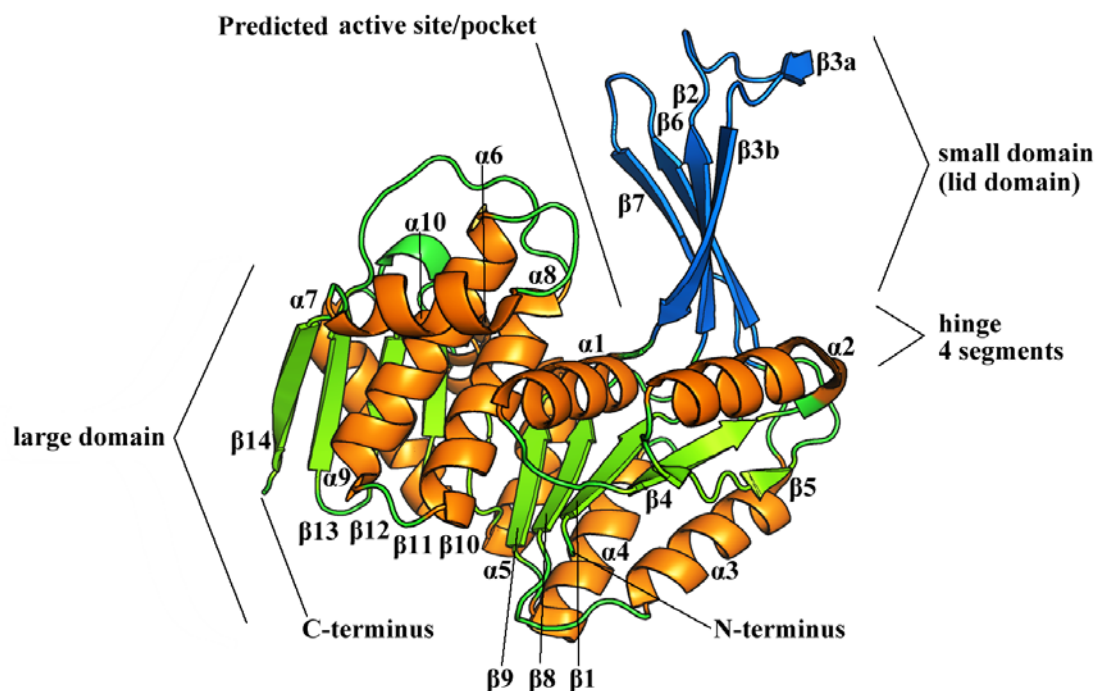
FIGURE 3.20: Cartoon representation of the crystal structure of *S .aureus* **PFK. Helices are shown in orange and labeled. β-sheets in large domain are colored in green. B-sheets from the lid domain are colored in blue and numbered accordingly.**
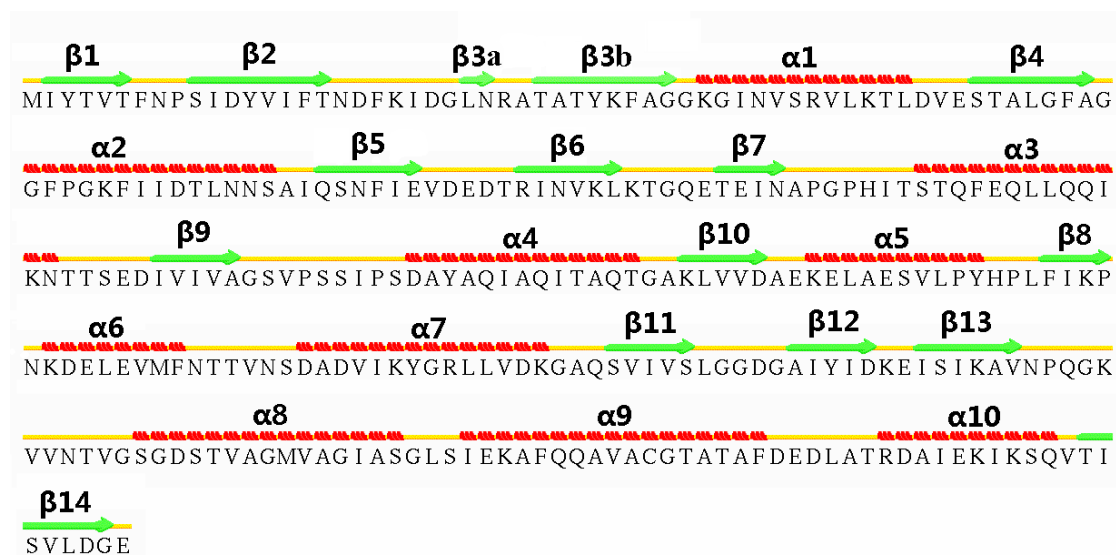
FIGURE 3.21: Secondary structure alignment of *S. aureus* **PFK monomer A. The secondary structure was assigned, using STRIDE (Frishman and Argos 1995) web-based software (http://webclu.bio.wzw.tum.de/cgi-bin/stride/stridecgi.py) and confirmed by visual inspection of the model.**
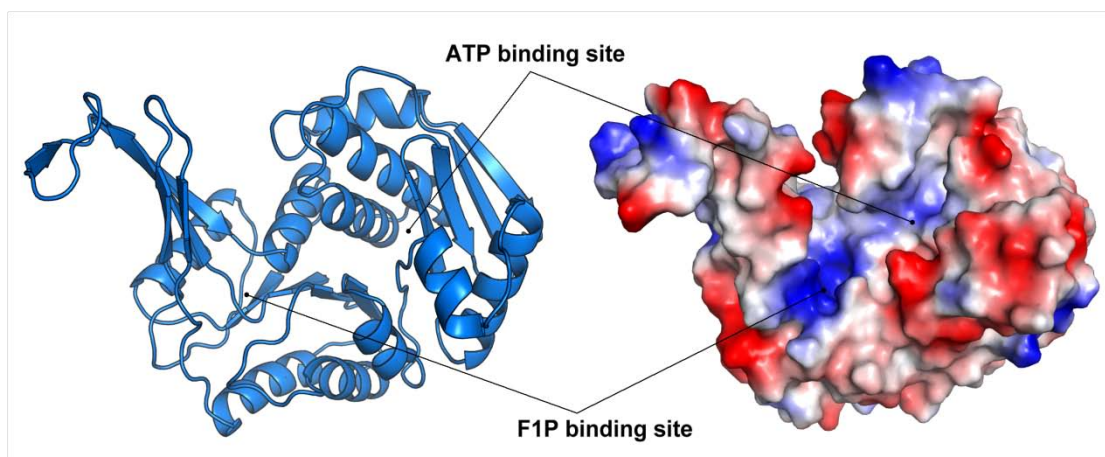
FIGURE 3.22: Cartoon representation and electrostatics surface potential of the active site of PFK. The solvent-accessible surface of PFK colored based on the electrostatics potential from -7 to +7 kT/e, calculated using ABPS tools in PyMol™. Positive charge is shown in blue and negative charge is shown in red. F1P is superimposed to indicate the active site of PFK
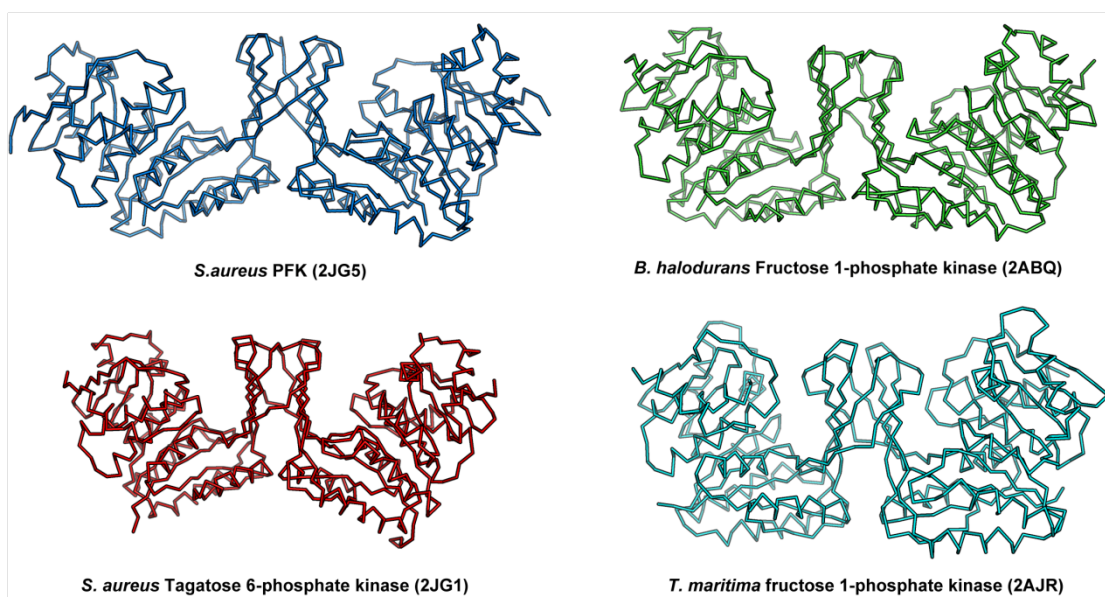
FIGURE 3.23: Ribbon representation of members of the pfkB family. Fructose-1-phosphate kinase from *S. aureus* (PDB code: 2JG5). Fructose-1-phosphate kinase from *Bacillus halodurans* (PDB code: 2ABQ), D-tagatose-6-phosphate kinase from *S. aureus* (PDB code: 2JG1) and fructose 1-phosphate kinase from *Thermotoga maritima* (PDB code: 2AJR)

A structure-based sequences alignment of the ribokinase family and ribokinase-pfkB subfamily enzymes indicates that there are several conserved structure motifs in these enzymes (FIGURE 3.29). Motifs I and II have been reported previously as the signature character for the ribokinase family members (Sigrell, Cameron et al. 1998; Cabrera, Caniuguir et al. 2006). Amino acid residues from these two motifs are considered to be vital for the phosphorylation process (Sigrell, Cameron et al. 1998; Li, Kwok et al. 2002; Zhang, Dougherty et al. 2004). Motif III has the sequence Val-Gly-Ala/Ser-Gly-Asp-Ser-X-Val and this conserved structure motif is located close to the γ-phosphate of AMP-PNP/ATP and the sugar binding site. Motif IV which has the sequence Ala/Ser-Gly-Ser-X-Pro, and is located around the phosphate groups of the co-factor, is believed to stabilize the transition state. Motif IV is involved in sugar base substrate binding and such architecture is believed to be critical for the phosphate transfer (Chapter 3.4.5). Motif III and IV are common to the ribokinase-pfkB subfamily members of carbohydrate kinase, but not to the ribokinase family members in general (Cabrera, Caniuguir et al. 2006; Miallau, Hunter et al. 2007; Cabrera, Ambrosio et al. 2008). Motifs III and IV may be assigned as a signature structure motif of the ribokinase-pfkB family of carbohydrate kinases (Cabrera, Caniuguir et al. 2006; Miallau, Hunter et al. 2007). These features imply that with highly conserved active sites residues and locations (Chapter 3.4.3), the substrate and co-factor should occupy similar locations within the active sites in each structure.

FIGURE 3.24: Structural-based sequence alignment of ribokinase family members. A multiple structural-based sequence alignment of *S. aureus* PFK (PFK), Fructose-1-phosphate kinase from *Bacillus halodurans* (2ABQ), D-tagatose-6-phosphate kinase from *S. aureus* (2JG1), phosphofructokinase-2 from *Escherichia coli* (3CQD) and phosphofructokinase from *Listeria innocua* (3IE7). Identical residues in the sequences aligned are highlight in black, residues shaded grey indicate regions of sequence homology. The four red boxes indicate the conserved motifs in comparison. This alignment was generated with BioEdit program.
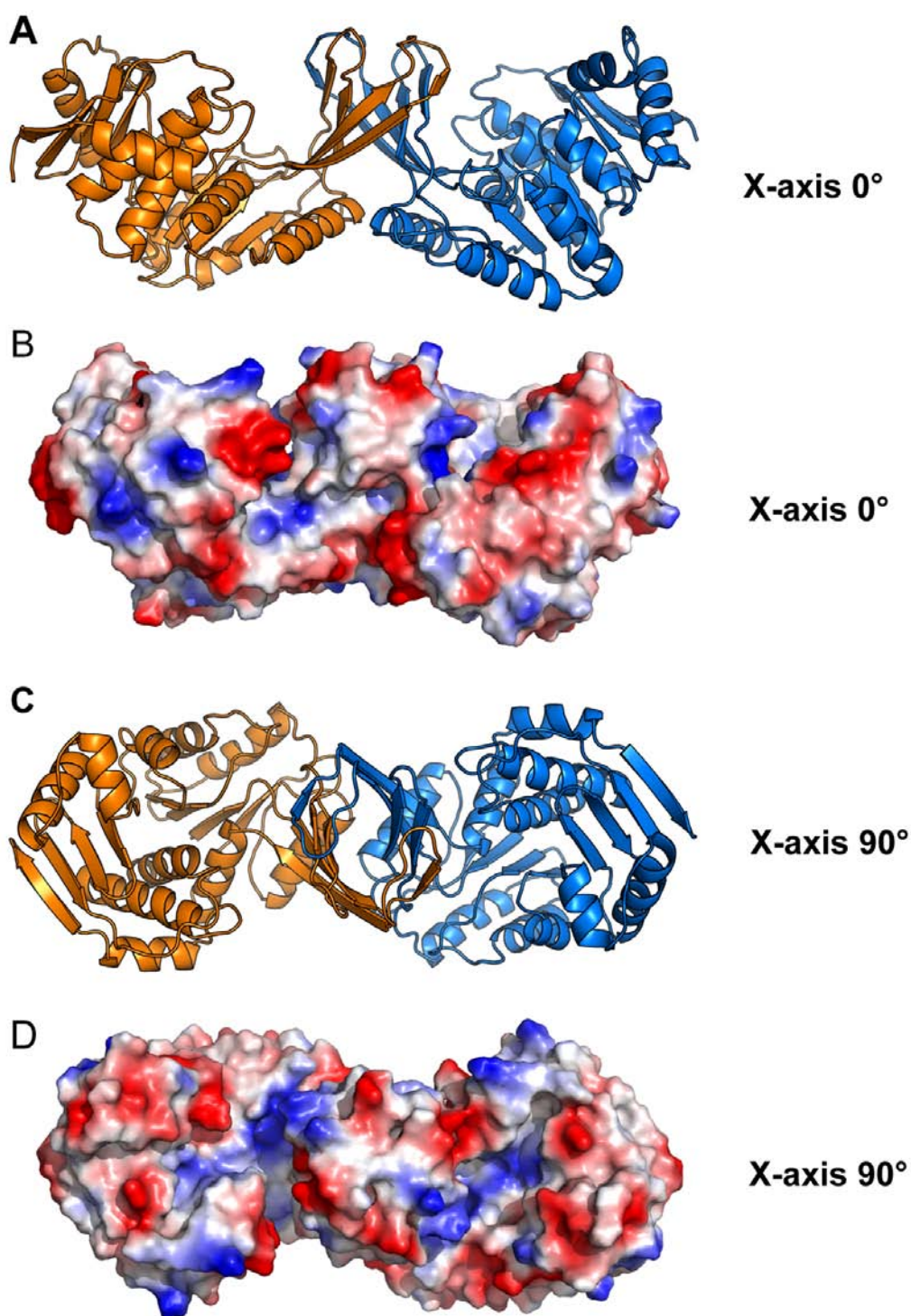
FIGURE 3.25: Cartoon representation of overall structure of PFK dimer [A] [B] [C] [D]The surface electrostatics potential of PFK. The solvent-accessible surface of PFK colored based on the electrostatics potential from -7 to +7 kT/e, calculated using ABPS tools in PyMol™. Positive charge is shown in blue and negative charge is shown in red.

3.4.2 Dimer interactions in *S. aureus* PFK

S. aureus PFK appears as a dimer in crystal form and this is consistent with gel filtration results. These results reveal that *S. aureus* PFK forms a functional dimer in common with other members of ribokinase-pfkB-like family such as *B. halodurans* PFK and *S. aureus* LacC (Miallau, Hunter et al. 2007) in both solution form and crystal form. A web-based "protein interfaces, surfaces and assemblies" (PISA) analysis software http://www.ebi.ac.uk/msd-srv/prot_int/pistart.html (Krissinel and Henrick 2005) was used to investigate the interactions between two subunits. The two subunits in the dimer are related by crystallographic symmetry and associate with each other via the interactions between their small domains (lid domain) and some part of the four loops that linking the two domains. An interface area of 1297 Å^2 is buried between the two monomers. β-sheets β3a, β3b and β7 from lid domain, along with the residues from the loop between β5 and β6 are the main elements that participated in monomer-monomer interactions. The β-sheets from the lid domain are placed face to face with the strand directions. In this 4+1 β-sheets domain, the smallest β-strand (β3a) between β2 and β3b interacts with the lid domain from the other monomer. This structure organization was initially identified and described as "β-clasp motif" in *E.coli* ribokinase (Sigrell, Cameron et al. 1998). The β-clasp motif is a main feature of the interface interactions between two subunits of the dimmer, the two lid domains come together to form a special "β-barrel" and rotate about 90 ° with respect to each other. The small β-strand (β3a) and the loop between β2 and β3b interact with β7 from the opposite monomer as a hook and an interaction parallel

ladder is formed by the residues from these structure elements. The interaction area of each monomer is extensive. This β-clasp motif is highly conserved and considered as a distinguishing feature of the ribokinase-pfkB family enzymes (Sigrell, Cameron et al. 1998; Sigrell, Cameron et al. 1999). Structure elements from the hinge segments are also involved in the interactions between two subunits. Residue Asp86 from the loop between β5 and β6 interacts with the residue Lys33 from the other subunit in the dimer also to contribute to the protein dimerization (FIGURE 3.26).
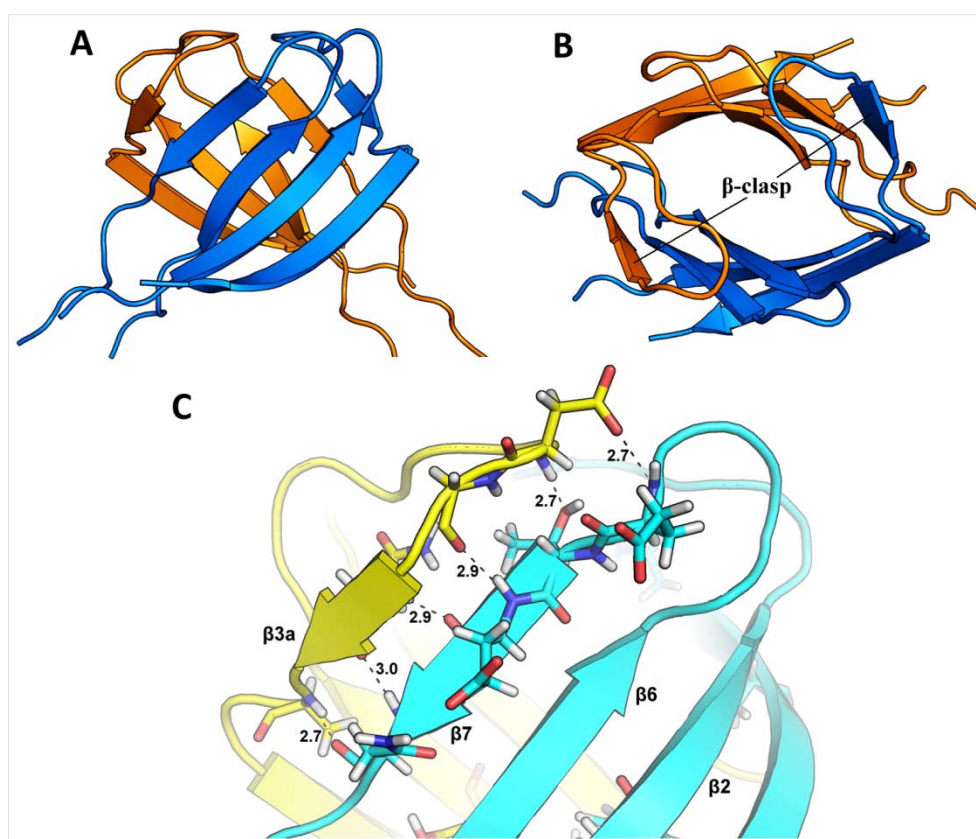
FIGURE 3.26: Cartoon representations of the interactions of the β-clasp motif between two subunits. [A] Cartoon representation of the interaction interface of the interactions between two subunits. [B] 90 ° turn X-axis view. [C] A closer look at the interactions between the residues from β-clasp motif and β7 from the other subunit. N, O and H atoms are shown in blue, red and white, respectively.

3.4.3 The potential active site of *S. aureus* PFK

The active site of *S. aureus* PFK can be predicted by superimposing with other similar structure. The proposed AMP-PNP/ATP binding site is located on the surface of the large domain, the cleft between helices α8-10 cluster and the four anti-parallel β-strands (β10-14). The proposed F1P binding site is located on the edge of the sandwich domain, close to the flexible hinge segments that link to the lid domain and the long loop between β9 and helix α4 (FIGURE 3.27). Modeling of ATP and F1P was tried with both superposition method and a visual docking program GOLD (Genetic Optimization for Ligand Docking) (Verdonk, Cole et al. 2003), respectively. Crystal structure of *S. aureus* LacC in complex with T6P and AMP-PNP (PDB entry: 2HFU) (Miallau, Hunter et al. 2007) was used as the model for superposition.

The proposed AMP-PNP/ATP binding site is composed of helices α8, α9, β11, β12 and the small turn between β11, β12. This pocket is perfectly shaped to accommodate the ribose group and the long chain of AMP-PNP/ATP. The surface electrostatics potential of the groove is strongly positively charged and quite close to the β- and γ-phosphate group of AMP-PNP/ATP. This setting can neutralize the negative charge of the transition state (FIGURE 3.27).
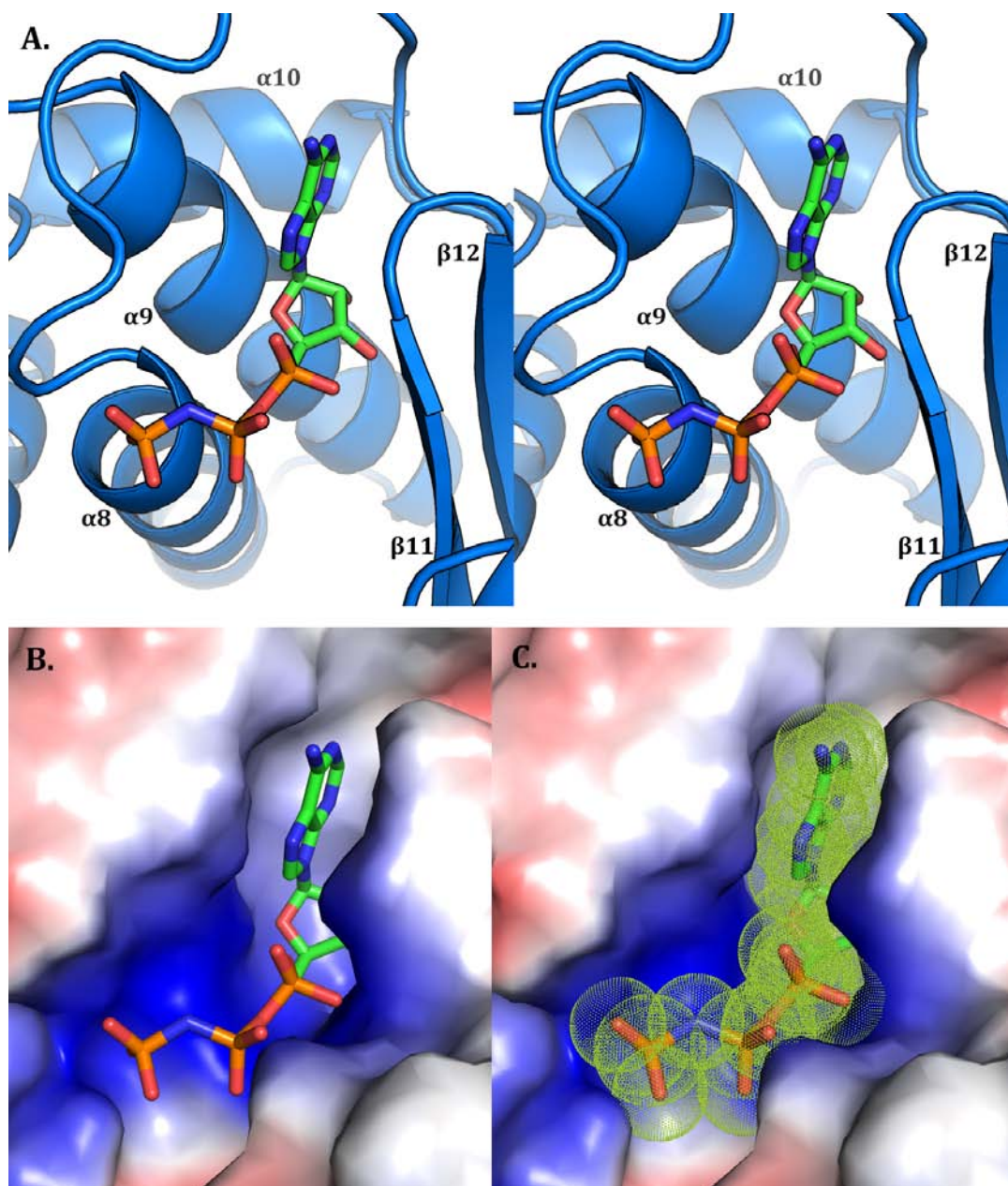
FIGURE 3.27: The proposed ATP binding site. [A] Stereo view of the proposed AMP-PNP/ATP binding site of PFK. [B] [C]. Electrostatics surface potential of the proposed AMP-PNP/ATP binding site of PFK. The solvent-accessible surface of PFK colored based on the electrostatics potential from -7 to +7 kT/e, calculated using ABPS tools in PyMol™. Positive charge is shown in blue and negative charge is shown in red. AMP-PNP is superimposed to indicate the potential ATP binding site of PFK.

In the *S. aureus* PFK/AMP-PNP model, the ribose group of AMP-PNP/ATP is deeply

buried in the binding pocket, between the loop that links the β-strands β11, β12 and

one side of the helix cluster α8-10. The tri-phosphate chain runs along the groove between α8 and the parallel strands β8, β9, sandwiched by motif II and motif III. The α-phosphate group is likely to accept the hydrogen bonds directly from Gly219 and Ser217. A water-mediated hydrogen bonds network is possibly involved with the α-phosphate group and Thr251. The β-phosphate group may accept some hydrogen bonds from Asn181 and Lys179. Residues Gly246, Gly248 and T251 from the conserved motif II were also predicted to interact with the β-phosphate group. Most of these active site residues are conserved except two residues Val273 and Thr277 (equivalent to Asn278 and Gly282 in *S. aureus* LacC). The phosphate groups are the key elements in the reaction. Comparison of the active site residues related to AMP-PNP/ATP binding shows the residues that might have interactions with the phosphate groups are highly conserved in ribokinase-pfkB family. These are Gly246, Gly248 Asp249, Thr251from conserved motif II, Lys179 and Asn181 from motif III. The γ-phosphate may interact with the residues from conserved Gly-Ala/Ser-Gly-Asp motif II (246-249) (α8). Residues Gly246 and Asp249 would be able to form direct hydrogen bonds with the γ-phosphate group. In addition, the conserved residue Gly248 could provide extra hydrogen bond to this phosphate group (FIGURE 3.28) Such arrangement is believed to catalyze the transfer of phosphoryl group (Zhang, Dougherty et al. 2004). The active site would be large enough to bind with ATP and admit the magnesium ions and solvent around the phosphate groups of ATP.
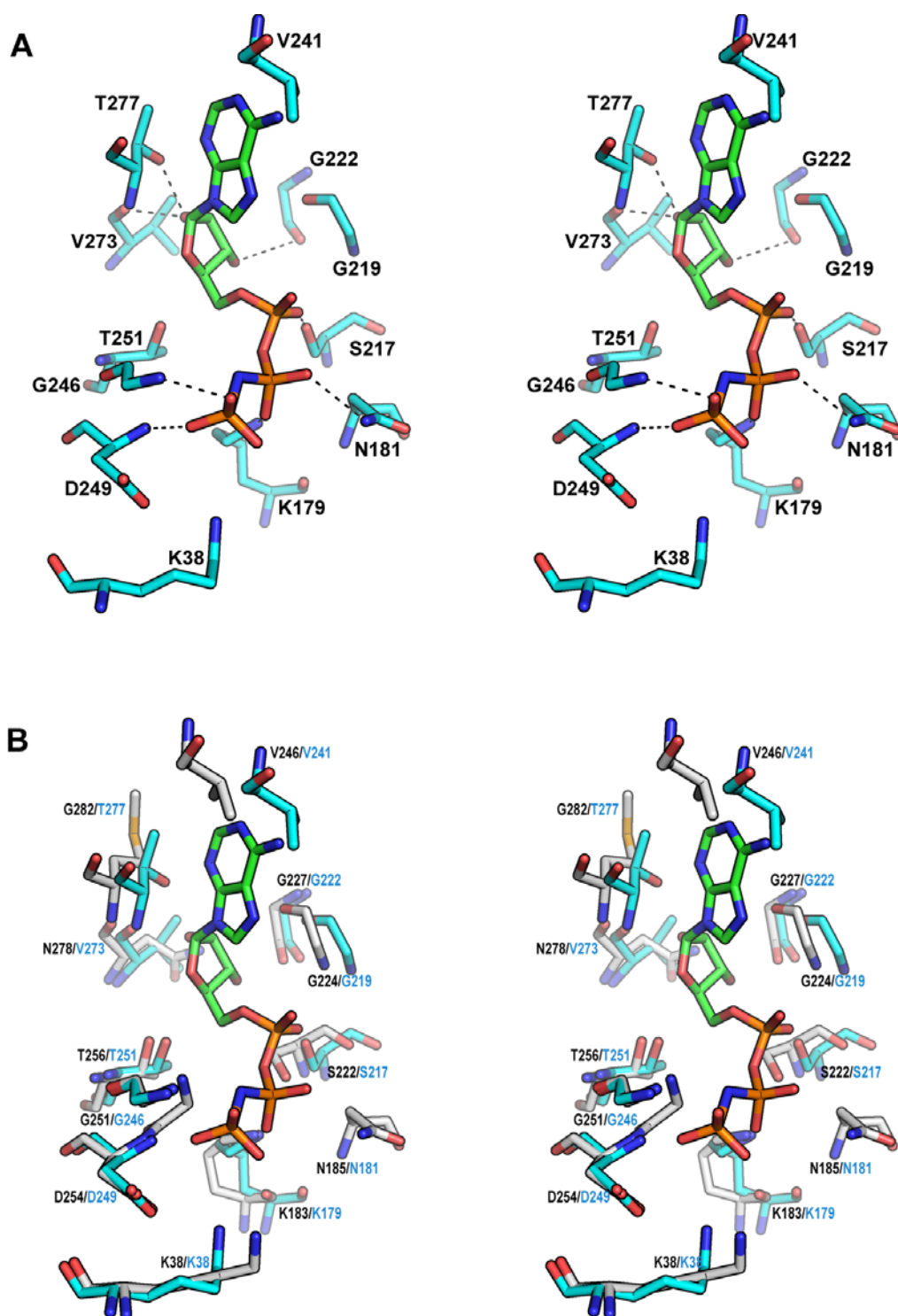
FIGURE 3.28: Stereo view of the proposed ATP binding site of *S .aureus* PFK [A] and *S. aureus* LacC [B]. PFK atoms are colored in cyan. *S. aureus* LacC atoms are colored in white. AMP-PNP is shown in green to indicate the potential ATP binding site. N, O and P atoms are shown in blue, red and orange, respectively. All the potential residues that might interact with AMP-PNP are labeled in the order of *S. aureus* LacC/*S. aureus* PFK.

The predicted F1P binding site is located at the surface of the large domain, close to the four loops and helix α1. The potential flexible hinge segments may the binding site. The hydroxyl group on ring moiety of F1P is close to the γ-phosphate of AMP-PNP/ATP. The electrostatic potential around the phosphate group of the substrate is strongly positive charged, and it is likely that such a distribution stabilizes the negative charged transition state phosphate group. Analysis of docking results suggests that F1P binds to the residues from both two domains of PFK and residues from the "hinge" loops.
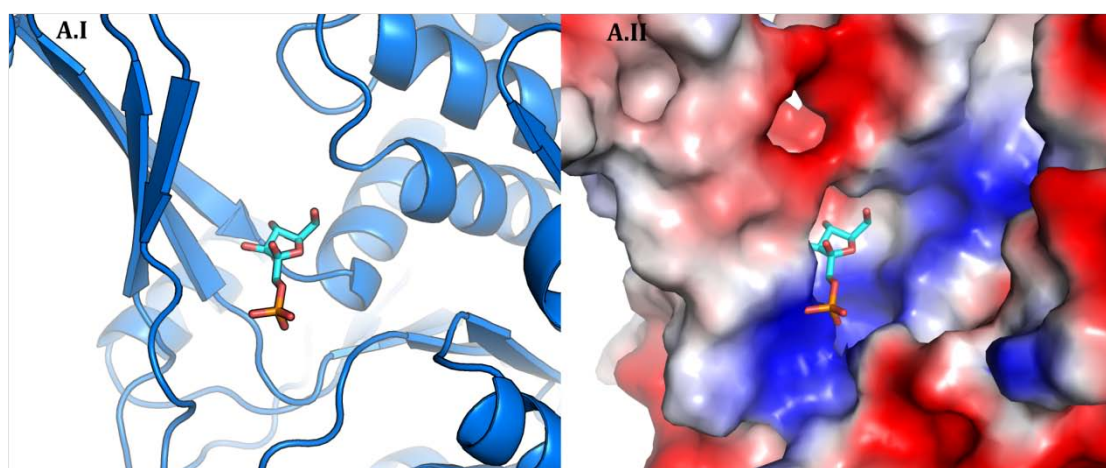
FIGURE 3.29: The proposed F1P binding site in *S. aureus* PFK and *S. aureus* LacC. [A.I] Cartoon representation of the proposed F1P binding site of *S. aureus* PFK suggested by program GOLD. [A.II] Electrostatics surface potential of the proposed F1P binding site of *S. aureus* PFK. F1P is shown in cyan to indicate the potential binding site. Ligand libraries were prepared using PRODRG (Schuttelkopf and van Aalten 2004). The solvent-accessible surface of TAG colored based on the electrostatics potential from -7 to +7 kT/e, calculated using ABPS tools in PyMol™. Positive charge is shown in blue and negative charge is shown in red.
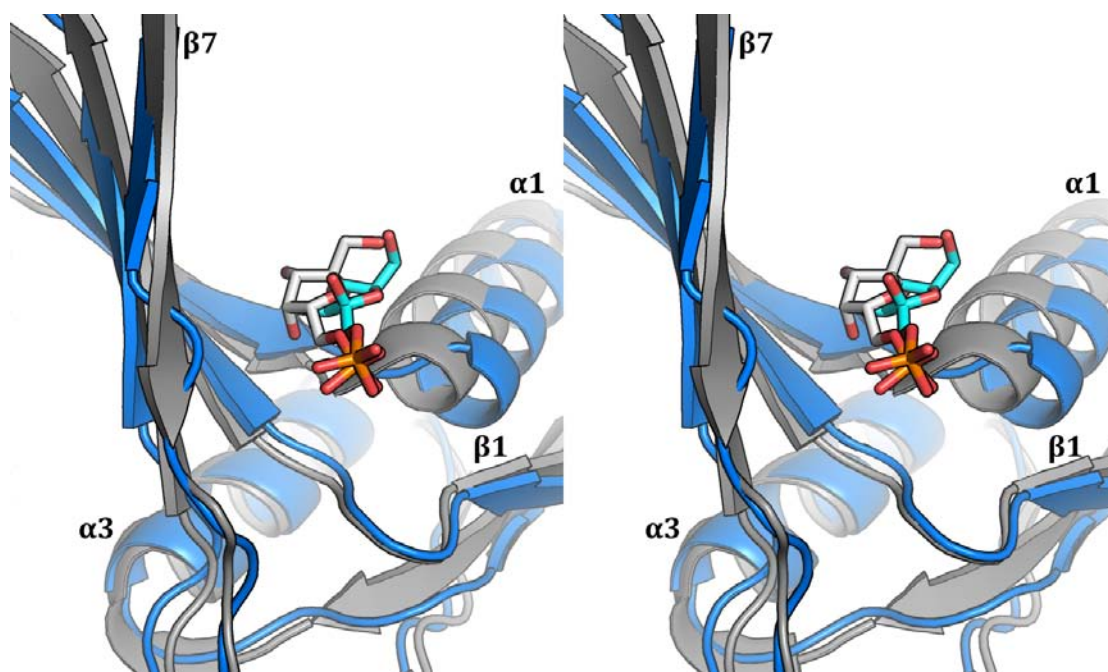
FIGURE 3.30: Stereo view of _S. aureus_ PFK with modeled F1P superimposed with _S. aureus_ LacC/T6P complex structure. _S. aureus_ PFK is colored in blue, _S. aureus_ LacC is shown in grey. Secondary structure elements from _S. aureus_ PFK are labeled in black. C atoms of F1P are shown in cyan. C atoms of T6P are colored in white, O and P atoms are shown in red and orange, respectively. Ligand libraries were prepared using PRODRG (Schuttelkopf and van Aalten 2004).

The C3 and C4 hydroxyl groups of F1P are likely to interact with residue Asp12 and Gly37 from motif I. These two residues may also help to fix the orientation of the C1 hydroxyl group. Both Arg88 and Ser134 from the motif IV which are highly conserved in ribokinase-pfkB family are likely to have potential interactions with the C1 phosphate group of the substrate and such interactions are predicted to help stabilize the flexible phosphate group. Residues Asn90 from β6 and Asn102 from β7 are predicted to recognize the C2 hydroxyl group (distance ~3.5 Å), respectively. Residues Lys38 from motif I and Asp249 from motif II locate around the C6 hydroxyl group of the docked F1P, these two conserved residues are also close to the γ-phosphate group of ATP and predicted to play important roles in the reaction.
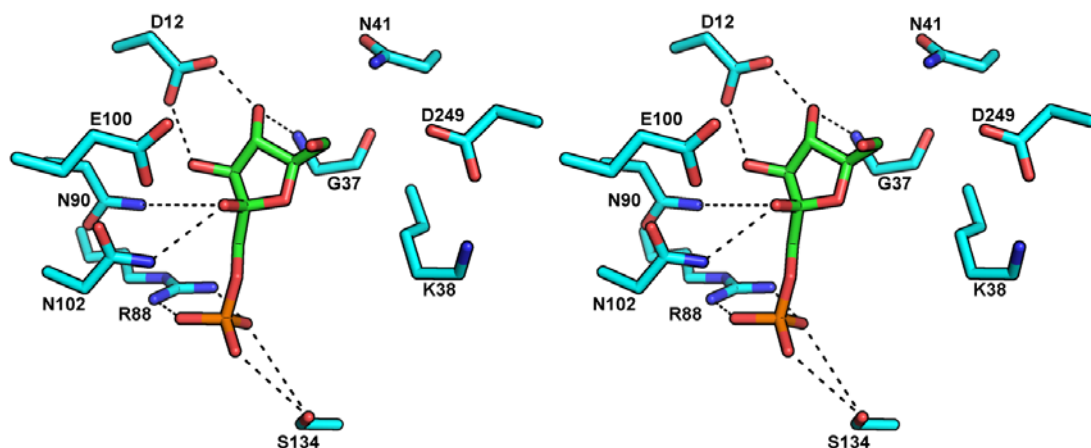
FIGURE 3.31: Stereo view of the proposed F1P binding site. Protein C atoms are shown in marine blue, C atoms of F1P are shown in green. N, O and P atoms are shown in blue, red and orange, respectively. F1P is docked to indicate the proposed substrate binding site.

Structure comparison between *S. aureus* PFK and *S. aureus* LacC indicates that these substrate-related residues are highly conserved. In LacC, residues Asp12 and Gly37 (equivalent to Asp12 and Gly37 in *S. aureus* PFK) interact with the C3, C4 hydroxyl groups of T6P, while residues Ser136 and Arg88 (Ser134 and Arg88 in *S. aureus* PFK) form hydrogen bonds with the phosphate group of T6P. Asn41 interacts with the C5 hydroxyl group of T6P. Only two active site residues, Cys90 and Leu103 (equivalent to Asn90 and Asn102 in *S. aureus* PFK) are not conserved. These two residues are conserved in other fructose 1-phosphate kinases, they are able to form much stronger interactions with the C2 hydroxyl group of F1P than residues Cys90 and Leu103 in LacC. Previous studies on fructose 1-phosphate kinase from other species such as *E. coli* indicated that the enzyme is specific for F1P over T6P, with no reaction observed in the assay when F1P was replaced by F6P or T6P (Davies, Detheux et al. 1990; Veiga-da-Cunha, Hoyoux et al. 2000). Our model predicts that N90 and N102 of *S.*

aureus PFK are positioned to recognize the C2 hydroxyl of F1P. In T6P, however the hydroxyl is on the opposite face of the sugar ring and thus presents a hydrophobic surface. This hydrophobic surface of T6P is matched by Leu103 (distance ~ 3.9 Å) in LacC. This mutual incompatibility of

the C2 hydroxyl recognition site is the best candidate for the observed substrate discrimination.
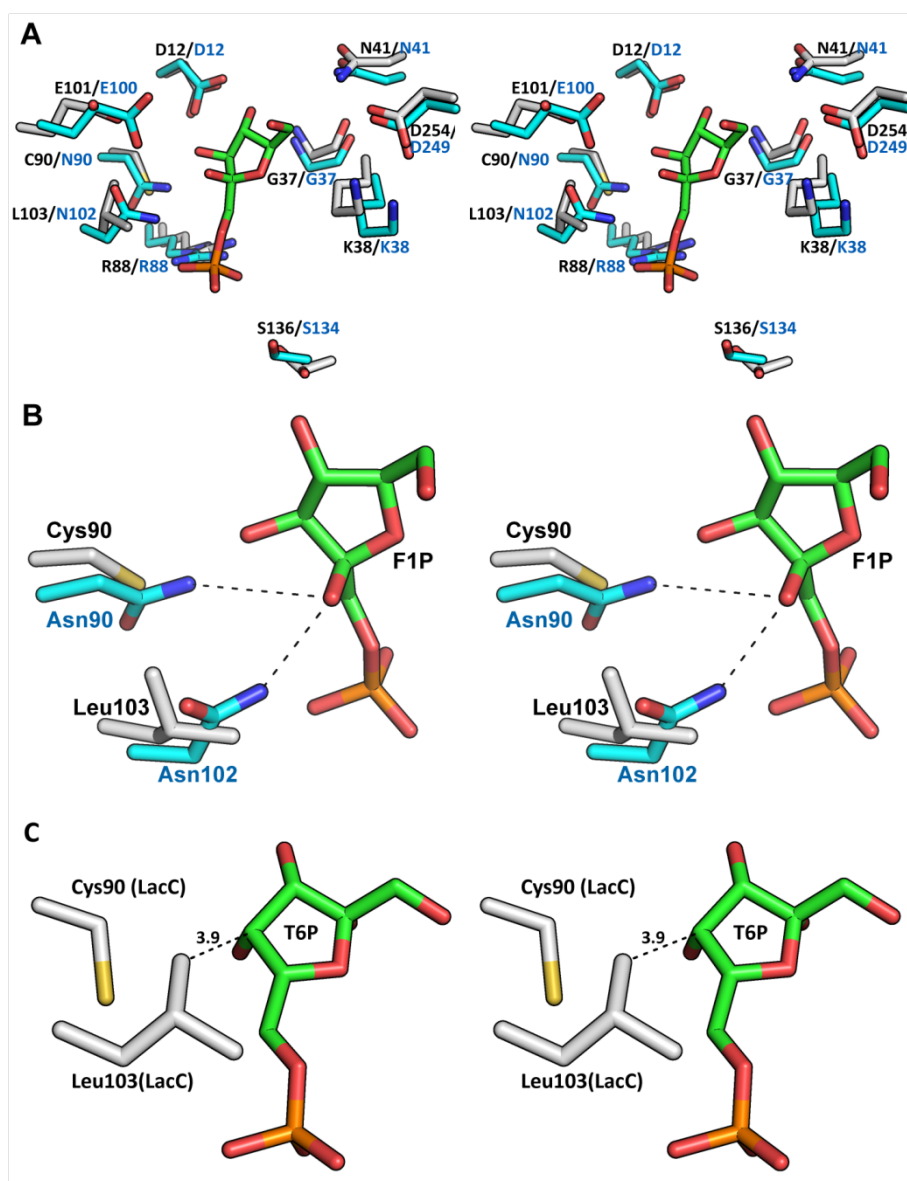
FIGURE 3.32: Stereo view of superimposed of the active site residues of *S. aureus* PFK and *S. aureus* LacC. [A] Stereo view of superimposed of all F1P binding site residues of *S. aureus* PFK and *S. aureus* LacC. [B] Stereo view of the two distinct residues that might interact with C2

hydroxyl group of F1P in *S. aureus* **PFK and** *S. aureus* **LacC. [C] hydrophobic interactions in** *S. aureus* **LacC**

A model of F1P and ATP binding in *S. aureus* PFK is generated according to our prediction (FIGURE 3.33). Protein surface shows that both ATP and F1P can fit into the active pocket of *S. aureus* PFK. The surface electrostatics potential of ribose group of ATP and the ring moiety of the F1P are neutral, while the surface around phosphate groups of ATP and F1P are reasonable positively charged. We predict that such settings can significantly stabilize and neutralize the phosphate group during the phosphoryl transfer process.
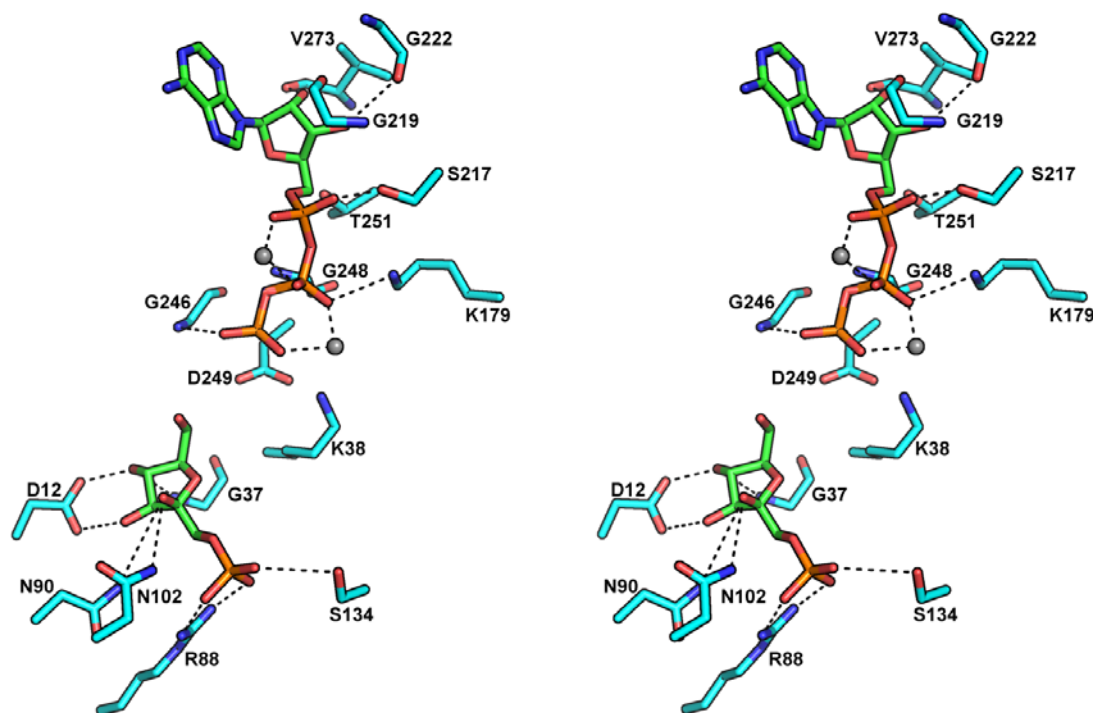
FIGURE 3.33: Stereo view of the proposed active site of *S. aureus* **PFK. Protein C atoms are shown in marine blue, C atoms of the substrate are shown in green. N, O and P atoms are shown in blue, red and orange, respectively. Potential hydrogen bonds between protein and ligands are shown as black dashes. ATP, Mg ions and F1P are docked to indicate the proposed binding site, respectively. Main chains of the selected residues are hidden for clarity purpose.**
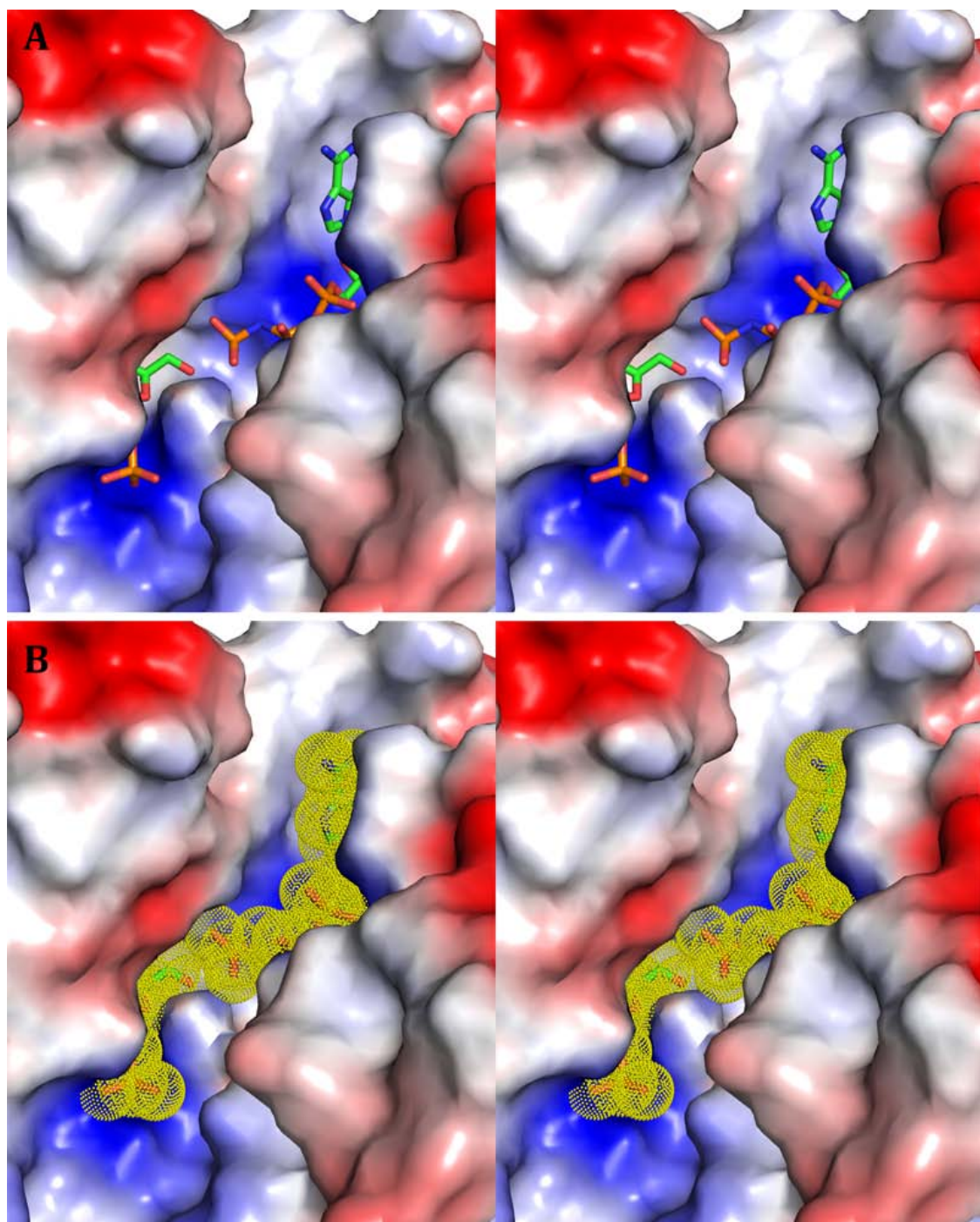
FIGURE 3.34: Stereo view of electrostatics surface potential of the proposed ATP and F1P binding site of S. aureus PFK. The solvent-accessible surface of TAG colored based on the electrostatics potential from -7 to +7 kT/e, calculated using ABPS tools in PyMol™. Positive charge is shown in blue and negative charge is shown in red. AMP-PNP and F1P are superimposed to indicate the potential binding site of PFK.

Structure comparison between the apo-form of *S. aureus* PFK and complex structures of other ribokinase-pfkB family enzymes reveal a conformational change. When binding with the substrate, the region between lid domain and sandwich domain is closed down like a "clam shell". The lid domain covers the groove between two domains, with the four flexible loops that linking the two domains act as the hinge joint. This closed conformation presumably holds the ligands more tightly and may create the catalytic environment for the reaction (FIGURE 3.35).
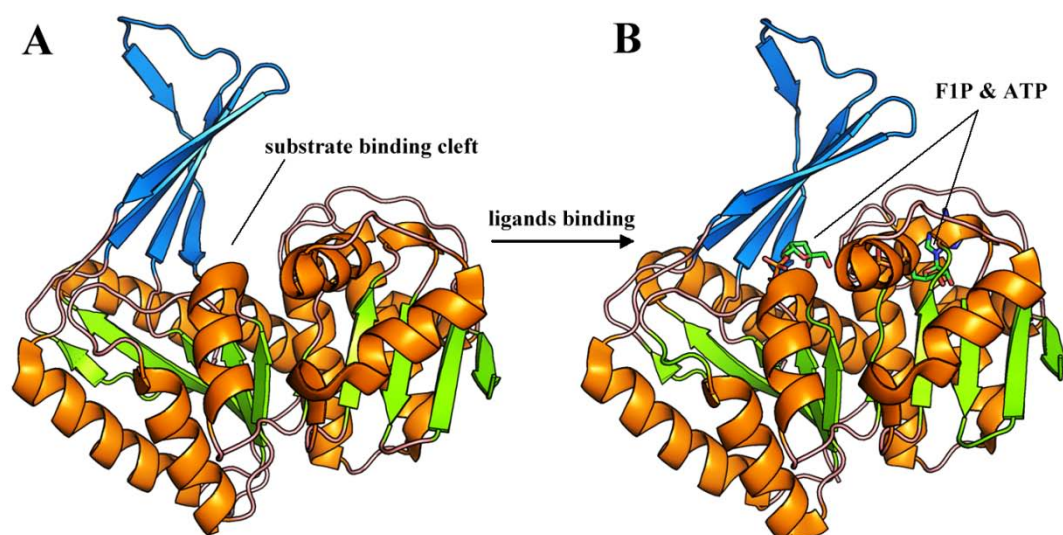
FIGURE 3.35: The proposed conformational change in PFK upon substrate binding. The small domain (lid domain) is shown in marine blue. The β-strands in the large domain (sandwich domain) are shown in orange and the α-helices are shown in green. F1P and ATP are superimposed to indicate the proposed binding site of substrate and co-factor.

The movements can be thought of as a small rotation of the large domain against the fixed small dimerization domain. Similar phenomenon (domain closure) of conformational change has been observed in some other members of the ribokinase family like 6-phosphofructokinase from *Pyrococcus horikoshii* OT3 (Currie, Merino

et al. 2009) and many other multi-domain proteins (Ito, Fushinobu et al. 2001; Cheng, Bennett et al. 2002). This domain movement is essential for the phosphoryl group transfer in its reaction (Sigrell, Cameron et al. 1998) and this strategy is well known and widely applied in nucleotide-dependent transferases . The catalytic amino acids are positioned at their proper location by such conformational change (Matte, Tari et al. 1998). As the domains close, the active site is set for catalysis bringing the hydroxyl and phosphate close together.
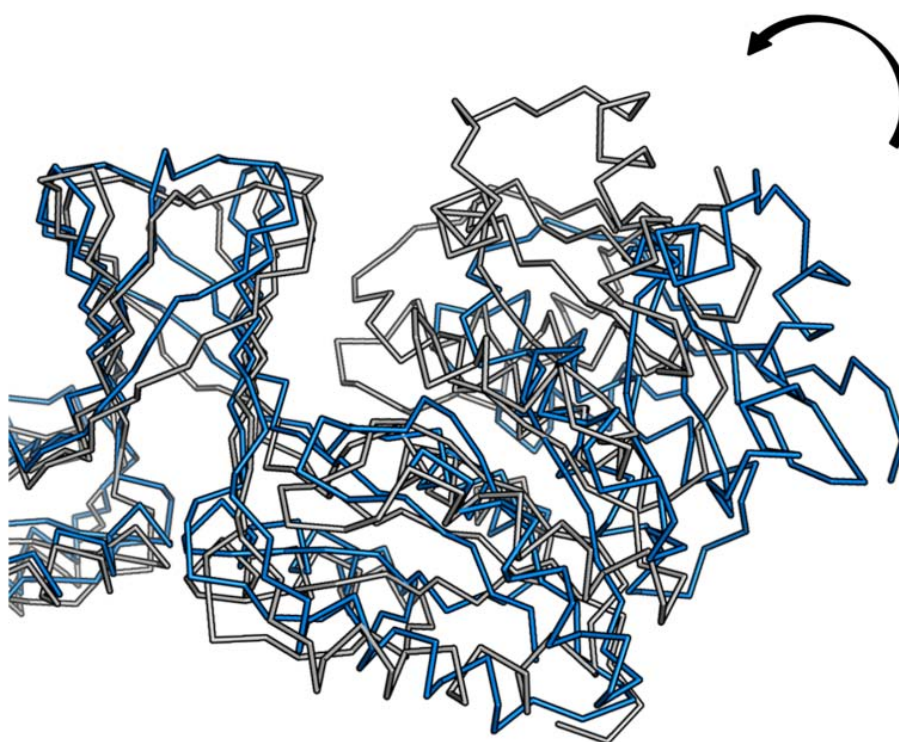
FIGURE 3.36: Stereo view of the conformation change of open-form and closed-form structure. The open-form (apo-form) structure is shown in marine blue. The closed-form structure is shown in grey.

3.4.4 The proposed catalytic mechanism of *S. aureus* PFK

The mass spectra results and activity assay have been used to confirm the putative *S. aureus* PFK. The apparent K_m of *S. aureus* PFK for F1P was approximately 490 µM when enzyme was measured in the presence of 2 mM ATP and 5 mM $MgCl_2$. This value is comparable to other PFKs. The *S. aureus* PFK is also capable of binding to the substrate F1P and co-factor ATP as reported for similar enzymes.

	initial velocity (nmol/min)
Michaelis-Menten	
Best-fit values	
VMAX	27.11
KM	0.4924
Std. Error	
VMAX	0.7007
KM	0.04492
95% Confidence Intervals	
VMAX	25.68 to 28.54
KM	0.4008 to 0.5840
Goodness of Fit	
Degrees of Freedom	31
R²	0.9799
Absolute Sum of Squares	51.26
Sy.x	1.286
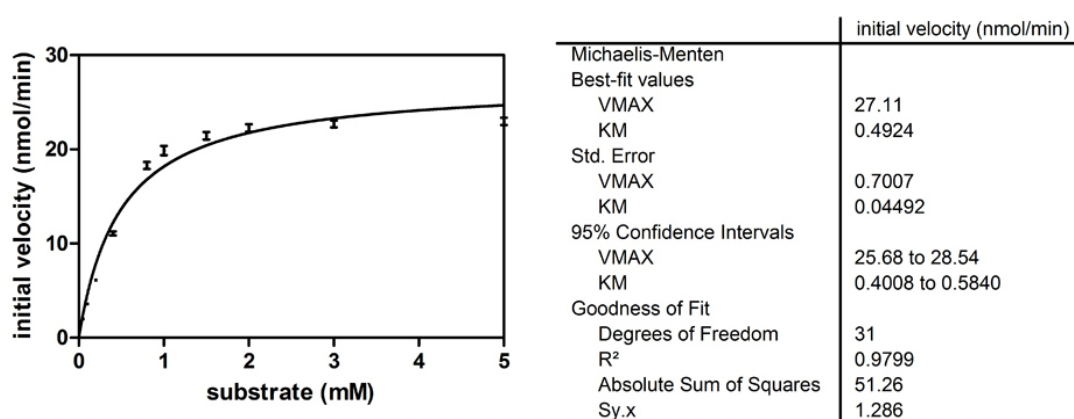
Source	K_m for *S. aureus* PFK (mM)	citations
E. coli	0.36	(Veiga-da-Cunha, Hoyoux et al. 2000)
A. aerogenes	0.75	(Sapico and Anderson 1969)
C. difficile	0.16	(Davies, Detheux et al. 1990)
S. aureus	0.49	This work

TABLE 3.6: K_m for *S. aureus* PFK and other PFKs.

Structure-based and sequence comparison between *S. aureus* PFK and other ribokinase-pfkB family enzymes provide a general idea of the location of the substrate

and how the reaction proceeds. The predicted catalytic centre is located at the cleft between lid domain and sandwich domain, the interface between the substrate (F1P) and co-factor (ATP). The Lys38 from conserved motif I and Asp249 from conserved motif II are close to γ-phosphate group of AMP-PNP/ATP and C1 hydroxyl group of F1P. The side chain of Asp249 is likely to function as a base that attracts the proton from the C1 hydroxyl group of F1P, then a nucleophile is generated to attack the γ-phosphate group of ATP, leading to phosphorylation and eventually producing fructose 1,6-bisphosphate. Lys38 would serve to stabilize and neutralize the negative charge during the transition of phosphoryl group. This proposed catalytic mechanism of *S. aureus* PFK is similar to other ATP-independent phosphoryl transferases/kinase and consistent to the catalytic mechanism proposed by Sigrell (Sigrell, Cameron et al. 1999).

FIGURE 3.37: Selected sequences are strictly conserved in ribokinase-pfkB family enzymes. Identical residues in the sequences aligned are highlight in black, residues shaded grey indicate regions of sequence homology. The three highly conserved motifs are shown The two predicted key catalytic residues Lys38 and Asp249 are indicated by red arrows and labeled. This alignment was generated with the BioEdit program
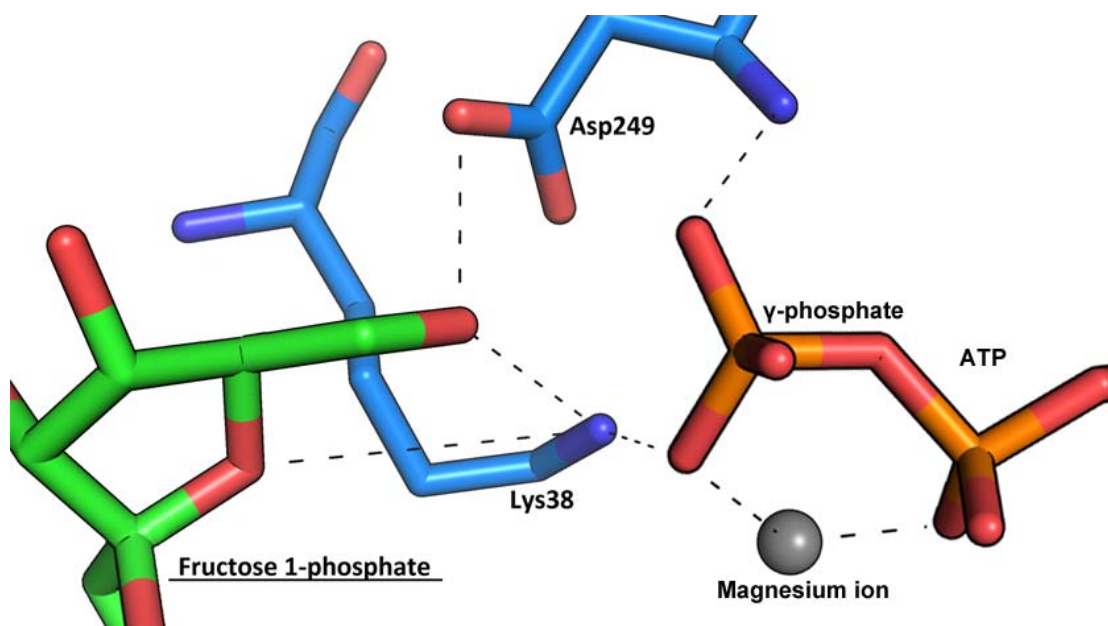
FIGURE 3.38: Cartoon representation of the catalytic centre for *S. aureus* PFK. Protein C atoms are shown in marine blue, C atoms of F1P are shown in green. N atoms, O and P atoms are shown in blue, red and orange, respectively. F1P, AMP-PNP and the two key residues Asp249 and Lys38 are shown to indicate the interactions with the hydroxyl and phosphate group. The potential interactions are shown as black dashes.

The metal ion is a critical element for the reactions (Mathews, Erion et al. 1998; Arnfors, Hansen et al. 2006). Mg^{2+} ions are found within the active sites of related structures e.g. human adenosine kinase, and are proposed to establish the cation bridges between the γ- and β-phosphates of the ATP, or the β- and α-phosphate of ADP. Furthermore, Mg^{2+} ion and the side chains are involved in the creation of a water-mediated interaction network with other amino acids in active site. These interactions are critical for transition state stabilization (Abele and Schulz 1995; Sabini, Ort et al. 2003; Liu, Timm et al. 2006). This architecture is also predicted to help orient the side chain that involved in transition, stabilize any negative charge during the reaction. The Mg^{2+} ion may also be essential for making the P-O bond between the γ- and β-phosphate more sensitive to nucleophilic attack by polarizing the

P-O bond (Pappu, Gregory et al. 1994) (Schumacher, Scott et al. 2000). This Mg-nucleotide complex setting can facilitate the effective attack by the activated hydroxyl group of F1P.
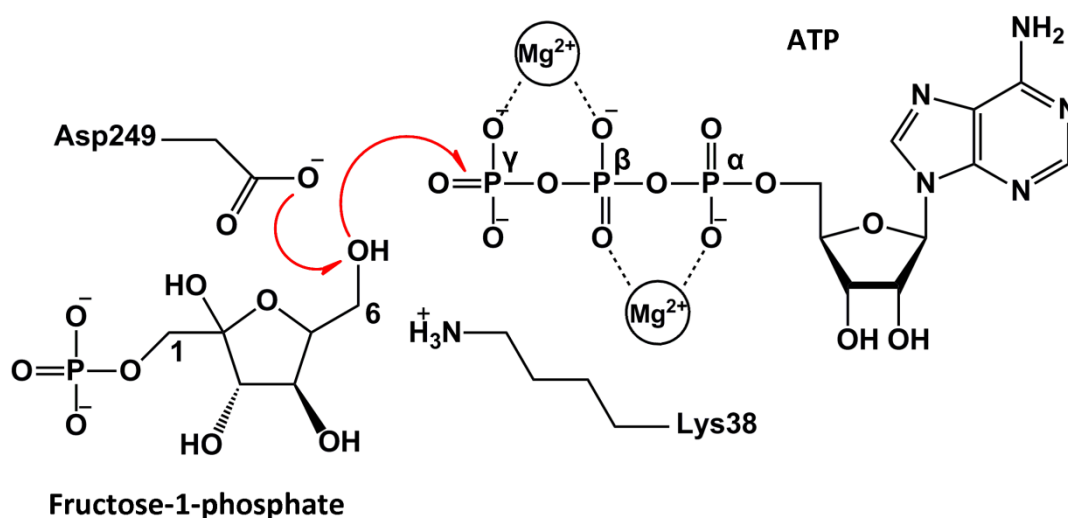
FIGURE 3.39: The proposed mechanism for the γ-phosphate of the ATP transfer to fructose 1-phosphate by 1-phosphofructokinase.

3.4.5 Future work

Although we have solved the PFK native structure, the proposed mechanism of enzyme needs further experimental work, namely site directed mutagenesis. In order to understand the interactions between protein and ligand, better quality crystals of PFK in complex with its substrate F1P and AMP-PNP are needed. To further validate the thermofluor data, an NMR assay or co-crystallization is necessary. The compounds can now be tested for inhibition using the assay described here. Mutational analysis would also provide valuable information on enzyme activities and provide useful information for inhibitor design.

Chapter 4

Structural studies of the mevalonate kinase from Methicillin-resistant *Staphylococcus aureus*, a member of the GHMP kinase family.

4.1 <u>Summary</u>

Mevalonate Kinase (MK) is an important enzyme that catalyzes the first step in the Mevalonate pathway. The 32.4 kDa protein from *S. aureus,* has been over-expressed, purified and crystallized. The enzyme crystallizes in the space group P6222 with a cell dimension of a=b= 94.6, c=169.0; α=β= 90°. γ=120°. A data set diffracting to 2.2 Å has been collected at ESRF, however molecular replacement attempts were unsuccessful. Heavy atom soaks were attempted by soaking various solutions into the native crystals. The structure was solved using multiple isomorphorus replacement (MIR). Citrate was bound at the active site and it was not possible to obtain a co-complex structure with mevalonate or ATP analogue. A Thermofluor assay was also applied to investigate the interactions between the enzyme and some potential fragments. The enzyme was assayed for activity and kinetic constants determined.

4.2 <u>Introduction</u>

4.2.1 Isoprenoids and the mevalonate pathway

Isoprenoids are a class of organic compounds comprising a huge family of more than 30,000 different natural products (Lange, Rujan et al. 2000; Wilding, Brown et al. 2000). Isoprenoids are essential for cell membranes and cell wall biosynthesis (Reusch 1984), and are also involved in electron transport (Reusch 1984; Kwon, Bhattacharyya et al. 1996). Isoprenoids are normally synthesized from the five-carbon starter unit, isopentenyl diphosphate (IPP) (Reusch 1984). IPP is synthesized by two different pathways, the mevalonate pathway (Goldstein and Brown 1990) and a non-mevalonate pathway, the glyceraldehydes-3-phosphate pyruvate (GAP-pyruvate) pathway (Rohmer, Knani et al. 1993; Rohmer 1999) (Lange, Rujan et al. 2000). The mevalonate pathway (mevalonate-dependent pathway) is widely used by many organisms such as mammals, yeast and archaea (Barnes and Goodfellow 1971; Porter 1985; Goldstein and Brown 1990). While the GAP-pyruvate pathway was discovered recently in some microorganisms and plants (Rohmer 1999; Kim, Stauffacher et al. 2000; Wilding, Brown et al. 2000).

The mevalonate-dependent biosynthetic route was first proposed in eukaryotes in the 1960s reviewed in (Kuzuyama 2002). In this pathway, two molecules of acetyl coenzyme A (Acetyl-CoA) are first polymerized into acetoacetyl coenzyme A (Acetoacetyl-CoA), and then this intermediate combines with another molecule of

acetyl-CoA to give 3-hydroxy-3-methylglutaryl-CoA (HMG-CoA), which is reduced by HMG-CoA reductase (Wang and Tong 1999). Mevalonate is then double phosphorylated to mevalonate 5-pyrophosphate by mevalonate kinase and phosphomevalonate kinase, then decarboxylated by diphosphomevalonate decarboxylase and finally dehydrated to form the IPP for further biosynthesis (Goldstein and Brown 1990; Wilding, Brown et al. 2000; Wilding, Kim et al. 2000; Dewick 2002). (FIGURE 4.1)

Some bacteria such as *E. coli* (Lange, Rujan et al. 2000; Kuzuyama and Seto 2003) can use the distinct GAP-pyruvate pathway to generate IPP. However, some Gram-positive bacteria such as *Streptococcus pneumonia, Enterococcus faecalis and S. aureus* (Wilding, Kim et al. 2000) can use the mevalonate-dependent pathway to form the IPP. Given its importance for membrane and cell wall biosynthesis, if any stage of this pathway is blocked, the growth of bacteria will be inhibited.
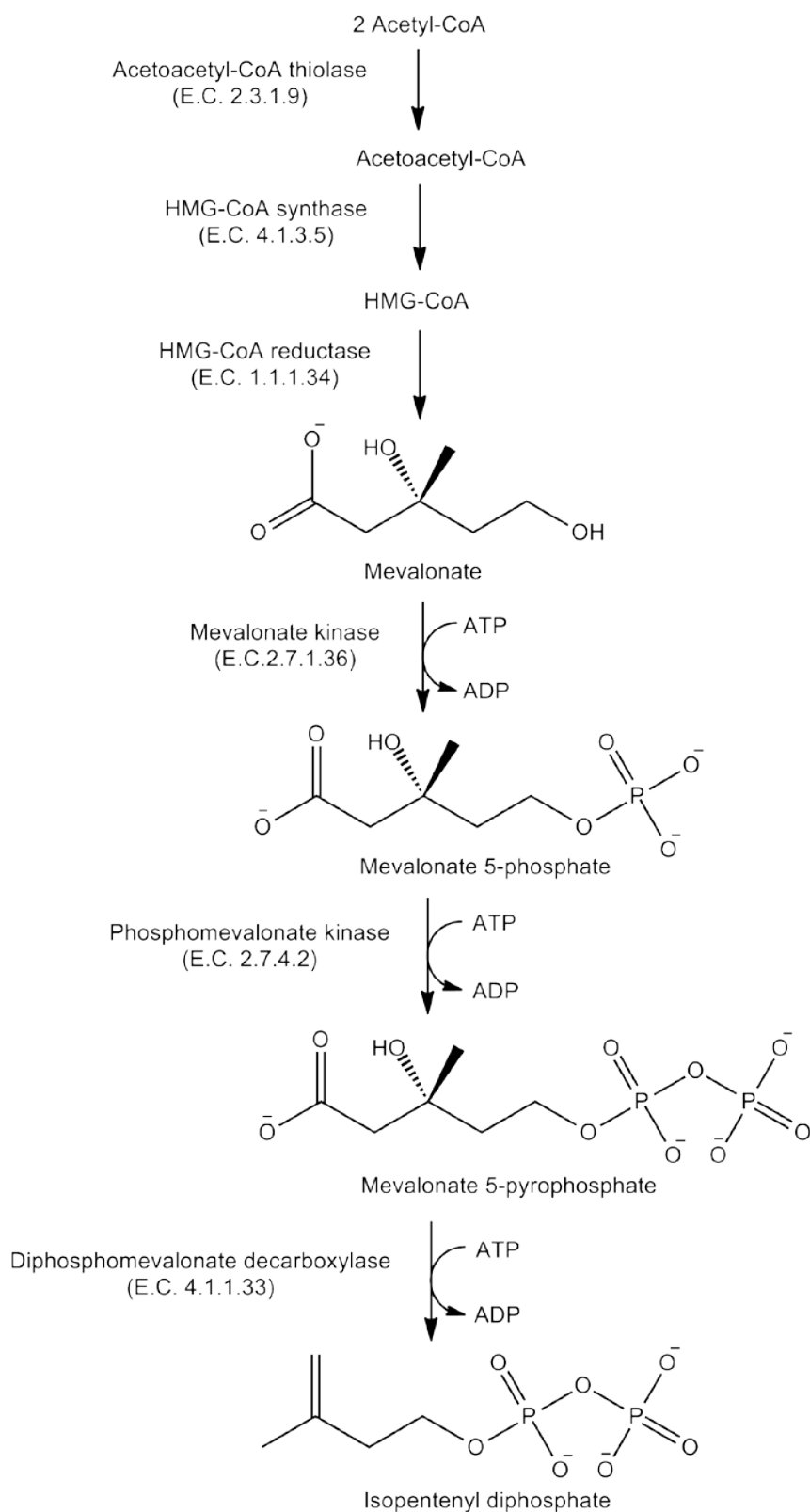
FIGURE 4.1: Mevalonate pathway. The acronyms: MK, mevalonate kinase (ATP:(R)-mevalonate phosphotransferase, E.C 2.7.1.36); PMK, phosphomevalonate kinase (ATP: (R)-phosphomevalonate kinase, (E.C 2.7.4.2); and DPM-DC, diphosphomevalonate decarboxylase (ATP: (R)-5-diphosphomevalonate carboxy-lyase, E.C 4.1.1.33).

4.2.2 The GHMP Kinase family

Kinase can be classified into three major distinct super-families according to their basic structure overall fold and sequence similarities (Azzi, Boscoboinik et al. 1992; Zhou, Daugherty et al. 2000; Andreassi and Leyh 2004) The first group is composed primarily of protein kinase, which usually use a conserved loop connecting two anti-parallel β-sheet for the binding of phosphate (Bossemeyer 1994; Zhou, Daugherty et al. 2000). The second group is called the classical phosphate-binding-loop-containing kinases, they share a common motif consisting of a helix-loop-strand, and use this loop for phosphate binding (Matte, Tari et al. 1998), for instance the homoserine kinases (Zhou, Daugherty et al. 2000). The third group include sugar kinases and actin, which use two β-hairpins to bind the phosphate group (Bork, Sander et al. 1993).

Crystal structures of eukaryotic MK and bacteria MK show that this enzyme is a typical member of the GHMP kinase family, this family belongs to the second kinase group (Bork, Sander et al. 1993; Fu, Wang et al. 2002; Yang, Shipman et al. 2002) GHMP derive from its members Galactokinase (G), Homoserine kinase (H), mevalonate kinase (M) and phosphomevalonate kinase (P) originally (Tsay and Robinson 1991; Bork, Sander et al. 1993). These proteins share a common overall fold and a highly conserved motif with an invariant arrangement of Gly-X-Gly-Ser-Ser-Ala-Ala. (FIGURE 4.2). This motif was first identified in 1991 (Tsay and Robinson 1991) and considered as the signature structure motif for GHMP kinase family. This motif is found as a loop between α-helix and a β-strand and is

believed to be involved in the phosphate group binding of ATP. (FIGURE 4.3)

In the past 10 years, new members of GHMP kinase family have been identified, such as mevalonate 5-diphosphate decarboxylase (MDD) (Cordier, Lacombe et al. 1999), 4-diphosphocytidyl-2C-methylerythritol kinase (CDPME) (Luttgen, Rohdich et al. 2000) and isopentenyl monophosphate kinase (IMK) (Lange and Croteau 1999). Shikimate kinases have also been identified as a member of this kinase family (Daugherty, Vonstein et al. 2001)
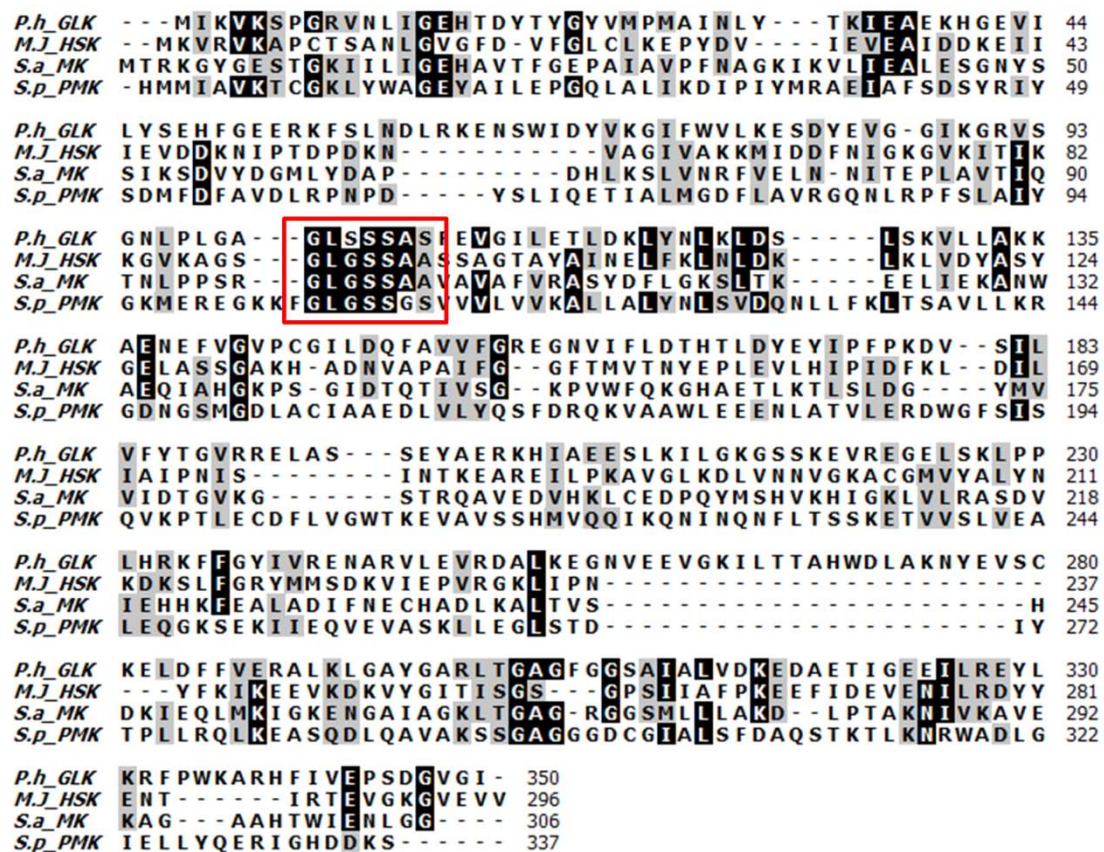
FIGURE 4.2: The conserved phosphate-binding-loop in classical p-loop-containing group of kinases family. The signature motif phosphate-binding-loop is highlighted by a red square. Sequence alignment using BioEdit (Hall 1999) and DALI (Holm and Sander 1993) server.
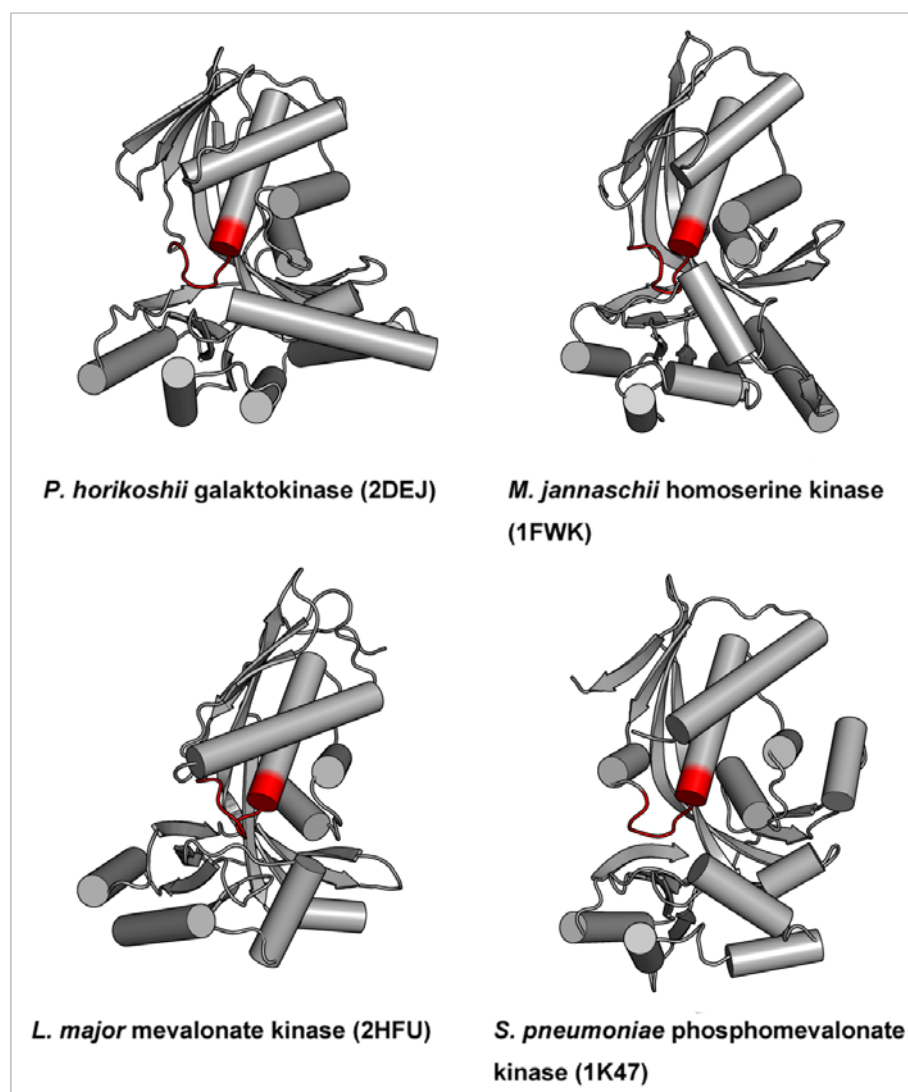
FIGURE 4.3: Structures of the classic GHMP kinase family enzymes. Helices and β-strands are shown as grey cylinders and arrows. The signature phosphate-binding-loop are shown in red. The r.m.s.d value between these structures is in a range of 2.2-3.0. These values are suggested by the web-based protein structure comparison service SSM at European Bioinformatics Institude (EBI) http://www.ebi.ac.uk/msd-srv/ssm/.

4.2.3 Mevalonate Kinase from *S. aureus*

Mevalonate kinase (MK) (E.C. 2.7.1.36) transfers the γ-phosphoryl group of ATP to the C5 hydroxyl oxygen group in mevalonate, converting mevalonate to mevalonate 5-phosphate. The systematic name of mevalonate kinase is: ATP: mevalonate

5-phosphotransferase. Studies have suggested that this enzyme is essential for the biosynthesis of IPP in both the mevalonate-dependent (Goldstein and Brown 1990) and non-mevalonate pathway (Contin, van der Heijden et al. 1998; Schulte, van der Heijden et al. 2000). Mevalonate kinase was first discovered in 1950s (Amdur 1957; Tchen 1958). This enzyme has been found in eukaryotes (Goodman and Popjak 1960), archaeal sources (Williamson and Kekwick 1965), plants (Rogers, Shah et al. 1966) and animals including human (Soler, Jabalquinto et al. 1979; Porter 1985) where it plays an important role in all of these organisms. A deficiency of mevalonate kinase in human can lead to inherited diseases such as hyperimmunoglobulemia D syndrome (HIDS) and mevalonic aciduria (Houten, Wanders et al. 2000). *S. aureus* requires the mevalonate-dependent pathway to generate the basic building block IPP for isoprenoids biosynthesis (Kuroda, Kuroda et al. 2003). Although kinase is shared with humans, the generation of kinase inhibitors now in development as anticancer agents (Mani, Wang et al. 2000) holds out the hope of engineering specific targeted inhibitors.
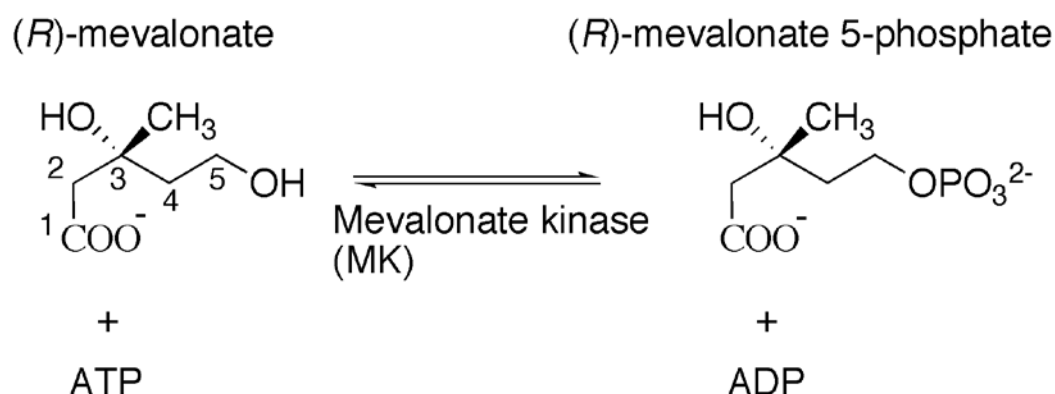
FIGURE 4.4: Reaction catalyzed by mevalonate kinse (E.C 2.7. 1. 36). With the conversion of ATP to ADP.

The mevalonate-dependent pathway is essential for survival of *S. aureus* on skin and nose mucosa (Peacock, de Silva et al. 2001; Voynova, Rios et al. 2004). *S. aureus* MK, in common with other bacterial enzymes, is much smaller than the eukaryotic MKs. Crystal structures of bacterial and animal MK such as the rat MK in complex with ATP has provided insights into how the eukaryote protein binds with the co-factor. However, there is no bacterial MK structure in complex with substrate and co-factor. *S. aureus* mevalonate kinase is up-regulated in strain MRSA252, but down-regulated in strain MSSA476, such proteomic differences suggesting that this enzyme may be particularly important for the pathogenic strain. In addition, the structural and functional differences between *S. aureus* MK and animal (human) MK might provide some novel ideas for inhibitors design. When the project began there was no prokaryotic ATP analogue co-complex structure known.

4.3 Materials & Methods

4.3.1 Over-expression and purification of MK

IPTG induction and Auto-induction

The small scale IPTG induction method was used to test solubility. The *S. aureus* mevalonate kinase plasmid was firstly transformed into *E. coli* BL21 (DE3) cells (Novagen) and plated onto Ampicillin agar plates. Single colonies were grown in 10 ml LB medium at 37 ℃ for 4 hours, grown to an OD_{600} of 0.6–0.8 at 37 ℃, supplemented with 100 µg/ml ampicillin. The temperature was then reduced to 25 ℃

and 16 °C, respectively. Protein over-expression was achieved by induction with 1.0 mM isopropyl β-D-1-thiogalactopyranoside (IPTG) for 6 hours.

The auto-induction method was employed to test the expression and solubility (Studier 2005). 1ml of a 10 ml overnight culture was used to inoculate 50 ml of LB and the cells were harvested, after overnight incubation at 37 °C, at 2000 g and re-suspended in 20 ml PBS. This was then used to inoculate auto-induction medium for over-night expression of protein, as detailed by Studier (Studier 2005). 500 ml of auto-induction growth medium in a 2L baffled flask, supplemented with 100 µg/ml ampicillin, was inoculated with 5 ml re-suspended cells and grown at 37 °C, using shaking at 300 r.p.m for 4 hours to start bacterial growth. The temperature was then lowered to 16 °C and left for 48 hours to reach saturation (OD$_{600}$ ~ 2.6). The results indicate that more soluble *S. aureus* MK resulting using the auto-induction method (FIGURE 4.5). Large scale (4 L) expression using auto induction was then performed to produce the target protein. Induced cells were harvested by centrifugation at 10500 x g for 15 minutes (Beckman Avanti J20-XP, JL8.100 rotor). The cells were re-suspended in PBS to remove any excess growth media and stored at -80 °C until required.
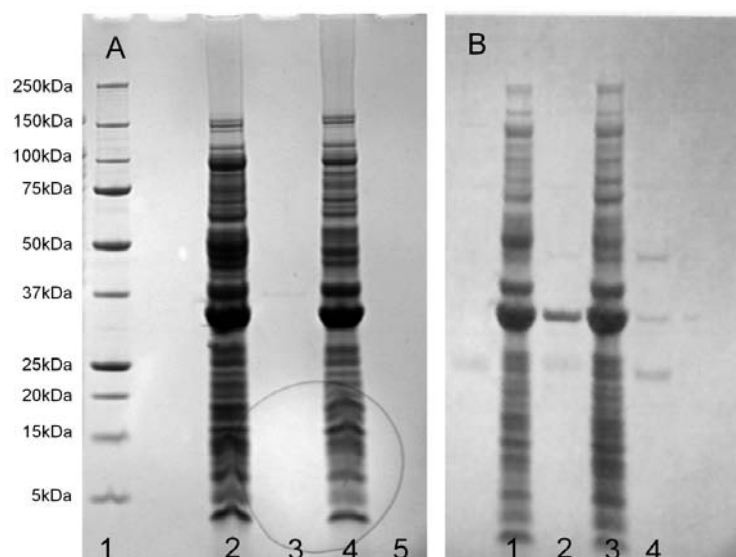
FIGURE 4.5: Coomassie Blue stained SDS-PAGE gels of *S. aureus* **PFK. [A.1] protein marker. [A.2] crudes flow through of IPTG induction at 16 ℃.[A.3] first elution of IPTG induction at 16 ℃. [A.4]crudes flow through of IPTG induction at 25 ℃. [A.5] first elution of IPTG induction at 25 ℃. [B.1] crudes flow through of auto induction at 16 ℃. [B.2] first elution from auto induction at 16 ℃. [B.3] first elution from auto induction at 25 ℃. [B.4] first elution from auto induction at 25 ℃.**

Purification

A standard purification protocol was applied as described in chapter II. The buffer system for MK purification is slightly different from PFK protein. 50 mM phosphate buffer (11.25 mM NaH_2PO_4, 38.75 mM Na_2HPO_4) replaced the 50 mM Tris-HCl in *S. aureus* MK purification approach. The induced cells were re-suspended in binding buffer at room temperature for 30 minutes. The cells were disrupted by sonication for 8 cycles of 45 seconds, interrupted by 1 minute periods on ice after addition of 20μg/ml DNAse I and one tablet of protease inhibitor (ROCHE). To ensure that the DNA was digested by DNAse I, the mixture was kept at 4℃ for another 20 minutes. After addition of 2 mM EDTA, the mixture was centrifuged for 45 minutes at 105000 x g at 4 ℃. Then the supernatant fraction was passed through a 0.22 µm syringe filter

(Millipore) and collected for further purification.

The supernatant containing mevalonate kinase protein was applied to a charged Histrap Nickel Sepharose, high performance column (Amersham Biosciences), which had been equilibrated already with binding buffer. Unbound and weakly bound proteins were removed by extensive washing with washing buffer. Essentially pure mevalonate kinase protein was eluted and collected with elution buffer. Eluted protein was incubated with 1 ml of 2 mg/ml tobacco etch virus protease (TEV) (approximate ratio 20:1 protein: protease) to remove the polyhistidine tag at room temperature (25 ℃). The MK protein and TEV mixture was dialyzed against 500 mM NaCl, 2 mM DTT, 50 mM phosphate buffer, pH 8.0 and 10% glycerol for 6 hours to remove imidazole. The progress of cleavage was checked by sodium dodecyl sulphate polyacrylamide gel electrophoresis (SDS-PAGE) (FIGURE 4.6).
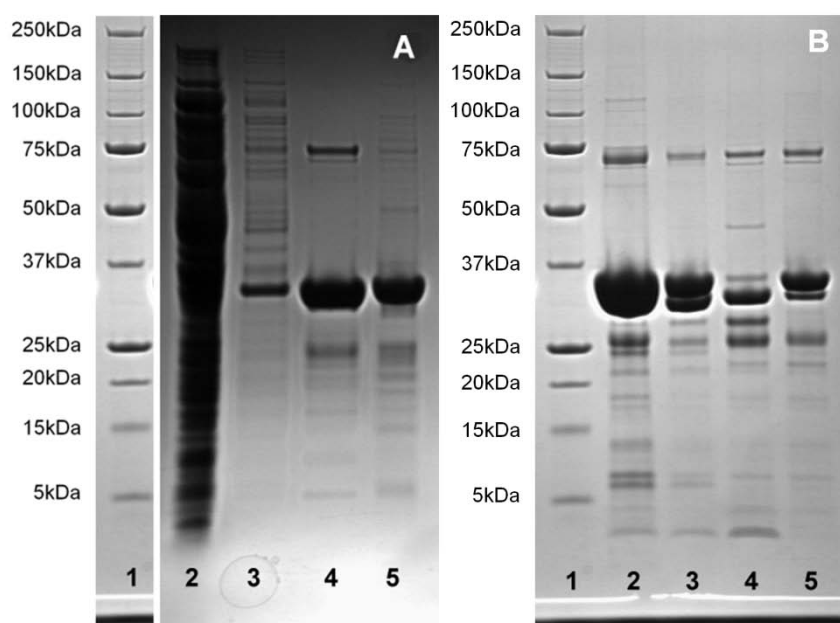
FIGURE 4.6: Coomassie Blue stained SDS-PAGE gels of *S. aureus* MK. [A.1] protein marker. [A.2] crudes flow through. [A.3] first wash through. [A.4]first elution. [A.5] second elution. [B.1]protein marker. [B.2]before tev cleavage. [B.3] 2 hours after addition of tev. [B.4]6 hours after addition of tev. [B.5] elution from second nickel column.

The protein-TEV mixture was passed through a 0.22 μM syringe filter membrane (Millipore) and a second Ni-NTA column to remove any non-cleaved protein, tag and protease (Liu and Naismith 2005). Then the flow through was concentrated to approximately 5 mL before further purification by size exclusion gel filtration. Some precipitant was removed by centrifugation at 75000 x g for 10 min (4°C, Beckman Avanti J20-XP JA25.50 rotor). Size exclusion gel filtration was applied on a Superdex™ 200 size exclusion chromatography column (Amersham Biosciences) After the gel-filtration step proteins were judged to be pure by Coomassie™ Blue-stained gels and their integrity was confirmed by mass spectrometry (University of St Andrews) (FIGURE 4.7). In total it was estimated 20 mg pure *S. aureus* mevalonate kinase native protein was obtained from 4 L of cell culture. According to the results of the Pre-Crystallization Test (PCT), the protein was then concentrated to 10 mg/ml and 5 mg/ml respectively prior to crystallization. Some of the protein was flash-frozen in liquid nitrogen for long term storage. The buffers used in each step were summarized in TABLE 4.1

Binding buffer	500 mM NaCl, 2 mM DTT, 50 mM phosphate buffer, pH 8.0, (11.25 mM NaH$_2$PO$_4$, 38.75 mM Na$_2$HPO$_4$), 10 mM imidazole
Wash buffer	500 mM NaCl, 2 mM DTT, 50 mM phosphate buffer, pH 8.0, (11.25 mM NaH$_2$PO$_4$, 38.75 mM Na$_2$HPO$_4$), 35 mM imidazole
Elution buffer	500 mM NaCl, 2 mM DTT, 50 mM phosphate buffer, pH 8.0, (11.25 mM NaH$_2$PO$_4$, 38.75 mM Na$_2$HPO$_4$), 500 mM imidazole
Dialysis buffer	500 mM NaCl, 2 mM DTT, 50 mM phosphate, pH 8.0, (11.25 mM NaH$_2$PO$_4$, 38.75 mM Na$_2$HPO$_4$), 500 mM imidazole, 10% glycerol. 1mM EDTA
Gel-filtration buffer (Crystallization buffer)	150 mM NaCl, 50 mM phosphate buffer (11.25 mM NaH$_2$PO$_4$, 38.75 mM Na$_2$HPO$_4$), pH 8.0

TABLE 4.1 Buffers used in each step of *S. aureus* MK purification.

Protein View   **B**

Match to: **Q6GJ78** Score: **795** Expect: 2e-073
Mevalonate kinase - Staphylococcus aureus (strain MRSA252)

Nominal mass (M_r): **33026**; Calculated pI value: **6.64**
NCBI BLAST search of Q6GJ78 against nr
Unformatted sequence string for pasting into other applications

Taxonomy: Staphylococcus aureus subsp. aureus MRSA252

Sequence Coverage: **69%**

Matched peptides shown in **Bold Red**

```
  1 MTRKGYGEST GKIILIGEHA VTFGEPAIAV PFNAGKIKVL IEALESGNYS
 51 SIKSDVYDGN LYDAPDHLKS LVNRFVELNN ITEPLAVTIQ TNLPPSRGLG
101 SSAAVAVAFV RASYDFLGKS LTKEELIEKA NWAEQIAHGK PSGIDTQTIV
151 SGKPVWFQKG HAETLKTLSL DGYMVVIDTG VKGSTRQAVE DVHKLCEDPQ
201 YMSHVKHIGK LVLRASDVIE HHKFEALADI FNECHADLKA LTVSHDKIEQ
251 LNKIGKENGA IAGKLTGAGR GGSMLLLAKD LPTAKNIVKA VEKAGAAHTW
301 IENLGG
```

FIGURE 4.7: Gel-filtration results and mass spectrometry analysis of S. aureus mevalonate kinase. [A] selected fraction of gel-filtration elution. [B] mass spectrometry output of the protein.

4.3.2 Crystallization and optimization of MK crystals

The substrate of MK, (R)-Mevalonate was not commercially available, so mevalonatelactone purchased from Sigma-Aldrich was purchased to prepare mevalonate according to the protocol described in (Skilleter and Kekwick 1967). A standard stock solution was prepared by using 1g of Mevalonatelactone (SIGMA, MW: 130) added to 4.62ml of 1M NaOH, the solution were incubated at 37 °C for 2 hours to hydrolyze the mevalonolactone, the pH was adjusted to 7.2 with HCl and the final volume was brought to 7.69ml with distilled water.
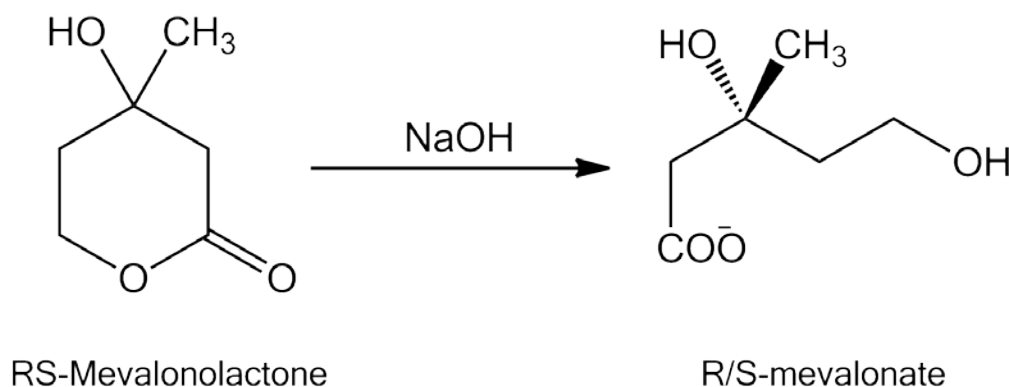
FIGURE 4.8: Mevalonolactone hydrolysised by NaOH and converted to mevalonate.

156

In order to produce complex crystals of mevalonate kinase with its substrate and co-factor, co-crystallization method was attempted using 20 mM substrate mevalonate and 10 mM AMP-PNP. AMP-PNP is an analogue of ATP, and it resistant to hydrolysis because th e O between γ- and β-phosphate is replaced by N. Mevalonate and AMP-PNP were both dissolved in mevalonate kinase crystallization buffer to avoid any disruption to the protein solution. The protein and ligands solution were mixed gently and pre-incubated for 6 hours at 4°. The protein and ligands mixture was then centrifuged at 35000 x g for 2 min (Eppendorf Centrifuge 5415D) to remove any insoluble compounds and precipitated protein.

The sitting drop method was employed for crystal screening, using a drop size of 0.3 μl, containing 0.15 μl proteins and 0.15 μl precipitant, against 80μl screen buffer. The same nano-drop crystallization robot (Cartesian Honeybee) from Hamilton-Thermo Rhombix system was also used to perform this screening. The crystal screens employed for this initial crystal screening including JMac, Nextal-The Classics, Nextal-JCSG, Nextal-PEGs (Hampton Research). All the sitting drop trials were kept in a quiet room at 20 ℃ for crystal growing. The best crystals judged by shape and size appeared after approximately 5 days from Hampton PHClear condition 19 [0.1 M citric acid pH 4.0, 4 M sodium chloride]. An optimization screen around this condition was attempted to produce better quality crystals suitable for X-ray diffraction. Some large crystals were observed in an optimized condition containing 0.1 M Citric acid, pH 3.8, 3.6 M NaCl. Using a drop with 3 µL protein and 3µL

precipitant equilibrated against a reservoir of 100 µL optimized screen buffer. Crystallization conditions had to be translated and optimized from nanodrop to microliter drop size. The best results were obtained using sitting drop plates (Hampton Research CrystalClear Strips™ 96 wells plates) with 2 µl MK protein plus 2 µl precipitant. Changing of the NaCl concentration from 3 M to 4 M did not change the form of the crystal, and the crystals grew to typically 0.1 to 0.3 mm in the longest dimension. The diffraction quality was tested by an in house X-ray generator, Crystals were cryo-protected with 20% – 25% glycerol added to screen buffer before being flash-frozen for synchrotron source data collection before being flash-frozen for synchrotron source data collection. The improvement of the size and quality of the crystals can be seen in FIGURE 4.9
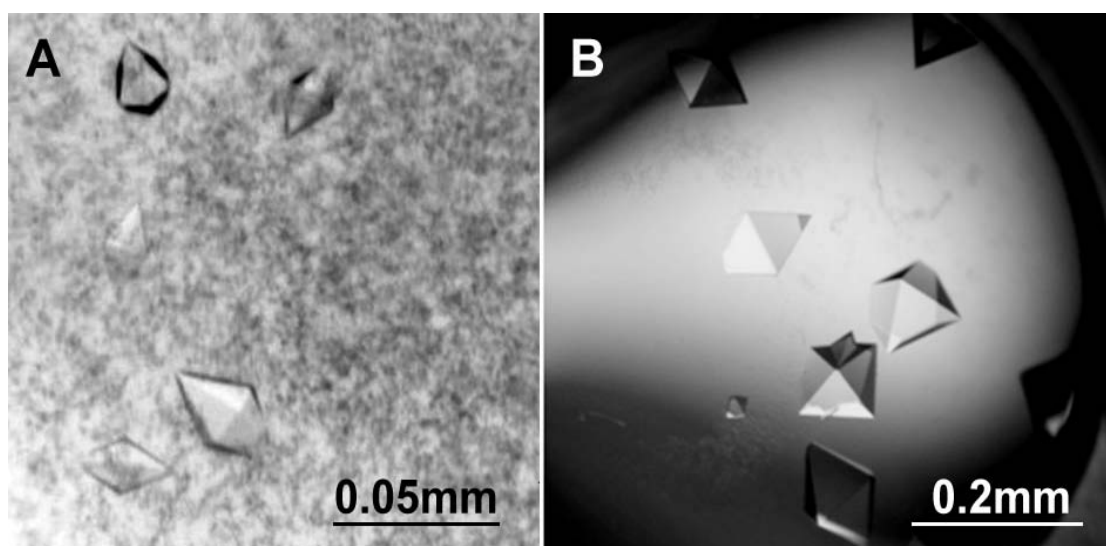
FIGURE 4.9: *S. aureus* **MK crystals. [A]** *S. aureus* **MK complex crystals grown in nano drop. [B] Larger crystals of** *S. aureus* **MK complex after optimization at similar condition.**

4.3.3 Data collection and initial processing

Crystals were cryo-cooled in liquid nitrogen using a cryo-protectant of screen buffer containing 20% glycerol, 0.1 M Citric acid, pH 3.8, 3.6 M NaCl. A dataset diffracting to 2.2 Å was collected on crystals at ESRF Beamline BM14. 308 images were collected using an exposure time of 20 seconds and a crystal to detector distance of 225.9 mm. The wavelength used for data collection is 0.953 Å. The data set was first indexed with the program DENZO (Otwinowski and Minor 1997). The suggested crystal lattice belonged to a primitive hexagonal Laue group with cell dimensions of a=b= 94.6 Å, c=169.0 Å; α=β= 90° γ=120°. Data were integrated with these parameters and then merged in SCALEPACK (Otwinowski and Minor 1997). Diffraction image and data collection statistics are shown in FIGURE 4.10 and TABLE 4.2 respectively.
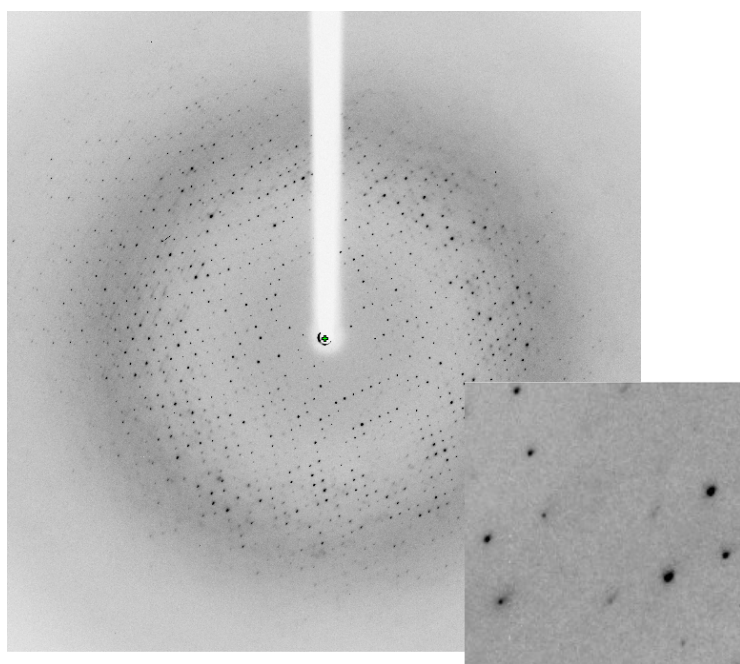
FIGURE 4.10: X-ray diffraction pattern of *S. aureus* MK crystals from beamline BM14 ESRF.

The resolution at the edge of the detector is 2.0 Å.

Data collection	*S. aureus* mevalonate kinase
Wavelength (Å)	0.953
Resolution (Highset Shell)	81.92 – 2.20 (2.26-2.20)
Unit cell	a=b=94.589., c=169.010 α=β=90, γ=120
Space Group	P6$_2$22
Unique reflections	17784 (1937)
Average redundancy	4.6 (4.2)
Completeness (%)	100 (78.3)
R$_{merge}$	0.095 (0.34)
I/σ (I)/	17.7 (4.7)

TABLE 4.2: Summary of data collection statistics for *S. aureus* MK crystal collected in ESRF.

4.3.4 MR attempts and heavy atom soaking.

Attempts to solved the structure by Molecular Replacement were made with AMoRe (Navaza 1994), MOLREP (Vagin and Teplyakov 2000) and PHASER from CCP4 suite using crystal structure of *L. major* mevalonate kinase (PDB entry: 2HFU) (Sgraja, Smith et al. 2007). However these attempts ultimately proved unsuccessful, the programs only giving a partial solution with a Rotation Function Z of 4.3. This may have been due to the limited sequence identities with the potential search models (highest sequence identity was 29%).

Since the structure could not be solved by molecular replacement we tried to use other techniques to solve the structure including the use of heavy atom. Several heavy metal salts were selected by signal strength at 1.541 Å in an attempt to obtain derivative

crystals (FIGURE 4.8), including pCMBS, $Hg(NO_3)_2$, $K_2Hg(NO_3)_4$, $Au[CN]_2$, $Sm(NO_3)_3$ and $K_2Pt[CN]_4$. The apo-form crystals was transferred to "heavy atom soaking solution" containing cryo-protectant of 25% glycerol, 0.1 M Citric acid, pH 3.8, 3.6 M NaCl, and 2-20 mM heavy metal derivatives for a short time (10 min) or a long time (overnight) to assessed for stability. Crystals usually tolerated soaking, however in some cases the crystals began to dissolve in the solution, or cracked. Crystals that survived soaking using low concentration (2 mM) were also soaked using a higher concentration (20 mM). Those crystals that survived were assessed for X-ray diffraction. The in-house Rigaku-MSC Micromax-007 hf X-RAY generator system ($\lambda=1.541$Å) was used to collect these heavy atom data, the oscillation angle was 0.5 degree from -180° to 180° and the distance between the crystal to detector was 70 mm. At this stage, 6 heavy atom datasets were collected.
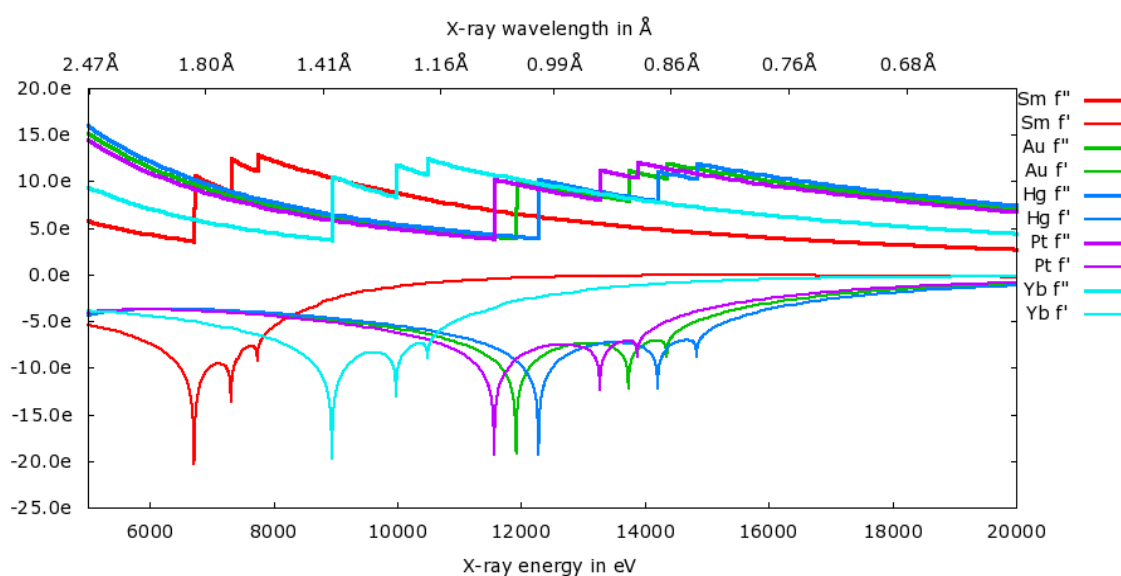
FIGURE 4.11: Plot of theoretical f' and f" for different heavy atoms under different X-ray wavelength. Image was made by a web-based X-ray Anomalous Scattering Coefficients check tool http://skuld.bmsc.washington.edu/scatter/

4.3.5 Data processing, structure solution and model refinement

For the multiple isomorphorus replacement (MIR) attempts, the phase calculations and heavy atom sites localization were performed with the PHENIX program (Adams, Grosse-Kunstleve et al. 2002) using two heavy atom soaking datasets combinations. However, most of the electron density maps generated from those heavy atoms were ambiguous and difficult to interrupt, possibly due to non-isomorphism between the datasets. However a $Sm(NO_3)_3$ and a $K_2Pt[CN]_4$ dataset collected to 2.6 Å and 2.7 Å, respectively, were able to localize 2 heavy atom sites using PHENIX. The AutoBuild program in PHENIX suite then significantly improved the initial phases and a partial model was built with 223 residues. Although this model was incomplete, it still showed a GHMP kinase family basic overall fold (FIGURE 4.12).

Data collection	MK-Sm	MK-Pt
Wavelength (Å)	1.541	1.541
Resolution (Highset Shell)	30 – 2.60 (2.65-2.60)	30-2.70 (2.74-2.70)
Unit cell	a=b=94.10., c=169.10 $\alpha=\beta=90, \gamma=120$	a=b=94.00., c=168.90 $\alpha=\beta=90, \gamma=120$
Space Group	$P6_2 22$	$P6_2 22$
Unique reflections	34293 (4937)	35120 (4968)
Average redundancy	5.6 (4.2)	5.9 (4.3)
Completeness (%)	100 (78.3)	98 (80.6)
R_{merge}	0.095 (0.34)	0.095 (0.43)
$I/\sigma (I)$	17.7 (3.7)	19.7 (3.9)

TABLE 4.3: Summary of data collection statistics for heavy atom soaked MK crystals.
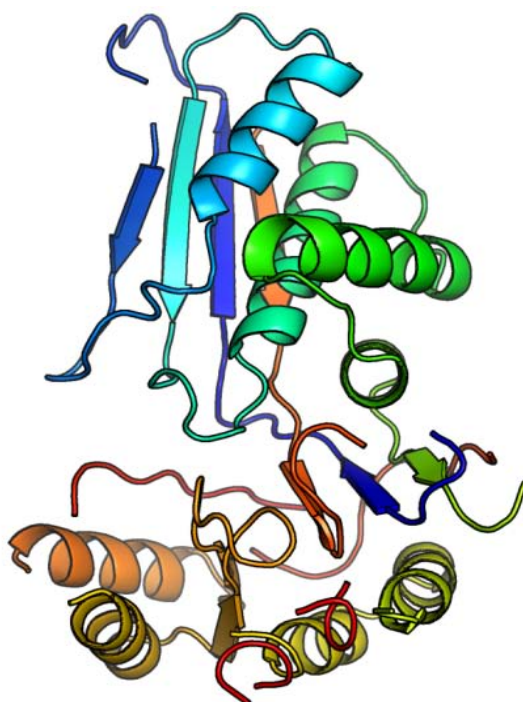
FIGURE 4.12: Cartoon representation of the model build by Autobuild in PHENIX suite. 212 residues were build in this model with an initial R/R$_{free}$ = 0.37/0.42.

The ARP/wARP program was then used to auto build the initial mevalonate kinase model with the MTZ file generated from program PHENIX and the mevalonate kinase sequence file of 306 amino acids. 9 chains of 269 residues in total were built in the new model after 50 building cycles with an R factor/R free of 0.31/0.38. Although there were 37 amino acid residues still missing in this new model, it was possible to rebuild the model manually using WinCoot and REFMAC5 subsequently. "Translation, libration and screw rotation parameters" (TLS) (Potterton, Briggs et al. 2003; Winn, Murshudov et al. 2003) was used in model refinement. Water molecules were added to the model automatically using ARP/wARP (Perrakis, Morris et al. 1999) in CCP4 program suite. Ligand libraries were prepared using PRODRG (Schuttelkopf

and van Aalten 2004). The MK model refinement statistics are summarized in TABLE 4.4.

Refinement	*S. aureus* MK
Clashscore (percentage)	8.84 (92%)
Rotamer outliers (%)	0.85
Cβ deviations >0.25 Å	0
Residues with bad bonds/angles (%)	0.00
MolProbity Score (percentage)	1.49 (99%)
Ramachandran favoured/outliers (%)	97.92/0.69
R_{factor}	0.213
R_{free}	0.257
r.m.s.d bond lengths(Å)/angles	0.008/1.070

TABLE 4.4: Model refinement and validation statistics of *S. aureus* MK

4.3.6 *S. aureus* MK enzyme activity assay

S. aureus mevalonate kinase enzyme activity assay was based on that previously described by Porter (Porter 1985) with some modification and carried out. The enzyme activity was measured by coupling the formation of ADP to the oxidation of NADH via two related enzymes, lactate dehydrogenase (LDH) and pyruvate kinase (PK), determined by measuring the decrease of absorbance at 340 nm using a spectrometer at room temperature (25 ℃).

mevalonate + ATP $\xrightarrow{\text{mevalonate kinase (MK)}}$ mevalonate 5-phosphate +ADP

ADP + phosphenolpyruvate $\xrightarrow{\text{lactate dehydrogenase (LDH)}}$ ATP + pyruvate

pyruvate + NADH + H $\xrightarrow{\text{pyruvate kinase (PK)}}$ lactate + NAD
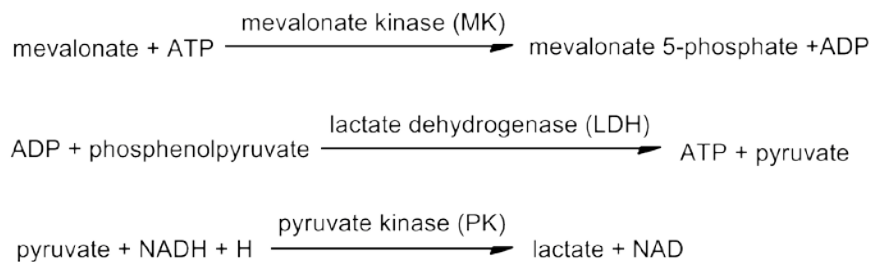
FIGURE 4.13: reactions in the measurement of mevalonate kinase enzyme activity using the coupled assay with pyruvate kinase (PK) and lactate dehydrogenase (LDH).

Mevalonate

mevalonate + ATP $\xrightarrow{\text{mevalonate kinase (MK)}}$ mevalonate 5-phosphate +ADP

ATP

ADP

Mevalonate 5-phosphate

ADP

phosphoenolpyruvate (PEP)

ADP + phosphenolpyruvate $\xrightarrow{\text{lactate dehydrogenase (LDH)}}$ ATP + pyruvate

ADP

ATP

pyruvate

pyruvate + NADH + H $\xrightarrow{\text{pyruvate kinase (PK)}}$ lactate + NAD

NADH

NAD$^+$
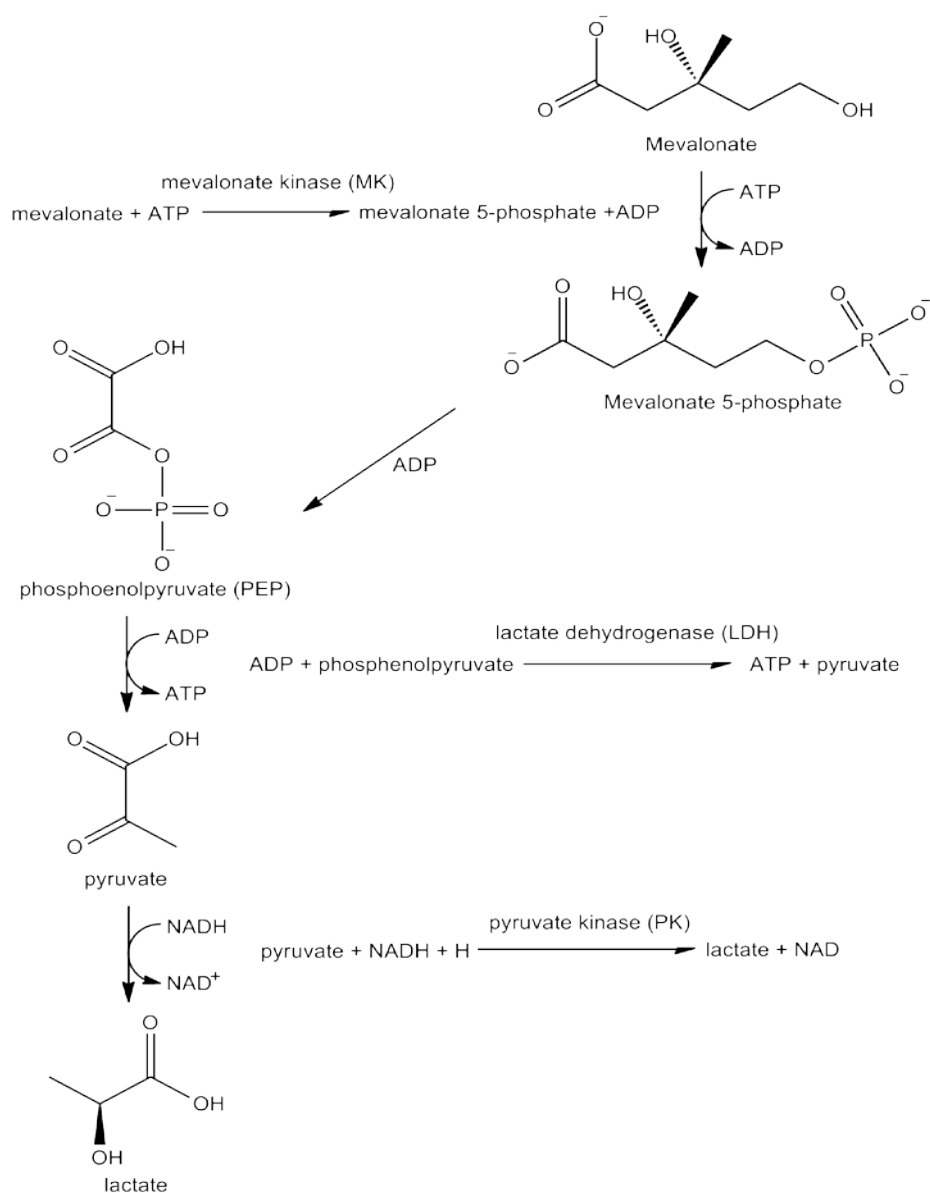
lactate

FIGURE 4.14: Diagram of the coupled reaction of formation of mevalonate 5-phosphate and ADP to the oxidation of NADH via two related enzymes, lactate dehydrogenase (LDH) and pyruvate kinase (PK).

165

The reaction mixture for this coupled assay containing 50 mM potassium phosphate buffer (KH_2PO_4/K_2HPO_4), pH 7.5, 0.2 mM NADH, 4 mM ATP, 8 mM $MgCl_2$, 1 mM phosphoenolpyruvate (PEP), 35 units pyruvate kinase, 55 units lactate dehydrogenase and 2 mM mevalonate. The final volume of the reaction mixture was 1 ml. The mixture was mixed gently and the background rate for the oxidation of NADH was measured for 3 minutes before addition of MK. The reaction was monitored for an additional 60 seconds. A unit enzyme activity is defined as the amount of enzyme producing 1 µmol mevalonate 5-phosphate per minute. All coupling enzymes and chemicals were tested in absence to make sure that the rate of the standard assay is not limited by them. All the reagents and assays auxiliary enzymes were purchased from Sigma-Aldrich.

The K_m for mevalonate was determined using an enzymes assay mixture containing 4 mM ATP, mevalonate concentration between 0.01 – 2 mM, and 1µg of pure *S. aureus* MK. Three repeat measurements were carried out to make sure the data are consistent. Data replotted in Grafit graphic analysis program. K_m of *S. aureus* MK for mevalonate was obtained using the Michaelis – Menten equation.
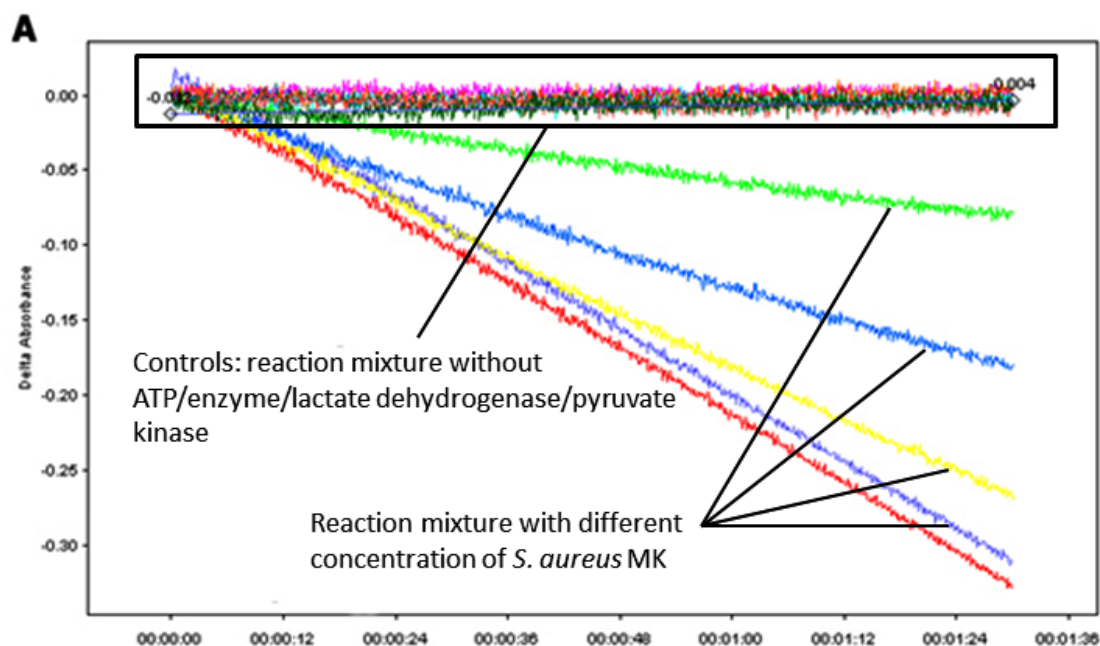
FIGURE 4.15: Enzyme kinetics study on *S. aureus* MK. The apparent K_m of *S. aureus* MK for mevalonate was approximately 110 μM when enzyme was measured in the presence of 4 mM ATP and 8 mM MgCl$_2$.
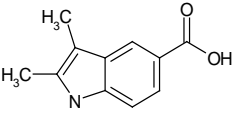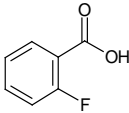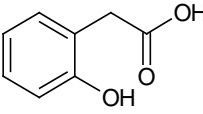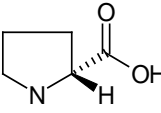
4.3.7 Thermofluor study on *S. aureus* MK

The Thermofluor assay is also applied for finding the potential hits for *S. aureus* MK. The same sample preparation and assay protocol are employed as described before (Chapter 2.3.6). All the samples were repeated twice at the same condition. The melting curves were also generated by the program iCycler iQ Optical System. The data could be further processed using the same program and Origin. Those fragments that shifted Tm over 2 ℃ were classed as hits.

Fragments	Structure	Formula	ΔT_m (℃)
2-methyl-3-furoic acid		C6 H6 O3	3

Name	Structure	Formula	
3-(2-methoxyphenyl)propanoic acid		C10 H12 O3	2
3-(2-hydroxyphenyl)propanoic acid		C9 H10 O3	2
1-methyl-5-(trifluoromethyl)-1H-pyrazol-3-ol		C5 H5 F3 N2 O	2
3-oxoindane-1-carboxylic acid		C10 H8 O3	2
2-ethyl-6-methylpyridine		C8 H11 N	3
4-hydroxy-1-methyl-1,2-dihydroquinolin-2-one		C10 H9 N O2	3
2,5-dimethyl-3-furoic acid		C7 H8 O3	2
2-furoic acid		C5 H4 O3	3
benzo[b]furan-3-ylacetic acid		C10 H8 O3	3
1-methyl-1H-indole-6-carboxylic acid		C10 H9 N O2	4
2-(benzylthio)acetic acid		C9 H10 O2 S	2
2-hydroxy-2-phenylacetic acid		C8 H8 O3	3
2-(1,3-benzothiazol-2-yl)acetonitrile		C9 H6 N2 S	3
2-fluoro-4-hydroxybenzonitrile		C7 H4 F N O	3

168

3-chloro-4-fluorophenol		C6 H4 Cl F O	2
2-fluorobenzoic acid		C7 H5 F O2	3
2-(2-hydroxyphenyl)acetic acid		C8 H8 O3	3
D-proline		C5 H9 N O2	4

TABLE 4.5: The positive hits of the thermal shift assay

These potential hits all are aromatic hetrocycles and possibly mimic the adenosine group. This mimicry is often seen in kinase type inhibitors (Ramdas and Budde 1998).

4.4 Results & Discussion

4.4.1 Crystal structure of *S. aureus* MK

Monomer

The crystal structure of *S. aureus* MK was determined to 2.20 Å. The final refined model of *S. aureus* MK monomer contains 295 residues with an R_{factor} and R_{free} of 0.21/0.26. The monomer appears as a bell-shape with two distinct structural domains. There are 11 β-strands and 9 α-helices in the final refined model.

The N-terminal domain is composed of residues 2-168, comprising the first seven β-strands (β1-β7) and four α-helices (α1-α4). The outer side of the large β-strands β1,

β3-β5 is mostly exposed to the solvent. The C-terminal domain is formed by residues 169-306 and contains four β-strands (β8-11) and five α-helices (α5-9). The four anti-parallel β-sheets β8-β10 are sandwiched by helices α5, α6 α7 and α8. The electron density of residues 182-183, 191-198 that located between helix α5 and strand β8 is weak. These residues lie at the surface of the *S. aureus* MK molecule. There is a deep cleft between the N- and C-terminal domains, and this cleft is predicted to contain mevalonate binding, ATP binding and catalytic site (FIGURE 4.16). The predicted ATP binding site has a strong positive charge (FIGURE 4.17). A citric acid molecule is bound in this cleft, presumably from the crystallization condition. (Chapter 4.4.2).
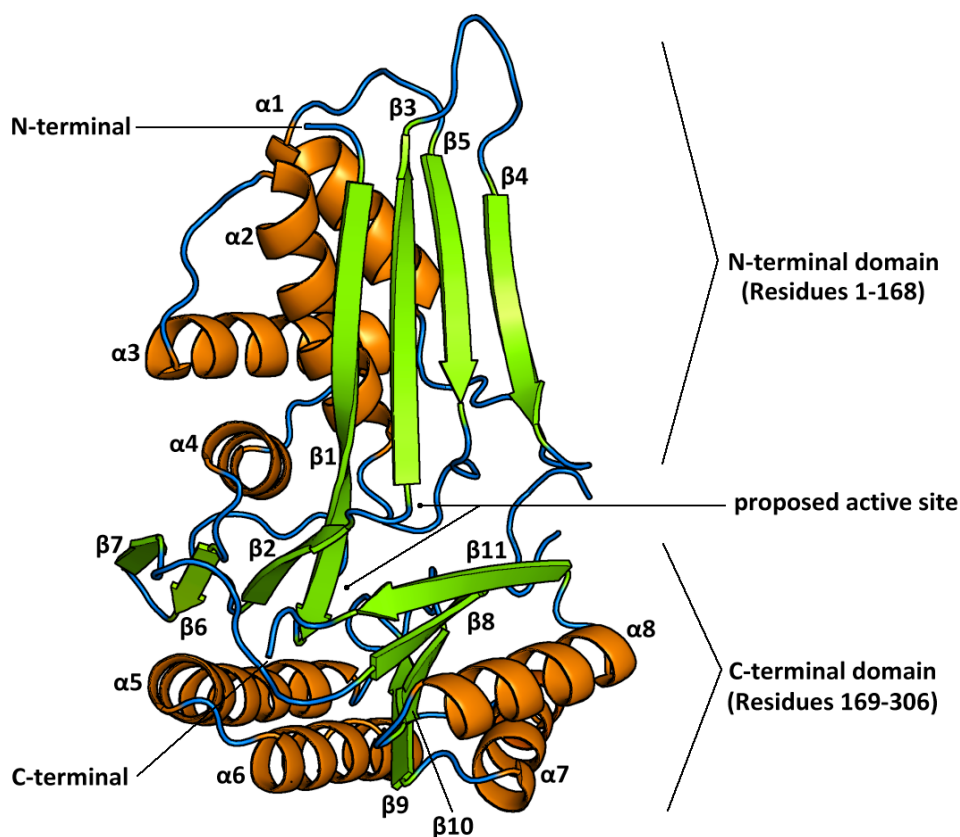
FIGURE 4.16: Cartoon representation of *S. aureus* mevalonate kinase monomer. Helices are

shown in orange and labeled, β-sheets in large domain are colored in green and loops are shown in blue.
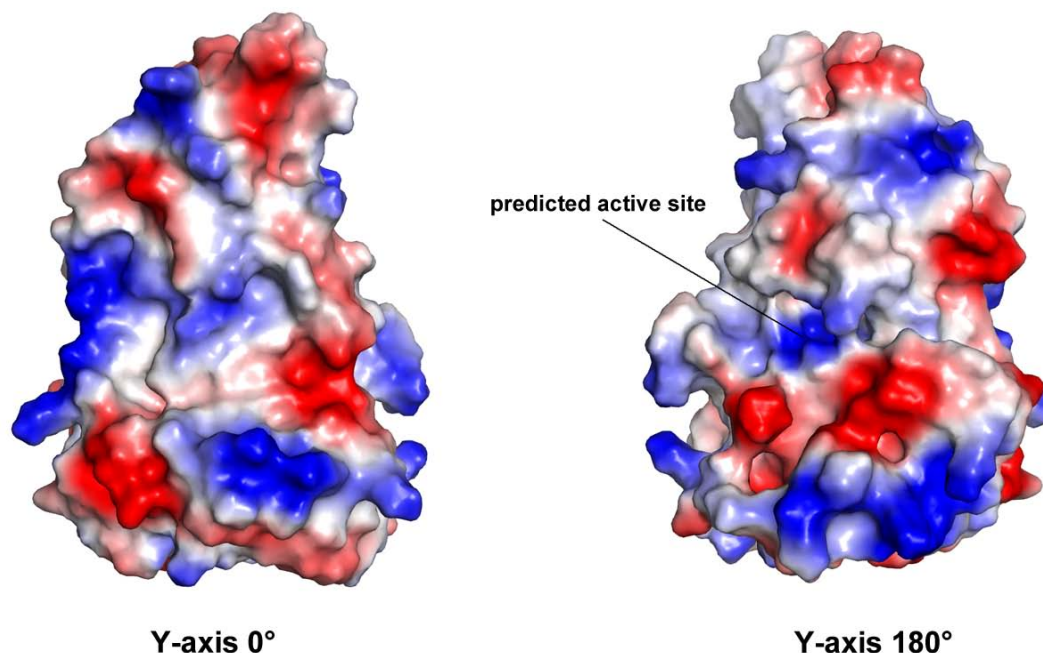
FIGURE 4.17: The surface electrostatics potential of *S. aureus* mevalonate kinase. The solvent-accessible surface of MK colored based on the electrostatics potential from -7 to +7 kT/e, calculated using ABPS tools in PyMol™. Positive charge is shown in blue and negative charge is shown in red.

The overall sequence similarity within the GHMP kinase family is low. An examination of the Protein Data Bank (PDB) for similar structures using the web-based protein structure comparison service SSM at European Bioinformatics Institute (EBI) http://www.ebi.ac.uk/msd-srv/ssm/ (Krissinel and Henrick 2004) shows that the *S. aureus* MK still shares a common overall fold with other GHMP kinase family enzymes with a r.m.s.d range of 2.5 – 4.2 Å. The locations of active site for mevalonate and ATP binding are likely to be conserved across the GHMP kinase family. The overall structure fold of *S. aureus* MK is more close to bacterial and *L.*

major (r.m.s.d of Cα atoms 2.5-3.5 Å) rather than mammalian enzymes (r.m.s.d 3.7-4.2 Å) (TABLE 4.6 and FIGURE 4.18)

Source	N_{align}	r.m.s.d(Å)
L. major mevalonate kinase	265	2.77
S. pneumonia mevalonate kinase	238	3.21
Rat mevalonate kinase	210	4.27
Human mevalonate kinase	189	3.72
P. horikoshii galactokinase	238	2.82
M. jannaschii homoserine kinase	233	3.29
S. pneumonia phosphomevalonate kinase	242	3.51

TABLE 4.6: Structure alignment of *S. aureus* mevalonate kinase using SSM at European Bioinformatics Institude (EBI) http://www.ebi.ac.uk/msd-srv/ssm/ (Krissinel and Henrick 2004). N_{align} indicates the Cα atoms aligned.
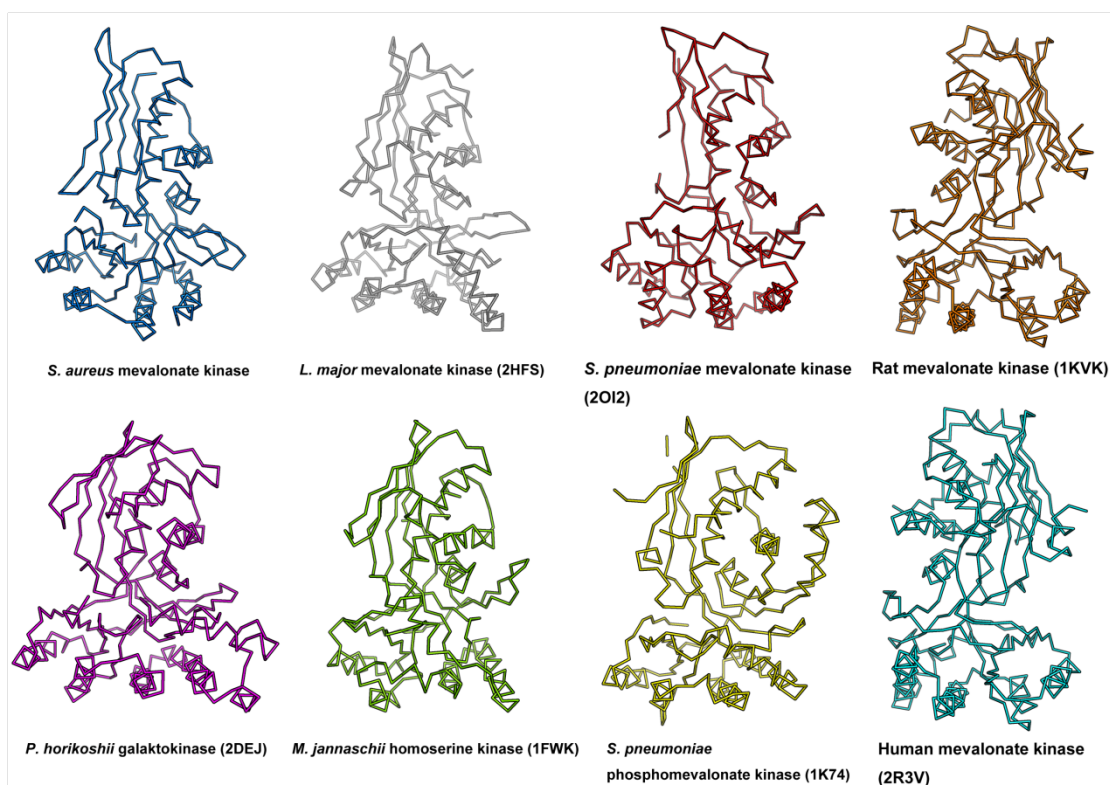
FIGURE 4.18: Ribbon view of the GHMP kinase family members' structures. MK from *S. aureus* (PDB code: 2X7I), MK from *L. major* (PDB code: 2HFS), galactokinase from *P. horikoshii* (PDB code: 2DEJ) homoserine kinase from *M. jannaschii* (PDB code: 1FWK) and phosphomevalote kinase from *S. pneumoniae* (PDB code: 1K74)

Structure comparison between these enzymes shows that they all comprise two domains. The N-terminal domain of the GHMP kinase family enzymes is mainly responsible for ATP binding and also participates in the formation of the catalytic centre in the GHMP kinase family (Zhou, Daugherty et al. 2000; Fu, Wang et al. 2002). The C-terminal domain in the GHMP kinase family enzymes is considered as the substrate binding domain (Zhou, Daugherty et al. 2000; Romanowski, Bonanno et al. 2002). There are some differences in some structure elements between *S. aureus* MK and other members of the GHMP kinase family. Some other GHMP kinases have more residues compare with *S. aureus* MK (306 residues), such as human MK (396

residues), rat MK (394 residues) and *P. horikoshii* galactokinase (346 residues). These additional residues form some extra structural elements in the N-terminal domain.

In rat MK, the sequence insertion forms a strand and a short helix. These additional structural elements create an open cavity that leads to the phosphate-binding-loop (motif II) and contributes to the binding of adenosine moiety of ATP. In *S. aureus* MK model, strand β4 is followed by a tight turn (loop) that links to helix α1 (residues 57-68). As a result the loop lies across the surface of the phosphate-binding-loop, which is the predicted ATP binding cavity. This loop denoted the "adenosine strap loop" could restrict the access of ATP/AMP-PNP by hindering the binding of adenosine group of ATP/AMP-PNP (FIGURE 4.19).
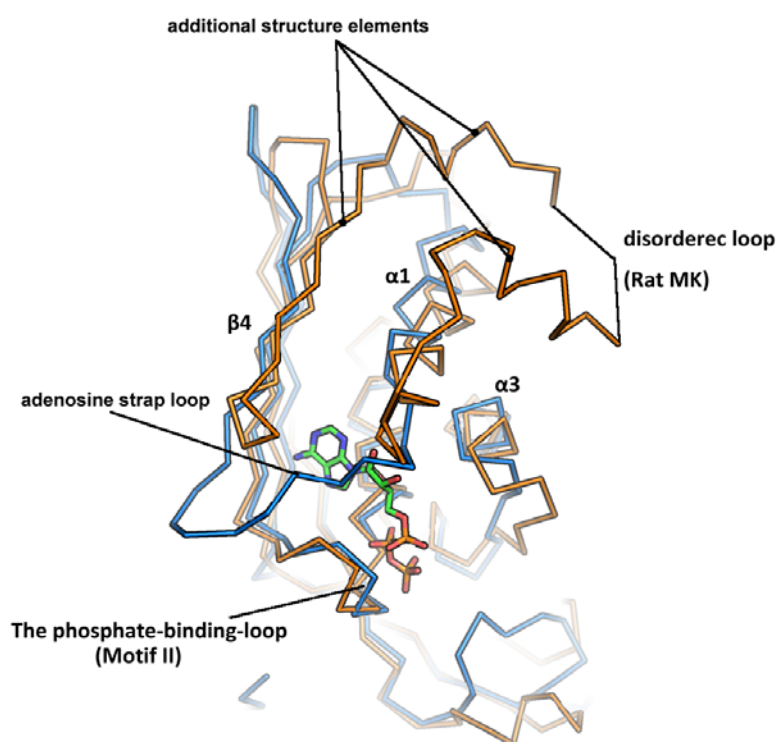
FIGURE 4.19: Cα-trace structure alignment of the N-terminal domains of the *S. aureus* MK and Rat MK. The *S. aureus* MK structure is shown in blue, the Rat MK is shown in orange. ATP molecule from Rat MK is superimposed to indicate the potential ATP binding site. N atoms, O and P atoms are shown in blue, red and orange, respectively. The related secondary structure elements of *S. aureus* MK are labeled.

Mammalian MKs (e.g. human MK) (Fu, Voynova et al. 2008) appear to conserve the insertion, presumably the same open binding cavity as rat MK. Some bacteria MKs also have sequence insertion in the N-terminal domain such as the *M. jannaschii* MK (Yang, Shipman et al. 2002). Currently the "adenosine strap loop" is only observed in a few bacteria enzymes of the GHMP kinase family such as *S. aureus* MK and *M. jannaschii* homoserine kinase (Zhou, Daugherty et al. 2000). MK from *Leishmania major* (Sgraja, Smith et al. 2007) exhibits this "adenosine strap loop" as well. No ATP or other ATP analogs complex structures were reported for these enzymes with the "adenosine strap loop". Attempts to obtain such complex structures with ATP/AMP-PNP binding were unsuccessful (Zhou, Daugherty et al. 2000; Sgraja, Smith et al. 2007). It seems that the ATP binding in these "adenosine strap loop" group MKs is more difficult than the other MKs with sequence insertion, which forms the open active site. Although this "adenosine strap loop" seems to block the access to ATP binding cavity, the enzyme assay shows that *S. aureus* MK is functional performing the phosphorylation reaction. Because this loop is located at the surface of the protein, we predict that the conformation of this loop could be influenced by crystal packing.
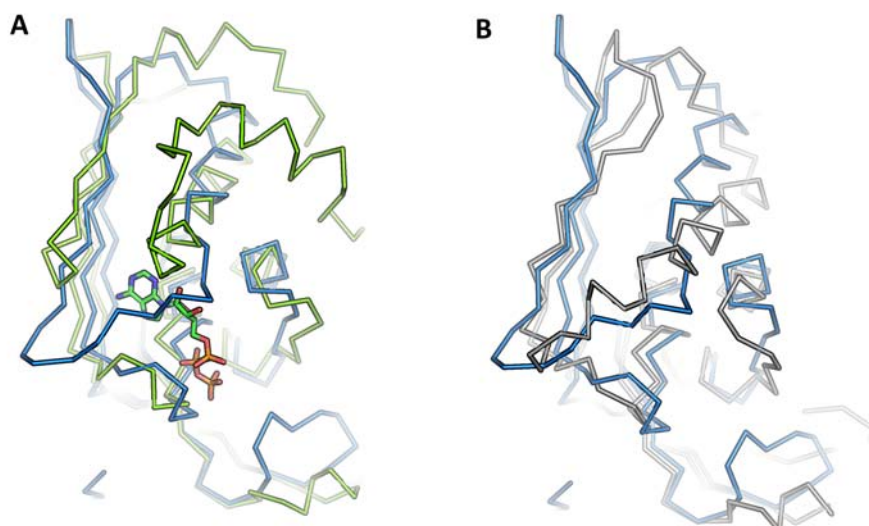
FIGURE 4.20: Cα-trace overlay for the N-terminal domains of *S. aureus* MK and other members of the GHMP kinase family. [A] *S. aureus* MK (blue) and Human MK (green). [B] *S. aureus* MK (blue) and *L. major* MK (grey).

A multiple sequence alignment of MKs from different species and *S. aureus* MK

indicates that there are three conserved structural motifs in MKs and other members

of the GHMP kinase family (e.g. galactokinase from *Pyrococcus furiosus)*. The

conserved structural motif I of the GHMP kinase family, in *S. aureus* MK, comprises

the last part of strand β1 and the loop link to β2, including residues 11-20. This motif

usually has the sequence of Lys-Ile/Val-Ile-Leu-X-Gly-Glu-His (Yang, Shipman et al.

2002). As a part of the N-terminal domain, motif I mainly contributes to the formation

of active site and interacts with the substrate (Zhou, Daugherty et al. 2000;

Romanowski, Bonanno et al. 2002). Motif II locates at the edge of N-terminal domain,

close to motif I, has an invariant residue arrangement of Gly-X-Gly-Ser-Ser-Gly-Ala

(residues 98-106 in *S. aureus* MK). These residues compose the loop after β5 and the

initial part of helix α2. This β-turn-α motif is the signature structural motif

"phosphate-binding-loop" that interacts with the β- and α- phosphate groups of ATP in the GHMP kinase family (Bork, Sander et al. 1993). Motif III is formed by part of β8 and the loop which connects to β9, and has a sequence of Lys-Leu-Thr/Ser-Gly-X-Gly-X-Gly-Gly residues order (residues 266-274 in *S. aureus* MK). This motif is considered to stabilize the phosphate binding loop (Zhou, Daugherty et al. 2000).

FIGURE 4.21: structure-based sequence alignment of Mevalonate kinases and galactokinase from the GHMP family. The mevalonate kinase sequences from *S. aureus (MK_Sa), Streptococcus. pneumoniae (MK_Sp), Methanocaldococcus. jannaschii (MK_Mj) Leishmania. Major (MK_Lm)* and galactokinase from *Pyrococcu. furiosus (GK_Pf)*. Identical residues in the sequences aligned are highlight in black, residues shaded grey indicate regions of sequence homology. The three conserved motifs are highlighted in red box.

FIGURE 4.22: stereo view of the three conserved GHMP kinase family structure motifs in *S.aureus* mevalonate kinase. Motif I is shown in purple, motif II and III are shown in green and blue, respectively. The related strands and helices are labeled for clarity.

Some conformational changes around the predicted active site were observed around the substrate binding site of *S. aureus* MK when superimposed with other MKs. The main difference is the conformation of motif I. In other structures, this motif appears as a short helix, ~12 Å from motif II. In *S. aureus* MK, these two motifs are ~6 Å apart. Motif III in *S. aureus* MK is closer to motif I and the distance from motif I is about ~ 5 Å. These major changes in *S. aureus* MK is probably due to the binding of citric acid. However, the conformational changes in the three loops appear to be coupled, if one or two of the three loops were to adopt the conformation seen in other structures, residues would clash. It seems that the loops adopt one arrangement or the other. This coupling of structural movements may be significant as these loops from the binding site.
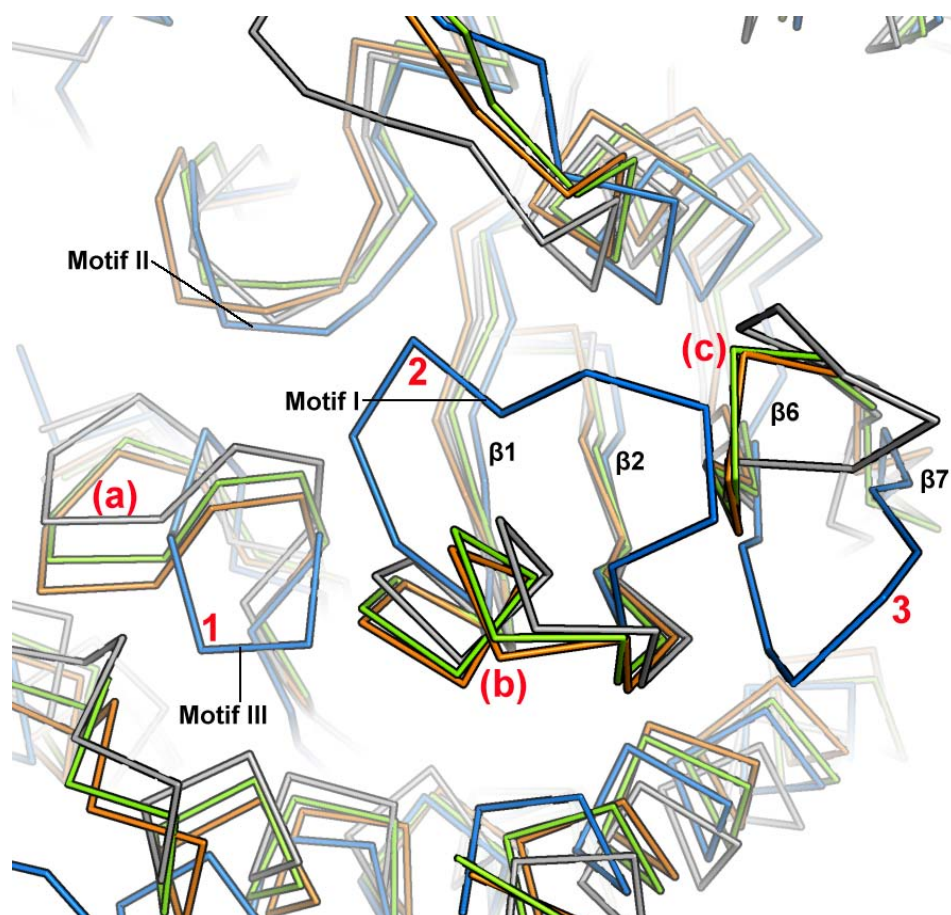
FIGURE 4.23: ribbon view of superimposed mevalonte kinases family members and *S. aureus* MK. The *S. aureus* MK is shown in blue, *L. major* MK in grey, human MK in green and Rat MK in orange. The three conserved motifs are labeled in black and main conformational changes in S. aureus MK are labeled by red arabic numbers 1, 2 and 3. The possible original conformation for the conformational changes 1, 2 and 3 are indicated by (a), (b) and (c), respectively.

The web-based analysis tool PISA "protein interfaces, surfaces and assemblies" http://www.ebi.ac.uk/msd-srv/prot_int/pistart.html (Krissinel and Henrick 2005) was used to analysis the crystal packing of *S. aureus* MK. The results indicate that *S. aureus* MK is stable as both dimer and tetramer form. The dimer form is consistent with the gel-filtration result which suggested that the *S. aureus* MK is a stable dimer in solution form. The fact that PISA predicts a tetramer may be a function of crystal packing.

PQS set		mm Size	Formula	Composition	Id	Stable	Surface area, sq. Å	Buried area, sq. Å
NN	«»							
1	◉	4	A_4a_4	$A_4[CIT]_4$	1	yes	45170	11530
2	◯	2	A_2a_2	$A_2[CIT]_2$	2	yes	25110	3250
3	◯	2	A_2a_2	$A_2[CIT]_2$	3	yes	24990	3360

FIGURE 4.24: Analysis output of S. aureus MK structure by PISA server.

In the dimer form, the two subunits of the dimmer are related by crystallographic symmetry and associate with each other via the interactions between their N-terminal domain, α1, β4 and the loop (adenosine strap loop) between them are the main structural elements that participated in monomer-monomer interactions. An interface area of ~3300 Å2 is buried between the two monomers. The dimer form of S. aureus MK is shown in FIGURE 4.25. The β4 from each subunit interacts with each other and extend the anti-parallel β-sheets conformation. While the α1 and adenosine strap loop from unit A interacts with the adenosine strap loop and α1 from subunit B, respectively. Notably the distance between α1/A and adenosine strap loop/B (α1/B and adenosine strap loop/A) are close (~4.8 Å), we predict that the interaction between this two elements may leads to a conformational change on adenosine strap loop and recesses to accommodate the ATP molecules. (FIGURE 4.26)
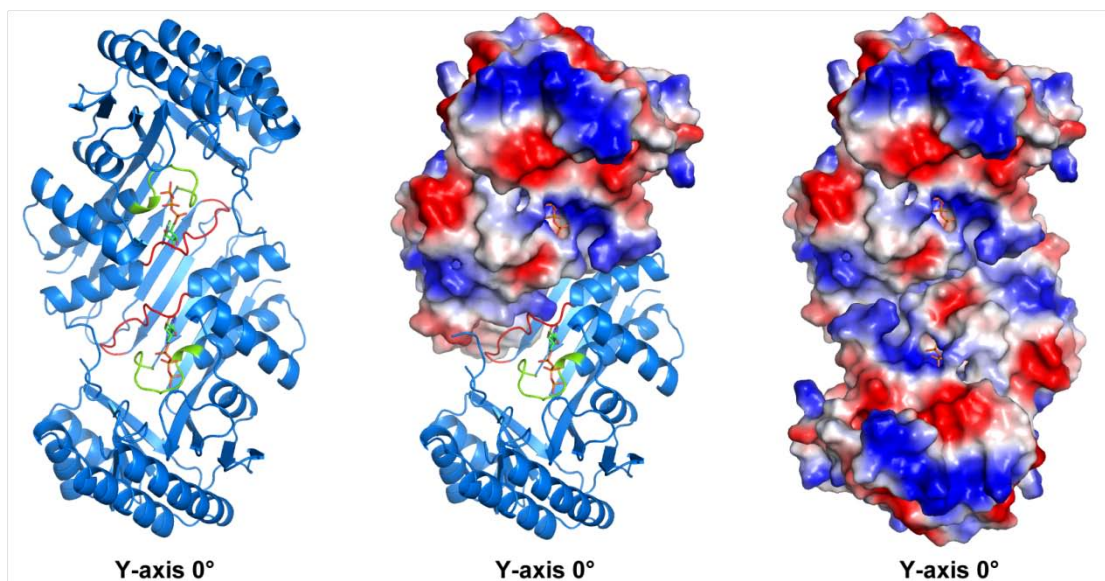
FIGURE 4.25: Surface electrostatics potential of S. aureus MK dimer suggested by PISA program. The solvent-accessible surface colored based on the electrostatics potential from -7 to +7 kT/e, calculated using ABPS tools in PyMol™. Positive charge is shown in blue and negative charge is shown in red.
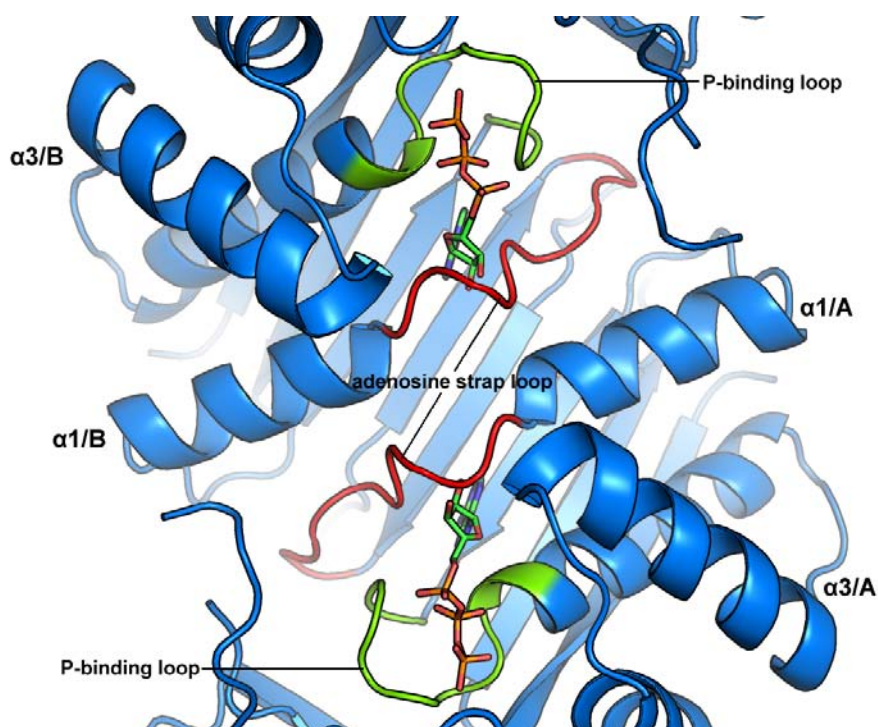
FIGURE 4.26: Cartoon representation of a close look of the dimer interface of *S. aureus* MK. The adenosine strap loop is highlighted in red, the phosphate-binding-loop is shown in green and labeled as "P-binding loop". ATP molecules are superimposed to indicate the predicted binding site.

The tetramer can be thought of a dimmers of dimmers. In FIGURE 4.27 the dimers are AB and CD. The AB (CD) interface buries about 12100 $\mathring{A}^2$ areas by each other. The four subunits in the tetramer are related by crystallographic symmetry and associate with each other via the interactions between with the β-strands β7 and β4 and form an extended and linked β-sheet area. The tetramer appears as a "hollow barrel" shape, surrounding by anti-parallel β-sheets in a row. The hole in the centre is about 15 Å wide. The active sites of each monomer are located at the surface of the hole inside the barrel. The hole is considered to be the entry point for substrate and ATP. The tetramer form suggested by PISA is shown in FIGURE 4.27.
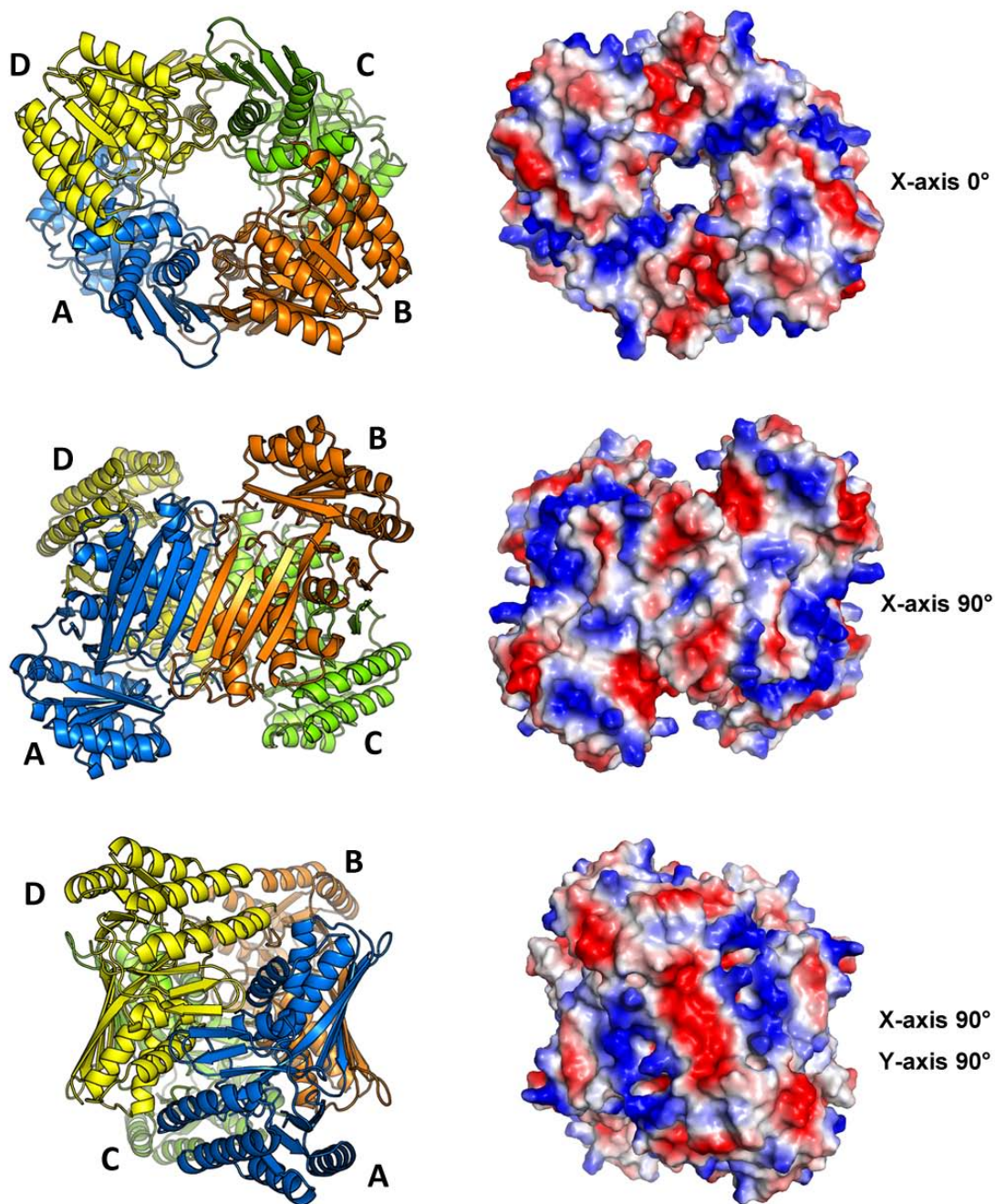
FIGURE 4.27: Cartoon representation and Surface electrostatics potential of *S. aureus* MK tetramer. The solvent-accessible surface colored based on the electrostatics potential from -7 to +7 kT/e, calculated using ABPS tools in PyMol™. Positive charge is shown in blue and negative charge is shown in red.

4.4.2 The proposed active site and citric acid binding.

The predicted ATP binding site of *S. aureus* MK locates in the cleft between the N-terminal and C-terminal domain. The signature motif II (phosphate-binding-loop), along with the adjacent helix α2 and β5, forms a deep cavity in the protein surface. The surface electrostatics potential shows this groove is strongly positively charged, consistent with ATP binding. (FIGURE 4.28)
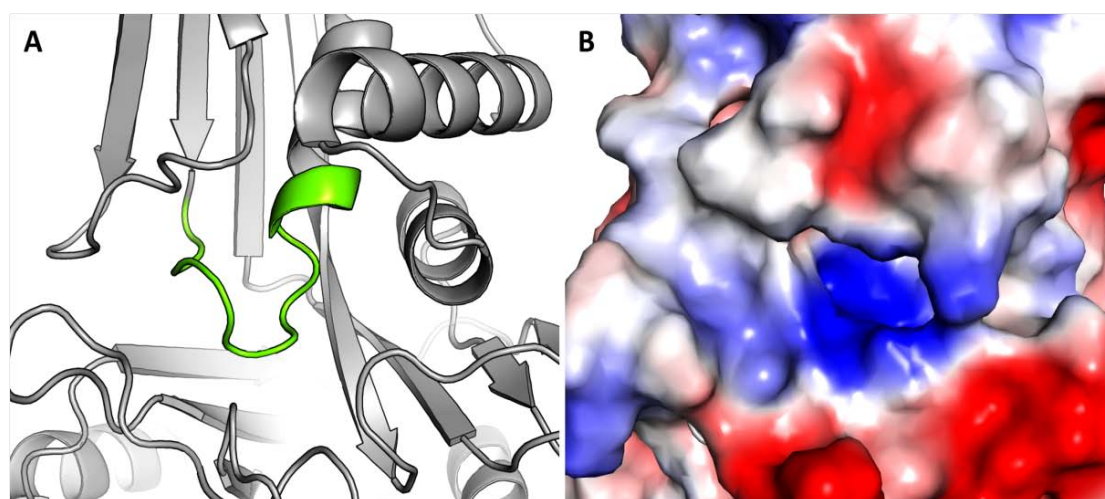
FIGURE 4.28: Cartoon representation and surface electrostatics potential of the phosphate binding loop of *S. aureus* MK. [A] Cartoon representation of the conserved signature structure motif of the GHMP kinase family, phosphate-binding-loop. The loop is shown in green. [B] Surface electrostatics potential of the phosphate-binding-loop in *S. aureus* MK. The solvent-accessible surface colored based on the electrostatics potential from -7 to +7 kT/e, calculated using ABPS tools in PyMol™. Positive charge is shown in blue and negative charge is shown in red.

A citric acid molecule is bound in the "phosphate-binding cavity", about 2.8 Å and 3.2 Å from the amide chain of Gly98 and Gly100, about 3.0 Å from the side chain of Ser101and Ser102 (FIGURE 4.30). These four residues from the motif II and helix α2 are highly conserved among MK family. The C3 hydroxyl group and C6 carboxyl

group of the citric acid form hydrogen bonds with these four residues. Ser96 bonds to

the C5 hydroxyl group of citric acid. Asp63 from the loop between β4 and helix α1

also hydrogen bond to the C5 carboxyl group. His19 and Ala20 from motif I both

interact with the citric acid molecule via a water-mediated network. Residues Lys12

from β1 and Asp145 from α3 pointing to the C1 carboxyl group of citric acid and

form a water-mediated network, these two residues are highly conserved in MKs and

considered as the key catalytic residues (Voynova, Rios et al. 2004). (FIGURE 4.29).

Water molecules surrounding the citric acid, indicating the cavity is a highly

hydrophilic environment. This positive-charged and hydrophilic cavity is ideal for the

phosphate donor of ATP binding.
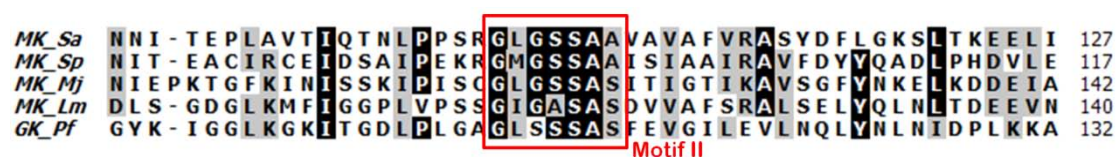
FIGURE 4.29: The conserved structure motif II of the GHMP kinase family. Identical residues in the sequences aligned are highlight in black. The red boxes indicate the highly conserved motif in MKs. This alignment was generated with BioEdit program.
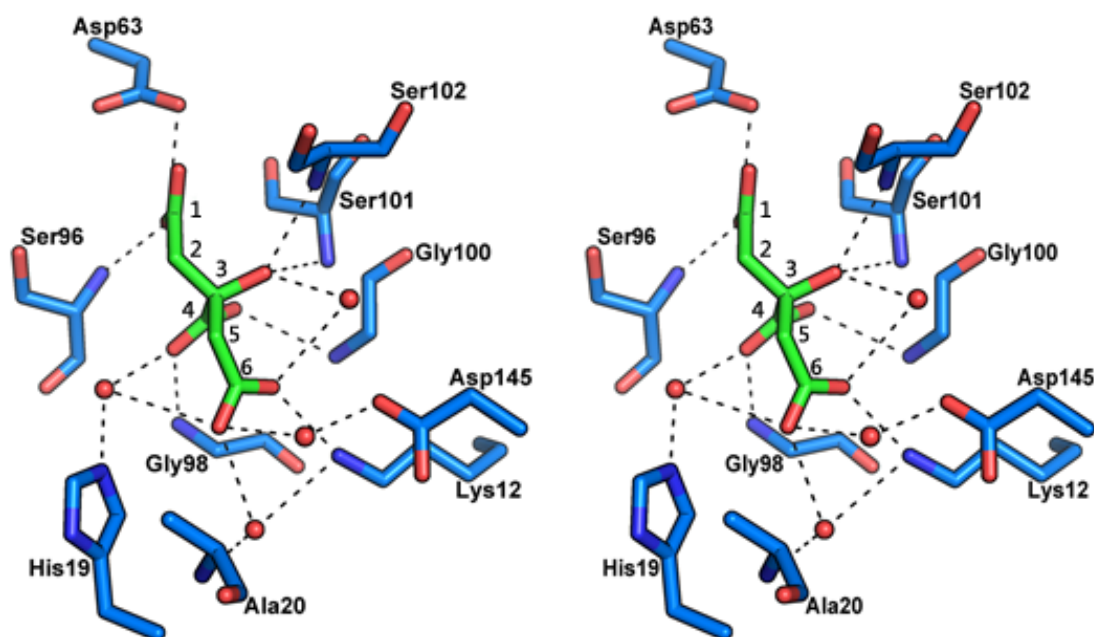
FIGURE 4.30: Stereo view of key interactions of protein with citric acid. Protein residues are shown in green, citric acid in green and blue, and water molecules as red sphere. Hydrogen bonds are depicted as black dashed lines. Residues that might interact with the ligand are labeled in black letters.
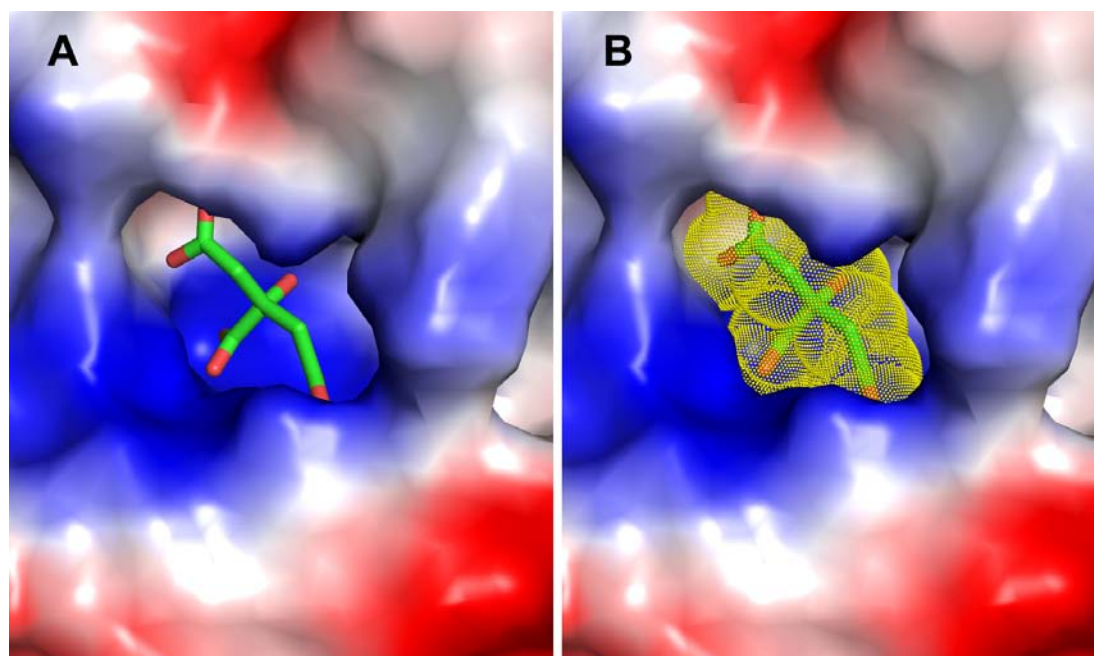
FIGURE 4.31: Surface electrostatics potential of the citric acid binding of *S. aureus* MK. The solvent-accessible surface colored based on the electrostatics potential from -7 to +7 kT/e, calculated using ABPS tools in PyMol™. Positive charge is shown in blue and negative charge is shown in red.

Our attempts to obtain a complex structure of *S. aureus* MK with ATP or AMP-PNP
(ATP analog) have been unsuccessful. This is probably due to the binding of citrate
which both blocks the binding site and alters the structure. In order to investigate the
binding mode and interactions between protein and co-factor, the ATP molecule was
docked into the predicted binding site by superimposing the rat MK/ATP complex
crystal structure with *S. aureus* MK structure.

The adenine group is anti with respect to the ribose group, and the ribose group is
binding with the residues Asn104 and Ser108 in Rat MK with reasonable distances
(2.6 Å and 2.8 Å, respectively). In the *S. aureus* MK monomer, the modeled ATP
clashes with the residues from the "adenosine strap loop" which presumably has
prevented binding in our experiments
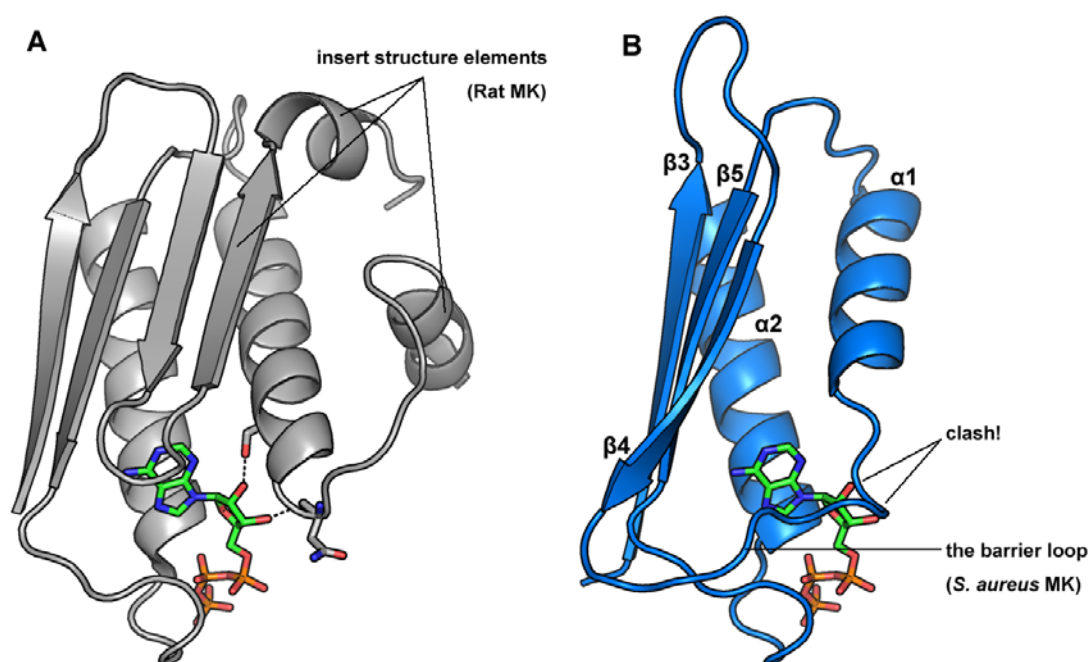
**FIGURE 4.32: Cartoon representation of the phosphate-binding-loop motif of Rat MK and *S.
aureus* MK. [A] Cartoon representation of the ATP binding at the phosphate-binding-loop of Rat
MK, the insert structure elements are labeled. [B] Cartoon representation of the superimposed
ATP at the phosphate-binding-loop of *S. aureus* MK. The barrier loop and predicted clash are
labeled.**
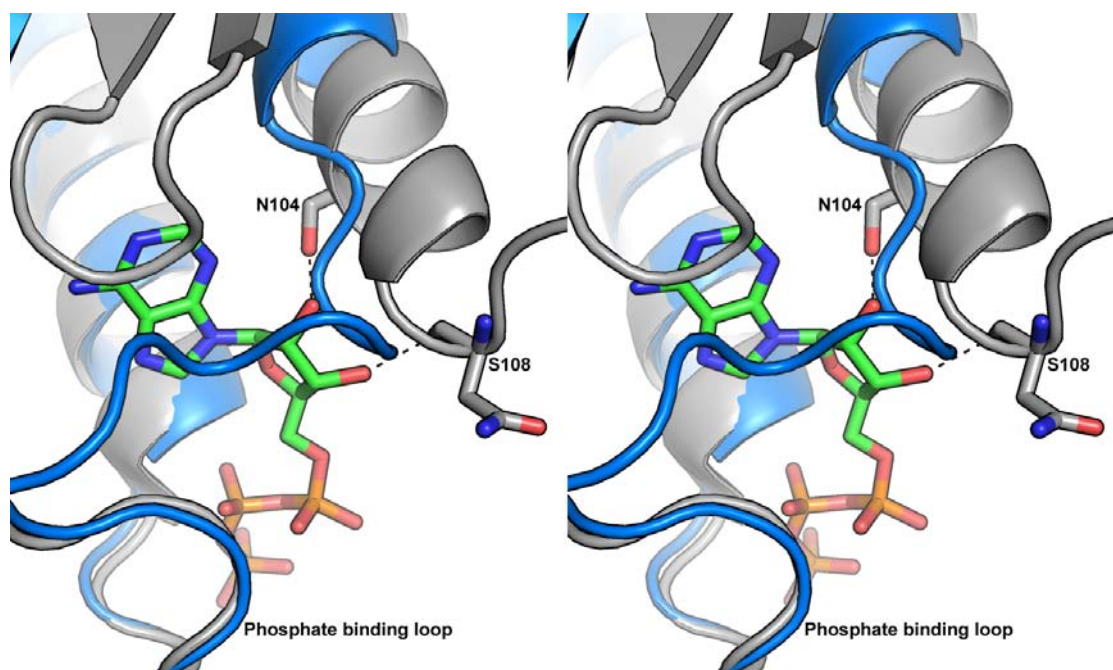
FIGURE 4.33: Stereo view of superimposed phosphate-binding-loop of Rat MK and *S. aureus* MK. The two residues which interacts with the ribose group are labeled. The Rat MK is shown in grey, the S. aureus MK is shown in blue, the ATP molecule is superimposed to indicated the predicted biding site.

Although the conformation of adenosine binding pockets are distinct due the additional insertion sequences in rat MK, the conformation of phosphate binding site is almost identical. In rat MK/ATP complex structure, the tri-phosphate interacts with the conserved motif II. The α-phosphoryl group of ATP hydrogen bonds to His197 and indirect interacts with Gly140 via a water-mediated network. The β- and γ-phosphoryl group of ATP coordinates an Mg^{2+}-water network using residues Gly140, Gly 144, Ser145, Ser146 and Asp204 the side chain of Lys13 and Asp204 point towards the γ-phosphoryl group.

In *S. aureus* mevalonate kinase/ATP model, these interactions are similar. The phosphate group binding residues are conserved; Gly140, Gly144, Ser145, Ser146, Asp204 and Lys13 in rat MK match Gly99, Gly100, Ser101, Ser102, Asp145 and

Lys12 in *S. aureus* MK. The strictly conserved residues Lys12 and Asp145 which close to the modeled γ-phosphoryl group (<2.8 Å) are predicted to be the key catalytic residues.
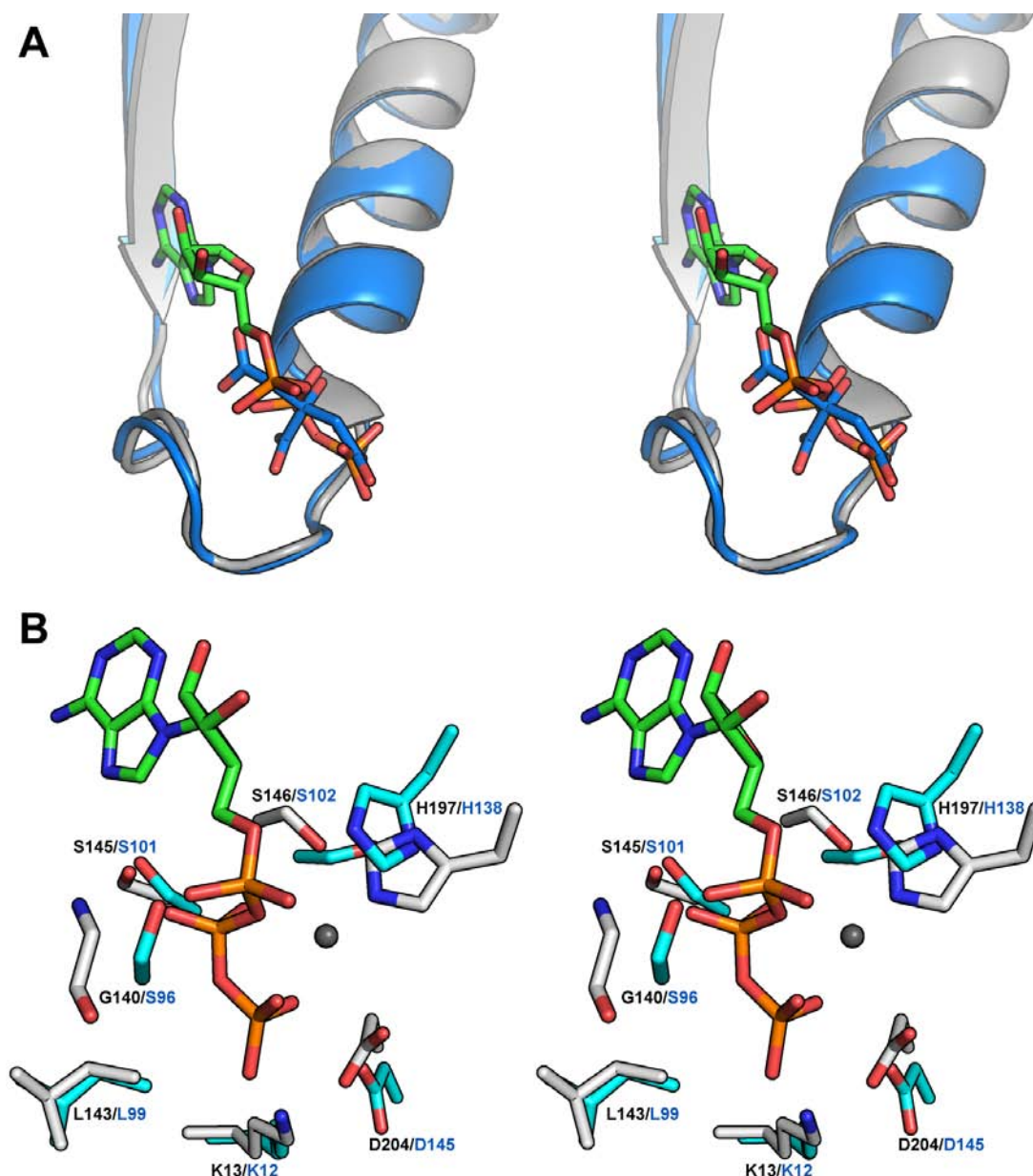
FIGURE 4.34: Stereo view of the cartoon representation of the potential triphosphate moiety interaction with protein. [A] A stereo view the conserved phosphate-binding-loop of *S. aureus* MK and Rat MK, ATP and citric acid molecules are superimposed. [B] Superposition of the related residues from the conserved motif 2 of *S. aureus* MK and Rat MK in complex with ATP. The *S. aureus* MK is colored in cyan, Rat MK is shown in white. ATP and Mg molecules are superimposed to indicate the proposed binding site. The residues at similar positions are labeled in the order of Rat MK/*S. aureus* MK. Single letter code of amino acid is used for concision.

A water-mediated network is formed around the citric acid molecule. Water molecules W1 and W2 interact with the C1 hydroxyls of citric acid and residues His19 and Ala20 from conserved motif I by hydrogen bonds. Motif I in *S. aureus* MK/citric acid complex structure occupies the predicted mevalonate binding site, and conformational change would be required to bind mevalonate.

This suggests that the conformation of structure elements between β1 and β2 may be flexible, These multiple interactions (mainly hydrogen bonds) between water molecules and residues "drag" motif I towards to the phosphate-binding-loop (motif II) and induce a conformational change of motif I and motif III in *S. aureus* MK, The conformational change of the loop between β6 and β7 would be achieved by the movement of motif I.

In *L. major* MK/mevalonate complex structure, residues Lys18, Ile20, Glu24, His25 and Val27 from conserved motif I and Ser152, Tyr167, Arg169, Thr195 and Val202 interact with the mevalonate with a water-mediated network. These residues are highly conserved and matching Lys12, Ile14, Glu18, His19 Val21, Ser142, Phe157, Gln159, Thr179 and Val190 in *S. aureus* MK. There are two residues, Phe157 and Gln159 in *S. aureus* MK, and Tyr167 and Arg169 in *L. major* MK, that might have similar interactions with mevalonate. The changes are relatively conservative preserving aromatic and amino groups (hydrogen bond donor).
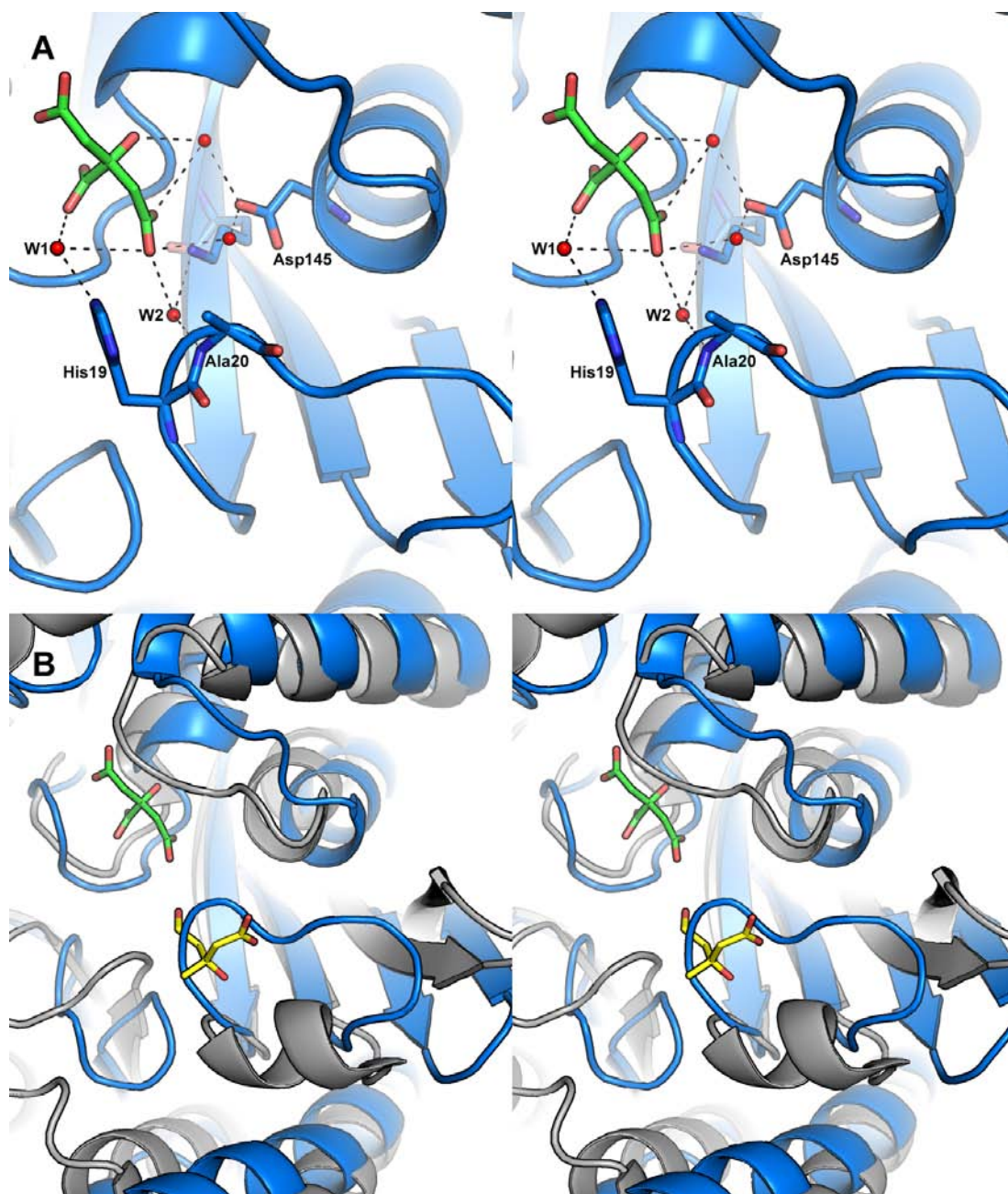
FIGURE 4.35: Stereo view of the predicted MEV binding site of *S. aureus* **MK and** *L.major* **MK.** *S. aureus* **MK is shown in blue,** *L.major* **MK in grey color. The citric acid (green) and the mevalonate (yellow) are superimposed to indicate the predicted ATP and mevalonate binding site, respectively.**

4.4.3 Mechanistic implications of *S. aureus* MK

Despite the crystal structure conformation of the "adenosine strap loop", the enzyme still shows normal activity, indicating the conformation we see is an artifact of packing. The apparent K_m of *S. aureus* MK for mevalonate was approximately 111.3($\pm$6.1) µM. This value is comparable to other enzymes.

	initial velocity (nmol/min)
Michaelis-Menten	
Best-fit values	
VMAX	34.75
KM	0.1113
Std. Error	
VMAX	0.4545
KM	0.006099
95% Confidence Intervals	
VMAX	33.82 to 35.68
KM	0.09887 to 0.1238
Goodness of Fit	
Degrees of Freedom	31
R²	0.9922
Absolute Sum of Squares	39.09
Sy.x	1.123
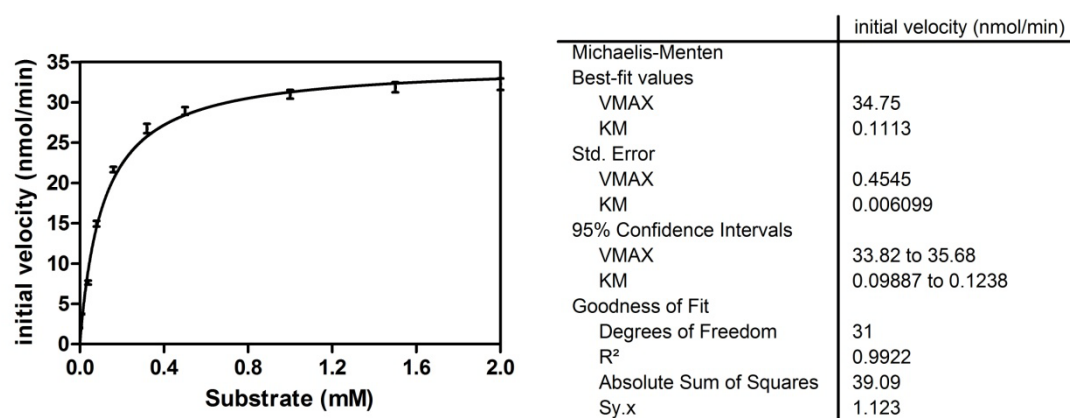
Source	K_m for Mevalonate (mM)	citations
Pig liver	0.019	(Beytia, Dorsey et al. 1970)
Rat liver	0.271	(Tanaka, Lee et al. 1990)
Human liver	0.074	(Popjak 1969)
E. faecalis	0.33	(Hedl, Rodwell al. 2003)
M. jannaschii	0.068	(Huang, Scott et al. 1999)
S. aureus (other strain)	0.041	(Voynova, Rios et al. 2004)
S. aureus (this study)	0.111	

TABLE 4.7: K_m for *S. aureus* MK and other MKs.

There are four strictly conserved residues at the catalytic centre that have been identified to be critical for the reaction, (Lys12, Ser102, Glu134 and Asp 145 in *S. aureus* MK). Ser102 and Glu134 from motif II is considered as the key elements interact with the phosphate donor and Mg ion (Cho, Rios et al. 2001). The position of Lys/Asp is almost identical in MKs from *S. aureus*, *L. major*, *M. jannaschii* and human. In mutational studies of human MK, the mutants Asp145Ala and Asp145Asn did not show any significant activity. Whist the mutant Lys12Met resulted in an almost 80-fold decrease of Vmax (Potter, Wojnar et al. 1997). This indicates that the residues Lys12 and Asp145 are very important residues of the catalytic mechanism.
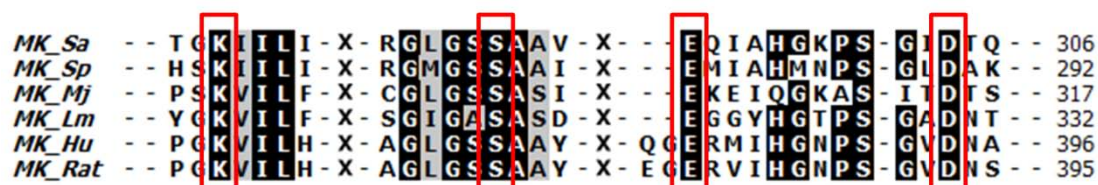
FIGURE 4.36: Selected sequences that strictly conserved in MKs. Identical residues in the sequences aligned are highlight in black. The four red boxes indicate the strictly conserved sequences in MKs. This alignment was generated with BioEdit program.

In the phosphorylation reaction, the Asp145 is likely to act as the essential catalytic base (acceptor) with its hydroxyl group in position to attract the proton from C5 hydroxyl group of mevalonate and generate a potent nuleophilie. Lys12 is thought to be responsible for fixing the orientation of the C5 hydroxyl group and also stabilizing the transition state (Chu and Li 2003). Ser146 may also provide some stabilizing effect of the transition state. Such arrangement is also observed in some other kinases such as *Escherichia coli* phosphofructokinase and *Trypanosoma brucei*

phosphoglycerate Kinase (Bossemeyer 1994; Matte, Tari et al. 1998). The residues from conserved motif III might have a water-mediated interaction with the magnesium ion and neutralize and stabilize the environment of the reaction. This potential catalytic mechanism is consistent with the Miziorko Lab model (Cho, Rios et al. 2001).
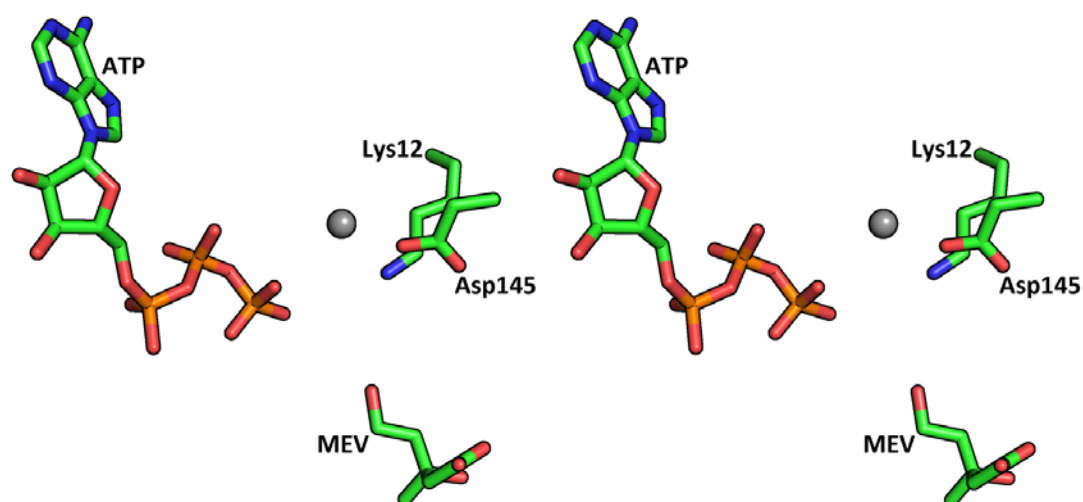
FIGURE 4.37: Stereo view of the proposed catalytic centre for *S. aureus* MK. Protein C atoms are shown in marine blue, C atoms of F1P are shown in green. N atoms, O and P atoms are shown in blue, red and orange, respectively. Magnesium ion is shown as grey sphere. MEV, ATP and the two key residues Asp145 and Lys12 are shown to indicate the potential interactions with the hydroxyl and phosphate group.
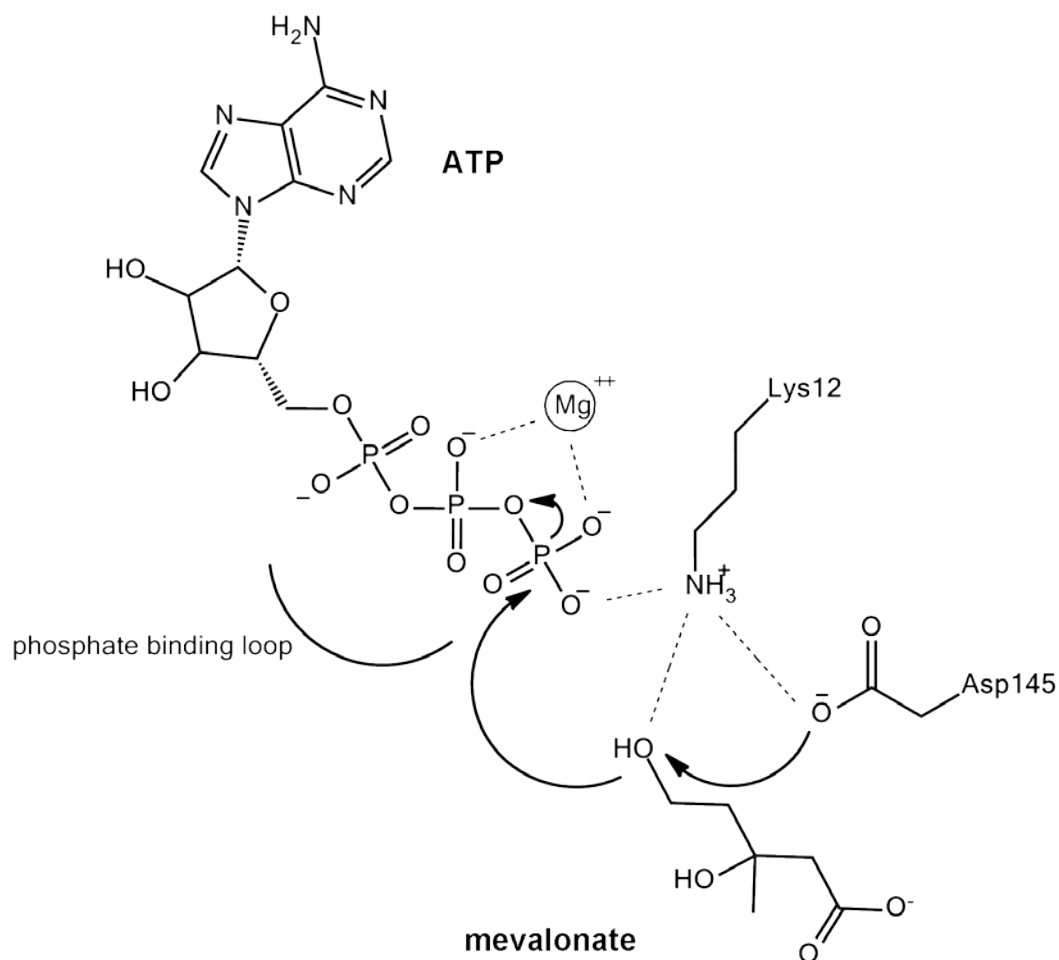
FIGURE 4.38: The possible mechanism of *S. aureus* MK.

4.4.4 Future work

It is important to obtain structures for both mevalonate and AMP-PNP in the active site of crystal. The problem is the citrate binding which appears to lock the structure into a non-binding mode. Validations of the results of thermofluor assay, co-crystallization soaking with potential hits in library is also necessary. New compounds could then be synthesized to inhibit the enzyme activities.

References:

(1982). "Treatment of methicillin-resistant Staphylococcus aureus infections." <u>Med Lett Drugs Ther</u> **24**(624): 107-108.

(2001). "Methicillin-resistant Staphylococcus aureus skin or soft tissue infections in a state prison--Mississippi, 2000." <u>MMWR Morb Mortal Wkly Rep</u> **50**(42): 919-922.

Abele, U. and G. E. Schulz (1995). "High-resolution structures of adenylate kinase from yeast ligated with inhibitor Ap5A, showing the pathway of phosphoryl transfer." <u>Protein Sci</u> **4**(7): 1262-1271.

Ackerman, E. J. and L. M. Iakoucheva (2000). "Nucleotide excision repair in oocyte nuclear extracts from Xenopus laevis." <u>Methods</u> **22**(2): 188-193.

Adams, P. D., R. W. Grosse-Kunstleve, et al. (2002). "PHENIX: building new software for automated crystallographic structure determination." <u>Acta Crystallographica Section D-Biological Crystallography</u> **58**: 1948-1954.

Allen, B. G., M. Johnson, et al. (2006). "Base excision repair of both uracil and oxidatively damaged bases contribute to thymidine deprivation-induced radiosensitization." <u>Int J Radiat Oncol Biol Phys</u> **65**(5): 1544-1552.

Altschul, S. F., T. L. Madden, et al. (1997). "Gapped BLAST and PSI-BLAST: a new generation of protein database search programs." <u>Nucleic Acids Res</u> **25**(17): 3389-3402.

Amano, M. (2004). "NMR studies of the alternative conformation of hammerhead ribozyme in the solution." <u>Nucleic Acids Symp Ser (Oxf)</u>(48): 215-216.

Amdur, M. O. (1957). "The influence of aerosols upon the respiratory response of guinea pigs to sulfur dioxide." <u>Am Ind Hyg Assoc Q</u> **18**(2): 149-155.

Andreassi, J. L., 2nd and T. S. Leyh (2004). "Molecular functions of conserved aspects of the GHMP kinase family." <u>Biochemistry</u> **43**(46): 14594-14601.

Arnfors, L., T. Hansen, et al. (2006). "Structure of Methanocaldococcus jannaschii nucleoside kinase: an archaeal member of the ribokinase family." <u>Acta Crystallogr D Biol Crystallogr</u> **62**(Pt 9): 1085-1097.

Arthur, M. and P. Courvalin (1993). "Genetics and mechanisms of glycopeptide resistance in enterococci." <u>Antimicrob Agents Chemother</u> **37**(8): 1563-1571.

Asaoka, Y., K. Yoshida, et al. (1992). "The family of protein kinase C in transmembrane signalling for cellular regulation." <u>J Nutr Sci Vitaminol (Tokyo)</u> **Spec No**: 7-12.

Azzi, A., D. Boscoboinik, et al. (1992). "The protein kinase C family." <u>Eur J Biochem</u> **208**(3): 547-557.

Baba, T., F. Takeuchi, et al. (2002). "Genome and virulence determinants of high virulence

community-acquired MRSA." <u>Lancet</u> **359**(9320): 1819-1827.

Baker, N. A., D. Sept, et al. (2001). "Electrostatics of nanosystems: application to microtubules and the ribosome." <u>Proc Natl Acad Sci U S A</u> **98**(18): 10037-10041.

Balakrishnan, V. and C. Van den Broeck (2005). "Analytic calculation of energy transfer and heat flux in a one-dimensional system." <u>Phys Rev E Stat Nonlin Soft Matter Phys</u> **72**(4 Pt 2): 046141.

Bang, S. S., P. Baumann, et al. (1977). "Properties of 1-phosphofructokinase from Pseudomonas putida." <u>Can J Microbiol</u> **23**(6): 721-725.

Barnes, F. J. and R. D. Goodfellow (1971). "Mevalonate kinase: localization and variation in activity during the development of Sarcophaga bullata." <u>J Insect Physiol</u> **17**(8): 1415-1427.

Baute, J. and A. Depicker (2008). "Base excision repair and its role in maintaining genome stability." <u>Crit Rev Biochem Mol Biol</u> **43**(4): 239-276.

Berg, J. M. (1990). "Zn2+ finger domains: hypotheses and current knowledge." <u>Annu Rev Biophys Biophys Chem</u> **19**: 405-421.

Berg, J. M. (1990). "Zn2+ fingers and other metal-binding domains. Elements for interactions between macromolecules." <u>J Biol Chem</u> **265**(12): 6513-6516.

Berman, D. S., S. Schaefler, et al. (1986). "Tourniquets and nosocomial methicillin-resistant Staphylococcus aureus infections." <u>N Engl J Med</u> **315**(8): 514-515.

Beytia, E., J. K. Dorsey, et al. (1970). "Purification and mechanism of action of hog liver mevalonic kinase." <u>J Biol Chem</u> **245**(20): 5450-5458.

Binet, M. R., M. N. Rager, et al. (1998). "Fructose and mannose metabolism in Aeromonas hydrophila: identification of transport systems and catabolic pathways." <u>Microbiology</u> **144 (Pt 4)**: 1113-1121.

Bjelland, S., M. Bjoras, et al. (1993). "Excision of 3-methylguanine from alkylated DNA by 3-methyladenine DNA glycosylase I of Escherichia coli." <u>Nucleic Acids Res</u> **21**(9): 2045-2049.

Bjelland, S. and E. Seeberg (1996). "Different efficiencies of the Tag and AlkA DNA glycosylases from Escherichia coli in the removal of 3-methyladenine from single-stranded DNA." <u>FEBS Lett</u> **397**(1): 127-129.

Boiteux, S., O. Huisman, et al. (1984). "3-Methyladenine residues in DNA induce the SOS function sfiA in Escherichia coli." <u>EMBO J</u> **3**(11): 2569-2573.

Borges-Walmsley, M. I. and A. R. Walmsley (2001). "The structure and function of drug pumps." <u>Trends Microbiol</u> **9**(2): 71-79.

Bork, P., C. Sander, et al. (1993). "Convergent evolution of similar enzymatic function on different protein folds: the hexokinase, ribokinase, and galactokinase families of sugar kinases." <u>Protein Sci</u> **2**(1): 31-40.

Bossemeyer, D. (1994). "The glycine-rich sequence of protein kinases: a multifunctional element." Trends Biochem Sci **19**(5): 201-205.

Bovill, B. A. and W. R. Weir (1994). "Staphylococcal infections." Br J Hosp Med **51**(11): 589-593.

Boyce, J. M., R. L. White, et al. (1983). "Impact of methicillin-resistant Staphylococcus aureus on the incidence of nosocomial staphylococcal infections." J Infect Dis **148**(4): 763.

Branger, C., C. Gardye, et al. (2003). "Genetic relationship between methicillin-susceptible and methicillin-resistant Staphylococcus aureus strains from France and from international sources: delineation of genomic groups." J Clin Microbiol **41**(7): 2946-2951.

Bruner, S. D., D. P. Norman, et al. (2000). "Structural basis for recognition and repair of the endogenous mutagen 8-oxoguanine in DNA." Nature **403**(6772): 859-866.

Burrus, V., G. Pavlovic, et al. (2002). "Conjugative transposons: the tip of the iceberg." Mol Microbiol **46**(3): 601-610.

Cabrera, R., A. L. Ambrosio, et al. (2008). "Crystallographic structure of phosphofructokinase-2 from Escherichia coli in complex with two ATP molecules. Implications for substrate inhibition." J Mol Biol **383**(3): 588-602.

Cabrera, R., A. Caniuguir, et al. (2006). "Crystallization and preliminary crystallographic analysis of the tetrameric form of phosphofructokinase-2 from Escherichia coli, a member of the ribokinase family." Acta Crystallogr Sect F Struct Biol Cryst Commun **62**(Pt 9): 935-937.

Cao, C., K. Kwon, et al. (2003). "Solution structure and base perturbation studies reveal a novel mode of alkylated base recognition by 3-methyladenine DNA glycosylase I." J Biol Chem **278**(48): 48012-48020.

Carretero-Paulet, L., I. Ahumada, et al. (2002). "Expression and molecular analysis of the Arabidopsis DXR gene encoding 1-deoxy-D-xylulose 5-phosphate reductoisomerase, the first committed enzyme of the 2-C-methyl-D-erythritol 4-phosphate pathway." Plant Physiol **129**(4): 1581-1591.

Chang, S. C., L. Y. Hsu, et al. (1988). "Methicillin-resistant Staphylococcus aureus infections." Taiwan Yi Xue Hui Za Zhi **87**(2): 157-163.

Chen, C. J., L. H. Su, et al. (2007). "Clinical features and molecular characteristics of invasive community-acquired methicillin-resistant Staphylococcus aureus infections in Taiwanese children." Diagn Microbiol Infect Dis **59**(3): 287-293.

Cheng, G., E. M. Bennett, et al. (2002). "Crystal structure of 4-amino-5-hydroxymethyl-2-methylpyrimidine phosphate kinase from Salmonella typhimurium at 2.3 A resolution." Structure **10**(2): 225-235.

Cho, Y. K., S. E. Rios, et al. (2001). "Investigation of invariant serine/threonine residues in mevalonate kinase. Tests of the functional significance of a proposed substrate binding motif and a site implicated

in human inherited disease." <u>J Biol Chem</u> **276**(16): 12573-12578.

Chu, D. T., J. J. Plattner, et al. (1996). "New directions in antibacterial research." <u>J Med Chem</u> **39**(20): 3853-3874.

Chu, X. and D. Li (2003). "Expression, purification, and characterization of His20 mutants of rat mevalonate kinase." <u>Protein Expr Purif</u> **32**(1): 75-82.

Contin, A., R. van der Heijden, et al. (1998). "The iridoid glucoside secologanin is derived from the novel triose phosphate/pyruvate pathway in a Catharanthus roseus cell culture." <u>FEBS Lett</u> **434**(3): 413-416.

Cordier, H., C. Lacombe, et al. (1999). "The Saccharomyces cerevisiae mevalonate diphosphate decarboxylase (erg19p) forms homodimers in vivo, and a single substitution in a structurally conserved region impairs dimerization." <u>Curr Microbiol</u> **38**(5): 290-294.

Crabtree, T. D., S. J. Pelletier, et al. (1999). "Analysis of aminoglycosides in the treatment of gram-negative infections in surgical patients." <u>Arch Surg</u> **134**(12): 1293-1298; discussion 1298-1299.

Crouzoulon, G. (1973). "[Proceedings: Intestinal absorption of fructose in the rat]." <u>J Physiol (Paris)</u> **67**(3): 337A.

Currie, M. A., F. Merino, et al. (2009). "ADP-dependent 6-phosphofructokinase from Pyrococcus horikoshii OT3: structure determination and biochemical characterization of PH1645." <u>J Biol Chem</u> **284**(34): 22664-22671.

Daugherty, M., V. Vonstein, et al. (2001). "Archaeal shikimate kinase, a new member of the GHMP-kinase family." <u>J Bacteriol</u> **183**(1): 292-300.

Daum, R. S. (1998). "Community-acquired methicillin-resistant staphylococcus aureus infections." <u>Pediatr Infect Dis J</u> **17**(8): 745-746.

Davies, D. R., M. Detheux, et al. (1990). "Fructose 1-phosphate and the regulation of glucokinase activity in isolated hepatocytes." <u>Eur J Biochem</u> **192**(2): 283-289.

Davies, J. (1994). "Inactivation of antibiotics and the dissemination of resistance genes." <u>Science</u> **264**(5157): 375-382.

Davies, J. (1996). "Bacteria on the rampage." <u>Nature</u> **383**(6597): 219-220.

Dewick, P. M. (2002). "The biosynthesis of C5-C25 terpenoid compounds." <u>Nat Prod Rep</u> **19**(2): 181-222.

Dianov, G. L., N. Souza-Pinto, et al. (2001). "Base excision repair in nuclear and mitochondrial DNA." <u>Prog Nucleic Acid Res Mol Biol</u> **68**: 285-297.

Dionne, K. E., B. M. Cain, et al. (1996). "Transport characterization of membranes for immunoisolation." <u>Biomaterials</u> **17**(3): 257-266.

Dizdaroglu, M. (2005). "Base-excision repair of oxidative DNA damage by DNA glycosylases." <u>Mutat Res</u> **591**(1-2): 45-59.

Dodson, M. L. and R. S. Lloyd (2002). "Mechanistic comparisons among base excision repair glycosylases." <u>Free Radic Biol Med</u> **32**(8): 678-682.

Doherty, A. J., L. C. Serpell, et al. (1996). "The helix-hairpin-helix DNA-binding motif: A structural basis for non-sequence-specific recognition of DNA." <u>Nucleic Acids Research</u> **24**(13): 2488-2497.

Doherty, A. J., L. C. Serpell, et al. (1996). "The helix-hairpin-helix DNA-binding motif: a structural basis for non-sequence-specific recognition of DNA." <u>Nucleic Acids Res</u> **24**(13): 2488-2497.

Draborg, H., D. Villadsen, et al. (1999). "Cloning, characterization and expression of a bifunctional fructose-6-phosphate, 2-kinase/fructose-2,6-bisphosphatase from potato." <u>Plant Mol Biol</u> **39**(4): 709-720.

Drohat, A. C., K. Kwon, et al. (2002). "3-Methyladenine DNA glycosylase I is an unexpected helix-hairpin-helix family member." <u>Nat Struct Biol</u> **9**(9): 659-664.

Ehringer, W. D., B. Chiang, et al. (2001). "The uptake and metabolism of fructose-1,6-diphosphate in rat cardiomyocytes." <u>Mol Cell Biochem</u> **221**(1-2): 33-40.

Eichman, B. F., E. J. O'Rourke, et al. (2003). "Crystal structures of 3-methyladenine DNA glycosylase MagIII and the recognition of alkylated bases." <u>EMBO J</u> **22**(19): 4898-4909.

Emsley, P. and K. Cowtan (2004). "Coot: model-building tools for molecular graphics." <u>Acta Crystallogr D Biol Crystallogr</u> **60**(Pt 12 Pt 1): 2126-2132.

Enright, M. C., N. P. Day, et al. (2000). "Multilocus sequence typing for characterization of methicillin-resistant and methicillin-susceptible clones of Staphylococcus aureus." <u>J Clin Microbiol</u> **38**(3): 1008-1015.

Fairclough, S. H. and K. Houston (2004). "A metabolic measure of mental effort." <u>Biol Psychol</u> **66**(2): 177-190.

Farr, B. M. (1999). "Methicillin-Resistant Staphylococcus aureus Infections." <u>Curr Infect Dis Rep</u> **1**(4): 328-333.

Feder, H. M., Jr. (2000). "Methicillin-resistant Staphylococcus aureus infections in 2 pediatric outpatients." <u>Arch Fam Med</u> **9**(6): 560-562.

Feil, E. J., J. E. Cooper, et al. (2003). "How clonal is Staphylococcus aureus?" <u>J Bacteriol</u> **185**(11): 3307-3316.

Fletcher, C. (1984). "First clinical use of penicillin." <u>Br Med J (Clin Res Ed)</u> **289**(6460): 1721-1723.

Foster, T. J. (2004). "The Staphylococcus aureus "superbug"." <u>J Clin Invest</u> **114**(12): 1693-1696.

Frank, A. L., J. F. Marcinak, et al. (2002). "Clindamycin treatment of methicillin-resistant Staphylococcus aureus infections in children." <u>Pediatr Infect Dis J</u> **21**(6): 530-534.

Friedberg, E. C., A. Aguilera, et al. (2006). "DNA repair: from molecular mechanism to human disease." <u>DNA Repair (Amst)</u> **5**(8): 986-996.

Frishman, D. and P. Argos (1995). "Knowledge-based protein secondary structure assignment." <u>Proteins</u> **23**(4): 566-579.

Fromme, J. C., A. Banerjee, et al. (2004). "Structural basis for removal of adenine mispaired with 8-oxoguanine by MutY adenine DNA glycosylase." <u>Nature</u> **427**(6975): 652-656.

Fromme, J. C. and G. L. Verdine (2002). "Structural insights into lesion recognition and repair by the bacterial 8-oxoguanine DNA glycosylase MutM." <u>Nat Struct Biol</u> **9**(7): 544-552.

Fromme, J. C. and G. L. Verdine (2004). "Base excision repair." <u>Adv Protein Chem</u> **69**: 1-41.

Fu, Z., N. E. Voynova, et al. (2008). "Biochemical and structural basis for feedback inhibition of mevalonate kinase and isoprenoid metabolism." <u>Biochemistry</u> **47**(12): 3715-3724.

Fu, Z., M. Wang, et al. (2002). "The structure of a binary complex between a mammalian mevalonate kinase and ATP: insights into the reaction mechanism and human inherited disease." <u>J Biol Chem</u> **277**(20): 18134-18142.

Fujii, S. and Y. Yamagata (2000). "Structural bases for substrate recognition and repair system of base-excision DNA repair proteins." <u>Nucleic Acids Symp Ser</u>(44): 57-58.

Fujisawa, T., J. Riby, et al. (1991). "Intestinal absorption of fructose in the rat." <u>Gastroenterology</u> **101**(2): 360-367.

Gao, L. Y., F. Laval, et al. (2003). "Requirement for kasB in Mycobacterium mycolic acid biosynthesis, cell wall impermeability and intracellular survival: implications for therapy." <u>Mol Microbiol</u> **49**(6): 1547-1563.

Garman, E. (1999). "Cool data: quantity AND quality." <u>Acta Crystallogr D Biol Crystallogr</u> **55**(Pt 10): 1641-1653.

Giamarellou, H., M. Papapetropoulou, et al. (1981). "'Methicillin resistant' Staphylococcus aureus infections during 1978-79: clinical and bacteriologic observations." <u>J Antimicrob Chemother</u> **7**(6): 649-655.

Gilboa, R., D. O. Zharkov, et al. (2002). "Structure of formamidopyrimidine-DNA glycosylase covalently complexed to DNA." <u>J Biol Chem</u> **277**(22): 19811-19816.

Goldstein, J. L. and M. S. Brown (1990). "Regulation of the mevalonate pathway." <u>Nature</u> **343**(6257): 425-430.

Goodman, D. S. and G. Popjak (1960). "Studies on the biosynthesis of cholesterol. XII. Synthesis of

allyl pyrophosphates from mevalonate and their conversion into squalene with liver enzymes." J Lipid Res **1**: 286-300.

Gouet, P., X. Robert, et al. (2003). "ESPript/ENDscript: Extracting and rendering sequence and 3D information from atomic structures of proteins." Nucleic Acids Res **31**(13): 3320-3323.

Graham, P. L., 3rd (2002). "Staphylococcal and enterococcal infections in the neonatal intensive care unit." Semin Perinatol **26**(5): 322-331.

Gschaedler, A., N. Thi Le, et al. (1994). "Glucose and acetate influences on the behavior of the recombinant strain Escherichia coli HB 101 (GAPDH)." J Ind Microbiol **13**(4): 225-232.

Guan, Y., R. C. Manuel, et al. (1998). "MutY catalytic core, mutant and bound adenine structures define specificity for DNA repair enzyme family." Nat Struct Biol **5**(12): 1058-1064.

Gunther, M. A., A. Sillero, et al. (1967). "Fructokinase assay with a specific spectrophotometric method using 1-phosphofructokinase." Enzymol Biol Clin (Basel) **8**(5): 341-352.

Hagopian, K., J. J. Ramsey, et al. (2005). "Fructose metabolizing enzymes from mouse liver: influence of age and caloric restriction." Biochim Biophys Acta **1721**(1-3): 37-43.

Haley, R. W., A. W. Hightower, et al. (1982). "The emergence of methicillin-resistant Staphylococcus aureus infections in United States hospitals. Possible role of the house staff-patient transfer circuit." Ann Intern Med **97**(3): 297-308.

Hansen, T., L. Arnfors, et al. (2007). "The phosphofructokinase-B (MJ0406) from Methanocaldococcus jannaschii represents a nucleoside kinase with a broad substrate specificity." Extremophiles **11**(1): 105-114.

Herold, B. C., L. C. Immergluck, et al. (1998). "Community-acquired methicillin-resistant Staphylococcus aureus in children with no identified predisposing risk." Jama **279**(8): 593-598.

Hers, H. G. and T. Kusaka (1953). "[The metabolism of fructose-1-phosphate in the liver.]." Biochim Biophys Acta **11**(3): 427-437.

Higashi, Y., A. Wakabayashi, et al. (1999). "Role of inhibition of penicillin binding proteins and cell wall cross-linking by beta-lactam antibiotics in low- and high-level methicillin resistance of Staphylococcus aureus." Chemotherapy **45**(1): 37-47.

Holden, M. T., E. J. Feil, et al. (2004). "Complete genomes of two clinical Staphylococcus aureus strains: evidence for the rapid evolution of virulence and drug resistance." Proc Natl Acad Sci U S A **101**(26): 9786-9791.

Hollis, T., Y. Ichikawa, et al. (2000). "DNA bending and a flip-out mechanism for base excision by the helix-hairpin-helix DNA glycosylase, Escherichia coli AlkA." EMBO J **19**(4): 758-766.

Holm, L. and C. Sander (1993). "Protein structure comparison by alignment of distance matrices." J Mol Biol **233**(1): 123-138.

Hone, R. and C. T. Keane (1974). "A clinical study of infections caused by methicillin-resistant Staphylococcus aureus." <u>Infection</u> **2**(4): 213-217.

Houten, S. M., R. J. A. Wanders, et al. (2000). "Biochemical and genetic aspects of mevalonate kinase and its deficiency." <u>Biochimica Et Biophysica Acta-Molecular and Cell Biology of Lipids</u> **1529**(1-3): 19-32.

Huang, K. X., A. I. Scott, et al. (1999). "Overexpression, purification, and characterization of the thermostable mevalonate kinase from Methanococcus jannaschii." <u>Protein Expr Purif</u> **17**(1): 33-40.

Hughes, W. H. (1952). "Variation in penicillin resistance in single-cell cultures of Staphylococcus aureus." <u>J Gen Microbiol</u> **6**(1-2): 175-180.

Ikeda, S. and S. Seki (2001). "[Base excision repair: DNA glycosylase and AP endonuclease]." <u>Tanpakushitsu Kakusan Koso</u> **46**(8 Suppl): 916-923.

Ito, S., S. Fushinobu, et al. (2001). "Structural basis for the ADP-specificity of a novel glucokinase from a hyperthermophilic archaeon." <u>Structure</u> **9**(3): 205-214.

Jasanoff, A., M. Kochoyan, et al. (1992). "Aromatic-aromatic interactions in the Zn2+ finger motif. Analysis of the two-dimensional nuclear magnetic resonance structure of a mutant domain." <u>J Mol Biol</u> **225**(4): 1035-1047.

Johnson, A. P., H. M. Aucken, et al. (2001). "Dominance of EMRSA-15 and -16 among MRSA causing nosocomial bacteraemia in the UK: analysis of isolates from the European Antimicrobial Resistance Surveillance System (EARSS)." <u>J Antimicrob Chemother</u> **48**(1): 143-144.

Kaatz, G. W. (2002). "Inhibition of bacterial efflux pumps: a new strategy to combat increasing antimicrobial agent resistance." <u>Expert Opin Emerg Drugs</u> **7**(2): 223-233.

Kanra, G., M. K. Caglar, et al. (1985). "Successful treatment with mezlocillin of a child infected by penicillin G-resistant Staphylococcus aureus." <u>Turk J Pediatr</u> **27**(4): 213-217.

Karanas, Y. L., M. A. Bogdan, et al. (2000). "Community acquired methicillin-resistant Staphylococcus aureus hand infections: case reports and clinical implications." <u>J Hand Surg Am</u> **25**(4): 760-763.

Kareiviene, V., A. Pavilonis, et al. (2006). "Staphylococcus aureus resistance to antibiotics and spread of phage types." <u>Medicina (Kaunas)</u> **42**(4): 332-339.

Katayama, Y., H. Z. Zhang, et al. (2003). "Effect of disruption of Staphylococcus aureus PBP4 gene on resistance to beta-lactam antibiotics." <u>Microb Drug Resist</u> **9**(4): 329-336.

Kayser, F. H., E. J. Benner, et al. (1970). "Acquired and native resistance of Staphylococcus aureus to cephalexin and other beta-lactam antibiotics." <u>Appl Microbiol</u> **20**(1): 1-5.

Keane, C. T. and M. T. Cafferkey (1983). "Severe infections caused by methicillin-resistant Staphylococcus aureus." <u>Eur J Clin Microbiol</u> **2**(4): 299-302.

Kim, D. Y., C. V. Stauffacher, et al. (2000). "Dual coenzyme specificity of Archaeoglobus fulgidus HMG-CoA reductase." Protein Sci **9**(6): 1226-1234.

Kirthi, N. and H. S. Savithri (2003). "A conserved Zn2+ finger motif in the coat protein of Tomato leaf curl Bangalore virus is responsible for binding to ssDNA." Arch Virol **148**(12): 2369-2380.

Kizaki, Z. and T. Sawada (1997). "[Fructose pathway]." Nippon Rinsho **55 Suppl 1**: 239-243.

Klungland, A., M. Bjoras, et al. (1994). "Increased removal of 3-alkyladenine reduces the frequencies of hprt mutations induced by methyl- and ethylmethanesulfonate in Chinese hamster fibroblast cells." Nucleic Acids Res **22**(9): 1670-1674.

Klungland, A., L. Fairbairn, et al. (1992). "Expression of the E.coli 3-methyladenine DNA glycosylase I gene in mammalian cells reduces the toxic and mutagenic effects of methylating agents." EMBO J **11**(12): 4439-4444.

Korolev, B. G. (2005). "[Base excision repair of DNA: glycosylases]." Genetika **41**(6): 725-735.

Korolev, V. G. (2005). "[Base excision repair: AP endonucleases and DNA polymerases]." Genetika **41**(10): 1301-1309.

Krissinel, E. and K. Henrick (2004). "Secondary-structure matching (SSM), a new tool for fast protein structure alignment in three dimensions." Acta Crystallographica Section D-Biological Crystallography **60**: 2256-2268.

Krissinel, E. and K. Henrick (2005). "Detection of protein assemblies in crystals." Computational Life Sciences, Proceedings **3695**: 163-174.

Krokan, H. E., H. Nilsen, et al. (2000). "Base excision repair of DNA in mammalian cells." FEBS Lett **476**(1-2): 73-77.

Krokan, H. E., R. Standal, et al. (1997). "DNA glycosylases in the base excision repair of DNA." Biochem J **325 (Pt 1)**: 1-16.

Kuo, C. F., D. E. McRee, et al. (1992). "Atomic structure of the DNA repair [4Fe-4S] enzyme endonuclease III." Science **258**(5081): 434-440.

Kuroda, M., H. Kuroda, et al. (2003). "Two-component system VraSR positively modulates the regulation of cell-wall biosynthesis pathway in Staphylococcus aureus." Mol Microbiol **49**(3): 807-821.

Kuzuyama, T. (2002). "Mevalonate and nonmevalonate pathways for the biosynthesis of isoprene units." Biosci Biotechnol Biochem **66**(8): 1619-1627.

Kuzuyama, T. and H. Seto (2003). "Diversity of the biosynthesis of the isoprene units." Nat Prod Rep **20**(2): 171-183.

Kwon, K., C. Cao, et al. (2003). "A novel Zn2+ snap motif conveys structural stability to 3-methyladenine DNA glycosylase I." J Biol Chem **278**(21): 19442-19446.

Kwon, O., D. K. Bhattacharyya, et al. (1996). "Menaquinone (vitamin K2) biosynthesis: overexpression, purification, and properties of o-succinylbenzoyl-coenzyme A synthetase from Escherichia coli." J Bacteriol **178**(23): 6778-6781.

Kwon, Y. and M. J. Smerdon (2003). "Binding of Zn2+ finger protein transcription factor IIIA to its cognate DNA sequence with single UV photoproducts at specific sites and its effect on DNA repair." J Biol Chem **278**(46): 45451-45459.

Labahn, J., O. D. Scharer, et al. (1996). "Structural basis for the excision repair of alkylation-damaged DNA." Cell **86**(2): 321-329.

Lachowicz, T. M. (1960). "The mechanism of development in vitro of penicillin-resistant variants of Staphylococcus aureus. II. Further investigation on the fluctuation test in the study of the origin of penicillin-resistance." Acta Microbiol Pol **9**: 143-150.

Lange, B. M. and R. Croteau (1999). "Isopentenyl diphosphate biosynthesis via a mevalonate-independent pathway: isopentenyl monophosphate kinase catalyzes the terminal enzymatic step." Proc Natl Acad Sci U S A **96**(24): 13714-13719.

Lange, B. M., T. Rujan, et al. (2000). "Isoprenoid biosynthesis: the evolution of two ancient and distinct pathways across genomes." Proc Natl Acad Sci U S A **97**(24): 13172-13177.

Larkin, M. A., G. Blackshields, et al. (2007). "Clustal W and Clustal X version 2.0." Bioinformatics **23**(21): 2947-2948.

Lau, A. Y., M. D. Wyatt, et al. (2000). "Molecular basis for discriminating between normal and damaged bases by the human alkyladenine glycosylase, AAG." Proc Natl Acad Sci U S A **97**(25): 13573-13578.

Levy, S. B. (1992). "Active efflux mechanisms for antimicrobial resistance." Antimicrob Agents Chemother **36**(4): 695-703.

Levy, S. B. (1998). "The challenge of antibiotic resistance." Sci Am **278**(3): 46-53.

Li, M. H., F. Kwok, et al. (2002). "Crystal structure of brain pyridoxal kinase, a novel member of the ribokinase family." J Biol Chem **277**(48): 46385-46390.

Lindahl, T. (1976). "New class of enzymes acting on damaged DNA." Nature **259**(5538): 64-66.

Lindahl, T. (1993). "Instability and decay of the primary structure of DNA." Nature **362**(6422): 709-715.

Lindsay, J. A. and M. T. Holden (2004). "Staphylococcus aureus: superbug, super genome?" Trends Microbiol **12**(8): 378-385.

Liu, J. Y., D. E. Timm, et al. (2006). "Pyrithiamine as a substrate for thiamine pyrophosphokinase." J Biol Chem **281**(10): 6601-6607.

Lo, M. C., A. Aulabaugh, et al. (2004). "Evaluation of fluorescence-based thermal shift assays for hit identification in drug discovery." Anal Biochem **332**(1): 153-159.

Lovell, S. C., I. W. Davis, et al. (2003). "Structure validation by Calpha geometry: phi,psi and Cbeta deviation." Proteins **50**(3): 437-450.

Lundstrom, T. S. and J. D. Sobel (2000). "Antibiotics for gram-positive bacterial infections. Vancomycin, teicoplanin, quinupristin/dalfopristin, and linezolid." Infect Dis Clin North Am **14**(2): 463-474.

Luttgen, H., F. Rohdich, et al. (2000). "Biosynthesis of terpenoids: YchB protein of Escherichia coli phosphorylates the 2-hydroxy group of 4-diphosphocytidyl-2C-methyl-D-erythritol." Proc Natl Acad Sci U S A **97**(3): 1062-1067.

Luz, D. A., A. K. Rodrigues, et al. (2008). "Adsorptive separation of fructose and glucose from an agroindustrial waste of cashew industry." Bioresour Technol **99**(7): 2455-2465.

Lye, W. C., S. O. Leong, et al. (1993). "Methicillin-resistant Staphylococcus aureus nasal carriage and infections in CAPD." Kidney Int **43**(6): 1357-1362.

Mani, S., C. Wang, et al. (2000). "Cyclin-dependent kinase inhibitors: novel anticancer agents." Expert Opin Investig Drugs **9**(8): 1849-1870.

Martinez-Aguilar, G., W. A. Hammerman, et al. (2003). "Clindamycin treatment of invasive infections caused by community-acquired, methicillin-resistant and methicillin-susceptible Staphylococcus aureus in children." Pediatr Infect Dis J **22**(7): 593-598.

Massova, I. and S. Mobashery (1998). "Kinship and diversification of bacterial penicillin-binding proteins and beta-lactamases." Antimicrob Agents Chemother **42**(1): 1-17.

Mathews, II, M. D. Erion, et al. (1998). "Structure of human adenosine kinase at 1.5 A resolution." Biochemistry **37**(45): 15607-15620.

Matte, A., L. W. Tari, et al. (1998). "How do kinases transfer phosphoryl groups?" Structure **6**(4): 413-419.

McCoy, A. J. (2007). "Solving structures of protein complexes by molecular replacement with Phaser." Acta Crystallogr D Biol Crystallogr **63**(Pt 1): 32-41.

McGahee, W. and F. D. Lowy (2000). "Staphylococcal infections in the intensive care unit." Semin Respir Infect **15**(4): 308-313.

Meira, L. B., N. E. Burgis, et al. (2005). "Base excision repair." Adv Exp Med Biol **570**: 125-173.

Memisoglu, A. and L. Samson (2000). "Base excision repair in yeast and mammals." Mutat Res **451**(1-2): 39-51.

Metz, A. H., T. Hollis, et al. (2007). "DNA damage recognition and repair by 3-methyladenine DNA

glycosylase I (TAG)." EMBO J **26**(9): 2411-2420.

Miallau, L., W. N. Hunter, et al. (2007). "Structures of Staphylococcus aureus D-tagatose-6-phosphate kinase implicate domain motions in specificity and mechanism." J Biol Chem **282**(27): 19948-19957.

Milatovic, D. (1986). "Vancomycin for treatment of infections with methicillin-resistant Staphylococcus aureus: are there alternatives?" Eur J Clin Microbiol **5**(6): 689-692.

Mitsuda, T. (2002). "[MRSA infection]." Rinsho Byori **Suppl 123**: 42-48.

Mlynarczyk, A., G. Mlynarczyk, et al. (1979). "[Mechanisms of resistance to antibiotics in Staphylococcus aureus]." Pol Tyg Lek **34**(39): 1537-1540.

Mol, C. D., C. F. Kuo, et al. (1995). "Structure and function of the multifunctional DNA-repair enzyme exonuclease III." Nature **374**(6520): 381-386.

Moore, P. C. and J. A. Lindsay (2002). "Molecular characterisation of the dominant UK methicillin-resistant Staphylococcus aureus strains, EMRSA-15 and EMRSA-16." J Med Microbiol **51**(6): 516-521.

Murshudov, G. N., A. A. Vagin, et al. (1997). "Refinement of macromolecular structures by the maximum-likelihood method." Acta Crystallogr D Biol Crystallogr **53**(Pt 3): 240-255.

Nash, H. M., S. D. Bruner, et al. (1996). "Cloning of a yeast 8-oxoguanine DNA glycosylase reveals the existence of a base-excision DNA-repair protein family." Curr Biol **6**(8): 968-980.

Navaza, J. (1994). "Amore - an Automated Package for Molecular Replacement." Acta Crystallographica Section A **50**: 157-163.

Nettleship, J. E., J. Brown, et al. (2008). "Methods for protein characterization by mass spectrometry, thermal shift (ThermoFluor) assay, and multiangle or static light scattering." Methods Mol Biol **426**: 299-318.

Niculescu, L., M. Veiga-da-Cunha, et al. (1996). "Enzymatic assays of fructose-1-phosphate and fructose-1,6-bisphosphate in the picomole range." Anal Biochem **235**(2): 243-244.

O'Rourke, E. J., C. Chevalier, et al. (2000). "A novel 3-methyladenine DNA glycosylase from helicobacter pylori defines a new class within the endonuclease III family of base excision repair glycosylases." J Biol Chem **275**(26): 20077-20083.

Okumura, A., Y. Muraishi, et al. (1993). "[Clinical studies on methicillin-resistant Staphylococcus aureus (MRSA) infections]." Hinyokika Kiyo **39**(12): 1157-1161.

Olofsson, A., J. H. Ippel, et al. (2004). "Probing solvent accessibility of transthyretin amyloid by solution NMR spectroscopy." J Biol Chem **279**(7): 5699-5707.

Orchard, L. M. and H. L. Kornberg (1990). "Sequence similarities between the gene specifying 1-phosphofructokinase (fruK), genes specifying other kinases in Escherichia coli K12, and lacC of

Staphylococcus aureus." <u>Proc Biol Sci</u> **242**(1304): 87-90.

Otwinowski, Z. and W. Minor (1997). "Processing of X-ray diffraction data collected in oscillation mode." <u>Macromolecular Crystallography, Pt A</u> **276**: 307-326.

Panzaru, C., D. Gotia, et al. (2002). "Tolerance to penicillin in Staphylococcus pyogenes isolated from skin infections." <u>Rev Med Chir Soc Med Nat Iasi</u> **107**(2): 356-359.

Papadopoulos, N. M. and J. H. Roe (1957). "Fructose phosphorylation and dephosphorylation by the intestinal mucosa of the rat during fructose absorption." <u>Am J Physiol</u> **189**(2): 301-306.

Pappu, K. M., J. D. Gregory, et al. (1994). "Substrate activity of Rh(III)ATP with phosphoglycerate kinase and the role of the metal ion in catalysis." <u>Arch Biochem Biophys</u> **311**(2): 503-508.

Park, Y. K. and E. A. Yetley (1993). "Intakes and food sources of fructose in the United States." <u>Am J Clin Nutr</u> **58**(5 Suppl): 737S-747S.

Patelski, R. and G. L. Hobby (1952). "The first decade of antibiotics; 1941-51; penicillin to terramycin." <u>Med Illus</u> **6**(4): 155-166.

Paulsen, I. T., M. H. Brown, et al. (1996). "Proton-dependent multidrug efflux systems." <u>Microbiol Rev</u> **60**(4): 575-608.

Peacock, S. J., I. de Silva, et al. (2001). "What determines nasal carriage of Staphylococcus aureus?" <u>Trends in Microbiology</u> **9**(12): 605-610.

Pembroke, J. T., C. MacMahon, et al. (2002). "The role of conjugative transposons in the Enterobacteriaceae." <u>Cell Mol Life Sci</u> **59**(12): 2055-2064.

Peromet, M., E. Schoutens, et al. (1973). "Clinical and microbiological study of enduracidin in infections due to methicillin-resistant strains of Staphylococcus aureus." <u>Chemotherapy</u> **19**(1): 53-61.

Perrakis, A., R. Morris, et al. (1999). "Automated protein model building combined with iterative structure refinement." <u>Nat Struct Biol</u> **6**(5): 458-463.

Poole, K. (2004). "Resistance to beta-lactam antibiotics." <u>Cell Mol Life Sci</u> **61**(17): 2200-2223.

Porter, J. W. (1985). "Mevalonate kinase." <u>Methods Enzymol</u> **110**: 71-78.

Potter, D., J. M. Wojnar, et al. (1997). "Identification and functional characterization of an active-site lysine in mevalonate kinase." <u>J Biol Chem</u> **272**(9): 5741-5746.

Potterton, E., P. Briggs, et al. (2003). "A graphical user interface to the CCP4 program suite." <u>Acta Crystallogr D Biol Crystallogr</u> **59**(Pt 7): 1131-1137.

Powledge, T. M. (2004). "New antibiotics--resistance is futile." <u>PLoS Biol</u> **2**(2): E53.

Rafferty, J. B., S. M. Ingleston, et al. (1998). "Structural similarities between Escherichia coli RuvA

protein and other DNA-binding proteins and a mutational analysis of its binding to the holliday junction." J Mol Biol **278**(1): 105-116.

Rahman, M. (1998). "Alternatives to vancomycin in treating methicillin-resistant Staphylococcus aureus infections." J Antimicrob Chemother **41**(3): 325-328.

Ramage, G., S. Bachmann, et al. (2002). "Investigation of multidrug efflux pumps in relation to fluconazole resistance in Candida albicans biofilms." J Antimicrob Chemother **49**(6): 973-980.

Ramdas, L. and R. J. Budde (1998). "The instability of polyhydroxylated aromatic protein tyrosine kinase inhibitors in the presence of manganese." Cancer Biochem Biophys **16**(4): 375-385.

Rawal, B. D. (1969). "Induction of penicillin susceptibility in hospital strains of penicillin-resistant Staphylococcus aureus: a new therapeutic pathway." Med J Aust **1**(12): 612-614.

Reardon, J. T., T. Bessho, et al. (1997). "In vitro repair of oxidative DNA damage by human nucleotide excision repair system: possible explanation for neurodegeneration in xeroderma pigmentosum patients." Proc Natl Acad Sci U S A **94**(17): 9463-9468.

Reeves, R. E., L. G. Warren, et al. (1966). "1-Phosphofructokinase from an anaerobe." J Biol Chem **241**(6): 1257-1261.

Reusch, V. M., Jr. (1984). "Lipopolymers, isoprenoids, and the assembly of the gram-positive cell wall." Crit Rev Microbiol **11**(2): 129-155.

Richet, H. M., M. Benbachir, et al. (2003). "Are there regional variations in the diagnosis, surveillance, and control of methicillin-resistant Staphylococcus aureus?" Infect Control Hosp Epidemiol **24**(5): 334-341.

Rogers, L. J., S. P. Shah, et al. (1966). "Mevalonate-kinase isoenzymes in plant cells." Biochem J **100**(2): 14contd-17c.

Rohmer, M. (1999). "The discovery of a mevalonate-independent pathway for isoprenoid biosynthesis in bacteria, algae and higher plants." Nat Prod Rep **16**(5): 565-574.

Rohmer, M., M. Knani, et al. (1993). "Isoprenoid biosynthesis in bacteria: a novel pathway for the early steps leading to isopentenyl diphosphate." Biochem J **295 (Pt 2)**: 517-524.

Romano, A. C. (1953). "[Strain of Staphylococcus aureus of high resistance to antibiotics.]." Rev Sanid Milit Argent **52**(1): 107-108.

Romanowski, M. J., J. B. Bonanno, et al. (2002). "Crystal structure of the Streptococcus pneumoniae phosphomevalonate kinase, a member of the GHMP kinase family." Proteins **47**(4): 568-571.

Ross, H. (1985). "Postoperative wound infection with methicillin-resistant staphylococci in general surgical patients." Aust N Z J Surg **55**(1): 13-17.

Sabath, L. D., N. Wheeler, et al. (1977). "A new type of penicillin resistance of Staphylococcus

aureus." <u>Lancet</u> **1**(8009): 443-447.

Sabini, E., S. Ort, et al. (2003). "Structure of human dCK suggests strategies to improve anticancer and antiviral therapy." <u>Nat Struct Biol</u> **10**(7): 513-519.

Samson, L., J. Thomale, et al. (1988). "Alternative pathways for the in vivo repair of O6-alkylguanine and O4-alkylthymine in Escherichia coli: the adaptive response and nucleotide excision repair." <u>Embo J</u> **7**(7): 2261-2267.

Sapico, V. and R. L. Anderson (1969). "D-fructose 1-phosphate kinase and D-fructose 6-phosphate kinase from Aerobacter aerogenes. A comparative study of regulatory properties." <u>J Biol Chem</u> **244**(22): 6280-6288.

Sawaya, M. R., R. Prasad, et al. (1997). "Crystal structures of human DNA polymerase beta complexed with gapped and nicked DNA: evidence for an induced fit mechanism." <u>Biochemistry</u> **36**(37): 11205-11215.

Schulte, A. E., R. van der Heijden, et al. (2000). "Purification and characterization of mevalonate kinase from suspension-cultured cells of Catharanthus roseus (L.) G. Don." <u>Arch Biochem Biophys</u> **378**(2): 287-298.

Schumacher, M. A., D. M. Scott, et al. (2000). "Crystal structures of Toxoplasma gondii adenosine kinase reveal a novel catalytic mechanism and prodrug binding." <u>J Mol Biol</u> **296**(2): 549-567.

Schuttelkopf, A. W. and D. M. van Aalten (2004). "PRODRG: a tool for high-throughput crystallography of protein-ligand complexes." <u>Acta Crystallogr D Biol Crystallogr</u> **60**(Pt 8): 1355-1363.

Scott, K. P. (2002). "The role of conjugative transposons in spreading antibiotic resistance between bacteria that inhabit the gastrointestinal tract." <u>Cell Mol Life Sci</u> **59**(12): 2071-2082.

Seeberg, E., L. Eide, et al. (1995). "The base excision repair pathway." <u>Trends Biochem Sci</u> **20**(10): 391-397.

Selig, M., K. B. Xavier, et al. (1997). "Comparative analysis of Embden-Meyerhof and Entner-Doudoroff glycolytic pathways in hyperthermophilic archaea and the bacterium Thermotoga." <u>Arch Microbiol</u> **167**(4): 217-232.

Sgraja, T., T. K. Smith, et al. (2007). "Structure, substrate recognition and reactivity of Leishmania major mevalonate kinase." <u>BMC Struct Biol</u> **7**: 20.

Shaw, K. J., P. N. Rather, et al. (1993). "Molecular genetics of aminoglycoside resistance genes and familial relationships of the aminoglycoside-modifying enzymes." <u>Microbiol Rev</u> **57**(1): 138-163.

Sieradzki, K., T. Leski, et al. (2003). "Evolution of a vancomycin-intermediate Staphylococcus aureus strain in vivo: multiple changes in the antibiotic resistance phenotypes of a single lineage of methicillin-resistant S. aureus under the impact of antibiotics administered for chemotherapy." <u>J Clin</u>

Microbiol **41**(4): 1687-1693.

Sieradzki, K. and A. Tomasz (1997). "Suppression of beta-lactam antibiotic resistance in a methicillin-resistant Staphylococcus aureus through synergic action of early cell wall inhibitors and some other antibiotics." <u>J Antimicrob Chemother</u> **39 Suppl A**: 47-51.

Sigrell, J. A., A. D. Cameron, et al. (1998). "Structure of Escherichia coli ribokinase in complex with ribose and dinucleotide determined to 1.8 A resolution: insights into a new family of kinase structures." <u>Structure</u> **6**(2): 183-193.

Sigrell, J. A., A. D. Cameron, et al. (1999). "Induced fit on sugar binding activates ribokinase." <u>J Mol Biol</u> **290**(5): 1009-1018.

Skilleter, D. N. and R. G. Kekwick (1967). "An improved ion-exchange procedure for the chromatography of the metabolites of mevalonate." <u>Anal Biochem</u> **20**(1): 171-180.

Soler, M., A. M. Jabalquinto, et al. (1979). "Hog liver mevalonate kinase: inactivation by pyridoxal-5'-phosphate and evidence of dead-end inhibition by one of the substrates." <u>Int J Biochem</u> **10**(11): 931-935.

Song, M. D., M. Wachi, et al. (1987). "Evolution of an inducible penicillin-target protein in methicillin-resistant Staphylococcus aureus by gene fusion." <u>FEBS Lett</u> **221**(1): 167-171.

Spratt, B. G. (1994). "Resistance to antibiotics mediated by target alterations." <u>Science</u> **264**(5157): 388-393.

Spratt, B. G. and K. D. Cromie (1988). "Penicillin-binding proteins of gram-negative bacteria." <u>Rev Infect Dis</u> **10**(4): 699-711.

Stankovic, C. and P. V. Mahajan (2006). "Healthy children with invasive community-acquired methicillin-resistant Staphylococcus aureus infections." <u>Pediatr Emerg Care</u> **22**(5): 361-363.

Staudacher, E., F. Altmann, et al. (1999). "Fucose in N-glycans: from plant to man." <u>Biochim Biophys Acta</u> **1473**(1): 216-236.

Steinman, G. (1962). "[Role of penicillinase in the resistance of Staphylococcus aureus to benzyl penicillin.]." <u>Antibiotiki</u> **7**: 718-724.

Studier, F. W. (2005). "Protein production by auto-induction in high density shaking cultures." <u>Protein Expr Purif</u> **41**(1): 207-234.

Tanaka, R. D., L. Y. Lee, et al. (1990). "Molecular cloning of mevalonate kinase and regulation of its mRNA levels in rat liver." <u>Proc Natl Acad Sci U S A</u> **87**(8): 2872-2876.

Tchen, T. T. (1958). "Mevalonic kinase: purification and properties." <u>J Biol Chem</u> **233**(5): 1100-1103.

Terwilliger, T. C. (2003). "SOLVE and RESOLVE: automated structure solution and density modification." <u>Methods Enzymol</u> **374**: 22-37.

Thayer, M. M., H. Ahern, et al. (1995). "Novel DNA binding motifs in the DNA repair enzyme endonuclease III crystal structure." EMBO J **14**(16): 4108-4120.

Thornsberry, C. (1994). "Epidemiology of staphylococcal infections--a USA perspective." J Chemother **6 Suppl 2**: 61-65.

Tolmasky, M. E. (2000). "Bacterial resistance to aminoglycosides and beta-lactams: the Tn1331 transposon paradigm." Front Biosci **5**: D20-29.

Tsay, Y. H. and G. W. Robinson (1991). "Cloning and characterization of ERG8, an essential gene of Saccharomyces cerevisiae that encodes phosphomevalonate kinase." Mol Cell Biol **11**(2): 620-631.

Urisu, T., M. M. Rahman, et al. (2005). "Formation of high-resistance supported lipid bilayer on the surface of a silicon substrate with microelectrodes." Nanomedicine **1**(4): 317-322.

Vagin, A. and A. Teplyakov (2000). "An approach to multi-copy search in molecular replacement." Acta Crystallographica Section D-Biological Crystallography **56**: 1622-1624.

Van Rooyen, J., J. McCarthy, et al. (2002). "Increased glycolysis during ischaemia mediates the protective effect of glucose and insulin in the isolated rat heart despite the presence of cardiodepressant exogenous substrates." Cardiovasc J S Afr **13**(3): 103-109.

Van Schaftingen, E., M. Detheux, et al. (1994). "Short-term control of glucokinase activity: role of a regulatory protein." FASEB J **8**(6): 414-419.

Veiga-da-Cunha, M., A. Hoyoux, et al. (2000). "Overexpression and purification of fructose-1-phosphate kinase from Escherichia coli: application to the assay of fructose 1-phosphate." Protein Expr Purif **19**(1): 48-52.

Verdonk, M. L., J. C. Cole, et al. (2003). "Improved protein-ligand docking using GOLD." Proteins-Structure Function and Genetics **52**(4): 609-623.

Viriasov, S. N. and V. V. Perelygin (1984). "[Specific electric resistance of a narrow gap between two lipid bilayer membranes]." Biofizika **29**(5): 792-795.

Voynova, N. E., S. E. Rios, et al. (2004). "Staphylococcus aureus mevalonate kinase: isolation and characterization of an enzyme of the isoprenoid biosynthetic pathway." J Bacteriol **186**(1): 61-67.

Walsh, C. (2000). "Molecular mechanisms that confer antibacterial drug resistance." Nature **406**(6797): 775-781.

Walsh, C. T., S. L. Fisher, et al. (1996). "Bacterial resistance to vancomycin: five genes and one missing hydrogen bond tell the story." Chem Biol **3**(1): 21-28.

Wang, W. and T. J. Tong (1999). "[The key enzyme of cholesterol synthesis pathway: HMG-CoA reductase and disease]." Sheng Li Ke Xue Jin Zhan **30**(1): 5-9.

Washer, P. and H. Joffe (2006). "The "hospital superbug": Social representations of MRSA." Soc Sci

Med.

Whipp, P. (1987). "Staph aureus: resistance to antibiotics." Prof Nurse **2**(9): 282-284.

Wilding, E. I., J. R. Brown, et al. (2000). "Identification, evolution, and essentiality of the mevalonate pathway for isopentenyl diphosphate biosynthesis in gram-positive cocci." J Bacteriol **182**(15): 4319-4327.

Wilding, E. I., D. Y. Kim, et al. (2000). "Essentiality, expression, and characterization of the class II 3-hydroxy-3-methylglutaryl coenzyme A reductase of Staphylococcus aureus." J Bacteriol **182**(18): 5147-5152.

Williamson, I. P. and R. G. Kekwick (1965). "The formation of 5-phosphomevalonate by mevalonate kinase in Hevea brasiliensis latex." Biochem J **96**(3): 862-871.

Winn, M. D., G. N. Murshudov, et al. (2003). "Macromolecular TLS refinement in REFMAC at moderate resolutions." Methods Enzymol **374**: 300-321.

Wood, R. D. (1997). "Nucleotide excision repair in mammalian cells." J Biol Chem **272**(38): 23465-23468.

Wyatt, M. D., J. M. Allan, et al. (1999). "3-methyladenine DNA glycosylases: structure, function, and biological importance." Bioessays **21**(8): 668-676.

Xiao, C. L. and T. J. Yao (2004). "[Bacterial resistance and study of new antibiotics]." Zhongguo Yi Xue Ke Xue Yuan Xue Bao **26**(4): 351-353.

Yang, D., L. W. Shipman, et al. (2002). "Structure of the Methanococcus jannaschii mevalonate kinase, a member of the GHMP kinase family." J Biol Chem **277**(11): 9462-9467.

Yang, Z. R., R. Thomson, et al. (2005). "RONN: the bio-basis function neural network technique applied to the detection of natively disordered regions in proteins." Bioinformatics **21**(16): 3369-3376.

Zaoutis, T. E., P. Toltzis, et al. (2006). "Clinical and molecular epidemiology of community-acquired methicillin-resistant Staphylococcus aureus infections among children with risk factors for health care-associated infection: 2001-2003." Pediatr Infect Dis J **25**(4): 343-348.

Zhang, Y., M. Dougherty, et al. (2004). "Crystal structure of an aminoimidazole riboside kinase from Salmonella enterica: implications for the evolution of the ribokinase family." Structure **12**(10): 1809-1821.

Zharkov, D. O. (2008). "Base excision DNA repair." Cell Mol Life Sci **65**(10): 1544-1565.

Zhou, T., M. Daugherty, et al. (2000). "Structure and mechanism of homoserine kinase: prototype for the GHMP kinase family." Structure **8**(12): 1247-1257.